Imperial College London

Department of Earth Science & Engineering

Measurements of Zeta Potential for Improved Understanding of Controlled Salinity Waterflooding

Harry M. Collini

Supervised by:

Professor Matthew D. Jackson

Dr. Bilal Rashid

A thesis submitted in fulfilment of the requirements for the degree of Doctor of Philosophy in Earth Science & Engineering at Imperial College London

March 2022

Measurements of Zeta Potential for Improved Understanding of Controlled Salinity Waterflooding

Declaration of Originality

I hereby declare that all the work presented in this thesis is my own, completed under the supervision of Professor Matthew Jackson in the Department of Earth Science & Engineering at Imperial College London. Where other sources of information have been used these have been clearly indicated and acknowledged.

Harry Collini

Abstract

Improved oil recovery (IOR) processes increase the efficiency of oil extraction from subsurface reservoirs. Controlled salinity waterflooding (CSW) is an IOR process where brine of a specific ionic composition is injected into a reservoir. However, CSW does not always yield IOR and the underlying mechanism(s) responsible remain unclear. It is generally accepted that successful CSW is associated with a shift to a more water-wet state. The wetting state is thought to be controlled by the zeta potential, a measure of the electrical potential, at the mineral and oil interfaces.

This thesis explores how modifying the brine composition changes the zeta potential of these interfaces and impacts wettability in sandstones and carbonates. This is primarily done by streaming potential measurements (SPM) of natural, intact rock cores at conditions relevant to CSW. Results are discussed with specific focus on their application to CSW.

Under fully water saturated conditions, the zeta potential of carbonates becomes more negative with reduction of the divalent cations Ca^{2+} and Mg^{2+}. Sandstones exhibit more complex behaviour; however, the bulk clay content appears to be an important control.

Following wettability alteration with crude oil, the zeta potential of carbonate samples became more positive or negative with increasing oil-wetness. The direction of change is interpreted to represent the polarity of the oil-brine zeta potential. During CSW, if the injection brine yields a mineral-brine zeta potential polarity that is the same as the oil-brine zeta potential, then IOR is observed.

Determining the polarity of the oil-brine zeta potential appears critical in controlling CSW but directly measuring this under relevant conditions is challenging using conventional methods. A theoretical pore network model was developed which allows for prediction of the oil-brine zeta potential under such conditions. The model predicts that this was positive in most of the carbonate experiments. However, previous literature data from conventional methods

suggest positive values are rare. Therefore, a new method to directly measure the oil-brine zeta potential was also developed. Strongly oil-wet substrates were prepared using natural porous media and coated with crude oil. The zeta potential of these substrates reflects the oil-brine zeta potential. These results show Ca^{2+} is a key control, however, most of the data were negative, conflicting with prior results.

There is an apparent difference between the zeta potential of the 'pristine' oil-brine interface and that of the '*in-situ'* oil-brine interface present in the subsurface; the latter of which appears critical in controlling CSW. Understanding the *in-situ* oil-brine zeta potential contributes to better design and optimisation of CSW processes to maximise oil recovery.

Acknowledgments

First and foremost, I must thank my supervisor, Professor Matthew Jackson. None of this would have been accomplished without your guidance and support over the last few years and the confidence and trust you have given to me since day one. You have helped me become more precise, well-rounded and self-confident in preparation to begin my career.

I would like to thank BP for funding and providing samples. In particular, Bilal Rashid, John Couves, Ian Collins and Ugo Ekpo have all been important in contributing to this work and I thank each of them for their time. Graham Nash and Gary Jones have been vital in helping set up experiments, fixing equipment and keeping the lab running. Thank you to Professors Martin Blunt and Aksel Hiorth for agreeing to examine this thesis.

To Catherine and Ben, thank you both for being my closest friends throughout this time. I have always been able to rely on you to rant to when things have not been going well and have an extended coffee break with when I've needed a distraction. I've many fond memories together from conferences, coffee mornings and the various pubs around South Kensington and I know we will remain close regardless of what the future holds. I will miss the wider NORMS group, particularly those I have spent long hours in the lab with, and our Christmas parties. Hopefully one day I will be able to attend a summer BBQ.

Sam and Siobhan, thanks for making lockdown about as bearable as it possibly could have been. Tiggy, your love has kept me grounded and focused, and you have always been there for me. Lastly, I must thank my family. You have always supported my ambitions and encouraged me to pursue challenging goals. I would not be where I am today without you.

List of Publications

Peer Reviewed Journal Articles

Li, Shuai, **Harry Collini**, and Matthew D Jackson. 2018. 'Anomalous zeta potential trends in natural sandstones', *Geophysical Research Letters*, 45: 11,068-11,73.

Collini, Harry, Shuai Li, Matthew D Jackson, Nicolas Agenet, Bilal Rashid, and John Couves. 2020. 'Zeta potential in intact carbonates at reservoir conditions and its impact on oil recovery during controlled salinity waterflooding', *Fuel*, 266: 116927.

Alarouj, Mutlaq, **Harry Collini**, and Matthew D Jackson. 2021. 'Positive Zeta Potential in Sandstones Saturated with Natural Saline Brine', *Geophysical Research Letters*, 48: e2021GL094306.

Collini, Harry, and Matthew D Jackson. 2022. 'Relationship Between Zeta Potential and Wettability in Porous Media: Insights From a Simple Bundle of Capillary Tubes Model', *Journal of colloid and interface science*, 608: 605-21.

Collini, Harry, Bilal Rashid, Matthew D Jackson. 'Zeta Potential of Crude Oil in Aqueous Solution', *Advances in Colloid and Interface Science,* (Ready for submission).

Collini, Harry, Bilal Rashid, Matthew D Jackson. 'Zeta Potential of Intact Natural Sandstones at Reservoir Conditions', *Geophysical Research Letters,* (Ready for submission).

Conference Papers & Presentations

Harry Collini, Li, Shuai and Matthew D. Jackson. 2018. "Impact of Caclium on the Zeta Potential of Clay-Rich Sandstones." *IOR Norway 2018.* Stavanger, Norway.

Collini, H., and M. Jackson. 2019. 'Improved Understanding of Zeta Potentials in Intact Natural Rock Cores and Implications for Controlled Salinity Waterflooding', *81st EAGE Conference & Exhibition.* London, UK.

Jackson, M.D., **H. Collini**, S. Li, B. Rashid, J. Couves, K. Webb, I. Collins, and M. Maynard. 2019. 'Zeta Potential in Intact Carbonate Samples: Impact of Brine Composition, Temperature and Wetting State with Application to Controlled Salinity Waterflooding', *EAGE IOR 2019.* Pau, France.

Collini, H., and M. Jackson. 2019. 'A Modified Derjaguin-Landau-Verwey-Overbeek (DVLO) Model Accounting for Steric Effects at High Ionic Strength: Implications for Low Salinity Waterflooding'. *EAGE IOR 2019.* Pau, France.

Collini, H., and M. Jackson. 2019. 'Zeta Potential of the Mineral-Brine Interface in Natural, Intact Sandstones with Oilfield Applications'. *ELKIN 2019*. Boston, USA.

Collini, H., S. Li, and M. Jackson. 2019. "Zeta Potential of Intact Natural Sandstones in Subsurface Reservoirs: Impact of Mineralogy, Electrolyte Composition, Temperature and Wetting State." *AGU Annual Fall Meeting 2019.* San Francisco, USA.

Collini, Harry, and Matthew Jackson. 2020. "Zeta Potential of the Oil-Brine Interface and its Importance for Controlled Salinity Waterflooding." *SPE Improved Oil Recovery Conference*. Society of Petroleum Engineers. Tulsa, USA. (Withdrawn).

Collini, Harry, and Matthew Jackson. 2021. " Zeta Potential of the Crude Oil-Brine Interface and Implications for Controlled Salinity Waterflooding." *EAGE IOR 2021.* Online.

Collini, H., and M. Jackson. 2021. 'Zeta Potential in Intact Natural Carbonates at Reservoir Conditions and Implications for Controlled Salinity Waterflooding', *82nd EAGE Conference & Exhibition.* Amsterdam, The Netherlands.

Collini, H., and M. Jackson. 2021. 'Streaming Potential Measurements of Non-Aqueous Phase Liquids', *AGU Fall Meeting 2021.* New Orleans, USA.

Collini, H., and M. Jackson. 2021. 'Impact of Clay Content on the Zeta Potential of Intact Natural Sandstones', *AGU Fall Meeting 2021.* New Orleans, USA.

Table of Contents

List of Figures

List of Tables

Nomenclature

Acronyms

Abbreviation	Description
AN	Acid Number
AFM	Atomic Force Microscopy
BN	Base Number
BERB	Berea
BOCT	Bundle of Capillary Tubes
CAST	Castlegate
CEC	Cation Exchange Capacity
CSE	Controlled Salinity Effect
CSW	Controlled Salinity Waterflooding
COBR	Crude Oil/Brine/Rock
DI	De-ionised
dSW	Diluted Seawater
DODT	Doddington
DLE	Double Layer Expansion
EDL	Electrical Double Layer
EPM	Electrophoretic Method
EOR	Enhanced Oil Recovery
FB	Fontainebleau
FI	Forced Injection
FMB	Formation Brine
HIS	High Ionic Strength
HT	High Temperature
IOR	Improved Oil Recovery
IHP	Inner Helmholtz Plane
IFT	Interfacial Tension
IEA	International Energy Agency
iLSW	Inverse Low Salinity Waterflood
IEP	Iso-electric Point
LIS	Low Ionic Strength
LS	Low Salinity Brine
LSE	Low Salinity Effect
LSW	Low Salinity Waterflooding
LT	Low Temperature
MSW	Modified Salinity Waterflooding
MIE	Multi-Ion Exchange
pCa	Negative Logarithm of Calcium Concentration in mol/L
pMg	Negative Logarithm of Magnesium Concentration in mol/L
pSO_4	Negative Logarithm of Sulphate Concentration in mol/L

OHP	Outer Helmholtz Plane
pZc	Point of Zero Charge
PV	Pore Volume
PDI	Potential Determining Ion
P	Pressure
REV	Representative Elementary Volume
SW	Seawater
SCAL	Special Core Analysis
SI	Spontaneous Imbibition
STB	St. Bees
SPM	Streaming Potential Method
SCM	Surface Complexation Model
TDS	Total Dissolved Solids
USBM	United States Bureau of Mines
V	Voltage
WAG	Water Alternating Gas

Symbols

Symbol	Description	SI Units
A	Core Cross Sectional Area	m^2
C	Streaming Potential Coupling Coefficient	V/Pa
c	Distribution Scaling Parameter	N/A
Ca	Capillary Number	N/A
C_d	Diffuse Layer Capacitance	F/m^2
C_s	Stern Layer Capacitance	F/m^2
D	Core Diameter	m
e	Elementary Charge	C
F	Formation Factor	N/A
I_{AH}	Amott-Harvey Wettability Index	N/A
I_o	Amott Oil Wetting Index	N/A
IS	Ionic Strength	mol/L
$I_{s,c}$	Streaming Current Through a Capillary	A
I_{USBM}	USBM Wettability Index	N/A
I_w	Amott Water Wetting Index	N/A
k	Core Permeability	m^2
k_B	Boltzmann Constant	J/K
L	Core Length	m
L_c	Capillary Length	m
N	Number of Capillaries	N/A
Q	Volumetric Brine Flow Rate Through Core	m^3/s
$Q(y)$	Excess Counter Charge as a Function of Distance from Capillary Centre	C/m
r_c	Radius of Capillary	m
r_{max}	Maximum Capillary Radius	m
r_{min}	Minimum Capillary Radius	m

r_{omax}	Maximum Capillary Radius that is occupied by oil	m
r_{omin}	Minimum Capillary Radius Occupied By Oil	m
r_{owet}	Capillary Radius Which Determines Capillaries That Become Oil Wet After Aging	m
r_{Sor}	Minimum Capillary Radius that Can be Invaded by Water During Imbibition	m
r_{Swi}	Minimum Capillary Radius That is Actually Invaded by Oil	m
r_{Swirr}	Minimum Capillary Radius That Can Be Invaded by Oil	m
S_{or}	Residual Oil Saturation	N/A
S_w	Water Saturation	N/A
S_{wi}	Initial Water Saturation	N/A
S_{wirr}	Irreducible Water Saturation	N/A
T	Temperature	K
Vc	Volume of Capillary	m^3
V_{WFI}	Volume of Water Forcefully Imbibed	m^3
V_{WSI}	Volume of Water Spontaneously Imbibed	m^3
x	Distance from Capillary Surface	m
y	Distance from Capillary Centre	m
z	Charge Valency	N/A
γ	Inerfacial Tension	N/m
δ	Distance of Shear Plane from the Stern Plane	m
ΔP	Differential Pressure	Pa
ΔV	Differential Voltage	V
$\Delta\zeta_{CSW}$	Change in Zeta Potential Caused by Changing the Injection Brine	V
$\Delta\zeta_{IS}$	Change in Zeta Potential Caused by Changing the Ionic Strength	V
$\Delta\zeta_{Temp}$	Change in Zeta Potential Caused by Temperature	V
$\Delta\zeta_{wett}$	Change in Zeta Potential Caused by Wettability Alteration	V
ε_b	Brine Permittivity	F/m
ε_w	Electrolyte Permittivity	F/m
ζ	Zeta Potential	V
ζ_{mb}	Zeta Potential at the Mineral-Brine Interface	V
ζ_n	Normalised Zeta Potential	N/A
ζ_{ob}	Zeta Potential at the Oil-Brine Interface	V
κ	Inverse Deby-Huckle Length	m^{-1}
μ_b	Brine Viscosity	Pa.s
μ_w	Electrolyte Viscosity	Pa.s
$v(y)$	Flow Velocity as a Function of Distance from Capillary Centre	m/s
π	Pi	N/A
σ_b	Electrolyte Conductivity	S/m
σ_e	Brine Conductivity	S/m
σ_m	Saturated Porous Media Conductivity	S/m
σ_{rw}	Saturated Rock Conductivity	S/m
σ_{rwh}	Saturated Rock Conductivity at High Ionic Strength	S/m
σ_s	Surface Conductance	S
σ_{wh}	Brine Conductivity at High Ionic Strength	S/m
φ	Core Porosity	N/A
ψ	Surface Electrical Potential	V

Chapter 1 - Introduction

1.1 Background & Motivation

To achieve global net zero carbon emissions by 2050 the International Energy Agency (IEA) recently suggested total investment into new oil and gas field developments must end by 2030 (Bouckaert et al. 2021). Under this net zero 2050 scenario, oil and gas will continue to contribute about 15% of the energy supply. The IEA estimate that investment to support existing oil & gas operations will continue past 2030 at around $170 billion per year to meet this demand (Bouckaert et al. 2021). A portion of this investment will be used for developing and deploying enhanced and improved oil recovery (EOR/IOR) processes. EOR/IOR processes aim to increase the efficiency of oil and gas extraction by increasing the recovery factor (the percentage of oil recovered from that initially present) of existing, mature fields. The recovery factor for oil reservoirs averages about 30% globally (Kokal and Al-Kaabi 2010; Muggeridge et al. 2014). Accessing some of the remaining 70% by using EOR/IOR processes offers a pathway to meeting future oil demand without the need to develop new fields, in line with the IEA's 2050 net zero scenario.

Conventional EOR/IOR processes include waterflooding, gas injection, water alternating gas (WAG) injection, chemical flooding with surfactants or alkalis, polymer injection and thermal steam injection (Muggeridge et al. 2014). During waterflooding, water is injected into the reservoir to maintain pressure and improve the sweep efficiency (Muggeridge et al. 2014). This is usually done by re-injecting the connate water produced from the reservoir itself or by using seawater if the reservoir is offshore. Both brines typically contain high concentrations of ionic salt species. In recent years, injection of brine where the ionic composition/concentration was modified has been shown to yield an increase in the recovery factor compared to using connate brine or seawater.

This observation that oil recovery could be improved by adjusting the ionic composition of the injected brine gained traction in the 1990s (Tang and Morrow 1999). The process was first termed ‘low salinity waterflooding (LSW)’ because the total salinity/ionic strength of the injection brine was usually lower than the initial saturating connate brine. Consequently, the increase in oil recovery was termed the ‘low salinity effect’ (LSE). Since then, a plethora of studies have provided evidence for the LSE in both sandstone (Jackson et al. 2016b) and carbonate (Tetteh, Brady, and Ghahfaorkhi 2020) reservoirs. However, it is now accepted that the injection brine does not necessarily need to be of lower salinity for the LSE to be observed. Specifically adjusting the ionic composition, the concentration of specific ions or even increasing the total salinity/ionic strength can all yield improved oil recovery. To reflect these observations, the process is often more broadly referred to as “controlled salinity waterflooding (CSW)”, “modified salinity waterflooding (MSW)” or “smart waterflooding” depending on the authors, although all three terms refer to the same general process. Herein, CSW will be used for simplicity and consistency. CSW has certain advantages over the other conventional EOR processes including a strong economic potential, lower carbon emissions and lower environmental impact, that have made it a promising area of interest for both academia and industry (Smalley et al. 2020).

Plenty of evidence for IOR by CSW has been published using a range of experimental techniques across different scales (Jackson et al. 2016b; Tetteh, Brady, and Ghahfaorkhi 2020; Berg et al. 2010). However, there also exist numerous, similar experiments where CSW was performed but no additional oil was recovered when it was expected to. Moreover, many of these types of experimental results are likely to have not been published. The notion that IOR will always occur during CSW is far from conclusive. Various studies have sought to determine the underlying mechanism(s) controlling IOR during CSW, but none have yet been decisively proven. Given the complexity and heterogeneity of different crude-oil/brine/rock (COBR) systems it may be unlikely that one single mechanism exists. Similarly, the necessary and/or sufficient properties for CSW to yield IOR have not been determined so it is not possible

to screen potential candidate reservoirs. Despite the contradictory and conflicting data, it is commonly observed that successful CSW is associated with a change in wettability to a more water-wet state, for both sandstone and carbonate rocks.

Wetting describes the tendency of a fluid to spread over a solid surface in the presence of another fluid. Wettability is a measure of the extent of wetting. In oil and gas reservoirs, wettability is an important property as it controls the pore-scale distribution of fluids which affects the dynamics of multi-phase flow (Blunt 1997, 2017). COBR systems are qualitatively described as (i) water-wet, where water preferentially wets the rock surface and oil exists in the centre of the pore space (ii) oil-wet, where oil preferentially wets the rock surface and water exists in the centre of pores; or (iii) mixed-wet. Mixed wetting occurs when the rock surface has no preference to be wetted by oil or water, or when there are a variety of rock surfaces present which have different wetting preferences. Whilst wetting is a complex process that is dependent on a number of the COBR properties, the zeta potential at the mineral and oil surfaces are thought to be important controls (Buckley et al.1989b; Buckley 1996).

The zeta potential is an experimental measurement of the electrical potential at the interface between two phases (Hunter 1981a). Its magnitude and polarity control the interaction between the interface and polar species in adjacent phases. In a COBR system, the zeta potential at the mineral-brine and oil-brine interfaces are dependent on the physicochemical properties of the surface, the brine chemistry and other system parameters such as temperature and pressure. Modifying the brine composition during CSW will modify the zeta potential at both interfaces, changing the interaction between the two interfaces and altering the wettability.

The link between the zeta potential of the mineral-brine and oil-brine interfaces and wettability of COBR systems has been previously studied (Buckley et al.1989b; Buckley 1996; Strand, Høgnesen, and Austad 2006). Measuring the zeta potential is relatively routine by using a commercial device such as a Zetasizer which uses the electrophoretic method (Hunter 1981). The general method is to prepare a dispersion of crushed mineral particles or oil

droplets in the brine of interest and the device then applies an electrical voltage to the dispersion and measures the subsequent movement of the particles. The zeta potential can be calculated based on the direction and speed of the particle movement. However, this approach relies on the dispersion remaining stable throughout the measurement which can be challenging when using dispersions in high ionic strength brines or when measuring at elevated temperatures. Both these conditions are common in COBR systems and thus obtaining zeta potential measurements relevant to COBR systems using this approach is challenging.

The streaming potential method (SPM) is an alternative but less common approach to measuring the zeta potential. Here, brine is passed through a capillary, membrane or porous media sample whilst the electrical voltage and pressure differentials are measured, from which the zeta potential can be calculated. The SPM has been used to measure the zeta potential of intact natural rock cores at high ionic strength (Al Mahrouqi et al. 2017b; Jaafar et al. 2009; Jackson 2010) elevated temperature (Al Mahrouqi et al. 2016) and with brines and wetting states relevant to CSW (Jackson et al. 2016b). Furthermore, the SPM is advantageous over other methods when measuring the zeta potential for subsurface applications since it does not require the sample to be crushed, thus preserving the natural textures, rock structures and mineral distributions within the sample.

The SPM has been used to explore the relationship between the zeta potential of carbonate core samples and their wettability (Jackson et al. 2016b; Jackson and Vinogradov 2012). The zeta potential was measured at full water saturation before draining to the irreducible water saturation (S_{wirr}) with crude oil and aging at elevated temperature for several weeks to render oil-wet samples. After flooding with the same brine to the residual oil saturation ($S_w = 1 - S_{or}$) the zeta potential was measured again with the same procedure. In all samples the zeta potential showed a distinct change after wettability alteration. Some samples became more positive whilst others became more negative. This change in sample

zeta potential was interpreted to represent the polarity of the zeta potential at the oil-brine interface (Jackson et al. 2016b; Jackson and Vinogradov 2012).

The only published study that has investigated the impact of this change in zeta potential to CSW is that of Jackson et al. (2016b). They measured the zeta potential of carbonate core samples with brines relevant to CSW. Under fully water saturated conditions, brines of lower ionic strength/salinity caused the zeta potential to become more negative. The samples underwent wettability alteration with four crude oils. It was observed that three of these caused the zeta potential to become more negative, representing a negatively charged oil-brine interface. The remaining oil caused the zeta potential of the samples to become more positive, representing a positively charged oil-brine interface. When performing CSW on these samples, they found that IOR occurred only if the injection brine composition yielded a zeta potential at the mineral-brine and oil-brine interfaces of the same polarity. For example, during conventional LSW where the injection brine is of lower salinity and the mineral-brine interface becomes more negative, only the samples where the oil was interpreted to be negatively charged yielded IOR. The samples where the oil was interpreted to be positive did not. It was hypothesised that this similar polarity in the zeta potential caused an increased electrostatic repulsion between the two interfaces leading to improved stabilisation of a wetting water film acting between them resulting in a more water-wet state. Where this repulsive force exceeded the localised disjoining pressure, detachment of the oil droplets occurred leading to an overall increase in oil recovery. The positive oil did not yield IOR when the injection brine was diluted (as in a conventional LSW) since the mineral surface became more negative and caused an increased electrostatic attraction between the mineral and oil interfaces. They speculated that cases from literature where LSW was performed but no additional oil was recovered may have been dealing with an unknowingly positive oil.

The suggestion that the oil-brine interface could be positively charged in these experiments was contradictory to most previous literature data from electrophoretic measurements, however limited data was available at appropriate conditions to benchmark

against. The interpretation of the oil-brine interface polarity from the intact core experiments appeared to be a critical parameter for controlling the success of CSW, however, it was not possible to predict or model this property prior to conducting these experiments. Furthermore, no correlations between the COBR system properties and the oil-brine interface polarity were determined.

Although the study of Jackson et al. (2016b) yielded some promising insight into the relationship between the zeta potential, wettability and CSW, only one type of carbonate core sample and four crude oils were investigated. It is known that different rock types can exhibit different zeta potential values (Al Mahrouqi et al. 2017) and that crude oils can be significantly different from one another due to their complexity (Simanzhenkov and Idem 2003). Furthermore, it is not clear if, or how, this model would apply to other rock types such as sandstones.

1.2 Aims & Objectives

This thesis broadly aims to improve understanding of the link between the zeta potential and wettability in COBR systems. The primary application of the results will be focused on the challenges of predicting and optimising controlled salinity waterflooding processes. To achieve these aims, the main approach will be to conduct streaming potential measurements on various intact mineral cores when saturated with single- and multi-phase fluids of varying compositions and at conditions relevant to subsurface environments. Specifically, this work aims to:

- Explore further the link between the zeta potential, wettability and IOR by CSW for a wide variety of intact carbonate core samples, subsurface relevant brine compositions and crude oils. Test the model of Jackson et al. (2016b) to a larger dataset to identify any inconsistencies or critical COBR properties.
- Measure the zeta potential of a range of intact sandstone cores when saturated with brines representing those used in CSW processes at ambient and elevated temperatures.
- Investigate the link between zeta potential, wettability and IOR by CSW for a range of intact sandstone cores and compare this to carbonates.
- Develop an approach to measure the zeta potential of the oil-brine interface using the streaming potential method and benchmark this against existing electrophoretic techniques.
- Measure the zeta potential of the oil-brine interface using the streaming potential method when saturated with NaCl/$CaCl_2$ electrolytes at saline conditions (up to 2 mol/L ionic strength).

1.3 Thesis Overview

Chapter Two begins with an overview of controlled salinity waterflooding, briefly covering the evidence of its impact and reviewing the main mechanisms that have been discussed for both carbonate and sandstone reservoirs. Emphasis is paid to the impact of the zeta potential on wettability alteration and CSW. The chapter then provides a brief overview of the theory of the zeta potential and its control on polar species. The key controls on the carbonate, sandstone and crude oil zeta potential are discussed and reviewed considering the available data in literature.

Chapter Three reports zeta potential measurements made on intact carbonate cores saturated with brines relevant to CSW at full and partial water saturation and water- and oil-wet conditions. CSW corefloods are performed and the results discussed in context with the zeta potential measurements. An extensive dataset of experiments comprising different carbonate core samples, crude oils, measurement temperatures and flooding sequences are reported. The results and conclusions highlight the importance of the mineral-brine and oil-brine zeta potential in predicting and optimising CSW in carbonate samples.

Chapter Four reports zeta potential measurements made on intact natural sandstones comprising a range of mineralogical heterogeneity when saturated with brines relevant to CSW and the subsurface. The results show that the zeta potential trends made on intact samples with representative brines may differ to those observed on crushed samples under ideal conditions. The impact of these results for CSW in sandstones are discussed.

Chapter Five outlines a simple pore network bundle of capillary tubes model to investigate the link between zeta potential and wettability in porous media. The model outlines how the zeta potential changes as a function of water saturation for different wetting states, before being applied to the experimental data presented in Chapter Three. The model provides a procedure for estimating the magnitude and polarity of the zeta potential at the oil-brine

interface in these experiments. The results are discussed with regards to their implications on CSW.

Chapter Six presents zeta potential measurements of the oil-brine interface using the streaming potential method. Natural sandstone cores are chemically treated to render strongly oil-wet substrates which are coated with a range of crude oils. The zeta potential of these samples is measured using the streaming potential method and the results are compared to electrophoretic measurements obtained on emulsions of the same oil and brine. The results are compared to the interpretations of the oil-brine zeta potential from Chapters Three and Five and discussed in terms of the key controls on the oil-brine zeta potential and the implications for CSW.

Finally, Chapter Seven reviews the core conclusions from this work and provides recommendations for further work.

Chapter 2 - The Zeta Potential and Controlled Salinity Waterflooding

2.1 Wettability Alteration by Controlled Salinity Waterflooding

Numerous laboratory experiments and field trials have shown that oil recovery can be increased from both sandstone and carbonate reservoirs by modifying the injected brine composition and/or concentration (Jackson et al. 2016a; Tetteh et al. 2020; Bartels et al. 2019; Sheng 2014). This process is termed 'controlled salinity water-flooding' (CSW) and the observation of improved oil recovery by CSW is termed the 'controlled salinity effect' (CSE). CSW is appealing due to its relative simplicity, low cost, easy implementation and avoidance of complex engineering or chemical additives such as polymers or surfactants (Smalley et al. 2020). Typically, the injected brine is of lower salinity than the naturally present formation brine; it may comprise seawater and/or diluted seawater, or low-salinity water with a specific ionic composition. In this instance the process is commonly termed 'low salinity waterflooding' (LSW).

The earliest studies to report the CSE in sandstone core samples were published in the 1950's and 60's (e.g. Martin, (1959) and Bernard, (1967)). However, this initial work was primarily focused on understanding the phenomenon of formation damage. Interest in CSW as an IOR method only began to garner significant attention after work by Tang and Morrow (1999) who first proposed fines migration as an underlying mechanism for the CSE in sandstones. Since then, a plethora of studies have investigated CSW in both sandstone and carbonate reservoirs.

Bartels et al. (2019) broadly categorises these studies into three scales of focus. The first is the sub-pore scale. Here, studies utilise techniques such as zeta potential

measurements e.g. (Nasralla and Nasr-El-Din 2014a), atomic force microscopy (AFM) e.g. (Hilner et al. 2015), contact angle measurements e.g. (Haagh et al. 2017) and molecular dynamics e.g. (Chen et al. 2021) to investigate the physics and molecular interactions between the rock surfaces, crude oil components and ionic species in the brine. Results are typically used to enhance understanding of the underlying mechanism(s) controlling CSW and predict/screen reservoirs for their CSW potential. The sub-pore scale Is largely the focus of the academic community and represents approximately 30% of published literature.

The second category is the pore network scale. Network modelling e.g. (Boujelben et al. 2018), micro-CT imaging e.g. (Andrews et al. 2021; Bartels, Rücker, et al. 2017) and micro-models e.g. (Tetteh et al. 2021) are used to understand the pore filling and oil displacement processes. The pore-network scale links the sub-pore scale detachment processes to larger scale observations of changes in relatively permeability and oil recovery. Recent advancements in imaging techniques mean this area makes up the smallest contribution to the literature at just 13%, but is popular amongst both academia and industry (Bartels et al. 2019).

Finally, the remaining category covers the core/reservoir scale. This is largely the interest of the commercial oil industry and comprises special core analysis (SCAL), high temperature/pressure corefloods, well-tests, field trials and reservoir modelling (Bartels et al. 2019). Results are mainly used for risk management and quantification of uncertainties for deploying CSW on an industrial scale.

Figure 2-1 shows some examples of evidence supporting the CSE from some of the experimental methods mentioned above. Based on evidence from all three scales it is now widely accepted that CSW can lead to IOR. However, the underlying mechanisms controlling the CSE remain ambiguous and there is no acceptance on the necessary and/or sufficient conditions to screen candidate reservoirs for their IOR potential. One common theme across the various studies is that the CSE is associated with a change to a more water-wet state in both sandstones and carbonates. Despite the different mineralogies of the two rock types,

Bartels et al. (2019) report that many of the observations and proposed mechanisms are applicable in both instances. However, evidence suggests they may be subtly different (RezaeiDoust et al. 2009). The CSE in sandstones has been reported to only be observed when the total salinity of the injection brine is reduced below 5,000ppm (Lager, Webb, and Black 2007; Hilner et al. 2015). Conversely, IOR by CSW has been observed several times in carbonates when the injection brine was comparable to seawater at around 35,000ppm (Puntervold et al. 2007; Strand et al. 2006; Yousef et al. 2011a; Hiorth et al. 2010).

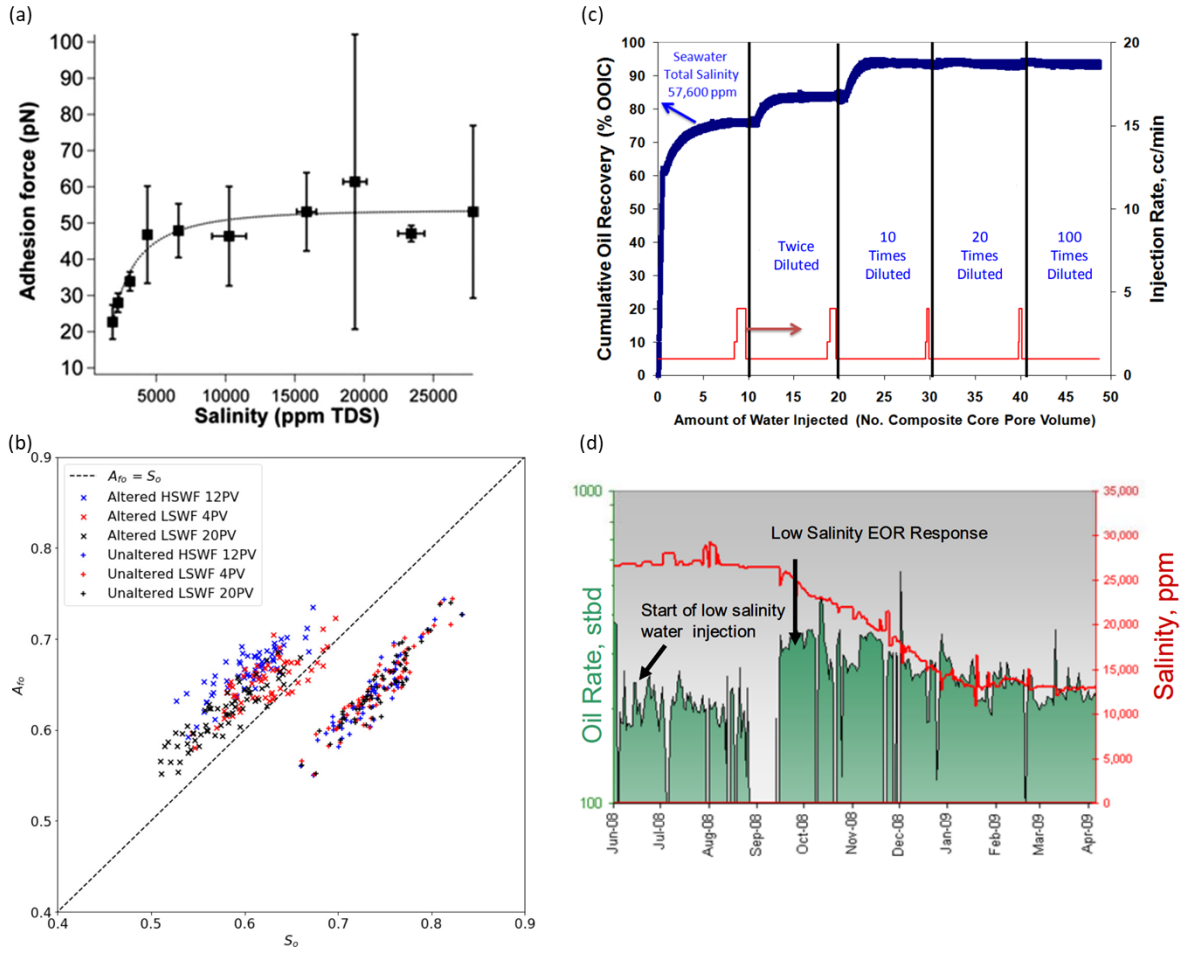

Figure 2-1: Evidence supporting the CSE across different scales. Plot (a) shows adhesion force between non-polar oil tips and sand grains as a function of salinity measured using AFM (Hilner et al. 2015). Plot (b) shows change in pore space area covered by oil in a sandstone sample with injection of low salinity water (LSWF) measured using Micro-CT imaging (Andrews et al. 2021). Plot (c) shows oil recovery from a laboratory coreflood experiment on a carbonate core sample with increasingly dilute sweater injection (Yousef et al. 2011b). Plot (d) shows increase in oil rate associated with injection of low salinity water during a field trial in a sandstone reservoir (Seccombe et al. 2010).

This section will briefly review wettability and CSW in sandstone and carbonate reservoirs. The more widely accepted mechanisms controlling wettability alteration in both cases will be summarised, discussed and compared. It should be noted that several review papers that examine and collate the various data investigating CSW have been published. These will primarily form the basis of this section although specific studies and results will be highlighted where relevant. For further detail the reader is directed to the following for carbonates (Tetteh et al. 2020; Ding and Rahman 2017; Nande and Patwardhan 2021; Derkani et al. 2018) and sandstones (Sheng 2014; Jackson et al. 2016a; Snosy et al. 2020; Katende and Sagala 2019). The review by Bartels et al. (2019) considers both rock types but focuses more on the challenges of CSW from a length and time scale and the industrial application, rather than the underlying physics responsible for the CSE.

2.1.1 Wettability

Wetting describes the tendency of one fluid to spread over a solid surface in the presence of a second fluid. Wettability defines the degree of wetting. Wettability is an important property of subsurface reservoirs since it governs the pore scale distribution of fluids (Dagan 2012). Consequently, this distribution of fluids governs the physics of multi-phase flow (Blunt 2017; Dagan 2012). In hydrocarbon reservoirs, wettability can be an important control on the flowrates and ultimate recoveries of oil & gas (Morrow 1990; Jadhunandan and Morrow 1995; Gandomkar and Rahimpour 2015).

Various methods exist to characterise wettability which will be summarised below, however this is challenging due to the complexity of subsurface reservoirs. Wettability is often described qualitatively as water-wet, oil-wet or mixed/intermediate-wet (Anderson 1986b). In water-wet reservoirs, water preferentially wets the rock surface whilst oil exists in the centre of the pore space. In oil-wet reservoirs, oil preferentially wets the rock surface whilst water exists in the centre of the pore space. Mixed-wet systems occur when the rock surfaces have

no preference to either fluid, or when a range of mineral surfaces exist that have different wetting states (Anderson 1986b). Carbonate reservoirs are typically thought to be mixed- to oil-wet whereas sandstones are thought to be more water- to mixed-wet (Anderson 1986b). However, a range of wetting states will be present in all systems and thus these terms do not fully capture the wettability of subsurface reservoirs.

2.1.1.1 Wettability Alteration

Most hydrocarbon reservoirs are thought to have been initially water-wet since the sediments were deposited in aqueous environments (Anderson 1986b). Once the reservoir has been formed, crude oil migrates upwards from the source rock below due to buoyancy forces and displaces water from the pore space (Abdallah et al. 1986). Under certain conditions, surface-active compounds within the crude oil may break the wetting water film and interact with the rock surface to alter its wettability towards a mixed- or oil-wet state (Anderson 1986b; Abdallah et al. 1986; Hirasaki 1991; Buckley 1996; Drummond and Israelachvili 2004). Several factors may influence the extent of wettability alteration including the rock, oil and brine chemistry, surface roughness and rock textures, the saturation history of the pore space and the temperature and pressure of the system (Abdallah et al. 1986; Morrow 1990; Hirasaki 1991; Buckley 1996). Four main mechanisms for wettability alteration are outlined by Buckley and Liu (1998):

- Polar interactions between rock and oil in the absence of a water film. Interactions between large, polar asphaltenes and the rock surface will dominate when no water is present. Strongly oil-wet reservoirs may be associated with this mechanism of wettability alteration (Anderson 1986b). However, water is typically present in most conventional reservoirs. Direct polar interactions between dry mineral surfaces and crude oil are likely to be less significant in the presence of water (Buckley and Liu 1998).

- Surface precipitation of asphaltenes. Crude oils vary in their ability to keep their constituent compounds suspended in the solvent. Large, high molecular weight asphaltene compounds in particular may precipitate out and become deposited on the rock surface if the solvent changes or the temperature/pressure of the COBR system changes (Buckley and Liu 1998). Salathiel (1973) showed sandstone cores could be altered to a more oil-wet state by diluting the crude oil with n-heptane. This wettability alteration was attributed to increased precipitation of heavy asphaltenes due to the modified, poorer, solvent.

- Acid/base interactions that control the surface charge at oil-brine and mineral-brine interface. In the presence of water, the oil-brine and mineral-brine interfaces are electrically charged (Buckley 1996). When these interfaces approach one another, the electrostatic forces between the two will determine whether the overall interaction is attractive or repulsive. If the force is attractive and sufficiently strong enough to overcome the disjoining pressure of the water film, the film can break, and the oil can wet the mineral surface.

- Ion-bridging between charged species and high valency ions. It is largely thought that negatively charged acid components in crude oil dominate the interfacial behaviour at pH > 5 (Buckley and Liu 1998). These can interact directly with positive sites on the mineral surface (as described above) or with negative sites via a divalent cation bridge (e.g. Ca^{2+}/Mg^{2+}). The cation can bind to negative sites on both the mineral and oil interfaces resulting in wettability alteration.

In most conventional reservoirs, where water is present and the oil is a sufficient solvent, the latter two mechanisms are primarily responsible for controlling wettability

alteration. Both mechanisms are dependent on the surface charges of the mineral and oil interfaces which can be measured and characterised by the zeta potential.

2.1.1.2 Characterising Wettability

I) Contact Angle

Contact angle measurements are one of the most widely used and direct measurements of wettability (Anderson 1986a). The sessile drop method is often used in the petroleum industry to measure contact angles (Anderson 1986a). Flat surfaces of mineral crystals (often quartz or calcite) are placed in a cell in contact with a fluid phase, usually brine. A droplet of another fluid phase, e.g. crude oil, is contacted to the mineral surface and allowed to equilibrate. The angle between the fluid-fluid interface and the flat surface is measured using cameras or other recording equipment. By convention the contact angle is measured through the more dense phase which in COBR systems is usually the brine (Anderson 1986a).

Figure 2-2 shows a schematic of a droplet of fluid on a flat surface with the contact angle shown.

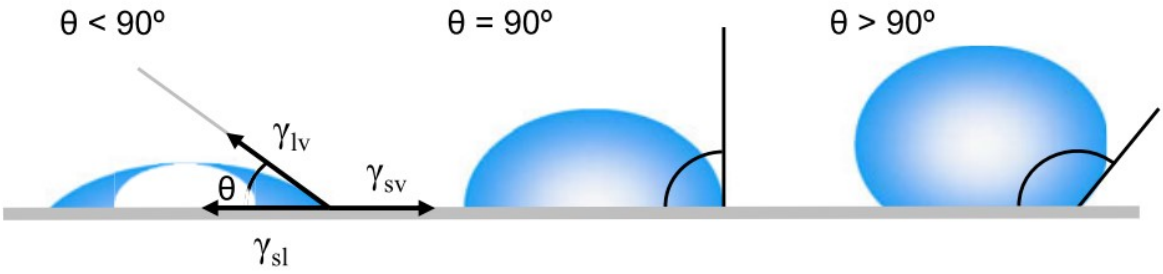

Figure 2-2: Schematic of a droplet of fluid on a flat surface in the presence of another fluid showing the contact angle(s) from Yuan and Lee (2013).

The wettability of the surface can be inferred from contact angle measurements by considering whether the fluid spreads over the surface. Contact angles in the range 0-80° imply the surface is water-wet, 80-100° is intermediate wet, 100-160° is oil-wet and 160-180° is strongly oil-wet (Anderson 1986b). However, there are several limitations with using these contact angles obtained on model, ideal systems to infer the wetting state of a real reservoir. Mineral surfaces are not flat homogenous ideal surfaces and effects such as chemical

heterogeneity and surface roughness may impact the wettability (Wenzel 1949). Additionally, there may be long equilibration times between the three phases that may not be captured within experimental timeframes. Crucially, different mineral surfaces will exhibit different contact angles and thus a range of values will be present in the reservoir. A single value does not represent or describe the distribution of contact angles within the reservoir which may be important controls on subsurface flow. Moreover, wetting is not a static process and so static contact angle measurements are not adequate to understand the wetting behaviour.

Understanding of this dynamic process has led to measurements of 'advancing' and 'receding' contact angles. Advancing contact angles are measured when the fluid (e.g. crude oil) is 'pushed' onto the flat crystal surface whilst receding contact angles are measured when the fluid is 'pulled' away from the surface (Yuan and Lee 2013). Hysteresis between advancing and receding contact angles can be significant and is usually attributed to surface roughness and heterogeneities (Yuan and Lee 2013). Therefore, it is inaccurate to interpret the wettability of a reservoir from a single contact angle measurement. However, changes in contact angle as the system parameters are changed (e.g. brine chemistry) can yield insight into the underlying wettability alteration mechanism(s). This point will be returned to in subsequent sections with reference to CSW.

In recent years, advances in pore scale imaging and computational processing have allowed for contact angle measurements to be made *in-situ* from micro-CT imaging of the pore space of natural core samples (Andrew et al. 2014; AlRatrout et al. 2017). This approach measures the contact angles of all the surfaces in the sample and returns a contact angle distribution rather than a single value. Comparing contact angle distributions of core samples instead of single static measurements of model systems may be a more accurate method to quantify the wetting state of COBR systems. Changes in the contact angle distribution with changes to the COBR system parameters may also yield insight into wettability alteration mechanism(s).

II) Amott-Harvey and USBM Tests

The Amott (Amott 1959) and US Bureau of Mines (USBM; Donaldson et al. 1969) methods are used to characterise the wettability of whole core samples. Both methods make use of capillary pressure curves to quantify the wettability and therefore require full displacement cycles to be performed.

Figure 2-3 shows an example of capillary pressure curves obtained from different fluid invasion cycles, in this case oil and water. Such results are usually obtained by centrifuging the sample (Mirzaei-Paiaman and Ghanbarian 2021). The USBM method makes use of the area under these curves to calculate wettability. The USBM index is given as:

$$I_{USBM} = \log\left(\frac{A_1}{A_2}\right) \qquad (2\text{-}1)$$

where A_1 is the area under the secondary drainage curve and the x-axis (e.g. the area under the green line between points B and E in Figure 2-3) and A_2 is the area between the waterflooding curve and the x-axis (e.g. the area between the blue line at negative capillary pressure and the x-axis between points C and D in Figure 2-3).

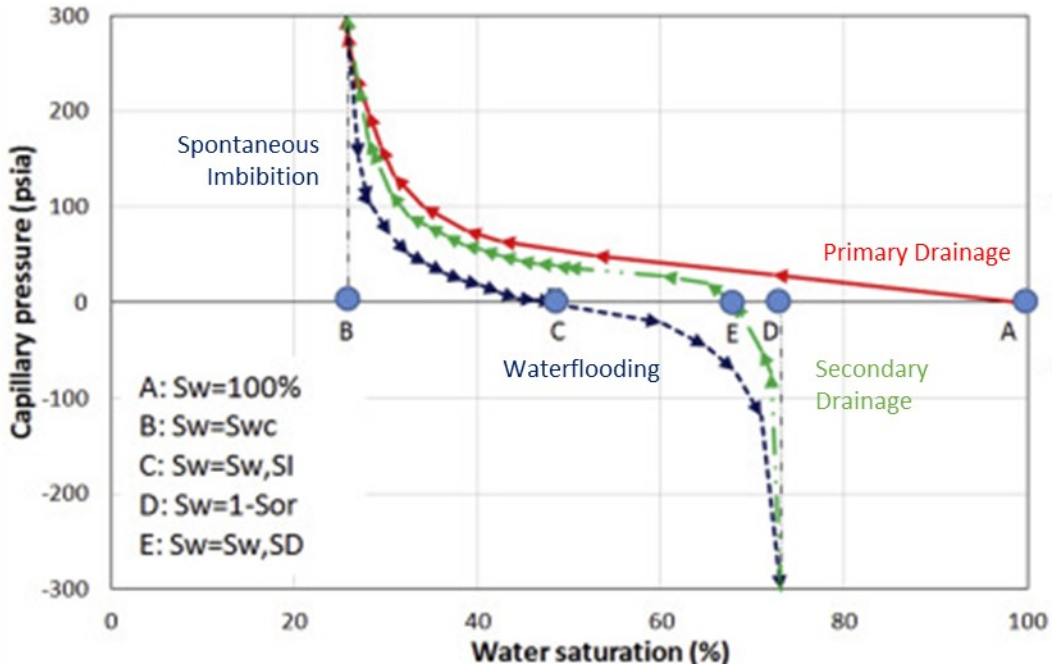

Figure 2-3: Example of capillary pressure curves during drainage/imbibition cycles modified from Mirzaei-Paiaman and Ghanbarian (2021).

An I_{USBM} value of zero indicates a neutral, or mixed-wet, sample that has no wetting preference to either phase. Increasingly positive values of I_{USBM} indicate increasingly water-wet samples whilst increasingly negative values indicate increasingly oil-wet samples (Donaldson et al.1969).

The Amott method also makes use of the capillary pressure curves but measures the volumes of water and oil produced during spontaneous imbibition (SI) and forced injection (FI) (Amott 1959). The Amott water- and oil-wetting indices are given respectively as:

$$I_w = \frac{V_{WSI}}{V_{WSI} + V_{WFI}} \qquad (2\text{-}2a)$$

$$I_o = \frac{V_{OSI}}{V_{OSI} + V_{OFI}} \qquad (2\text{-}2b)$$

where V_{WSI} represents the volume of water spontaneously imbibed; V_{WFI} represents the volume of additional water that can be forced into the sample; V_{OSI} represents the volume of oil spontaneously imbibed during secondary drainage and V_{OFI} represents the volume of additional oil that can be forced into the sample during secondary drainage. Assuming the total volume of pore space remains constant, equations 2-2a and 2-2b can be re-written as:

$$I_w = \frac{S_{spw} - S_{wirr}}{1 - S_{or} - S_{wirr}} = \frac{S_w(C) - S_w(B)}{1 - S_w(D) - S_w(B)} \qquad (2\text{-}3a)$$

$$I_o = \frac{S_{spo} - S_{or}}{1 - S_{or} - S_{wirr}} = \frac{S_w(E) - S_w(D)}{1 - S_w(D) - S_w(B)} \qquad (2\text{-}3b)$$

where S_{wirr} is the irreducible water saturation; S_{pw} is the water saturation after spontaneous imbibition; S_{spo} is the water saturation after spontaneous imbibition of oil during secondary drainage and S_{or} is the residual oil saturation. The terms $S_w(B)$, $S_w(C)$, $S_w(D)$ and $S_w(E)$ refer to the water saturation at the corresponding letters in Figure 2-3. The two Amott indices are often combined to give the Amott-Harvey wettability index as:

$$I_{AH} = I_w - I_o \quad (2\text{-}4)$$

An I_{AH} value of zero indicates a neutral, or mixed-wet, sample that has no wetting preference to either phase. An I_{AH} value of -1 indicates the strongest possible oil-wet sample and an I_{AH} value of +1 indicates the strongest possible water-wet sample.

The Amott-Harvey and USBM indices provide an indication of the average wettability of a core and account for natural roughness and heterogeneities that limit traditional contact angle measurements. However, neutral or weakly water- or oil- wet samples are difficult to discern and no indication of the range of wetting states on the mineral surfaces can be inferred. Moreover, wettability alteration is a molecular, sub-pore scale process whereas these tests are performed on the core scale. I_{USBM} and I_{AH} may not accurately capture or reflect underlying wettability alteration processes occurring.

III) In-Situ Wettability

Contact angle measurements on ideal surfaces give an indication of the wetting preferences of different minerals whilst core scale measurements of wettability give an overall indication of the wetting state and fluid connectivity of a porous media. However, neither of these necessarily reflect the wettability of the pore space *'in-situ'* and do not yield insight into the wettability alteration mechanisms, and how these contribute to oil recovery. For example, a change in contact angle to a more water-wet state may not necessarily yield detachment of oil from a surface or an increase in oil recovery on the core-reservoir scale. Conversely, the improved recovery on the core scale would imply a change to a more water-wet state but it is not clear where or how that additional oil has been produced.

Recent advances in high resolution imaging have led to new methods to characterise *'in-situ'* wettability within the pore space. µCT imaging can directly visualise the pore space and the contact angle of the COBR interface can be measured on real surfaces at reservoir conditions (e.g. Andrew et al. 2014, AlRatrout et al. 2017). These measurements give a more accurate representation of the contact angle since the real systems account for geological textures, roughness and displacement effects that may not be present on ideal flat surfaces. Moreover, the contact angle(s) can be measured at multiple points in multiple pores giving an

indication of the contact angle distribution within the subsurface (Figure 2-4, Alhammadi et al. 2017). A contact angle distribution gives a broader indication of the wetting state of the porous media. Moreover, changes in the contact angle distribution as the system parameters are changed can provide insight into the mechanism of wettability alteration by determining which pores/wetting states contribute to the overall change in wettability.

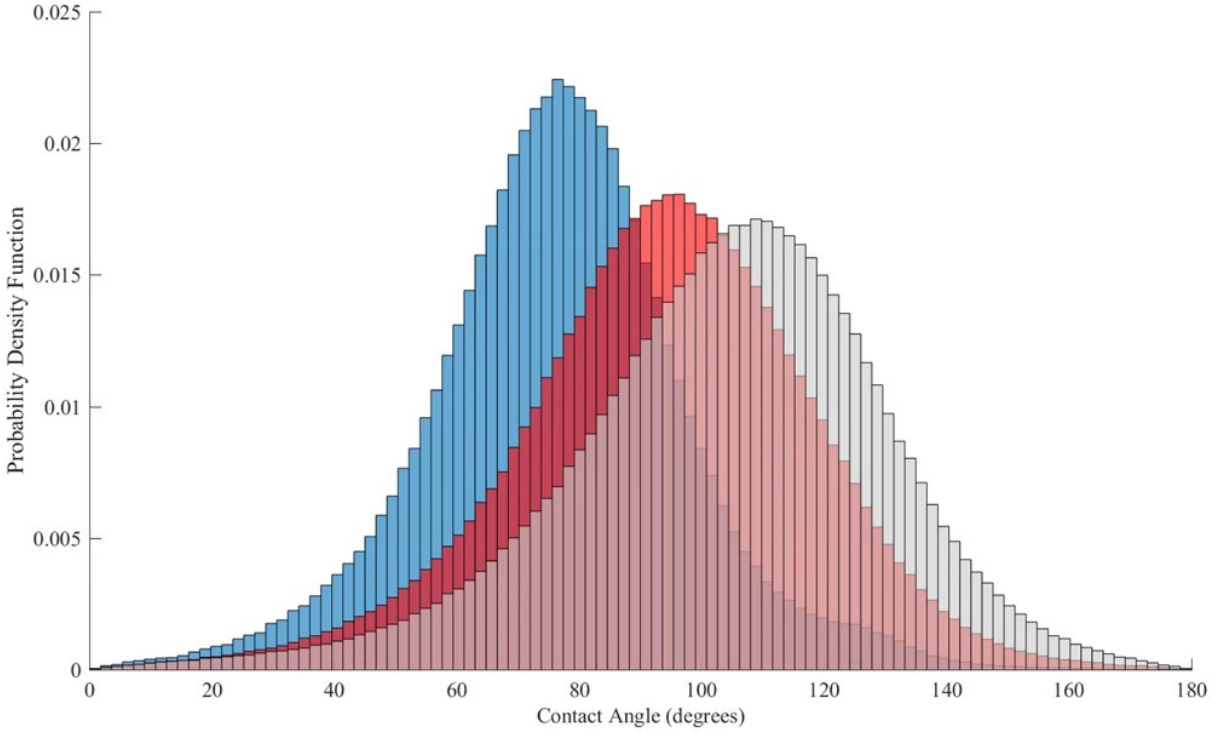

Figure 2-4: Example of contact angle distributions measured in-situ on different rock samples from Alhammadi et al. 2017.

Imaging of the spatial distribution of oil within the pore space is an alternate method of characterising wettability. Again, high resolution μCT images are used to identify the fluids in the pore space and the fraction of the pore space that is covered by a fluid can be measured (e.g. Andrews et al. 2021; Selem et al. 2021; Garfi et al. 2022;). If the surface area coverage of a fluid is higher than the saturation that implies the fluid is more wetting to the mineral surfaces. Imaging across the entire pore network produces a surface coverage map. As with contact angle distributions, changes in the surface coverage as the system parameters are changed can inform about the pore spaces in which wettability altering mechanisms are occurring (e.g. Andrews et al. 2021; Selem et al. 2021).

2.1.1.3 Wettability and Oil Recovery

Wettability is an important control on the overall oil recovery because it controls the distribution of fluids in the pore space and the connectivity of fluids through the pore network. Consequently, wettability is a key control on the flow paths of fluids through the pore network (Dagan 2012, Blunt 2017). During forced waterflooding, the wettability affects the flow paths of water through the pore network and thus the displacement mechanisms of oil from the pore space.

In water-wet systems, water will primarily flow through thin films of water wetting the mineral surfaces. Oil exists in the centre of the pore space and is displaced by the water films gradually thickening and mobilising the oil through connected channels (ganglia) through the pore network. Eventually, the water films will breakthrough the oil ganglia at narrow pore throats cutting off the connectivity of the oil ganglia and trapping the residual oil in the centre of pores in a process known as snap-off (Blunt, 2017). Conversely, in oil-wet systems, once the applied pressure is sufficient to overcome the capillary pressure, water will invade the centre of the pores and displace oil through the pore network. The water does not usually break the oil films and connectivity of the oil phase remains, allowing very low oil saturations to be reached, albeit at very low relative oil permeabilities as the water saturation increases (Blunt, 2017). In mixed-wet systems a combination of the displacement processes occurs, and both the oil and water phases remain connected throughout the pore network. The highest total recoveries on experimental timeframes have been observed in mixed-wet systems (Jadhunandan and Morrow, 1995).

During CSW, the mechanisms controlling the improved recovery and displacement of oil from the pore space will depend on the wettability. The majority of evidence and focus has suggested CSW is associated with a shift to a more water-wet state, implying the additional oil is caused by a detachment of oil droplets from the mineral surface at oil-wet portions.

However, evidence has shown other fluid-fluid mechanisms may occur. For example, a reduction in the oil-water interfacial tension may aid mobilisation of trapped oil ganglia (e.g. Tetteh and Barati 2019) and direct observations of formation of oil-in-water emulsions have also been reported (Sohrabi et al. 2017, Selem et al. 2021). These latter mechanisms will aid in the recovery of oil at water-wet mineral surfaces where the wettability of the mineral surfaces may not change. However, core scale methods of wettability quantification such as the Amott index would not necessarily highlight which mechanism(s) are occuring. The more widely accepted mechanisms of IOR by CSW in both sandstones and carbonates are discussed in subsequent sections.

2.1.2 CSW in Carbonates

2.1.2.1 Evidence for the CSE in Carbonates

Controlled salinity waterflooding in carbonates did not receive as much initial interest as sandstones. It was not until the mid-2000s that the first studies by Austad and co-workers reported the CSE in carbonate samples (Austad et al. 2005; Strand et al. 2006; Zhang and Austad 2006; Puntervold et al. 2007). Most of the evidence for the CSE in carbonates comes from coreflood experiments. Increases in oil recovery have been observed when injecting seawater and/or dilute seawater or specific low salinity brines into calcite or chalk core samples (Austad et al. 2005; Strand et al. 2006; Puntervold et al. 2007; Yousef et al. 2011a; Yousef et al. 2011b; Nasralla et al. 2016; Nasralla et al. 2018; Tetteh and Barati 2019; Jackson et al. 2016a). Increases in oil recovery have also been observed by subsequent injection of seawater and 10x diluted seawater into dolomite core samples (Shariatpanahi et al. 2016), however, dolomite has received significantly less attention compared to calcite or chalk. Despite evidence supporting the existence of the CSE in carbonates, there are also several coreflood studies where seawater and/or dilute brines were injected and the CSE was not observed (Seyyedi et al. 2018; Gandomkar and Rahimpour 2015; Ravari 2011).

Contact angle measurements of crude oil droplets on calcite crystals have been measured by some authors to investigate the effect of specific ions and temperature on carbonate wettability (Abdallah and Gmira 2014; Yousef et al. 2011a; Awolayo et al. 2014). Increasing SO_4^{2-} concentration (Abdallah and Gmira 2014; Awolayo et al. 2014) or decreasing Mg^{2+} concentration (Abdallah and Gmira 2014) was shown to make the samples more water-wet. Similar results have shown that seawater and/or dilute seawater can cause a reduction in contact angle and a more water-wet state on dolomite surfaces (Saikia et al. 2018; Kafili Kasmaei and Rao 2015). The zeta potential of carbonate rock samples has been studied extensively to understand the sub-pore scale mechanisms responsible for wettability alteration (Jackson et al. 2016a; Tetteh and Barati 2019; Mahani et al.2018). Injection of increasingly dilute and/or the removal of divalent cations and/or the addition of sulphate ions causes the zeta potential to become more negative. This increases the electrostatic repulsion between the mineral surface and the oil droplets leading to detachment and IOR. A discussion and review of the key controls on the carbonate-brine zeta potential is provided in section 2.2.2 or see Al Mahrouqi et al. (2017a).

Whilst evidence for the CSE in carbonates exists it has received much less attention than in sandstones. Experimental methods such as AFM have not been utilised to the same extent and fewer field trials of CSW have been conducted in carbonates than in sandstones. Yousef et al. (2012) conducted two single well chemical tracer tests in a carbonate reservoir and report a 7% decrease in residual saturation highlighting the potential of CSW in carbonates. Due to conflicting evidence for CSW, there is still debate regarding the underlying mechanisms which will be reviewed in the next section.

2.1.2.2 Mechanisms

I) Surface Charge Alteration

The surface charge of carbonates is highly complex and variable due to the equilibrium between the crystal lattice and the bulk fluid (Al Mahrouqi et al. 2017a) (see section 2.2.2 provides a review of the key controls on the carbonate surface charge). The surface charge is usually interpreted through measurements of zeta potential since it is difficult to measure directly (Al Mahrouqi et al. 2017a). In high salinity formation brines the carbonate-brine zeta potential is typically positive due to the high concentration of Ca^{2+} and Mg^{2+} ions adsorbed to the mineral surface (Al Mahrouqi et al. 2017a; Mahani et al.2018; Alotaibi et al. 2011; Alotaibi et al. 2018; Tetteh and Barati 2019). Dilution of the brine or injection of seawater/dilute seawater typically causes the zeta potential to become more negative due to the reduction of both ions. The increased concentration of SO_4^{2-} ions in seawater has also been shown to have a similar effect (Strand et al. 2006; Al Mahrouqi et al. 2017a).

This increasingly negative zeta potential with dilution of the injection brine suggests that the carbonate surface charge becomes increasingly negative during LSW. Mahani et al.(2018) show that the zeta potential of crude oil droplets in brine also become more negative in seawater and dilute seawater. They suggested that during LSW, both interfaces become increasingly negatively charged which causes an increased electrostatic repulsion between the carbonate-brine and oil-brine interfaces. If the electrostatic repulsion is sufficient to overcome the localised disjoining pressure, then the oil will detach from the mineral surface and lead to IOR.

Jackson et al. (2016a) used a similar argument to explain observations of IOR during CSW in carbonate core samples. They also observed that injection of seawater, and subsequent dilute seawater, caused the zeta potential to become more negative. In addition, they observed a measurable change in the sample zeta potential after wettability alteration with crude oil. In three of their experiments, the crude oil caused the zeta potential to become more negative and in the other, the crude oil caused the zeta potential to become more

positive. The carbonate core type and brine compositions were identical in all four experiments. They interpreted these results using a simple, qualitative pore scale model. They argued that mineral surfaces that become oil-wet return the zeta potential of the oil-brine interface, rather than the mineral-brine interface. Thus, if the measured zeta potential becomes more negative as the samples become increasingly oil-wet, then the oil-brine interface has a zeta potential that is more negative than the mineral-brine interface. Conversely, if the measured zeta potential becomes more positive as the samples become increasingly oil-wet, then the oil-brine interface has a zeta potential that is more positive than the mineral-brine interface.

The three samples where the oil-interface was interpreted to be negative all showed an increase in oil recovery when the injection brine was diluted. The one sample where the oil-brine interface was interpreted to be positive did not. These results were explained considering the electrostatic interactions. When the injection brine was diluted, the carbonate surface became more negative leading to an increased electrostatic repulsion with the three negative oils, and therefore detachment from the mineral surface and an increase in oil recovery. However, for the positive oil, making the mineral surface caused an increased electrostatic attraction between the rock and the oil, meaning no additional oil was recovered. They tested this hypothesis by repeating the experiments with the flooding sequence reversed. The samples underwent wettability alteration in the presence of dilute seawater before being injected with seawater and subsequently formation brine. This flooding sequence caused the surface charge of the carbonates to become more positive. Again, the same three oils were interpreted to have a negatively charged oil-brine interface whilst the remaining oil was interpreted to be positively charged. However, during this set of corefloods, the positive oil showed an increase in oil recovery whereas the three negative oils did not. These results were in keeping with the hypothesised electrostatic repulsion model and suggest that surface charge alteration is a dominant mechanism responsible for the CSE in carbonates. They

further suggested that examples in literature where the injection brine had been diluted but no additional oil was observed may have been dealing with an unknowingly positive oil.

II) Mineral Dissolution

Carbonates are known to interact readily with aqueous solutions and may precipitate or dissolve depending on the concentration and composition of the brine (Morse 2018). Dissolution of calcite (Hiorth et al. 2010; Chandrasekhar et al. 2018) and anhydrite (Yousef et al. 2011a; Austad et al. 2010) have both been suggested as underlying mechanisms of the CSE. Injection of seawater and/or dilute seawater typically reduces the concentration of Ca^{2+} and Mg^{2+} in the bulk fluid, promoting solid dissolution to maintain chemical equilibria. Hiorth et al. (2010) used geochemical modelling to suggest that dissolution of calcite directly altered the wettability and led to increased oil recovery. Alternatively, Austad et al. (2010) suggested that wettability alteration was not caused by the dissolution of anhydrite itself, but the *in-situ* generation of SO_4^{2-} ions which interact with the mineral surfaces to make them more water-wet. However, several studies note that the role of mineral dissolution at the reservoir scale is likely to be limited (Mahani et al.2015; Bartels et al. 2019; Nasralla et al. 2015). Any dissolution that would occur would likely be in the near wellbore region where equilibrium between the brine and rock would quickly be established (Nasralla et al. 2015).

III) Micro-Dispersions/Micro-Emulsions & Osmosis

It has been suggested that the CSE may be dependent on fluid-fluid interactions rather than the solid-fluid mechanisms discussed thus far (Bartels et al. 2019; Tetteh et al. 2020). Sohrabi et al. (2017) observed from micro-models the formation of water-in-oil dispersions during injection of low salinity water. They suggested these dispersions were formed by the generation of natural surfactants at the oil-water interface. These dispersions cause the mineral to become water-wet but also aid in the sweep efficiency and transport of crude-oil

through the porous media (Sohrabi et al. 2017; Tetteh and Barati 2019). The formation of micro-dispersions has alternatively been attributed to the osmotic pressure between high and low salinity brines, with the crude-oil acting as a semi-permeable membrane (Sandengen et al. 2016; Fredriksen et al. 2018, Selem et al. 2021). Injection of low salinity brine causes water ions to migrate through the crude-oil resulting in the formation of micro-dispersions and swelling of crude oil.

IV) IFT Reduction

Several authors have reported a decrease in the interfacial tension (IFT) between oil and water as the salinity of the water is reduced (Mahani et al.2015; Lashkarbolooki et al. 2016; Tetteh and Barati 2019; Moeini et al. 2014; Chávez-Miyauchi et al. 2016). A reduction in IFT would lead to a decrease in the capillary entry pressure allowing low salinity brine to displace oil from smaller pores (Sorbie and Collins 2010). A reduction in IFT has also been suggested to improve the viscoelasticity of the oil-brine interface, thereby reducing ganglia snap-off and improving the connectivity of the oil-phase through the porous media (Tetteh and Barati 2019).

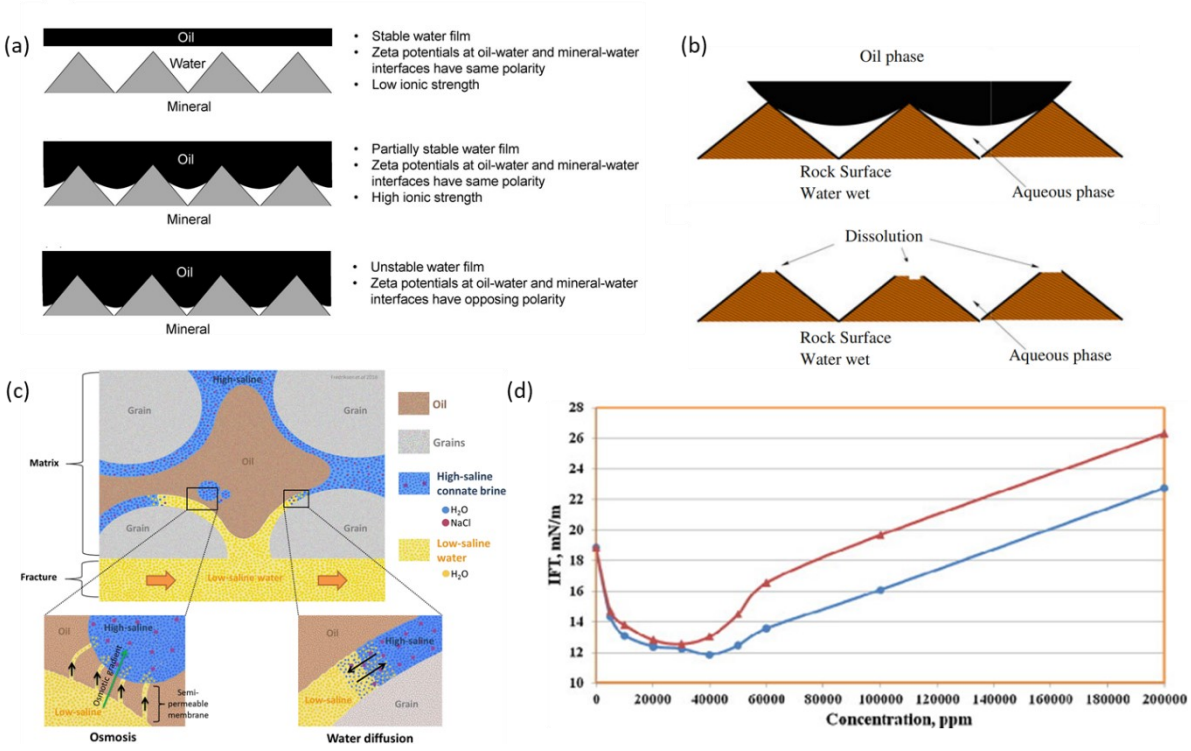

Figure 2-5: Schematics of the main mechanisms proposed for the CSE in carbonates. Figure (a) stability of water film between mineral and oil interfaces depending on the surface charge and oil polarity from Jackson et al. Vinogradov (2016a). Figure (b) detachment of oil droplets caused by dissolution of calcite asperities from Hiorth et al. (2010). Figure (c) formation of oil-water micro emulsions due to diffusion of water molecules through crude oil phase caused by osmotic gradient between high and low salinity brines from Fredriksen et al. (2018). Figure (d) reduction in interfacial tension (IFT) between water and oil as a function of NaCl and CaCl2 salinity from Moeini et al. (2014).

2.1.2.3 Comments

Although the CSE in carbonates has received less interest, it appears as though the underlying mechanisms are largely attributed to surface charge alteration and/or mineral dissolution. These two mechanisms do not necessarily have to occur independently of one another (Austad et al. 2010). Both mechanisms will contribute to changes in the zeta potential at the carbonate-brine interface through either direct alteration of the surface charge or changes to the brine chemistry.

The proposed fluid-fluid interaction mechanisms are less established. No studies have been conducted to determine the relationship between the oil, brine or system properties that affect the interactions and the majority have been conducted under ideal conditions (Tetteh et

al. 2020). Moreover, the fluid-fluid mechanisms imply that injection of lower salinity water should always yield an increase in oil recovery when it is well known this is not the case (e.g Seyyedi et al. 2018). These fluid-fluid interactions may be a secondary effect that aids transportation of crude-oil through the porous media but cannot solely be attributed as the underlying mechanism for the CSE in carbonates.

2.1.3 CSW in Sandstones

2.1.3.1 Evidence for the CSE in Sandstones

The CSE in sandstone core samples was first observed by Martin (1959) and Bernard (1967), however, it was not until Tang and Morrow (1999) first proposed fines migration as an underlying mechanism for the CSE that interest in the field became widespread. Since then, numerous studies have published evidence for the CSE across the multiple scales and techniques discussed by Bartels et al. (2019). Several authors have proposed underlying physical mechanisms to better predict and optimise CSW. This section will highlight some of the main evidence for the CSE in sandstones and summarise these key mechanisms.

As with carbonates, coreflood experiments make up the bulk of the experimental data. Katende and Sagala (2019) collated a database of over 500 different CSW coreflood experiments. Their analysis suggested that for the largest CSE the following criteria were desirable (i) presence of clays – specifically kaolinite – and calcite (ii) permeability > 2mD (iii) lower divalent cation concentration than monovalent cation, ideally below a 4% ratio and (iv) elevated temperature. However, none of these were deemed necessary. The CSE was still observed in experiments that did not match all four criteria. Results from field trials such as log-inject-log tests (Webb et al. 2004) and single well chemical tracer tests (McGuire et al. 2005; Seccombe et al. 2008) have also supported the CSE on the core and reservoir scale showing a reduction in residual oil saturation. Field trials have also shown successful responses to low salinity water injection (Seccombe et al. 2010) however these have often shown poorer results than what was expected based on laboratory measurements (Singh and Sarma 2021). The Clair Ridge field in the North Sea was the first major full reservoir deployment of LSW (Robbana et al. 2012).

Other experimental techniques have provided evidence for the CSE on the sub-pore scale. For example, Haagh et al. (2017) showed reductions in the contact angle of an oil droplet on a model system with a reduction in the divalent cation concentration. AFM

measurements have been used to understand the molecular interactions between surfaces and polar species as a function of salinity (Siretanu et al. 2014; Mugele et al. 2015; Van Lin et al. 2019). Hilner et al. (2015) showed the adhesion force between a quartz surface and a functionalised non-polar oil tip and decreased when the brine salinity decreased below 5,000ppm. Zeta potential measurements of the mineral-brine and oil-brine interface have shown that both become more negative with increasing brine dilution (Nasralla and Nasr-El-Din 2014a; Chen et al. 2018).

Recent advancements in Micro-CT imaging have provided new methods to measure wettability and investigate the CSE on the pore network scale. Direct imaging of pore occupancy changes has been observed when flooding with high and low salinity brines (Bartels et al. 2017; Lebedeva and Fogden 2011). These studies have shown that the fluid connectivity through the pore space can be important in determining the effectiveness of CSW in addition to the underlying detachment mechanism(s). Andrews et al. (2021) measured the fraction of the pore area covered by oil or water from Micro-CT images to assess the wetting state of a sandstone core. Upon injection of low salinity water, they showed a decrease in the fractional coverage indicative of a change to a more water-wet system.

Significant evidence supports the existence of the CSE in sandstones. However, there are still concerns about its use as an industrial IOR process due to the conflicting understanding and evidence regarding the underlying mechanism(s) and screening criteria (Singh and Sarma 2021). Challenges also remain in upscaling results and observations to full field models (Bartels et al. 2019). The academic community has largely focused on the former challenges, which are reviewed in the next section.

2.1.3.2 Mechanisms

The following focuses only on the solid-fluid mechanisms that have been proposed for the CSE in sandstones. The fluid-fluid mechanism discussed in the previous section are also relevant for sandstones (Bartels et al. 2019).

I) Clay Swelling & Fines Migration

It has been known since the 1960s that injection of dilute or freshwater into a clay-rich sandstone can cause a reduction in permeability (Martin 1959; Bernard 1967) in a phenomenon known as formation damage. Formation damage has been attributed to the swelling of clay minerals due to freshwater injection which leads to the detachment of small clay particles known as fines (Khilar et al. 1989). These fines travel through the pore space and accumulate at pore throats thereby blocking the pathway to fluid flow (Khilar et al. 1989; Vaidya and Fogler 1992).

Fines migration was first proposed as an underlying mechanism for CSW by Tang and Morrow (1999). They proposed that crude oil droplets adsorbed to fines could become mobilised when these fines detach upon low salinity waterflooding. The residual rock surface would consequently become more water-wet.

Whilst fines migration was one of the first mechanisms to garner significant attention, several studies have since shown the CSE in experiments where no evidence of fines migration was present (Sheng 2014; Jackson et al. 2016a; Katende and Sagala 2019). Whilst fines migration may be active in clay-rich sandstones, it is not the primary mechanism behind the CSE in all instances. Moreover, evidence suggests that the presence of clay particles is not a prerequisite for the LSE (Bartels et al. 2017).

II) (Localised) pH Increase & In-Situ Surfactant Generation

The majority of coreflood experiments on sandstones report an increase in the effluent brine pH during LSW (Sheng 2014; Jackson et al. 2016a; Katende and Sagala 2019). McGuire et al. (2005) suggested that the increase in pH could result in the formation of natural surfactants with polar acid compounds in the crude oil. These surfactants cause a decrease in the oil-water interfacial tension (IFT) and contact angle rending the mineral surfaces more water-wet. Furthermore, the surfactants can help dispersion of oil into the water phase to aid in transportation.

Increases in pH are common during low salinity water injection in sandstone cores however most experiments report effluent values in the range 7-8 (Jackson et al. 2016a; Sheng 2014; Katende and Sagala 2019). Saponification of acid compounds to form surfactants would be expected to occur only at pH values greater than 9 (Sheng 2014). Such high values of pH are unlikely to be encountered in sandstone reservoirs due to pH and CO_2 buffers (Jackson et al. 2016a). McGuire et al. (2005) note that for this mechanism to work the following are required (i) significant quantities of acidic species in the crude oil (AN > 0.2mgKOH/g) (ii) water sensitive minerals (iii) initial water saturation (iv) low salinity water injection (<5000ppm TDS). However, the CSE has been observed with low AN oils and no correlation between the CSE and AN has been identified (Jackson et al. 2016a). Whilst this mechanism may occur under the specific conditions mentioned, the CSE does not appear dependent on the presence of surfactants.

To explain the CSE in experiments where only a modest increase in pH was observed (effluent 7-8), Austad et al. (2010) proposed that significantly larger, localised increases in pH occur near the mineral/clay surfaces. Injection of low salinity brine causes desorption of cations from the clay surfaces, specifically divalent Ca^{2+} and Mg^{2+}, to maintain chemical equilibria. To compensate, H^+ ions near the clays adsorb to the negatively charged surface sites thus creating a loss of protons (and increase in pH) near the mineral surface. The localised increased pH then causes the formation of natural surfactants as suggested by

McGuire et al. (2005). Furthermore, Austad et al. (2010) suggested the localised increase in pH causes formation and precipitation of $Ca(OH)_2$ and $Mg(OH)_2$ to explain the reduction in divalent cation concentration observed in several studies.

These localised increases in pH are difficult to measure or prove and so this mechanism is unsettled. Ion exchange between brine and clay during injection of low salinity water and transient pH increases have been shown to occur (Kia et al. 1987; Vaidya and Fogler 1992). However, studies have shown increases in pH where the CSE was not observed (Sheng 2014; Jackson et al. 2016a; Katende and Sagala 2019).

III) Multi-Ion Exchange (MIE)

Lager et al. (2008) noted that during LSW in coreflooding experiments there was a significant reduction in the concentration of Ca^{2+} and Mg^{2+} ions in the effluent brine. They suggested that reduction in the brine salinity promotes preferential adsorption of these ions to the mineral surface. Polar oil components that were previously adsorbed to the mineral surface sites are exchanged in favour of these divalent cations. These oil components detach from the mineral surface leading to an increase in oil recovery.

Evidence directly supporting MIE and the CSE is sparse (Jackson et al. 2016a). Several studies have reported increases in oil recovery without observing a significant change in concentrations of Ca^{2+} or Mg^{2+} (Jackson et al. 2016a; Sheng 2014). the injection brine composition is different to that of the connate brine then a new equilibrium between the surface and bulk fluid will be established. However, for the MIE mechanism to occur polar oil components must be directly adsorbed to the clay mineral surface. This relates to the first of the wettability alteration mechanisms proposed by Buckley and Liu (1998) and discussed in section 2.1.1.1. This mechanism of wettability alteration is likely to dominate only in the absence of initial water presence which is rare in most conventional reservoirs.

IV) Double Layer Expansion (DLE)

Dilution of brine typically causes a reduction in the overall ionic strength causing an expansion of the diffuse part of the electrical double layer (see Hunter (2013) and section 2.2.1.1). Ligthelm et al. (2009) proposed double layer expansion (DLE) at the mineral-brine interface during LSW as an underlying mechanism of the CSE. DLE causes an increased in the electrostatic repulsion between the mineral-brine and oil-brine interfaces. If this electrostatic repulsion is sufficient to overcome the localised disjoining pressure, the oil components will detach from the mineral surface leading to improved oil recovery and a more water-wet mineral surface (Anderson 1986b; Buckley and Liu 1998).

Nasralla and Nasr-El-Din (2014a) concluded that DLE was a dominant mechanism controlling the CSE based on zeta potential measurements, contact angle measurements and coreflood experiments. They showed that the zeta potential of both the mineral-brine and oil-brine interfaces increased in magnitude and became more negative with brine dilution. The zeta potential of the sandstone-brine interface in simple NaCl electrolytes is typically negative and increases in magnitude with a reduction in the ionic strength of the brine, but is independent at higher values of brine ionic strength (~0.4 mol/L) (Walker and Glover 2017; Vinogradov et al. 2010). The 5,000ppm TDS salinity threshold at which the CSE is observed in sandstones (Lager et al. 2007) corresponds to an ionic strength of ~0.1 mol/L for a pure NaCl brine. If the brine contains divalent cations, then the total ionic strength will be higher. The increase in zeta potential that occurs at ~0.4 mol/L is roughly consistent with this salinity threshold. At the same salinity threshold, a reduction in the adhesion force between a quartz tip and a non-polar oil tip was observed from AFM measurements (Hilner et al. 2015). They proposed that DLE will always contribute to the CSE regardless of whether other mechanisms are also active.

The DLE mechanism is based on the fundamental assumption that the oil-brine and mineral-brine interfaces are negatively charged. If the oil-brine interface were positively charged, then a reduction in ionic strength would yield an increased electrostatic attraction.

Zeta potential measurements of the oil-brine interface suggest that this is negatively charged at pH > 5, however, many of these data were obtained at conditions unrepresentative of the subsurface (see section 2.2.4 for a review of the controls on the crude oil zeta potential). The DLE mechanism also implies that reduction of ionic strength will always yield an increase in oil recovery, yet it is well-known that this is not the case (Jackson et al. 2016a; Sheng 2014; Katende and Sagala 2019). Haagh et al. (2017) investigated the effect of divalent cations on contact angle measurements. They concluded that reducing the ionic strength of the brine whilst maintaining a constant divalent cation concentration showed no change in the wettability. DLE alone could not be the sole mechanism for the CSE. However, a reduction in the divalent cation concentration did yield an increase in the water-wetness of the surface along with a reduction in the overall ionic strength. Whilst DLE may occur in many instances due to a reduction in the brine ionic strength, the mechanism cannot explain the CSE on its own.

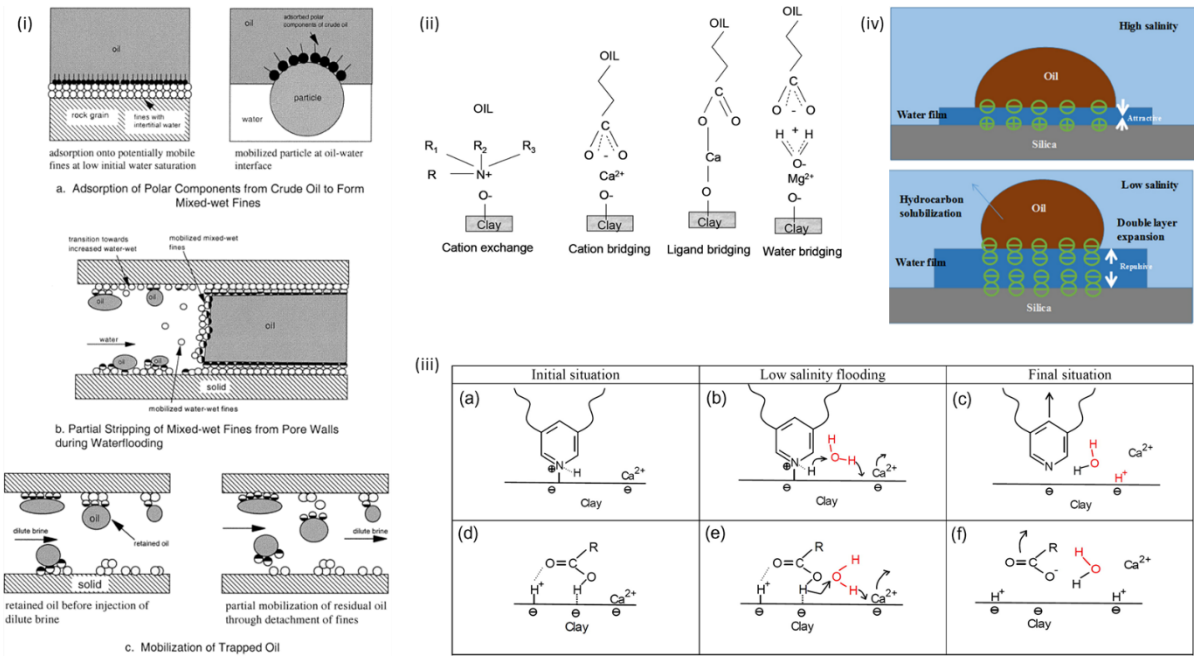

Figure 2-6: Schematics of the four main mechanisms explaining the CSE in sandstones. Figure (i) Fines Migration from Tang and Morrow (1999). Figure (ii) multi-ion exchange mechanism from Lager et al. (2008). Figure (iii) localised pH increase causing in-situ surfactant generation from Austad et al. (2010). Figure (iv) double layer expansion mechanism from Wei et al. (2017).

2.1.3.3 Comments

In comparison to carbonates, the CSE in sandstones appears more complex with multiple proposed mechanisms, none of which have been conclusively proven. There is still active debate around the role and importance of properties such as clay content, brine composition and oil properties. Inconsistency between experimental methods and reporting has been identified as a contributing factor to the conflicting evidence and lack of clarity on this topic (Jackson et al. 2016a; Bartels et al. 2019).

Of the main mechanisms, all should lead to a measurable change in the zeta potential of the sandstone-brine interface through alteration of the surface charge, changes in pH or changes in the brine chemistry. As with carbonates, the fluid-fluid interactions are thought to play a secondary role in the CSE (see section 2.1.2.2).

2.1.4 Summary

A wealth of evidence suggests the CSE is real and can lead to increases in oil recovery in sandstones and carbonates, at the laboratory and at the field scale. The CSE is also associated with a change to a more water-wet state. The underlying mechanisms of the CSE remain ambiguous but in almost all cases will lead to changes in the zeta potential of the mineral-brine interface. The zeta potential of the oil-brine interface would also be expected to change as the injection brine composition is modified, but has been studied to a lesser extent, particularly at conditions appropriate to subsurface hydrocarbon reservoirs. The controls on the mineral-brine and the oil-brine zeta potential in both sandstones and carbonates and their impact on wettability need to be fully understood. Such understanding will link changes in brine chemistry to wettability alteration and improved oil recovery to better predict and optimise CSW.

2.2 The Zeta Potential

The zeta potential is a measure of the electrical potential near an interface and is often considered a proxy for the surface electrical potential. Its polarity and magnitude control the electrostatic forces between the interface and other polar species in adjacent phases. This section begins with an overview of the theoretical origin of the zeta potential for a generic electrically charged surface. The zeta potential, and the key controls on the zeta potential, of carbonates, sandstones and crude oils are then discussed in subsequent sections.

2.2.1 Electrokinetics & The Origin of the Zeta Potential

2.2.1.1 The Electrical Double Layer & Electrokinetic Phenomena

When a charged particle or surface is in contact with an aqueous electrolyte, a separation of charge occurs in the electrolyte in a region near the interface. Counter-ions (those with an opposite polarity to the surface) are electrostatically attracted toward the surface and present in a higher concentration than co-ions (those with the same polarity as the surface). This increased counter-ion density yields an excess of counter charge in the near-interface region which balances the excess surface charge to ensure electroneutrality (Hunter 2013). This arrangement is termed the electrical double layer (EDL) (Figure 2-7).

The EDL is often further subdivided into the Stern layer, the diffuse layer, and the free electrolyte. The Stern layer contains ions which are directly adsorbed or attached to the surface, whereas ions in the diffuse layer are free to move in space. The Stern layer may also be further subdivided into the inner- and outer-Helmholtz planes (IHP and OHP respectively). The difference between the two is that the IHP contains smaller ions whereas the OHP contains larger, often hydrated, ions. In both instances the ions are still attached or adsorbed to the surface (Al Mahrouqi et al. 2017a). Typically, the counter charge in the Stern layer is insufficient to balance the excess surface charge. The residual excess charge at the Stern

plane is therefore balanced by an excess of charge in the diffuse layer. The movement of ions within the diffuse layer means the electrical potential decreases more gradually than in the Stern layer. In low ionic strength electrolytes (<0.1 mol/L) the electrical potential decreases exponentially until it reaches zero far from the surface, where electroneutrality is ensured and the co- and counter-ion charge is balanced (Hunter 2013).

The zeta potential is defined as the electrical potential at the 'shear' plane. It is assumed that the diffuse layer is mobile beyond the shear plane which lies some distance away from the surface, outward of the Stern layer. The shear plane is often assumed to coincide with the Stern plane or treated as a variable which can be tuned to match experimental data to surface complexation models (SCMs) (Glover et al. 2012; Bonto et al. 2019). Whilst the exact location is usually unknown, relative motion along the shear plane between the excess charge in the mobile diffuse layer and the immobile charged surface leads to electrokinetic phenomena. Experimental methods to measure the zeta potential make use of such electrokinetic phenomena.

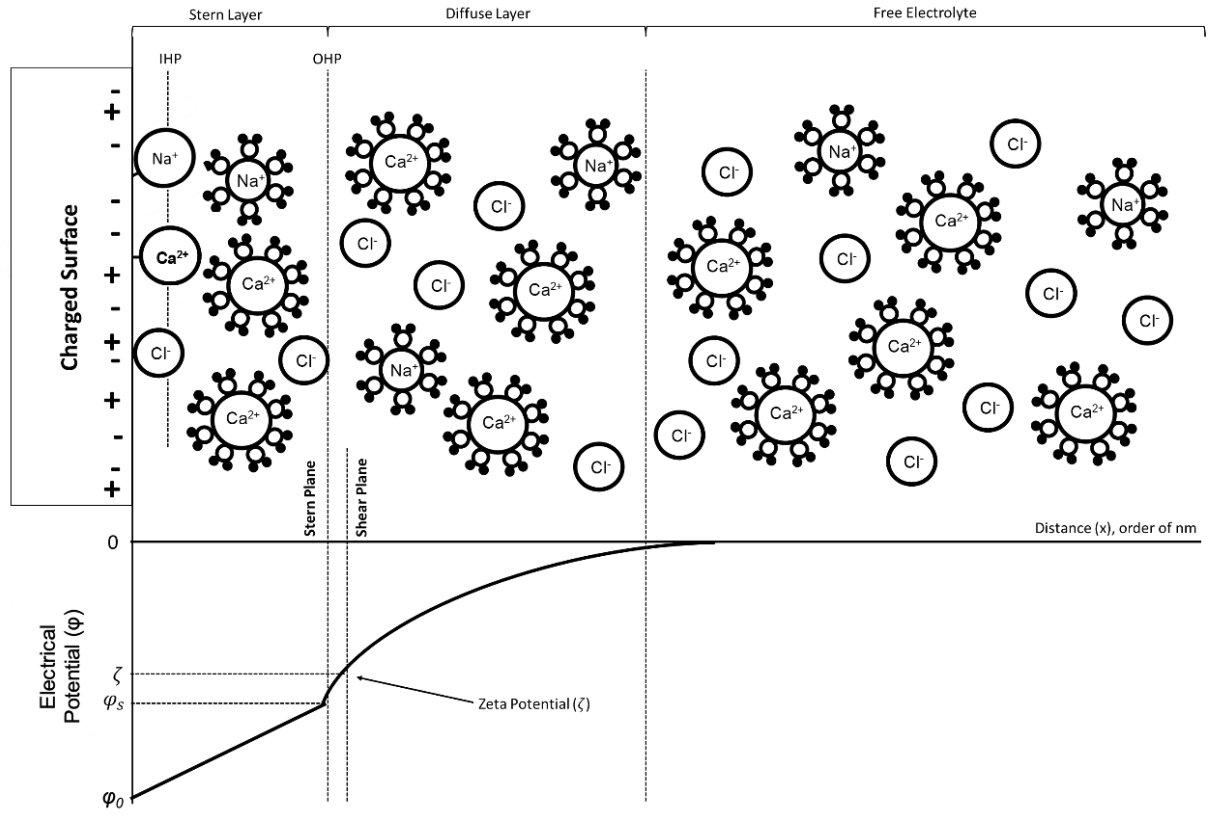

Figure 2-7: Schematic of the EDL for a generic electrically charged surface which is assumed to be negatively charged overall.

2.2.1.2 Measurement of Zeta Potential

The most common methods to determine the zeta potential are (1) electrophoresis, which is the mobilisation of charged particles, relative to a stationary solution, under the influence of an applied electrical field, and (2) streaming potential, which is the potential difference that arises when a solution is moved relative to a stationary solid under the influence of an applied pressure gradient.

I) Electrophoretic Methods

Electrophoretic methods (EPM) employ the first approach. Commercially available equipment, such as a Zetasizer (e.g. Nasralla and Nasr-El-Din (2014a)) are readily available and utilised across many disciplines. An alternating electric field is applied to a suspension of powdered or crushed solid particles, or to a dispersion of droplets of an immiscible fluid in

another. Due to electrokinetic phenomena, the electric field causes the particles to vibrate, and the speed and direction of these vibrations are measured. From these measurements, the zeta potential can be calculated (Hunter 2013). The zeta potential value that is reported is an average zeta potential across all particles in the suspension. For more detailed discussion on the measurements and calculations the reader is directed to the cited literature (Hunter 2013; Delgado et al. 2007).

Although widely used, EPM are limited in their operating conditions and applicability, particularly with regards to the subsurface, for several reasons. Primarily, the measurement is dependent on the ability to create and maintain a stable dispersion which can be challenging in high ionic strength electrolytes and/or at elevated temperatures (Mahani et al.2017). Both conditions are common in subsurface environments. In addition, when dealing with rock samples, these must be crushed to a fine powder which destroys the natural rock texture and distribution of minerals within the sample. Crushing samples may expose 'fresh' interfaces to the fluid which would not previously have been in contact in an intact sample, therefore altering the surface charge and surface charge distribution (Vernhet et al. 1994). The location of the shear plane may also be modified by destroying the natural geometry of the porous media (Vernhet et al. 1994; Alroudhan et al. 2016). Furthermore, EPM typically require a large volume/solid ratio compared to natural, intact porous media which may affect the bulk solid-liquid equilibrium, particularly in reactive systems where precipitation/dissolution may affect the surface charge or brine chemistry. Finally, EPM are limited to measuring the surface charge of one interface between two phases. Thus, multi-phase systems such as oil-water-rock where multiple interfaces exist simultaneously cannot be represented.

II) The Streaming Potential Method

Conversely to EPM, the streaming potential method (SPM) applies a pressure gradient to mobilise a fluid through a capillary, porous media or packed bed, or along a flat surface or membrane. The mobilisation of the excess charge in the diffuse layer relative to the charged

surface gives rise to a streaming current. Under steady state conditions when the total current density is zero, this streaming current must be balanced by an opposing conduction current to maintain electroneutrality. This conduction current is driven by an electrical potential difference (ΔV), termed the streaming potential, across the sample which is measured (Hunter 2013).

Measuring the pressure difference (ΔP) and the voltage difference (ΔV) across the sample as an aqueous electrolyte flows at steady state conditions allows for the zeta potential, ζ, to be calculated by the Helmholtz-Smoluchowski equation:

$$C = \frac{\Delta V}{\Delta P} = \frac{\varepsilon_w \zeta}{\sigma_e \mu_w} \qquad (2\text{-}5)$$

where ε_w is the permittivity of the electrolyte, μ_w is the viscosity of the electrolyte, C is the streaming potential coupling coefficient (V/Pa) and σ_e the electrolyte conductivity (S/m). In certain applications, such as natural porous media, when surface electrical conductivity may be significant, a modified form of equation (2-5) is necessary (Li et al. 2016):

$$C = \frac{\Delta V}{\Delta P} = \frac{\varepsilon_w \zeta}{\sigma_m \mu_w F} \qquad (2\text{-}6)$$

where σ_m represents the conductivity of the medium (S/m) when saturated with the electrolyte of interest and F is the formation factor of the medium, defined as the ratio of the electrolyte conductivity, σ_e, to the medium conductivity, σ_m, when surface electrical conductivity is negligible. Further detail regarding the derivation of equations (2-5) and (2-6) can be found in section 5.2.1 or in the cited literature.

2.2.2 The Zeta Potential of Carbonates

2.2.2.1 Controls on the Surface Charge of Carbonates and PDIs

Carbonates comprise a class of sedimentary rocks containing carbonate chemical groups (Morse and Mackenzie 1990). The more common carbonates are calcite ($CaCO_3$) and dolomite ($MgCO_3$) with the former more widely studied and of interest to oil & gas reservoirs (Morse and Mackenzie 1990). This section will focus on the zeta potential of calcite given the wider interest and available data. The surface charge of carbonates can be complex due to their ability to readily undergo dissolution/precipitation reactions based on the solid-liquid equilibria (Morse 2018; Al Mahrouqi et al. 2017a; Stumm et al. 1992). These reactions can be difficult to separate from adsorption reactions of specific ions to the mineral surface, which can in turn modify the surface charge (Al Mahrouqi et al. 2017a). Ions that can modify the surface charge are termed 'potential determining ions' (PDIs).

Al Mahrouqi et al. (2017a) published a recent review on the zeta potential of calcite and concluded that the surface charge (and zeta potential) of calcium carbonate mineral surfaces is primarily controlled by adsorption of the lattice species Ca^{2+} and Mg^{2+}. Decreasing the concentration of these divalent ions yields an increasingly negative zeta potential, and both behave identically within experimental error at laboratory conditions (Figure 2-8) (Al Mahrouqi et al. 2017a; Alroudhan et al. 2016). The total ionic strength of the brine also affects the magnitude of the zeta potential, because it controls the thickness of the diffuse part of the electrical double layer at the mineral-brine interface (Figure 2-7) Decreasing the total ionic strength increases the magnitude of the zeta potential via 'double layer expansion' (Hunter 2013).

The brine pH does not directly control the zeta potential of carbonate mineral surfaces; rather, varying the pH controls the equilibrium concentration of Ca^{2+} and Mg^{2+} for a given CO_2 partial pressure (pCO_2), and it is the concentration of Ca^{2+} and/or Mg^{2+} that controls the zeta potential (Al Mahrouqi et al. 2017a; Alroudhan et al. 2016; Foxall et al. 1979). Despite this,

many studies still report measurements of zeta potential on carbonates as a function of pH (Hiorth et al. 2010; Austad et al. 2012; Zhang and Austad 2006; Alotaibi et al. 2018; Alotaibi and Yousef 2017; Al Mahrouqi et al. 2017a; Mahani et al.2017a; Song et al. 2017; Chen et al. 2014; Kasha et al. 2015). The apparent correlation between pH and zeta potential obtained in these studies reflects the relationship between pCa (the negative logarithm of calcium concentration in mol/L) and zeta potential, with pCa varying in response to the imposed variation in pH. It is not possible to retrospectively extract the relationship between zeta potential and pCa from these studies, because calcium concentration was typically not measured. A relationship between SO_4^{2-} concentration and carbonate zeta potential has also been proposed, with increasing SO_4^{2-} yielding more negative zeta potential (Figure 2-8) (Alotaibi et al. 2018; Al Mahrouqi et al. 2017a; Mahani et al.2017a; Alotaibi and Yousef 2017; Song et al. 2017; Awolayo et al. 2016; Mahani et al.2015; Austad et al. 2012; Yousef et al. 2011b; Fathi et al. 2011; Hiorth et al. 2010; Zhang and Austad 2006).

In carbonates, where minerals can readily undergo precipitation/dissolution reactions, modifying the composition of specific ions in the bulk fluid may appear to act as PDIs to the mineral surface but in fact only indirectly affect the zeta potential by modifying the equilibrium concentration of other ions. For example, it has been suggested that SO_4^{2-} is not actually a PDI to the calcite surface and only affects zeta potential by removing Ca^{2+} from the bulk fluid (Al Mahrouqi et al. 2017a; Alroudhan et al. 2016, Hiorth et al. 2010). Other ions such as CO_3^{2-} (controlled by the pCO_2/pH) may yield similar observations (Al Mahrouqi et al. 2017a; Alroudhan et al. 2016, Hiorth et al. 2010). In such systems the evidence for PDIs may be more complicated since it is not easy to decouple the effects of direct surface interaction with fluid composition modification.

Previous studies have shown that the experimental conditions during zeta potential measurements are particularly important in carbonates to ensure consistent and repeatable data: it is essential to ensure that equilibrium has been reached between the mineral surfaces and the brine of interest, which may require 10’s or even 100’s hours of pre-equilibration to

achieve (Alroudhan et al. 2016). It is also important to control (or measure) pCO_2, as different pCO_2 (e.g., in open versus closed system experiments) will yield different equilibrium concentrations of Ca^{2+} (Song et al. 2017; Alroudhan et al. 2016). Some of the observed variability in zeta potential data in natural carbonates may reflect failure to reach equilibrium, or unknown/unreported variations in pCO_2.

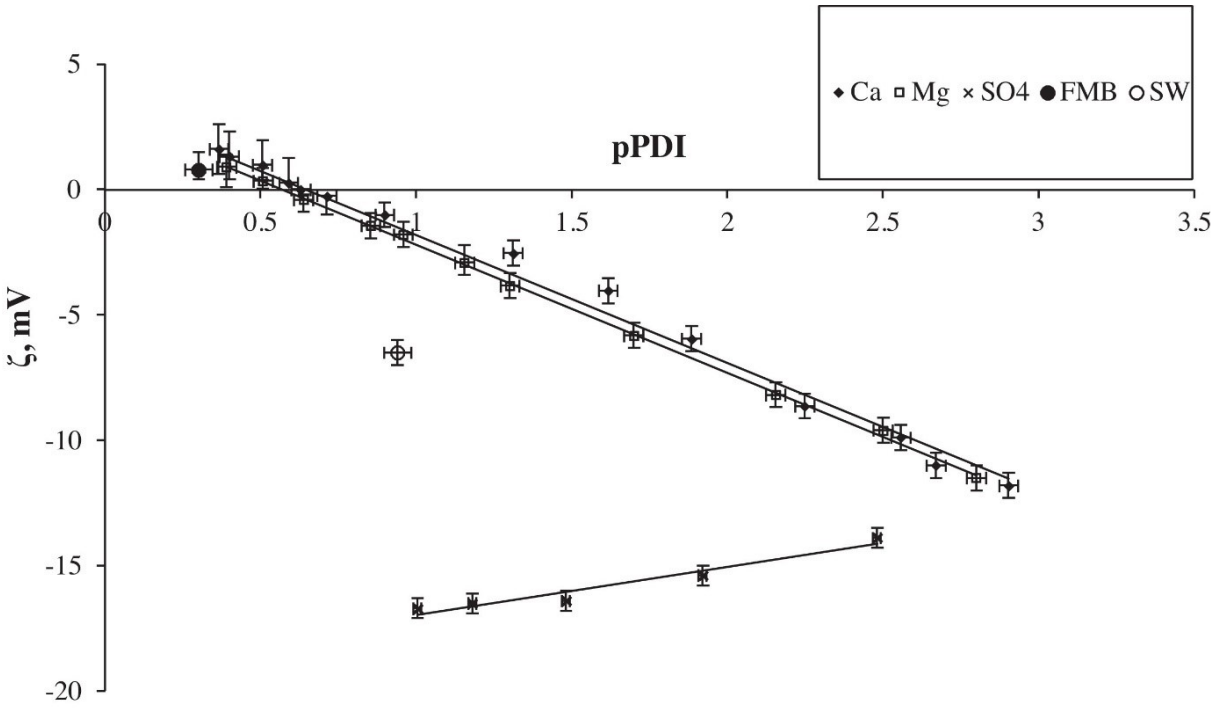

Figure 2-8: Zeta Potential of intact Portland limestone core samples showing effect of Ca^{2+}, Mg^{2+}, SO_4^{2-} Zeta potential in formation brine (FMB) and Seawater (SW) also shown. Figure from Alroudhan et al. (2016).

2.2.2.2 Zeta Potential of Carbonates at Reservoir Conditions

Despite the large number of published measurements of zeta potential in carbonates (Alroudhan et al. 2016), few measured data are relevant to carbonate oil reservoirs. Most studies obtain zeta potential data using commercially available laboratory equipment such as a Zetasizer (e.g. Mahani et al.2017a; Nasralla et al. 2011; Takeya et al. 2019; Pooryousefy et al. 2018; Nazarova et al. 2018; Mahani et al.2015; Kasha et al. 2015). As discussed in section 2.2.1.2I) electrophoretic measurements have a limited range of operating conditions that are far from those present in natural oil reservoirs. Primarily this is because rock samples must be

crushed to a sub-grain size powder, measurements in the high concentration electrolytes (>0.5 mol/L) and elevated temperatures (>60ºC) are difficult to perform and only one fluid phase is present.

The relatively limited relevant data published to date suggest that the zeta potential on natural, intact calcium carbonates in equilibrium with natural formation brines is typically positive, owing to the high concentration of Ca^{2+} in such brines, but is negative in lower salinity brines such as seawater, reflecting the lower Ca^{2+} concentration and, possibly, higher SO_4^{2-} concentration (Awolayo et al. 2014; Al Mahrouqi et al. 2017a; Alroudhan et al. 2016; Mahani et al.2017). However, different natural samples can exhibit different zeta potential values in the same brine, which may reflect differences in the texture, structure, and mineral distribution across samples (Li et al. 2020), or trace impurities and organic material on the mineral surfaces (Al Mahrouqi et al. 2017a). The impact of these small-scale variations on zeta potential may be lost in studies where samples are crushed (Mahani et al.2017a; Mahani et al.2015; Kasha et al. 2015). Moreover, most data published to date were obtained at laboratory conditions.

Al Mahrouqi et al. (2016) measured the temperature dependence of the zeta potential in intact natural carbonates and found that the zeta potential became smaller in magnitude with increasing temperature in low concentration brines (0.01 mol/L) but was independent of temperature in high concentration brines (>0.5 mol/L). However, they explored simple NaCl brines in which the Ca^{2+} present was sourced only from dissolution of the sample during initial equilibration; the temperature dependence of zeta potential in these experiments was directly correlated with the temperature dependence of the measured equilibrium Ca^{2+} concentration. Tetteh et al. (2020) reported electrophoretic measurements of the calcite-brine zeta potential at 25 ^{O}C and 40 ^{O}C for single-salt brines. Their results showed temperature had either no effect or caused the zeta potential to become slightly more positive. They report no change in zeta potential in reservoir formation brines, seawaters, or low salinity brines between 25 ^{O}C and 40 ^{O}C. However, many reservoirs are at much higher temperatures and thus

measurements of the zeta potential in natural carbonates saturated with oilfield brines at relevant temperatures are scarce.

Previous studies have shown that the zeta potential in natural carbonates saturated with brine and crude oil is affected by the wetting state. Jackson and Vinogradov (2012) measured a positive zeta potential on natural, water-wet reservoir carbonates which became less positive after aging in crude oil. Jackson et al. (2016a) extended this work and reported a correlation between wettability and the change in zeta potential after aging. In their work, three crude oils were observed to make the carbonate zeta potential more negative after wettability alteration and one was observed to make the zeta potential more positive. Figure 2-9 shows a schematic of the zeta potential for the calcite surface in (a) water-wet conditions and (b) after becoming oil-wet with crude oil.

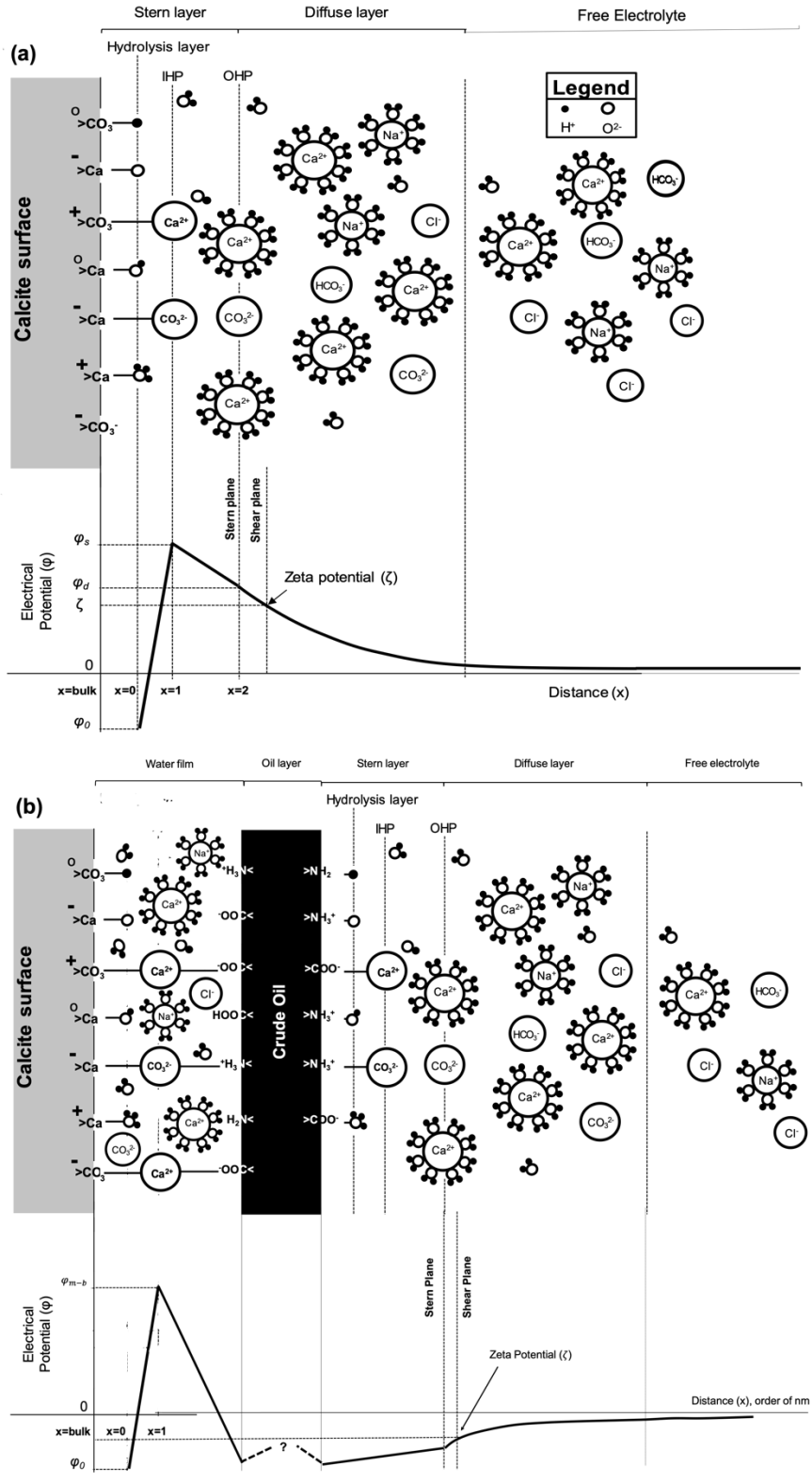

Figure 2-9: Schematic of a triple layer model for (a) the mineral-brine interface and (b) the same interface after aging and wettability alteration with a negatively charged crude oil. The crude oil is attached to the mineral surface via ion bridges (e.g. Ca^{2+}, CO_3^{2-}) within a thin water film between the two interfaces. On a water-wet surface (a), the zeta potential is dictated by the properties of the mineral-brine interface; however, on an oil-wet surface, the zeta potential is dictated by the properties of the oil-brine interface.

2.2.2.3 Comments

The controls on the surface charge and zeta potential of the calcite-brine interface are reasonably well understood. The divalent cations Ca^{2+} and Mg^{2+} appear to be the primary controls, however it is important that proper solid-fluid equilibrium is established. Dissolution or precipitation of carbonate material may alter the concentrations of these cations in the bulk fluid and modify the surface charge. The zeta potential of dolomite and other carbonates has been studied to a significantly lesser extent. Data surrounding the zeta potential of calcite at reservoir conditions is limited, but the importance of Ca^{2+} and Mg^{2+} is still evident. Further data are needed to confirm these observations. The impact of wettability alteration on the zeta potential also needs additional data to be better understood.

2.2.3 The Zeta Potential of Sandstones

2.2.3.1 Controls on the Surface Charge of Sandstones and PDIs

Sandstones are another classification of sedimentary rock primarily comprised of metal oxides, particularly quartz (SiOH) (McBride 1963). Different sandstones can vary significantly and exhibit high mineralogical heterogeneity including significant quantities of other metal oxides such as clay minerals (e.g. kaolinite, montmorillonite, Illite and chlorite); feldspars; plagioclase and traces of carbonate material such as calcite and dolomite (Garzanti 2019).

The origin of the surface charge in quartz and clay minerals is primarily due to the protonation and deprotonation of the metal oxide surface sites (Stumm et al. 1992; Hunter 1993) represented respectively by:

$$> \mathrm{MeOH} + \mathrm{H}^{+} \leftrightarrow > \mathrm{MeOH}_2^{+} \qquad \text{(2-7a)}$$

$$> \mathrm{MeOH} + \mathrm{OH}^{-} \leftrightarrow > \mathrm{MeO}^{-} + \mathrm{H}_2 \qquad \text{(2-7b)}$$

where >Me represents a metal ion site on the mineral surface. Si, Fe and Al are the more common metals in sandstones that contribute to the development of surface charge (Stumm et al. 1992). Consequently, the brine pH is a key control on the zeta potential of sandstones. Electrophoretic measurements on quartz/silica/glass beads (Farooq et al. 2011; Coreño et al. 2001; Gaudin and Fuerstenau 1955; Kosmulski et al. 2003; Boleve et al. 2007) and pure clay minerals (Kosmulski and Dahlsten 2006; Sondi, Biscan, and Pravdic 1995; Yukselen-Aksoy and Kaya 2011; Hunter 2013; Nasralla and Nasr-El-Din 2014b) show that increasing pH yields a more negative zeta potential. However, the magnitude of these measurements varies significantly. Different minerals exhibit different surface charges due to differences in their geochemistry, structure, and interaction with different ionic species in fluid phases (Figure 2-10 a-d).

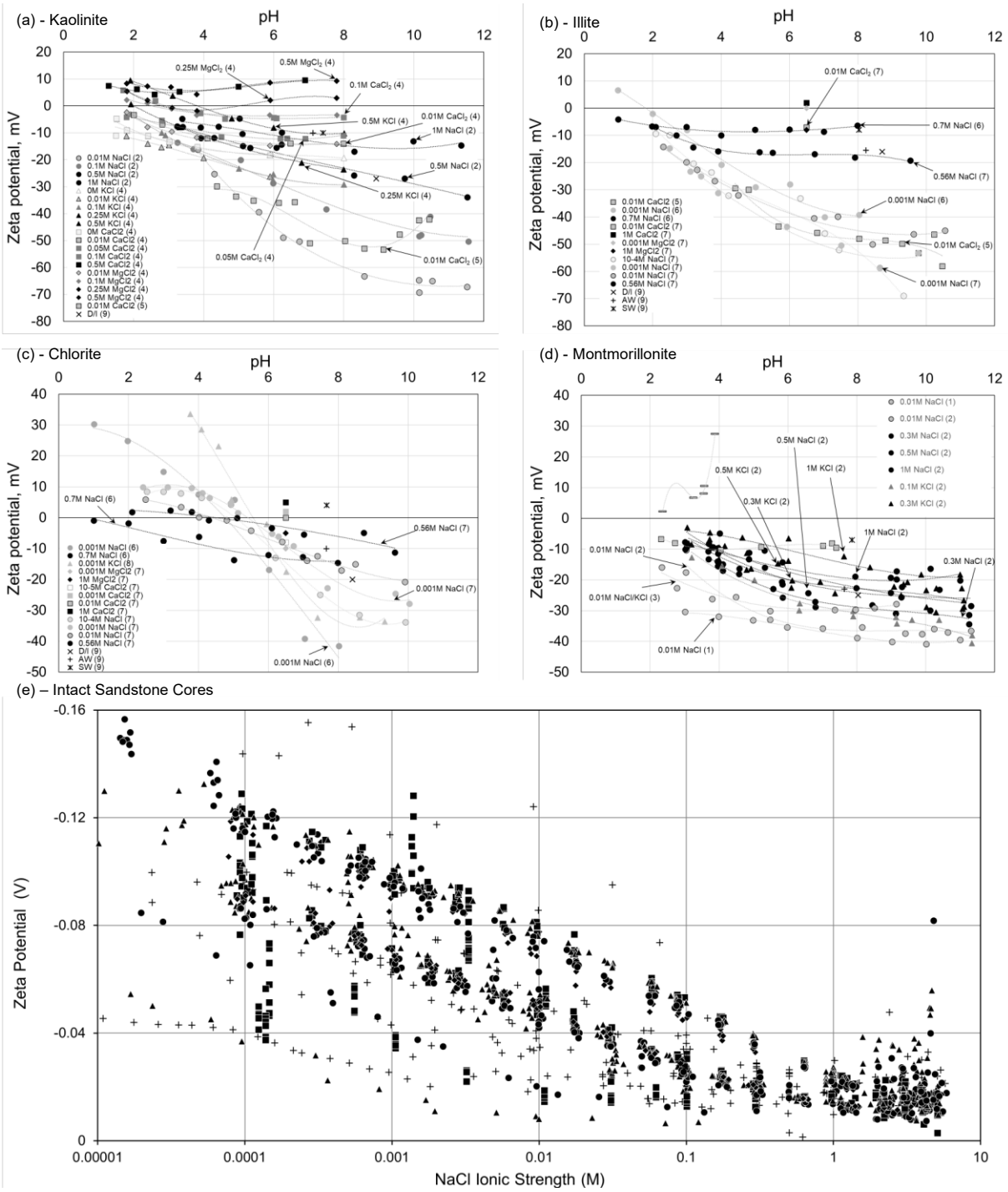

Figure 2-10: (a)-(d) from Jackson et al. (2016a) showing published zeta potential measurements as a function of pH for different clay minerals – (a) Kaolinite (b) Illite (c) Chlorite (d) Montmorillonite. Plot (e) shows zeta potential data obtained on a range of natural intact sandstones saturated with NaCl brines as a function of ionic strength. Data from Vinogradov et al. (2010) and Walker and Glover (2017).

Differences in the micro-scale zeta potential (i.e., that of the individual mineral surfaces typically considered on the nm scale) along with the quantity and distribution of these constituent minerals within porous sandstone systems can yield significant variability in the

macro-scale zeta potential (i.e. that of the entire system defined on the representative elementary volume (REV) on the mm scale). It is the macro-scale zeta potential that is of primary interest for most practical applications. Variation in the macro-scale zeta potential of natural, intact, quartz dominated sandstone cores when saturated with NaCl brines is evident in Figure 2-10(e).

Despite this variation in the magnitude, some general trends about the zeta potential of sandstones can be identified. The zeta potential is typically negative at pH > 3 consistent with the deprotonation of metal oxide surface sites yielding a negative surface charge (equations 2-7a and 2-7b) (Stumm et al. 1992; Walker and Glover 2017). Decreasing the total ionic strength typically increases the magnitude of the zeta potential via double layer expansion (Hunter 1981b; Walker and Glover 2017). However, at high salt concentrations (>0.4 mol/L) the zeta potential is independent of ionic strength (Vinogradov et al. 2010; Walker and Glover 2017) and has been termed the 'zeta potential offset'.

Limited data shows addition of Ca^{2+} and Mg^{2+} yields a more positive zeta potential in natural sandstones, sand packs, quartz, and clay minerals (Farooq et al. 2011; Sondi et al. 1995; Kosmulski and Dahlsten 2006; Vinogradov et al. 2018; Li et al. 2018; Thanh and Sprik 2016; Nasralla and Nasr-El-Din 2014b) suggesting these ions act as PDIs and can adsorb to the mineral surfaces to modify the surface charge. Other heavier metal/higher valency cations such as Al^{3+} also make the zeta potential more positive and can cause charge inversion (Duman and Tunç 2009).

2.2.3.2 Zeta Potential of Sandstones at Reservoir Conditions

Despite the broad range of interest few studies have measured the zeta potential of natural sandstones under conditions appropriate to the subsurface. As with carbonates, a key factor in the lack of data is the challenge of obtaining electrophoretic measurements under such conditions.

The ‘zeta potential offset’ measured in high ionic strength electrolytes was obtained on clean, quartz dominated sandstones when saturated with simple NaCl brines (Walker and Glover 2017; Vinogradov et al. 2010). Natural sandstones can exhibit much broader mineralogical heterogeneity and are typically saturated with brines containing multiple, multivalent ionic species in high concentrations (Alarouj et al. 2021). It has been shown that under these more complex conditions, the zeta potential may be significantly smaller in magnitude than the data obtained in NaCl brines may suggest (Alarouj et al. 2021). Furthermore, in highly heterogeneous samples, the zeta potential may in fact be positive (Alarouj et al. 2021). Adsorption of divalent cations to the mineral surfaces has been shown to make the zeta potential of sandstones more positive (Li et al. 2018) whilst the presence of carbonate material may carry a positive surface charge in the presence of high divalent cation concentrations (Al Mahrouqi et al. 2017a). If the carbonate material dominates the surface area of the pore space in heterogeneous sandstone samples this can cause the macro-scale zeta potential to become more positive (Alarouj et al. 2021).

Vinogradov and Jackson (2015) investigated the impact of temperature in natural intact sandstones. They report that increasing temperature decreases the magnitude of the zeta potential in NaCl electrolytes, but that it remains negative across the temperature investigated (20 – 150 ^{O}C). Vinogradov et al. (2018) report similar observations in sandpacks. The temperature dependence of the zeta potential was shown to be associated with the temperature dependence of the pH of the brine which modified the surface charge (Vinogradov and Jackson 2015; Vinogradov et al. 2018).

2.2.3.3 Comments

The zeta potential of sandstones is widely assumed to be negative and increases in magnitude with decreasing ionic strength. However, these two assumptions are based on data obtained under simple, idealised conditions, often in NaCl electrolytes. These conditions are far from those encountered in subsurface conditions and thus the zeta potential in these settings is poorly understood. The mineralogical heterogeneity of sandstones and the distribution of these minerals within the pore space can be an important factor. Thus, crushing samples for electrophoretic measurements may not accurately reflect the macro-scale zeta potential of the pore network. Furthermore, the impact of divalent cations (and other lesser studied ions) and the impact of temperature in complex brines remains ambiguous. No studies have investigated the impact of wettability alteration on the zeta potential of sandstones.

2.2.4 The Zeta Potential of Crude Oils

2.2.4.1 Development of Surface Charge at the Oil-Brine Interface

Crude oil is immiscible in the presence of water or brine and will develop an electrical surface charge along the oil-brine interface (Simanzhenkov and Idem 2003; Abdel-Raouf 2012). The origins of this surface charge are complex due to the complexity and variability of crude oils (Simanzhenkov and Idem 2003; Abdel-Raouf 2012). Crude oil covers of a broad range of fluids containing organic molecules in an organic solvent. Crude oils are primarily comprised of hydrocarbons, asphaltenes, resins, paraffins, sulfuric species and ash/residue (Simanzhenkov and Idem 2003). In comparison to the fixed structure of most solid-water interfaces, fluid-fluid interfaces are dynamic. Molecules can 'travel' from the bulk fluid to the interface and *vice-versa* (Simanzhenkov and Idem 2003; Abdel-Raouf 2012). The number of molecules that travel to the interface and are interfacially active (the surface site density), along with their electrical charge, will determine the overall surface charge of the interface (Hunter 2013).

Evidence suggests asphaltenes and resins play an important role in stabilising oil-brine emulsions and controlling wettability alteration; indirect indicators that these molecules are interfacially active and contribute to the development of surface charge (Abdel-Raouf 2012; Farooq et al. 2013; Szymula et al. 2000; Kokal et al. 1995; Buckley et al. 1997; Buckley and Liu 1998). It is thought that asphaltenes can become electrically charged due to the dissociation of carboxylic acid groups and/or the protonation of hydroxyl and basic amine groups (Szymula et al. 2000; Kokal et al. 1995; Dubey and Doe 1993; Buckley et al. 1997; Buckley et al.1989b; Abdel-Raouf 2012) The proportion of asphaltenes that are interfacially active is unclear. Chaverot et al. (2008) report 0.015% of the bulk asphaltene content is interfacially active whilst Yang et al. (2014) report it to be 2%. Furthermore, Yang et al. (2015) show that those interfacially active asphaltenes have a higher molecular weight and oxygen content than those in the bulk, implying the structure of the asphaltene may also be important

in controlling the interfacial properties. Asphaltenes are traditionally defined as the crude oil components that are soluble in aromatic solvents but precipitate in alkane solvents (Abdel-Raouf 2012). This bulk measurement of asphaltene content yields little insight into the properties and behaviours of the constituent molecules. Indeed, several authors comment that bulk asphaltene content is a poor indicator of emulsion stability and wettability alteration, implying it is a poor indicator of interfacial activity and surface charge (Yang et al. 2014; Czarnecki 2009; Buckley et al. 1997).

Other authors have suggested that acid and base hydrocarbon molecules are interfacially active. These molecules can develop an electrical charge through deprotonation and protonation of the acid and base groups respectively (Buckley et al.1989b; Farooq et al. 2013; Dubey and Doe 1993). The interfacial behaviour of acidic compounds has received more attention. The concentration of acids at the interface of oil-brine emulsions has been shown to be higher than in the bulk suggesting these molecules do indeed travel to the interface (Guo et al. 2006; Andersen et al. 2016). Evidence of increased emulsion stability (Rønningsen et al.1995; Havre et al.2003) and reduction in IFT (Hutin et al.2014a) with increased bulk acid concentration further suggest acids are interfacial active. Changes in IFT measurements have also been used to suggest that bases are less interfacially active than acids (Hutin et al.2014b; Nenningsland et al.2010; Bertheussen et al.2017). As with asphaltenes, it is unclear what proportion of acids or bases may be interfacially active.

Oils containing little to no polar molecules may develop a negative surface charge suggesting that non-polar hydrocarbons may also be interfacially active (Creux et al. 2007; Creux et al. 2009; Brooks and Seaman 1973; Gan et al. 2017; Gray-Weale and Beattie 2009). The development of negative charge at a non-polar interface, and at the air-water interface, is well documented and has been attributed to the affinity of the hydroxyl ion (OH^-) in the aqueous phase and/or the organisation of water molecules at the interface (Manciu and Ruckenstein 2012; Takahashi 2005; Creux et al. 2009). It was found that the zeta potential of different non-

polar oils was nearly identical with a consistent surface charge density of 1 site/3nm^2 (Creux et al. 2009).

The uncertainty regarding the type and quantity of molecules in crude oil that are interfacially active means it is challenging to determine the surface charge of the crude oil-brine interface. The surface charge of most solid-water interfaces can be measured by potentiometric titration (e.g., Chvedov et al. 2001). Solid particles are placed in an acid or base electrolyte and allowed to equilibrate before being neutralised. The surface charge can then be calculated from the amount of acid/base required to neutralise the sample. However, potentiometric titration of a fluid measures the total charge present in the bulk fluid rather, than that at the fluid-fluid interface (e.g., Dubey and Doe 1993). Potentiometric titration of crude oil measures the total concentration of negatively charged groups and positively charged groups present across all molecules (Dubey and Doe 1993) including hydrocarbons and asphaltenes (Szymula et al. 2000). These concentrations are termed the acid number (AN) and the base number (BN) respectively.

Since the surface charge cannot be determined directly, zeta potential measurements are the primary source of data available to understand the electrical properties of the crude oil-brine interface. Figure 2-11 collates published zeta potential data of different crude oils in NaCl electrolytes as a function of pH.

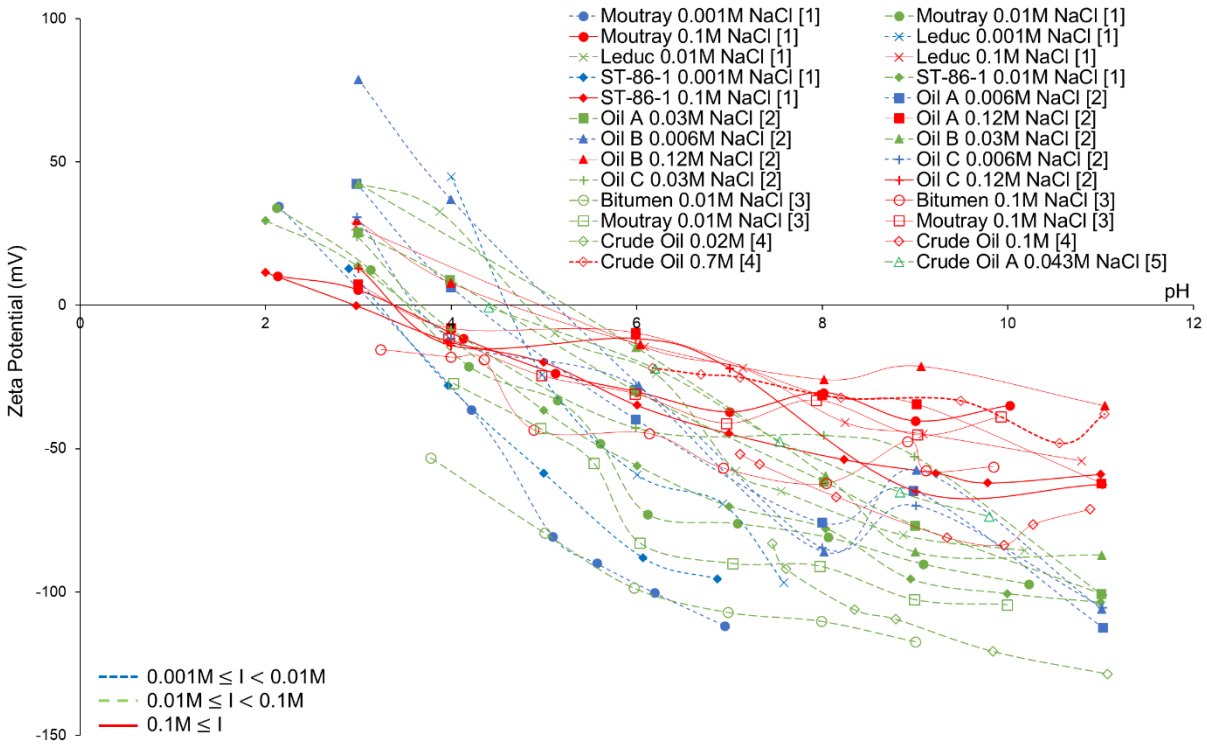

Figure 2-11: Published zeta potential data as a function of pH for crude oil in NaCl electrolytes measured using the EPM. Blue lines represent measurements obtained in the ionic strength range 0.001 < I ≤ 0.01 M; green lines in the range 0.01 < I ≤ 0.1 M and red lines at I > 0.1 M. Data from [1] Buckley et al. (1989) [2] Kolltveit (2016) [3] Chow and Takamura (1988) [4] Takeya et al. (2019) [5] Mahani et al.(2018).

It is generally accepted that the protonation/deprotonation of the interfacially active base/acid groups is the primary source of the surface charge at the oil-brine interface. Buckley et al.(1989b) proposed the following for the protonation/deprotonation reactions which have also been used in SCMs by other authors (Bonto et al. 2019; Tetteh et al. 2020; Brady et al. 2015):

$$> NH + H^+ \leftrightarrow > NH_2{}^+ \qquad \text{Log}K_{1a} = 5.25 \quad (2\text{-}8a)$$

$$> COOH \leftrightarrow > COO^- + H^+ \qquad \text{Log}K_{1b} = -4.75 \quad (2\text{-}8b)$$

where > represents a site on the oil-brine interface. The *K* values are those reported by Bonto et al. (2019) for their optimised model A. These reactions imply the surface charge is pH dependent and that increasing pH will yield an increasingly negative surface charge, and vice-versa. The pH dependency of the zeta potential can be observed in Figure 2-11.

The total surface charge (and zeta potential) will depend on the acid and base surface site density of the different oils. Indeed, there is a large range in the magnitude of the zeta potential measurements of different oils for a given pH and ionic strength (Figure 2-11) typically of around 50 mV or more at any given point, but particularly in dilute (10^{-3} mol/L) electrolytes around pH 4, where the range in zeta potential measurements can reach almost 100mV and include both positive and negative values. It is often assumed that the surface site density correlates directly with the bulk AN or BN (Buckley et al.1989b; Dubey and Doe 1993; Kolltveit 2016; Brady et al. 2015; Bonto et al. 2019; Takeya et al. 2019). Indeed, the iso-electric point (IEP) has been shown to correlate with the BN/AN ratio (Dubey and Doe 1993; Kolltveit 2016). The IEP is the pH at which the zeta potential is zero and the number of positive sites equals the number of negative sites (Hunter 1993). It has been argued that oils with a higher BN/AN ratio have a larger number of base sites to acid sites at the interface. To neutralise these sites, a greater proportion of the acid sites must be negatively charged to offset the positive charge of the base sites, which can be achieved by increasing the pH (Equations 2-8a and 2-8b) (Dubey and Doe 1993; Kolltveit 2016). However, this trend is not consistently observed across studies due to the weak correlation between bulk properties and interfacial activity as discussed previously. Furthermore, the IEP has been observed to change with the ionic strength (Kolltveit 2016) implying pH may not be the sole control on the surface charge.

These studies fail to consider the surface charge arising from non-polar hydrocarbons. Bonto et al. (2019) fail to model the data shown in Figure 2-11 by considering only equations (2-8a) and (2-8b) and so introduce a new pH dependent reaction to represent the affinity of the hydroxyl ion to the non-polar molecules:

$$> wOH \leftrightarrow > wO^- + H^+ \qquad \text{Log}K_2 = -8.93 \quad (2\text{-}9)$$

where >*w* represents a ‘weak’ surface site arising from a non-polar molecule and the *K* value is that reported by Bonto et al. (2019) for their optimised model A. They also constrict the weak surface site density in all models to 0.3 sites/nm^2, in line with the observations from Creux et al. (2009) that the surface site density of non-polar oils is independent of oil type.

2.2.4.2 Potential Determining Ions

The impact of the divalent cations Ca^{2+} and Mg^{2+} on the zeta potential of crude oil-brine emulsions has been studied by several authors. Figure 2-12 collates published data. For comparison, these data are plotted as a function of pPDI, the negative logarithm of the Ca^{2+} or Mg^{2+} concentration (in mol/L). The specific PDI and experimental pH are shown in the legend. The dashed line represents the trend line through all data obtained at a pH < 4 regardless of PDI. The dot-dash line represents the trend line through all data obtained at pH ≥ 7 regardless of PDI.

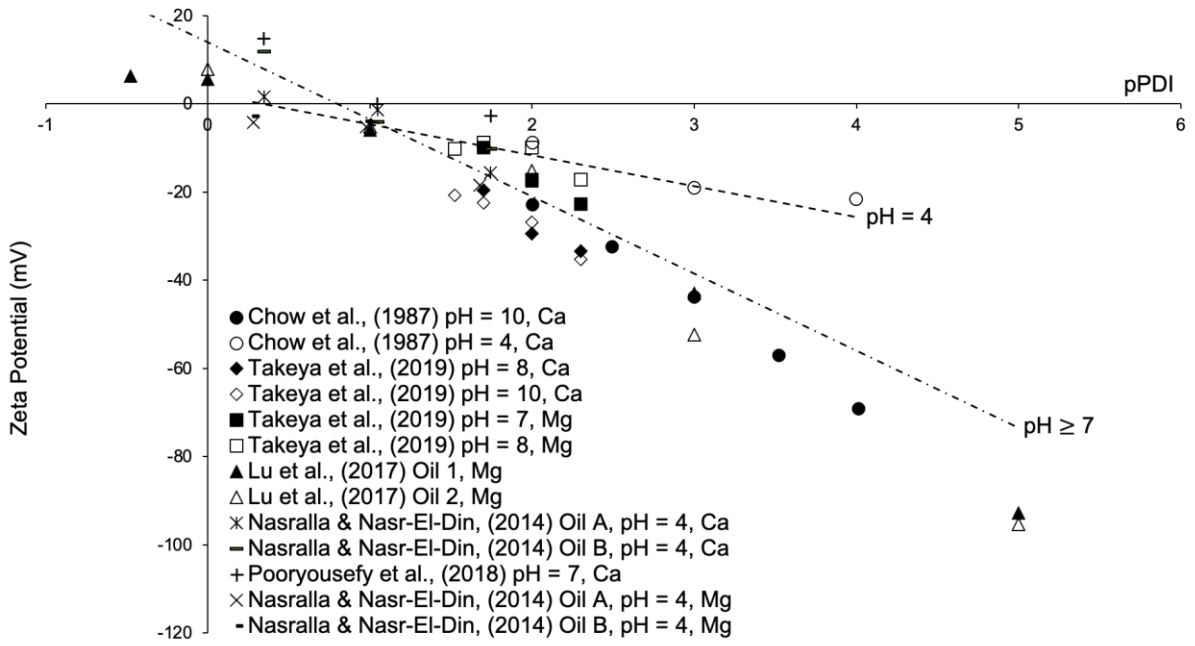

Figure 2-12: Published zeta potential data for crude oil in $CaCl_2$ and $MgCl_2$ electrolytes. Data plotted against pPDI, the negative logarithm of Ca^{2+} or Mg^{2+} concentration in mol/L. The value of pH is shown, when reported, in the legend. The dashed line represents the trend line through all data obtained at a pH < 4 regardless of PDI. The dot-dash line represents the trend line through all data obtained at pH ≥ 7 regardless of PDI.

The zeta potential is negative in the low concentration range (pPDI > 1) whilst charge inversion is observed at higher concentrations (pPDI < 0.5) with the point of zero charge (PZC) around pPDI = 0.5. For a given oil and pH a strong linear correlation between the zeta potential

and the pCa or pMg is observed, particularly in the low concentration range (pPDI > 1). This linear correlation, along with the ability of Ca^{2+} and Mg^{2+} to invert the polarity of the zeta potential suggests both ions act as PDIs to the crude oil surface. The sensitivity of the zeta potential to the concentration of both ions appears is comparable suggesting they interact with and modify the surface charge to a similar extent. However, there is some conflicting evidence. Takeya et al. (2019) report a more negative zeta potential values for their crude oil in the presence of Ca^{2+} compared to Mg^{2+} at a pH of 8. Nasralla and Nasr-El-Din (2014b) report a positive zeta potential at pCa = 0.34 and pH 4, but a negative zeta potential measurement for the same oil at a higher Mg^{2+} concentration of pMg = 0.28 and pH = 4.

Several authors (Tetteh et al. 2020; Brady et al. 2015; Bonto et al. 2019; Pooryousefy et al. 2018) have used the following reactions in their SCMs to model how Ca^{2+} and Mg^{2+} interact with the surface acid sites to modify the surface charge.

$$> COOH + Ca^{2+} \leftrightarrow > COO - Ca^{+} + H^{+} \qquad \text{Log}K_{3a} = -3.82 \qquad (2\text{-}10a)$$

$$> COOH + Mg^{2+} \leftrightarrow > COO - Mg^{+} + H^{+} \qquad \text{Log}K_{3b} = -3.47 \qquad (2\text{-}10b)$$

In addition, Bonto et al. (2019) proposed similar reactions could also occur at the weak sites they include in their model:

$$> wOH + Ca^{2+} \leftrightarrow > wO - Ca^{+} + H^{+} \qquad \text{Log}K_{4a} = -5.85 \qquad (2\text{-}11a)$$

$$> wOH + Mg^{2+} \leftrightarrow > wO - Mg^{+} + H^{+} \qquad \text{Log}K_{4b} = -5.85 \qquad (2\text{-}11b)$$

Equations (2-10a) – (2-11b) imply that the crude oil surface charge can be made more positive due to the divalent nature of the cations. In the presence of sufficiently high concentrations of the cations charge inversion may occur as observed in Figure 2-12. The similarity of the *K* values (in equations 2-10a and 2-11a; and 2-10b and 2-10b) imply that both ions have a similar affinity to the acidic surface sites and will modify the surface charge to a similar extent at the same pH and divalent cation concentration. However, this is not necessarily supported by the experimental data (Figure 2-12). Equations (2-10a) – (2-11b)

cannot explain the discrepancies in the zeta potential data of Nasralla and Nasr-El-Din (2014b) or Takeya et al. (2019).

Equations (2-10a) – (2-11b) further imply the interaction between the surface acid sites and the divalent cations is pH dependent. This dependency is evident from the experimental data in Figure 2-12. The gradient of the zeta potential as a function of pCa/pMg indicates the sensitivity of the surface charge to the divalent cation concentration. The gradient is pH dependent with two general trends apparent. For data obtained at a pH > 7 (dot-dash line) a steeper gradient than for data obtained at pH = 4 (dash line) can be seen. This change in gradient suggests an increased sensitivity and dependency of the zeta potential on the PDI with increased pH. Moreover, this pH dependency can be clearly seen for specific oils in the individual studies. Chow and Takamura (1988) show a large increase in the gradient of zeta potential against pCa for their oil when the pH was increased from 4 to 10. However, Takeya et al. (2019) show their oil exhibits little to no difference in the gradient as a function of pCa when increasing the pH from 8 to 10, or as a function of pMg when increasing the pH from 7 to 8. These observations suggest the oil may have limited dependency on the pH, or that the dependency on pH decreases at for pH > 7. No published data reports zeta potential measurements in the presence of Ca^{2+} or Mg^{2+} at pH values between 4 and 7 so it is not clear how the gradient changes in this range.

Figure 2-13 models how the state of the surface acid sites changes as a function of pPDI and pH based on equations (2-10a) and (2-11b). Plot (a) shows the interaction of the surface acid sites with Ca^{2+} whilst plot (b) shows the interaction of the surface acid sites with Mg^{2+}. Black lines correspond to a pH of 4 and red lines a pH of 7. In both plots, the curves are similar emphasising the proposed similarity between the extent of interaction of both ions with the surface sites. At pH of 4, only a small fraction of the surface sites exist in their negatively charged state across the range of pCa/pMg. Almost all sites are neutrally charged at high pCa/pMg and a fraction of these become positively charged as pCa/pMg decreases. Conversely, at a pH of 7, most of the sites are negatively charged at high pCa/pMg whilst

some are neutrally charged. This is consistent with the more negative zeta potential measurements at pH 7 compared to pH 4 in the low pPDI range in Figure 2-12. Decreasing pCa/pMg results in an increasing proportion of the surface sites becoming positively charged, consistent with the increasingly positive zeta potential measurements (Figure 2-12). The proportion of sites that are positively charged changes over a much broader pCa/pMg range at pH 7 than pH 4 indicating the increased sensitivity of the surface charge to the divalent cations at higher pH.

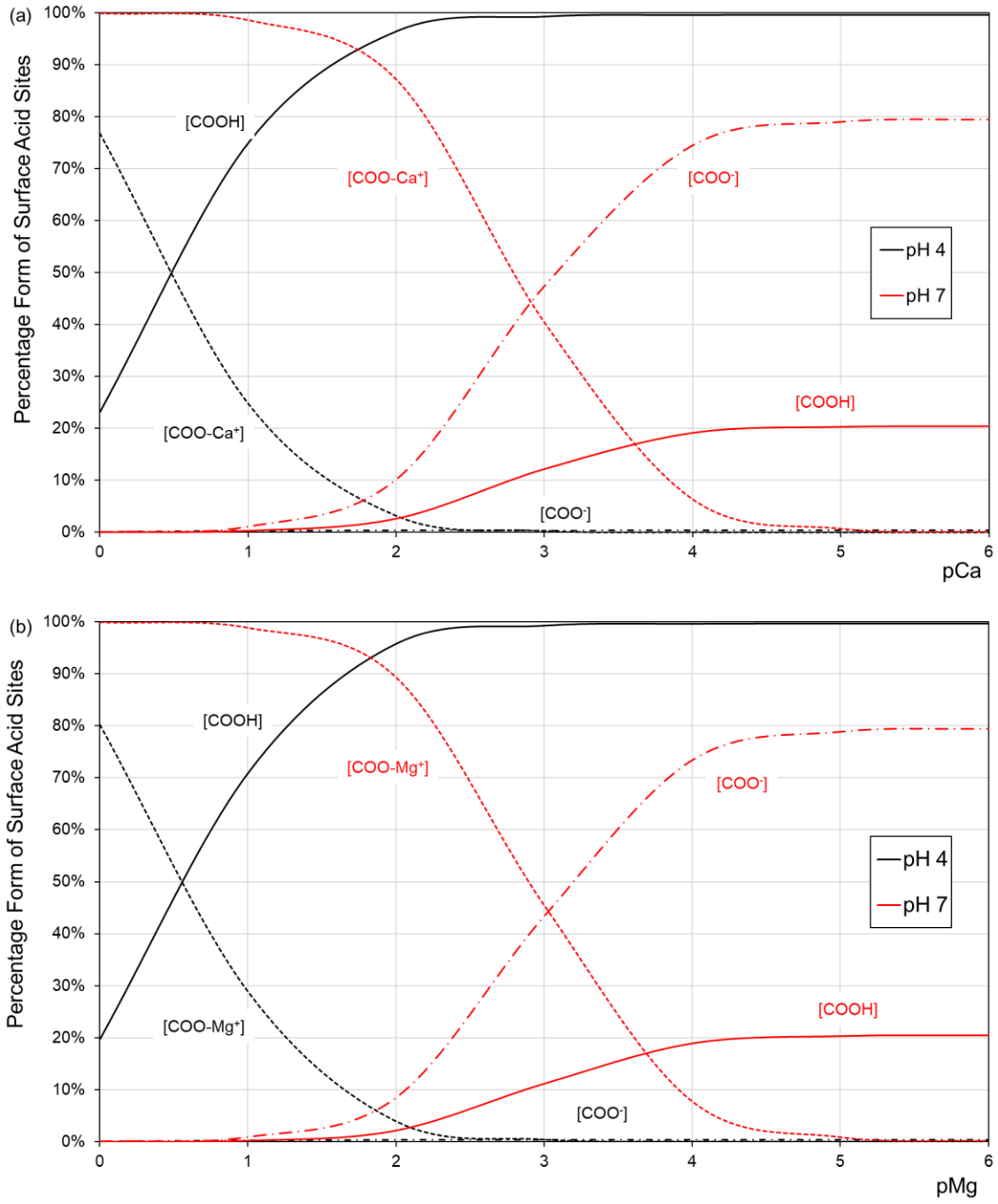

Figure 2-13: Surface complexation model showing the relative amounts of acidic species as a function of (a) pCa and (b) pMg. Solid lines represent neutrally charged acid species; dot-dashed lines represent negatively charged acid species and dashed lines represent positively charged acid-divalent cation complexes. Black lines represent pH 4 and red lines pH 7.

Although the pH is thought to be the primary control on the surface charge and the zeta potential of the crude oil-brine interface, SCMs have failed to model the experimental data shown in Figure 2-11 by considering only equations (2-8a) and (2-8b). Bonto et al. (2019)

showed that this approach typically led to over-estimations of the magnitude of the zeta potential. To account for the over estimation, they suggested that interactions with other ions may modify the surface charge. Na^+ may act as a PDI to neutralise some of the negatively charged surface sites through the following reactions:

$$> COOH + Na^+ \leftrightarrow > COO - Na + H^+ \qquad \text{Log}K_{5a} = -4.86 \qquad (2\text{-}12a)$$

$$> wOH + Na^+ \leftrightarrow > wO - Na + H^+ \qquad \text{Log}K_{5b} = -8.93 \qquad (2\text{-}12b)$$

The inclusion of Na^+ as a PDI is surprising as sodium is typically considered indifferent to most surfaces. The inclusion of equations (2-12a) and (2-12b) improved the model fit to the data shown in Figure 2-11 and reduced over-estimations of the magnitude of the zeta potential (Bonto et al. 2019). They concluded that equations (2-12a) and (2-12b) were necessary to the models.

The magnitude of the zeta potential decreases with increasing ionic strength in NaCl brines (Figure 2-11). This relationship is expected based on double layer collapse. If Na^+ is not a PDI to the crude oil surface and acts as an indifferent ion, then the zeta potential should be proportional to the logarithm of NaCl concentration (concentration is equivalent to ionic strength in a 1:1 electrolyte (Hunter 2013); see Al Mahrouqi et al. (2017a) for a similar argument for the calcite surface). Figure 2-14 plots the zeta potential measurements as a function of NaCl concentration for the data of Buckley et al.(1989b) and Kolltveit (2016) at a pH of 6. These data were chosen since the measurements were obtained at three or more NaCl concentrations. It is assumed the surface charge of each oil is consistent since the pH is the same in all measurements. Variation in the zeta potential is therefore considered to arise only from changes in the NaCl concentration.

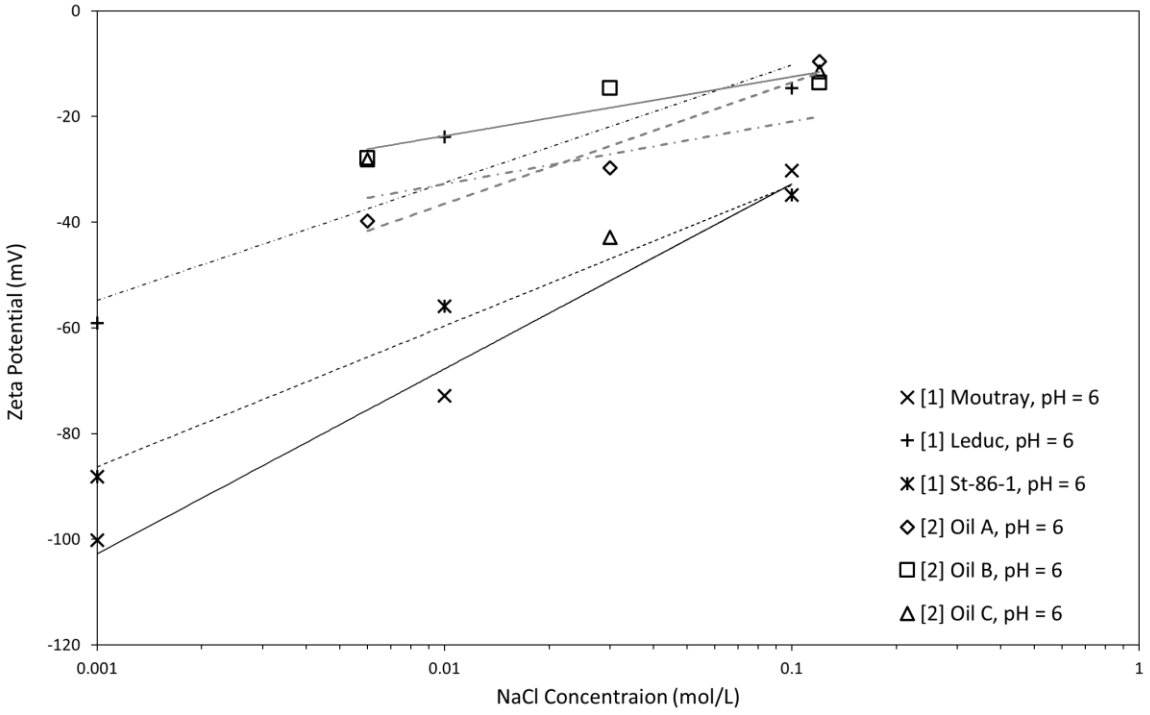

Figure 2-14: Zeta potential measurements on crude oil-brine emulsions as a function of NaCl concentration at a pH of 6. Reference [1] Buckley et al.(1989b); [2] Kolltveit (2016).

The sensitivity of the zeta potential to the NaCl concentration varies between different oils suggesting double layer expansion is not the only control on the zeta potential. Along with the conclusions of Bonto et al. (2019), Figure 2-14 suggests Na^+ may act as a PDI to the crude oil surface. Changes in the IEP with increasing NaCl concentration (Figure 2-11) provides further support to this notion.

2.2.4.3 Zeta Potential of Crude Oils at Reservoir Conditions

As with carbonates and sandstones, only a few studies have measured the zeta potential of crude oils at conditions relevant to subsurface reservoirs. Maintaining a stable dispersion of crude oil droplets in brine under high ionic strength and/or elevated temperatures is challenging, and thus conventional electrophoretic measurements of zeta potential are difficult to obtain.

Figure 2-15 collates published zeta potential measurements for the crude oil interface in the presence of complex, multi-ion brines representative of those found in the subsurface. The ionic composition of the brines used in these experiments are reported in Table 2-1. Plot (a) shows how the zeta potential varies as a function of pH in such brines whilst plot (b) shows data where the pH was not reported. Many of the trends observed in Figure 2-11 and Figure 2-12 are present in Figure 2-15. The zeta potential is positive at low pH and becomes increasingly negative with increasing pH (Figure 2-15 plot(a)) with an IEP around pH = 4. However, the impact of pH decreases with increasing ionic strength with the zeta potential of Crude Oil A in formation water reported by Mahani et al. (2017) largely independent of pH. The zeta potential increases in magnitude with increasing brine dilution and decreasing ionic strength. This is consistent with double layer expansion but also the reduction in PDI concentration (see equations 2-8a – 2-9b).

Table 2-1: Ionic composition of the brines used by various authors to represent those found in the subsurface.

		Concentration (mg/L)							
Reference	**Brine Code**	**Na**	**Ca**	**Mg**	**SO4**	**Cl**	**K**	**Sr**	**HCO3**
Mahani et al. (2017)	25dSW	536	20	65	135	967	19	1	7
	SW	13404	508	1618	3384	24141	483	17	176
	FW	49898	14501	3248	234	111812	0	0	162
Alshakhs and Kovscek (2016)	100dSW	172	0	21	43	310	0	0	0
	1000dSW	17.2	0	2.1	4.3	31	0	0	0
Mehraban et al. (2019)	SW	12653	498	1641	3037	23311	419	0	73
Tetteh et al. (2020)	FW	48000	11000	2800	260	101913	500	0	0
	SW	9600	2200	560	52	20383	100	0	0
	LS	585	134	34	3	1243	6	0	0
Takeya et al. (2019)	FW	12153	2133	320	72	22519	137	0	141
	SW	11345	441	1075	2676	18966	439	0	119
Jackson & Vinogradov (2012)	FMB	46420	14035	1134	241	99735	0	0	346
Jackson et al. (2016)	FMB	45960	16833	2211	192	107059	0	0	0

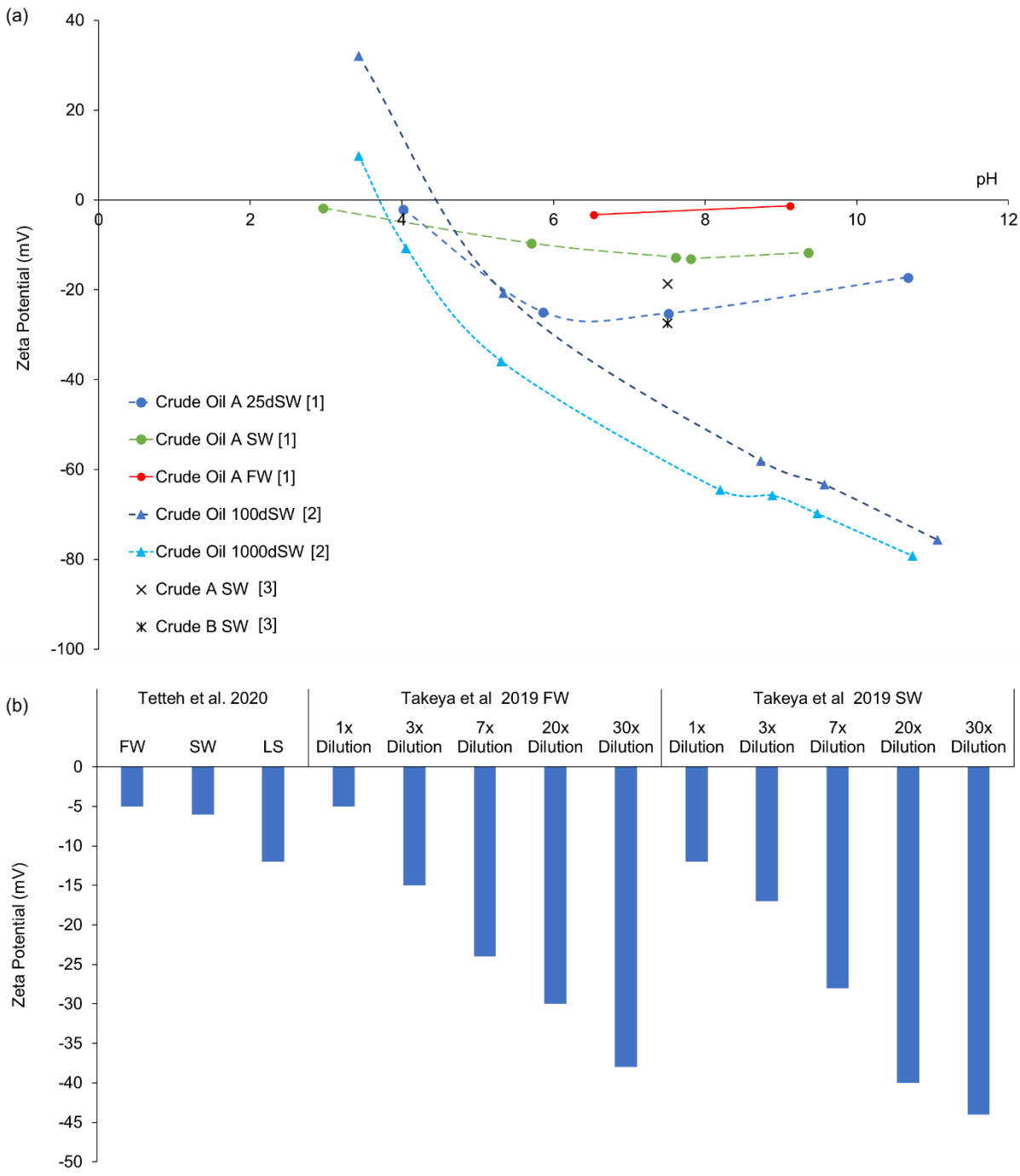

Figure 2-15: Published zeta potential data measured on crude oil emulsions in electrolytes containing mixtures of ionic species attempting to represent conditions found in natural subsurface environments. Plot (a) shows data as a function of pH where this was reported by the various studies [1] Mahani et al. (2017) [2] Alshakhs and Kovscek (2016) [3] Mehraban et al. (2019) Plot (b) shows data where the pH was not reported from Tetteh et al. (2020) and Takeya et al. (2019).

It has been shown that the zeta potential measured by the streaming potential method on natural carbonates saturated with brine and crude oil is affected by the wetting state. Jackson and Vinogradov (2012) measured a positive zeta potential on natural, water-wet

reservoir carbonates in a high salinity reservoir formation brine (FMB, Table 2-1) which became less positive after aging in crude oil. They proposed that the zeta potential at oil-wet mineral surfaces reflects the oil-brine interface rather than the mineral-brine interface in their model, a more negative zeta potential measured in an oil-wet sample is consistent with a negative zeta potential at the oil-brine interface. Jackson et al. (2016a) extended this work and reported a correlation between wettability and the change in zeta potential after aging in a different high salinity formation brine (FMB, Table 2-1). Of the four crude oils tested in their work, they found three yielded an increasingly negative zeta potential after aging, consistent with a negative oil-brine zeta potential (Figure 2-16). One crude oil yielded an increasingly positive zeta potential, consistent with a positive oil-brine zeta potential. The streaming potential method is potentially advantageous over electrophoretic measurements in measuring the zeta potential at reservoir conditions since it does not rely on the ability to maintain a stable dispersion and can therefore probe a wider parameter space. However, it does not provide a direct measurement of the oil-brine zeta potential. The approach of Jackson and Vinogradov (2012) and Jackson et al. (2016a) allows for an interpretation of the polarity of the oil-brine interface but not an accurate measurement of the magnitude.

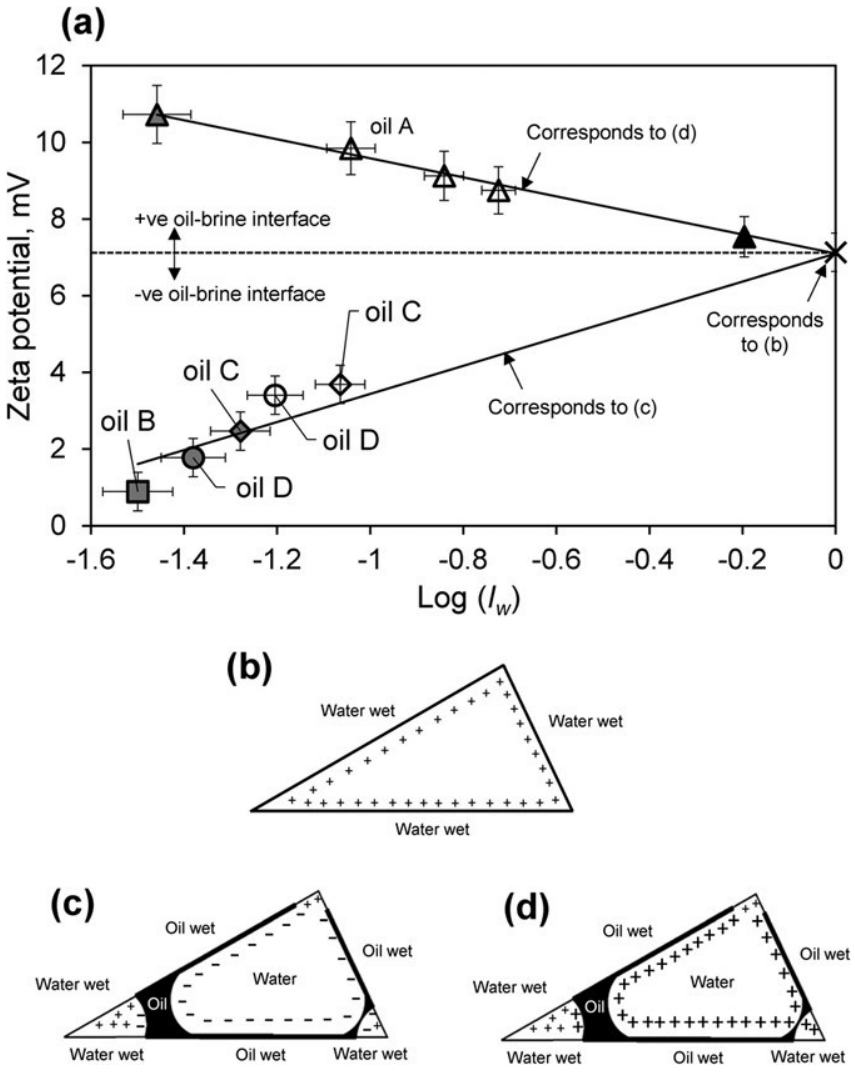

Figure 2-16: Plot (a) Zeta potential of intact Estaillades carbonate core samples as a function of Amott water wetting index after wettability alteration with different crude oils. Plot (b) model triangular pore showing positive charge on carbonate surface when fully saturated with water (c) change in surface charge after wettability alteration with a crude oil that has a negative charge at the oil-brine interface and (d) change in surface charge after wettability alteration with a crude oil that has a positive charge at the oil-brine interface. Figure from Jackson et al. (2016a).

Only three studies have examined the impact of temperature on the zeta potential of crude oil (Tetteh and Barati 2019; Lu et al. 2017; Mehraban et al. 2019). These data are collated and reported in Figure 2-17. Lu et al. (2017) report the temperature dependency of two crude oils in NaCl and $MgCl_2$ brines. The zeta potential of Oil 1 is independent of temperature whereas the zeta potential of Oil 2 decreases in magnitude with increasing temperature in dilute brines (<0.01 mol/L). In high concentration brines the zeta potential of both oils is independent of temperature. Tetteh et al. (2020) and Mehraban et al. (2019) report

zeta potential measurements in subsurface brines at 25 ^{O}C and 40 ^{O}C and 28 ^{O}C and 60 ^{O}C, respectively. Contrary to the data from Lu et al. (2017), the zeta potential increased in magnitude with increasing temperature in low salinity brine (Tetteh et al. 2020) and in seawater for two different oils (Mehraban et al. 2019). The zeta potential was independent of temperature in the higher concentration seawater and formation water (Tetteh et al. 2020).

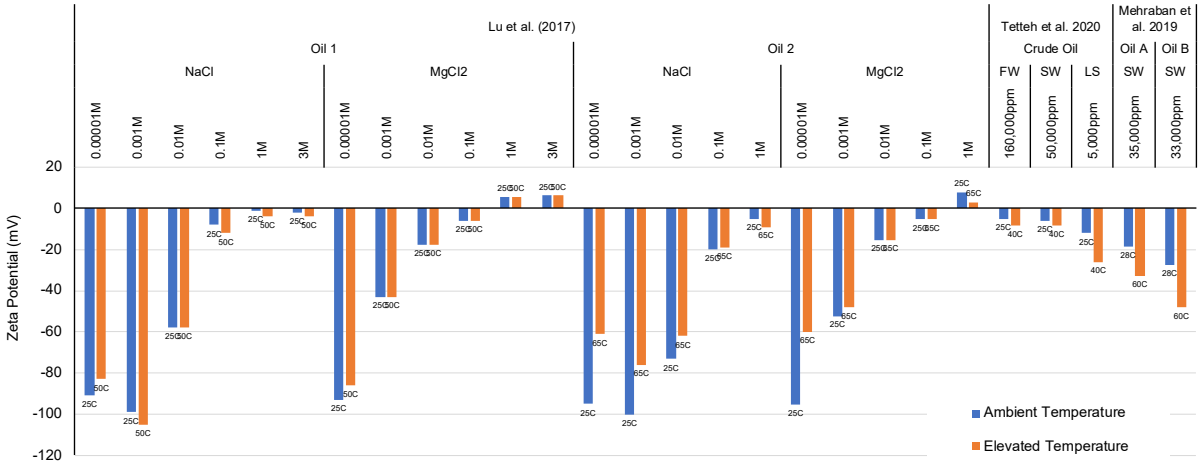

Figure 2-17: Published zeta potential data measured on crude oil emulsions in electrolytes at ambient laboratory (blue bars) and elevated (orange bars) temperature. The data labels correspond to the measurement temperature. The relevant study, oil and brine composition and ionic strength are listed above the data point. Electrolytes containing mixtures of ionic species to represent those encountered in natural environments are shown as FW (formation water), SW (seawater), and LS (low salinity brine) with the total dissolved solids listed below as reported by the relevant studies. Data from Tetteh et al. (2020); Mehraban et al. (2019) and Lu et al. (2017).

2.2.4.4 Comments

The zeta potential of the crude oil-brine interface is positive at low pH and becomes increasingly negative with increasing pH, which appears to be a primary control on the surface charge. The IEP where charge inversion occurs is in the pH range 3-5. The molecules responsible for the surface charge at the crude oil interface are unclear, although species containing carboxylic acid groups are thought to play an important role and have garnered the most attention. These can undergo interactions with the divalent cations Ca^{2+} and Mg^{2+} to modify the surface charge. Na^{+} may also be a PDI to the crude oil surface. However, there are significant gaps in understanding due to the limited data available. The role of basic amine groups at the interface, and their interaction with ionic species in the brine has largely been ignored. The zeta potential is thought to be negative at reservoir conditions but data supporting this notion is limited and conditions do not truly represent the subsurface due to experimental difficulties. Data highlighting the impact of temperature on the zeta potential is also limited and conflicting. Despite its importance for wettability alteration in the subsurface, the controls on the zeta potential of the crude oil-brine interface are poorly understood.

Significant gaps of knowledge surrounding the controls on the crude oil-brine interface therefore exist. As such, understanding of the interactions between crude oil droplets and mineral surfaces in the presence of brine to induce wettability altering interactions is limited. One of the major reasons for this is the limitations of existing experimental methods that are able to accurately probe the surface charge and/or zeta potential at relevant conditions. Better data is also needed to constrain modelling attempts to improve insight into the interfacial behaviour.

Chapter 3 - Zeta Potential in Intact Carbonates at Reservoir Conditions and its Impact on Oil Recovery During Controlled Salinity Waterflooding

---

The results and ideas presented in this chapter have been published in *Fuel as:*

Collini, H., Li, S., Jackson, M.D., Agenet, N., Rashid, B. and Couves, J., 2020. Zeta potential in intact carbonates at reservoir conditions and its impact on oil recovery during controlled salinity waterflooding. Fuel, 266, p.116927.

Abstract

This chapter presents zeta potential measurements obtained on natural intact carbonate core samples, saturated with brines of interest to CSW and at elevated temperatures representative of the subsurface. The impact of wettability alteration by aging with crude oil on the zeta potential of the core samples is explored with a range of crude oils. Some samples show a more positive zeta potential after aging whilst others show a more negative zeta potential after aging. The direction of change is interpreted to be indicative of the polarity of the zeta potential of the oil-brine interface. The data presented here represents a significant increase in the number of zeta potential measurements that are available in literature. The oil-brine zeta potential is interpreted to be positive in numerous cases and evidence of variable oil polarities depending on the experimental conditions is observed. During CSW, IOR is observed only if the change in zeta potential at the mineral-brine interface caused by changing the brine composition is of the same polarity as the oil-brine interface such as to induce an electrostatic repulsive force. Again, the number of CSW in tandem with zeta potential measurements presented here represents a significant increase in the available data.

3.1 Introduction

Carbonate reservoirs contain a substantial amount of the world's oil reserves, but recoveries are typically low (<40%) (Klemme and Ulmishek 1991). In chapter 2, we saw that there is substantial evidence that CSW in carbonates can lead to improved oil recovery. A common theme across the various mineral- to pore- scale mechanisms that have been proposed to underpin CSW is that they are associated with changes in the zeta potential at the carbonate mineral-brine interface (e.g. (Austad et al. 2012; Zhang and Austad 2006; Hiorth et al. 2010; Jackson et al. 2016a)).

It was also seen in Chapter 2 that the carbonate-brine zeta potential is primarily controlled by the concentration of the divalent cations Ca^{2+} and Mg^{2+} (see Chapter 2, Al Mahrouqi et al. (2017a)). However, measurements of the zeta potential in natural carbonates saturated with oilfield brines of interest at elevated temperature are scarce. This motivates the first aim of this chapter: to expand the existing experimental dataset by reporting measurements of zeta potential obtained in five intact reservoir carbonate samples and two outcrop carbonate samples, saturated with three synthetic formation brines, synthetic seawater, and three synthetic low salinity brines representative of those used in CSW. Data are obtained at laboratory temperature, and elevated temperatures relevant to oil reservoir conditions.

Previous studies have shown that the zeta potential in natural carbonates saturated with brine and crude oil is affected by the wetting state. It has been suggested that the change in zeta potential after wettability alteration is indicative of the oil-brine interface polarity (see Chapter 2, Jackson and Vinogradov (2012) and Jackson et al. (2016a)) since the zeta potential at oil-wet mineral surfaces reflects the oil-brine interface rather than the mineral-brine interface (Figure 2-9 (b)). Jackson et al. (2016a) found that of the four crude oils tested in their work three yielded an increasingly negative zeta potential after wettability alteration, indicating a negative oil-brine zeta potential consistent with literature data. The other crude oil yielded an increasingly positive zeta potential, consistent with a positive oil-brine zeta potential. This

result was unexpected and it is possible this result was an outlier, not typical of crude oils in general. Moreover, Jackson et al. (2016a) used only a single carbonate rock type. These observations motivate the second aim of this chapter: to expand the experimental dataset by reporting measurements of zeta potential after aging the five intact reservoir carbonate samples and two outcrop carbonate samples introduced above in three new crude oils.

Jackson et al. (2016a) also correlated changes in zeta potential observed in response to changing brine composition to IOR during CSW. They proposed a model for CSW in which IOR is observed only if the chosen injection brine yields a change in zeta potential at the mineral-brine interface that causes an increase in the electrostatic repulsion between the mineral-brine and oil-brine interfaces. This model has been tested so far only on one carbonate rock specimen and four crude oils. The third aim of this chapter is therefore to test their CSW model using the five intact reservoir carbonate samples, two outcrop carbonate samples and three new crude oils introduced above. Overall, the chapter reports a new suite of integrated experimental measurements of zeta potential and oil recovery during CSW in carbonates.

3.2 Materials and Methods

3.2.1 Materials

Table 3-1 summarises the materials used in this study. Samples of outcrop carbonates were used along with a range of reservoir samples. The crude oil samples labelled SR-A to SR-D were previously studied by Jackson et al. (2016a) and all measurements using these crude samples were made on samples of Estaillades natural carbonate rock. Artificial brines were prepared using deionised water and reagent grade salts.

Table 3-1: Materials used in this chapter. Oils SR-A to SR-D were previously reported by Jackson et al. (2016a).

Carbonate Core Samples

Sample	BA	BB	BC	BD	BF	BG	BH	TE	TR
Description	Reservoir	Reservoir	Reservoir	Reservoir	Reservoir	Reservoir	Reservoir	Outcrop	Outcrop
Permeability (mD)	10 ± 2	10 ± 2	120 ±20	10 ± 2	25 ± 5	10 ± 2	10 ± 2	85 ± 10	20 ± 5
Formation Factor (F)	35	20	25	20	50	35	20	40	20
Mineralogy	N/A	N/A	N/A	N/A	N/A	N/A	N/A	>99% Calcite	>99% Calcite

Brine Compositions (salt concentrations in ppm)

Brine Type	Formation Brine			Seawater	Low Salinity Brine		
Brine Name	BFB1	TFB1	BFB2	TSW	BLS1	TLS1	BLS2
NaHCO3	0	200	0	156	0	1	220
NaCl	89,442	109,550	177,440	29,000	648	760	90
CaCl2.2H2O	12,800	46,070	40,440	605	46	20	616
MgCl2.6H2O	12,827	11,240	21,040	405	186	296	903
KCl	0	0	2,190	900	0	35	13
SrCl2.6H2O	0	0	1,900	0	0	0	9
Na2SO4	0	140	1,020	26	0	87	1,000
NaBr	0	0	690	0	0	0	0
LiCl	0	0	30	0	0	0	0
TDS (ppm)	115,069	167,200	244,750	31,092	881	1,199	2,852
IS (mol/L)	1.99	3.03	4.29	0.53	0.01	0.02	0.05

Oil Properties

Oil Name	Acid Number (mg/KOH)	Base Number (mg/KOH)
SR-A	0.15	0.80
SR-B	0.20	1.77
SR-C	0.05	0.40
SR-D	0.20	1.20
Oil BD	0.05	0.60
Oil BM	0.20	1.80
Oil TT	0.34	0.41

3.2.2 Streaming Potential Measurements

3.2.2.1 Experimental Apparatus

Streaming potential measurements were made using the method of Vinogradov et al. (2010). Figure 3-1 shows a schematic of the experimental apparatus which is a modified version of a traditional core holder setup. Core samples are fully saturated with the brine of interest in a vacuum oven (not shown in Figure 3-1) at a pressure of -1 bar (-0.1 MPa) to remove any air inside the core. The sample is then placed inside the core holder and confined under a 20 bar (2 MPa) confining pressure. Bespoke core holder end caps made of polyether ether ketone (PEEK) ensure no metallic components are in contact with the core or the brine.

Two reservoirs either side of the core holder contain the brine of interest and a light mineral oil. The reservoirs are comprised of glass cylinders with PEEK endcaps to again ensure no metal is in contact with the brine. The mineral oil is used as a hydraulic fluid which passes through a pump to induce brine flow through the core holder. Using the mineral oil as a hydraulic fluid ensures the brine does not come into contact with any metal components in the pump; the pump does not need to be flushed of residual brine between experiments to avoid contamination; and creates a closed system which maintains a constant atmospheric pCO_2 (Song et al. 2017). All flowlines are comprised of perfluoroalkoxy (PFA) tubing, again ensuring the brine does not come into contact with metallic components.

The main modification from a conventional core holder setup is the inclusion of two Ag/AgCl electrodes situated either side of the core holder. The electrodes are bespoke and created by coating pure, smooth Ag rods (>99.99% purity) with a AgCl coating. This coating is applied electrochemically by oxidising chloride ions to form the AgCl coating on the Ag rods. The Ag/AgCl electrodes are situated in an NaCl electrolyte that is of a higher ionic strength than the experimental brine (typically 3 mol/L). This electrolyte bath is isolated from the experimental brine via a low permeability porous ceramic disc. The disc allows for electrical connectivity of the two fluids but prevents diffusion of ions into the NaCl electrolyte bath.

All components can be placed inside an oven (shown by the black box in Figure 3-1) to perform experiments at elevated temperatures up to 150 ^{O}C (Al Mahrouqi et al. 2016; Vinogradov and Jackson 2015). Experiments here were conducted at laboratory temperature, or at elevated temperatures of 70 ºC, 80 ^{O}C or 100 ^{O}C. A back-pressure regulator is used for elevated temperature experiments to prevent the formation of gas bubbles inside the core holder. Typically a back-pressure of 100psi (6.9 bar/0.69 MPa) was applied.

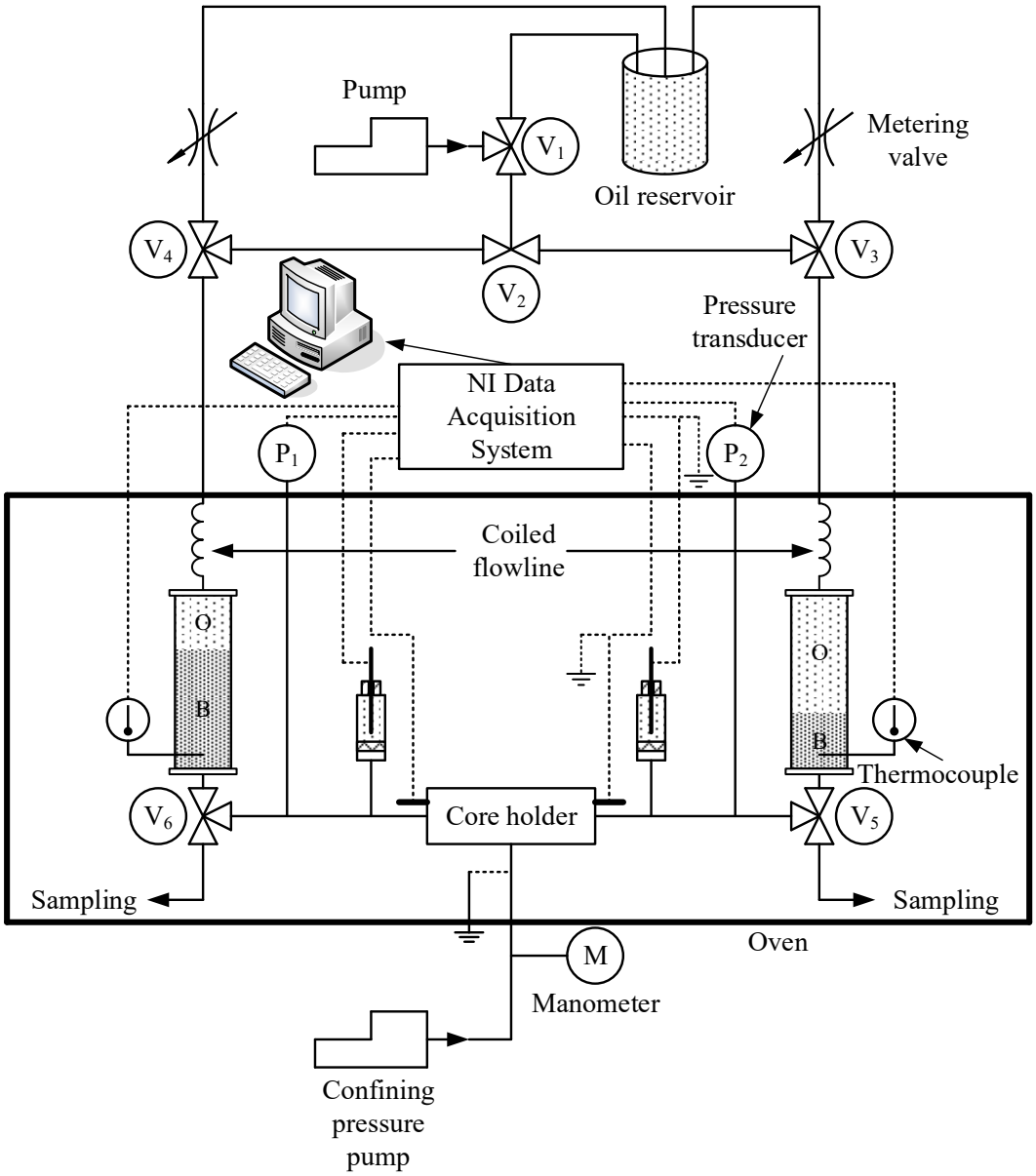

Figure 3-1: Schematic of the experimental apparatus used to measure the zeta potential (Vinogradov et al. 2010).

3.2.2.2 Experimental Procedure

Prior to each experiment the rock samples were equilibrated with the brine of interest for at least 24 hours. It has been shown that carbonate samples may take several hours to reach rock-fluid equilibrium due to dissolution/precipitation of calcite and other minerals (Alroudhan et al. 2016). In general, when dealing with complex reservoir brines equilibration was minimal and the effluent brine composition did not vary significantly or consistently from the initial brine composition, as determined by ion chromatography analysis. Rock-fluid equilibrium in carbonates takes longer when the brine contains minimal quantities of Ca^{2+}, Mg^{2+}, CO_3^{2-}, SO_4^{2-} and other ions that can readily precipitate/dissolve to for mineral species.

The pump is used to induce brine flow through the core via the mineral oil. The flow rate and pressure drop are allowed to stabilise and the stabilised values of pressure differential and voltage differential across the core holder were recorded for a given flowrate. Figure 3-1 shows an example of results from a typical experiment. Plot (a) shows the raw data that is recorded during an experiment showing the stability of the pressure and voltage differential measurements. Pressure differential values were typically stable to 0.1psi. The stability of the voltage differential values varied with salinity but in high salinity measurements they were typically stable to 10s of μV. The pressure differential was increased sufficiently high enough to observe a measurable change in the voltage differential signal. For some samples at high salinity the changes in voltage differential as the pressure differential changes are very small and thus large pressure differentials are required. It was observed that voltage differential signals were typically more stable when there was at least a pressure drop of 10-15psi across the core. Spikes in the voltage signal were commonly observed at low pressure drop.

Stabilised pressure and voltage differential measurements were recorded for several different flow rates, typically five to eight per zeta potential measurement, with flow reversed at each flow rate to ensure the pressure and voltage differential responses are symmetric with respect to flow direction. Negative values of pressure differential represent flow in the opposite direction through the core sample.

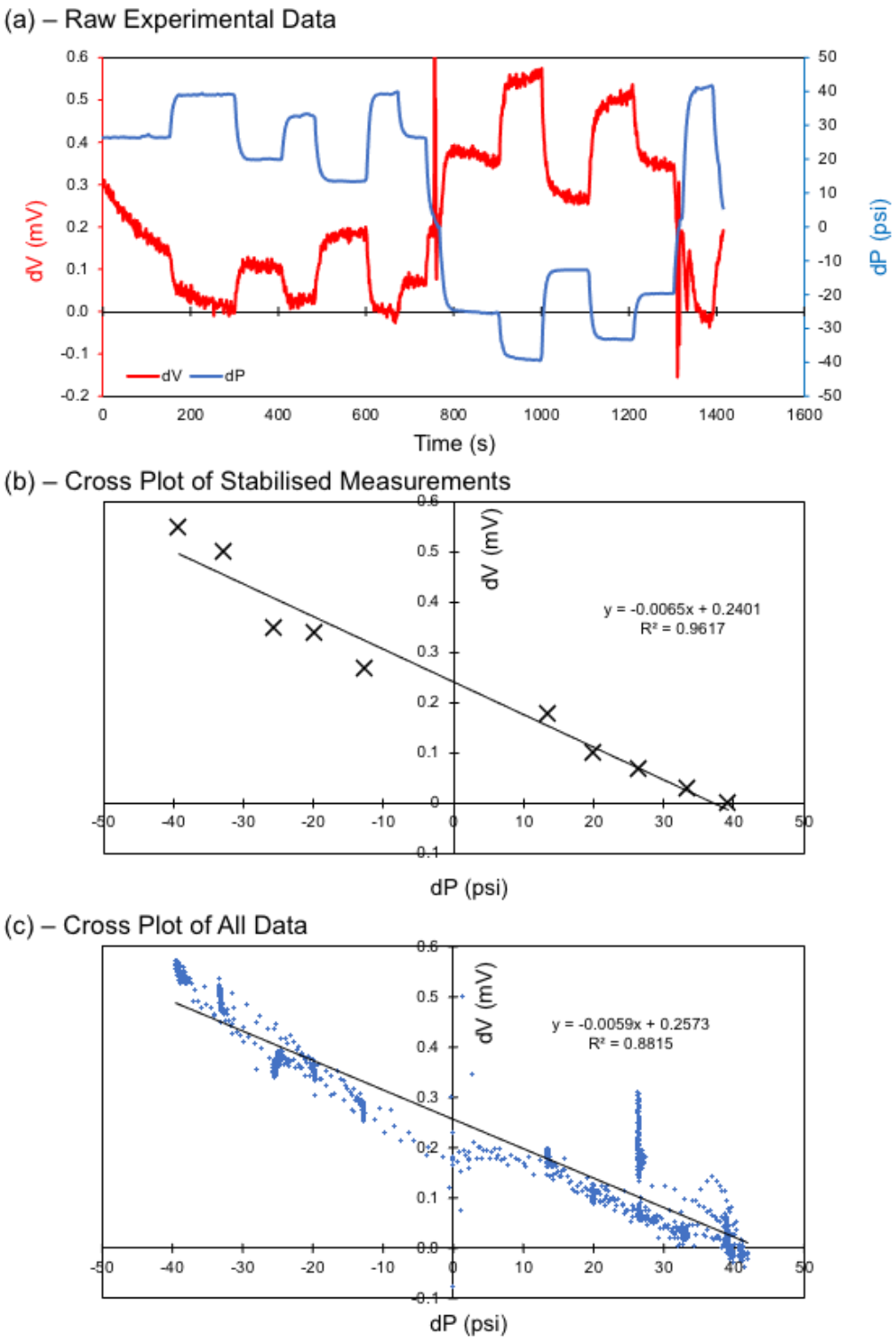

Figure 3-2: Example of typical streaming potential measurement. Plot (a) shows the raw pressure and voltage differential measurements recorded during the experiment. Plot (b) shows a cross plot of the stabilised values with a linear regression fitted. Plot (c) shows a cross plot of all the data points recorded during the experiment with a linear regression fitted.

The stabilised voltage differential was cross plotted against the stabilised pressure differential for each flow rate in each direction and a linear regression plotted through these points (Figure 3-2b). In an ideal experiment, the change in voltage differential as the pressure changes should be consistent at all times so for comparison a linear regression through all data points was also plotted (Figure 3-2c). The gradients of the two approaches were compared to ensure they were consistent, with any differences considered to be a source of error due to fluctuations and spikes in the voltage differential signal. The gradient of the two approaches was taken into account when determining errors in the measurements.

For confidence in the measurements, the streaming potential measurement was repeated. Typically, the sample would be left with brine flowing through at a constant pressure drop (usually around 20psi) for approximately 30 minutes at which point the flowrate would be changed and the resultant changes in pressure and voltage differential recorded again. If the gradient was consistent with previous measurements, then the experiment was concluded. If there were noticeable differences the sample was left for further time before repeating the measurement. Some samples were observed to take long periods of time (potentially up to two weeks) before measurements were consistent. There was not necessarily any obvious reason why this was the case but is thought to be due to small, pore-scale equilibration processes.

Samples of the effluent brine were collected following completion of the streaming potential measurements and the pH and electrical conductivity were measured. The conductivity of the brine saturated core sample was also measured.

3.2.3 Coreflooding Experiments

The coreflooding experimental workflow broadly followed that of Jackson et al. (2016a). Initially, mineral-brine streaming potential measurements were made using the methodology described above. Data were obtained at the temperature of interest for each of

the brines of interest (Table 3-1). The coreflooding procedure for a given sample began with the sample saturated in the aging brine of interest. The sample was then drained with the crude oil of interest at a low rate until the irreducible water saturation had been reached; the chosen rate depended on rock permeability but was typically in the range 0.01 – 0.5 mL/min (1.5×10^{-7} – 7.4×10^{-6} m/s). A minimum of 10 pore volumes (PV) of the crude oil were drained through the core. The core was then statically aged in an Amott cell at 80 ^{O}C for a minimum of four weeks, immersed in the aging crude oil. Following aging, the oil in the Amott cell was replaced with the aging brine and a spontaneous imbibition test was performed for a further three weeks at the chosen coreflooding temperature.

The volume of water spontaneously imbibed was recorded and the sample was then loaded into the coreholder and waterflooded with the aging brine until the first residual oil saturation (S_{or}) was reached, identified when coreflooding of at least 2 PVs yielded no additional oil. The volume of oil recovered was recorded as a function of PV injected, along with the flowrate of brine and the pressure drop across the core. Wettability change was characterised by the Amott water wetting index (see equation (2-2a), section 2.1.1.2II). The injection brine was switched to the controlled salinity brine of interest and any additional oil recovered by the CSW brine measured.

To ensure consistency across corefloods, the flowrate was chosen to ensure the capillary number was similar in magnitude. The capillary number used is defined as:

$$Ca = \frac{\mu_w L Q}{\gamma . A \sqrt{\Phi . k}} \qquad (3\text{-}1)$$

where γ is the interfacial tension of the oil-brine, assumed to be 35 mN/m for all crude oils. The remaining properties were all measured or calculated as part of the standard workflow. L is the sample length, A is the sample cross sectional area, ϕ the sample porosity, k the single-phase permeability and Q the volumetric flow rate through the core, which was varied across experiments to keep the capillary number consistent. Capillary numbers used in corefloods were initially of the order 0.05 (all properties defined in SI units) with high flowrate ‘bumps’ at

capillary numbers of approximately 0.08, 0.15 and 0.5 conducted when the residual saturation had been reached, to ensure any increases in oil recovery observed upon CSW brine injection were not the result of capillary end effects.

At each residual oil saturation, when there was only brine flowing through the core, the streaming potential was measured again. The procedure was slightly different to that described previously. Since the core flood experiments are conducted in only one direction and the capillary number dictated the maximum flowrate (and pressure differential) that was applied, the flowrate was gradually decreased and the resultant change in the voltage differential measured. The gradient of the linear regression through both the stabilised values and all the data was determined in the same way as in Figure 3-2. It was assumed that electrode polarisation effects were negligible. During these measurements brine is the only mobile fluid phase since mobile oil will disrupt the voltage differential signal.

For repeat experiments, samples were cleaned in a Soxhlet unit using toluene and methanol heated under reflux for several days, with regular replacement of the solvents until there was no further colour change of the solvents in the lower flask. Samples were dried for 24hrs to remove residual solvents. Petrophysical properties were then measured again to confirm cores had returned to their original state.

3.2.4 Interpretation of the Zeta Potential

3.2.4.1 Single-Phase Measurements

The gradient of the linear regression through the cross plot of voltage differential against pressure differential (Figure 3-2) gives the streaming potential coupling coefficient, *C*. The zeta potential is then interpreted using a form of the Helmholtz-Smoluchowski equation given by Li et al. (2016) which corrects for surface conductivity if significant:

$$C = \frac{\partial V}{\partial P} = \frac{\varepsilon_w \zeta}{\mu_w \sigma_{rw} F} \qquad (3\text{-}2)$$

The intrinsic formation factor ($F = \sigma_{wh}/\sigma_{rwh}$) represents the ratio of brine electrical conductivity (σ_{wh}) to saturated rock electrical conductivity (σ_{rwh}), measured using high ionic strength electrolyte (denoted by the subscript *h*) to ensure the contribution of surface electrical conductivity is negligible. Both properties were measured as part of the routine streaming potential measurement procedure. The brine viscosity (μ_w) and permittivity (ε_w) were calculated using published correlations based on the electrical conductivity (Jackson et al. 2012).

Equation (3-2) is classically derived by considering flow of fluid (brine) through a charged capillary or past a charged surface. The relative motion of charge in the mobile portion of the diffuse layer along the shear plane to the immobile charge inbound of the shear plane gives rise to a streaming current. To ensure steady flow conditions when there is zero flux of charge, the streaming current is balanced by an equal but opposite conduction current. The balance of these two currents yields equation (3-2). A full derivation can be found in section 5.2.1.

The streaming current is determined by multiplying the flowrate in the capillary by the charge density. In a capillary tube or porous media both the flowrate and the charge density will vary across the capillary area and so the total streaming current is determined by integrating across the entire capillary area. In deriving equation (3-2) the “thin double layer assumption” is invoked. This states that the size of the electrical double layer (where the mobile charge is contained) is small relative to the capillary size. Consequently, it can be assumed that in the centre of the capillary, far from the charged surface, charge neutrality is ensured, and the resultant charge density is zero. The total streaming current can be determined by integrating the streaming current from the centre of the capillary, where the charge density and electrical potential is zero, to the shear plane, where the electrical potential is described by the zeta potential (see Hunter, 1981 and 5.2.1 for full equations).

There is no assumption about, or requirement for the charge density distribution in the electrical double layer, only that it obeys Poisson’s equation (Hunter, 1981). Thus, as long as

the Poisson equation holds, there is no restriction on the electrolyte ionic strength which equation (3-2) can be applied to. Whilst many authors substitute the Poisson-Boltzmann equation which is dependent on the ionic strength (Hunter, 1981) it is not a requirement to do so. Furthermore, equation (3-2) is not dependent on the structure of the electrical double layer between the shear plane and the charged surface and only assumes the fluid is unaffected by the presence of the electrical field (Hunter, 1981). Thus, the only core assumptions in deriving equation (3-2) are (i) that some mobile charge exists at the shear plane and (ii) the "thin double layer assumption" is valid.

In most conventional porous media, the "thin double layer assumption" has been shown to be valid for the range of electrolyte ionic strengths that are typically encountered (Jackson and Leinov, 2012). Typical pore sizes are on the order of 10^{-6}m whilst the electrical double layer will be on the order of 10^{-10}m for high ionic strengths typical of reservoir formation brines and 10^{-8}m for lower ionic strengths typical of low salinity brines. Thus, the pore area is usually several orders of magnitude larger than the size of the electrical double layer. In fact, the "thin double layer assumption" is more likely to be valid in high salinity formation brines. The validity of the assumption, and the application of equation (3-2) may break down in sandstones with small-moderate pore sizes (10^{-7}m) when saturated with very dilute or freshwater brines, or in mudstones/shales where the pore sizes are on the order 10^{-9} – 10^{-7}m. Carbonate samples are known to exhibit a broader and more heterogeneous pore size distribution and the "thin double layer assumption", and the use of equation (3-2) to calculate the zeta potential may be invalid in the smallest pores. However, the flow of brine through such samples will be dominated by the flow through larger pore sizes and thus the flux of charge through the porous media will be dominated by flow in the larger pores where equation (3-2) is valid. It is assumed that the smallest pores will contribute negligibly to the total streaming current and in general, the "thin double layer assumption" and equation (3-2) remain valid in such cases.

The final assumption of importance to equation (3-2) is that the surface can be considered flat, smooth and homogeneous. Whilst this is certainly not the case for most mineral surfaces, it has been shown that the surface can be considered as such if the local radius of curvature is large compared to the size of the electrical double layer. This is assumed to be valid in most cases and, as with the “thin double layer assumption”, is more likely to be valid under conditions of high ionic strength.

3.2.4.2 Multi-Phase Measurements

Equation (3-2) is also used to calculate the zeta potential of the core samples from the streaming potential measurements obtained at the residual oil saturation after wettability alteration and waterflooding. The streaming potential coupling coefficient is determined from the gradient of the linear regression fitted through the cross plot of the voltage differential measurements against the pressure differential measurements.

During these measurements, brine is the only mobile phase through the core samples. In oil-wet porous media, the oil coats the pore surface and modifies the electrical surface charge due to interactions with the polar species in the oil (Figure 2-9). Brine flow through oil-wet pores will therefore be confined largely to the centre of the pore space and at the residual oil saturation, the majority of oil residing in oil-wet pores will be confined to the thin wetting layer. It is assumed that this wetting layer is volumetrically insignificant relevant to the pore size and will not modify the pore size radius enough to invalidate the “thin double layer assumption”. The flow profile of the mobile brine though oil-wet porous media will be largely similar to that of the single-phase measurements, except that the charge that is carried and the resulting streaming current will be dependent upon the surface charge of the oil. Oil-occupied pores are assumed, regardless of wetting state, to neither contribute to the streaming or conduction currents since flow of brine in these pores will be negligible and oil is assumed

to be non-conductive (Jackson, 2010). Therefore, these pores have no contribution to the zeta potential. Equation (3-2) is therefore assumed to be valid under oil wet conditions.

Under mixed-wet or more water-wet conditions, the characteristics of multi-phase flow are more complex. In such cases, brine flow in the corner of pores and within water-wetting films become important. The streaming current within these films may not be negligible and moreover, the “thin double layer assumption” may become invalid since the effective pore radius has been reduced due to the presence of the oil. The surface charge of the oil-brine interface may also influence the charge distribution within the thin wetting layer. The streaming and conduction currents through such porous media may not necessarily follow the same paths and the distribution of the residual oil within the pore space may therefore influence the zeta potential. Equation (3-2) may therefore break down in such cases and its validity to determining the zeta potential of mixed- or water-wet porous media may be questionable. More advanced models may be required to accurately interpreted the zeta potential in these cases, particularly if the oil is mobile along with the water.

3.3 Results

3.3.1 Carbonate-Brine Zeta Potential

The zeta potential of the carbonate-brine interface is necessary to understand how modifying the injection brine composition changes the electrostatic forces acting at COBR interfaces during CSW. Figure 3-3 shows zeta potential measured at ambient conditions on the intact outcrop and reservoir carbonate samples investigated here, saturated with complex brines typical of those used in CSW (Table 3-1). The equilibrium pH of the effluent brine is also reported for each measurement.

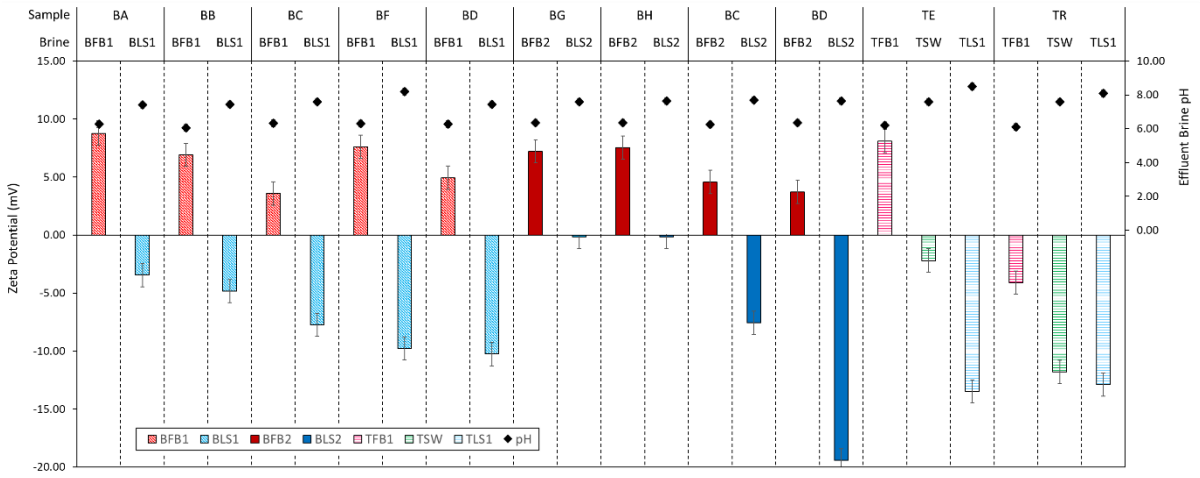

Figure 3-3: Mineral-brine zeta potential measurements at ambient conditions for the carbonate samples and brines reported in Table 1. Bars represent zeta potential with the different shades and colours corresponding to different brines; diamonds show equilibrium effluent brine pH.

Generally, the zeta potential in formation brines was positively charged and small in magnitude (< 10 mV), consistent with previous published data (e.g. Al Mahrouqi et al. (2017a) and reflecting the high concentrations of Ca^{2+} and Mg^{2+} (Table 3-1). However, a notable exception was sample TR. This was the only carbonate sample reported to date which has returned a negative zeta potential in formation brine. Seawater saturated samples yielded negative zeta potential values that are again small in magnitude (<5 mV) and again consistent with those reported previously (e.g. Al Mahrouqi et al. (2017a). In the low salinity brines, the

zeta potential was always negative, but with a large variation in magnitude across the different samples, with sample BD returning -19 mV but samples BG and BH only –1 mV. Note that the change in streaming potential during the experiments on BG and BH was clearly in the opposite sense to the change in pressure (see Alroudhan, Vinogradov, and Jackson (2016) for examples of raw streaming potential and pressure data) so there is confidence in the polarity of the zeta potential, despite the small magnitude.

Variations in the magnitudes for different samples or different brines would be expected based on previous published data (Al Mahrouqi et al. 2017a; Alroudhan, Vinogradov, and Jackson 2016). However, samples BC and BD are from the same subsurface reservoir formation yet returned zeta potential measurements that differed significantly in magnitude, especially in low salinity brines; moreover, samples TR and TE are compositionally indistinguishable, but returned not only differences in the magnitude of the zeta potential, but also opposing polarity when saturated with the same brine. Repeat measurements on these same samples with the same brines confirmed the data reported here.

There is no observed correlation between the variable zeta potentials observed across the samples and other parameters that are known control zeta potential in carbonates. The equilibrium brine pH was typically in the range 5-8, increasing with decreasing brine salinity and correlating with pCa, consistent with the trend reported by Al Mahrouqi et al. (2017a). However, no correlation between zeta potential and pCa and/or pH was observed that could explain the variability between samples for the same brines. Measurements of pCa in the effluent brine showed no significant differences from the values given in Table 1, so did not measurably change during equilibration. The variable zeta potentials may reflect differences in the texture, structure and mineral distribution across samples, or trace impurities and organic material on the mineral surfaces (Alroudhan, Vinogradov, and Jackson 2016; Li et al. 2020).

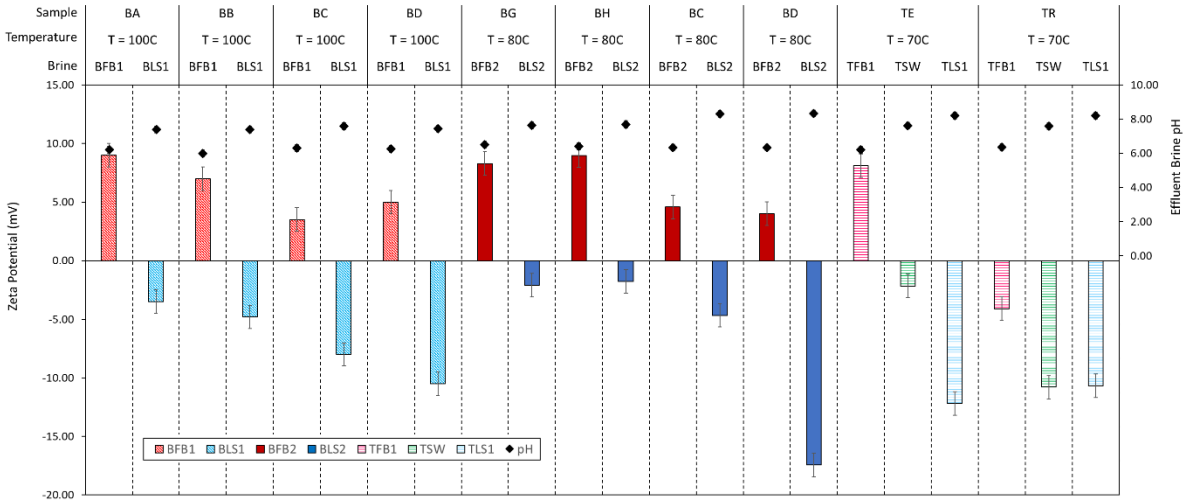

Figure 3-4: Mineral-brine zeta potential measurements at elevated temperature conditions for the carbonate samples and brines shown in Figure 3 and reported in Table 1. Bars represent zeta potential with the different shades and colours corresponding to different brines; diamonds show equilibrium effluent brine pH.

The main trends observed at laboratory temperature were replicated at elevated temperature (Figure 3-4). Zeta potential measurements were positive in formation brine, except for sample TR which again returned negative zeta potential. The zeta potential for all samples was negative in seawater and the dilute brines. The pH again correlated with pCa, and no consistent or significant changes in equilibrium pH were observed between ambient and elevated temperature.

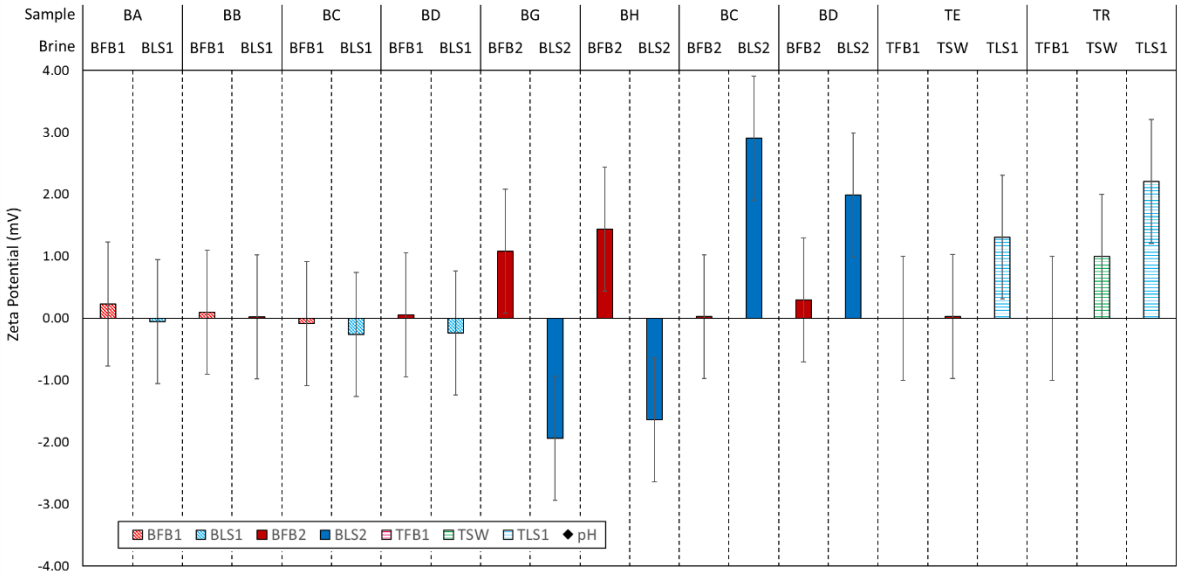

Figure 3-5: Change in zeta potential from ambient to elevated temperature for the carbonate samples and brines shown in Figure 3-3 and Figure 3-4 and reported in Table 3-1

Overall, the data suggest that temperature does not play a consistent or significant role in modifying zeta potential for carbonates saturated with complex, mixed brines. Of the samples and brines tested here, the zeta potential was identical within experimental error at low and high temperature for 14 of the 22 carbonate/brine combinations tested (Figure 3-5). In the remaining 8 carbonate/brine combinations, the zeta potential became more positive in formation brine at high temperature for two carbonate samples, and more negative at high temperature in dilute brine for the same two samples. However, the zeta potential became more positive in seawater and dilute brine in the other samples. No change in pH outside of experimental error was observed between ambient and elevated temperature. Thus, the change in zeta potential caused by changing the brine composition (which is termed here $\Delta\zeta_{CSW}$) was essentially independent of temperature (Figure 3-6). Injection of a dilute brine, as in a conventional low salinity waterflood, yields a more negative zeta potential at the mineral-brine interface irrespective of temperature and carbonate sample tested. However, the magnitude of the change in zeta potential depends on carbonate sample, with the smallest change observed of -8 mV for sample BG and BH at laboratory temperature, and the largest of -24 mV observed for sample BD, also at laboratory temperature (Figure 3-6).

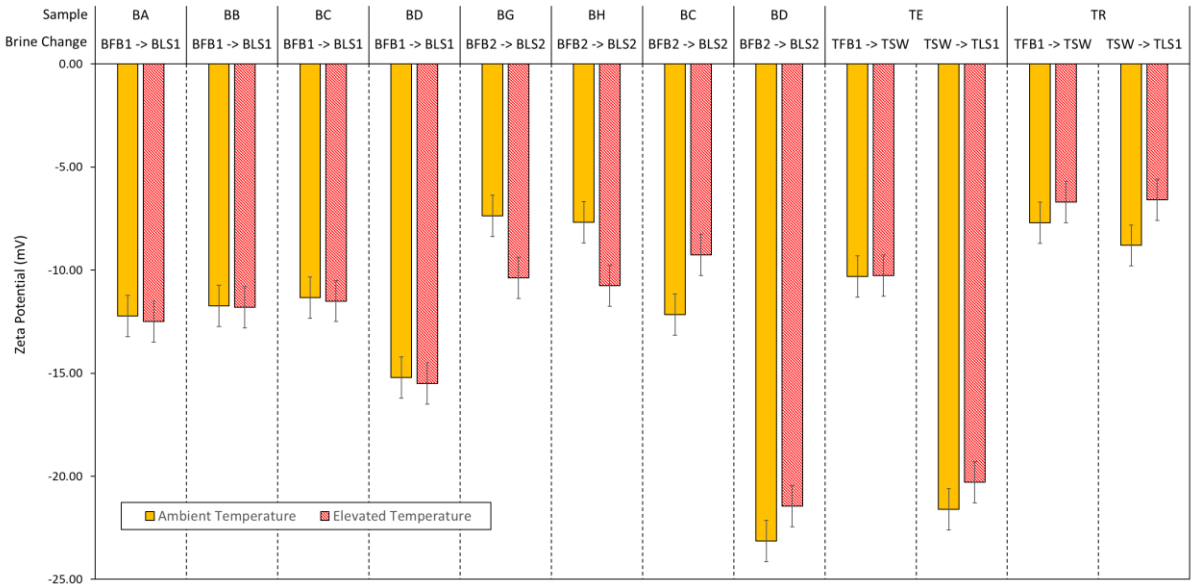

Figure 3-6: Change in zeta potential between high and low ionic strength brines at both ambient and elevated temperature for various carbonate samples and brine compositions.

3.3.2 Zeta Potential and Wettability

Figure 3-7 shows the effect of wettability alteration on the zeta potential for several different samples and crude oils initially saturated with formation brine. The zeta potential of the fully water saturated samples ($S_w = 1$) and the same samples at residual oil saturation ($S_w = 1 - S_{or}$) after aging are shown, along with the difference between these two values (which is termed here $\Delta\zeta_{wett,}$) which represents the change in zeta potential caused by wettability alteration.

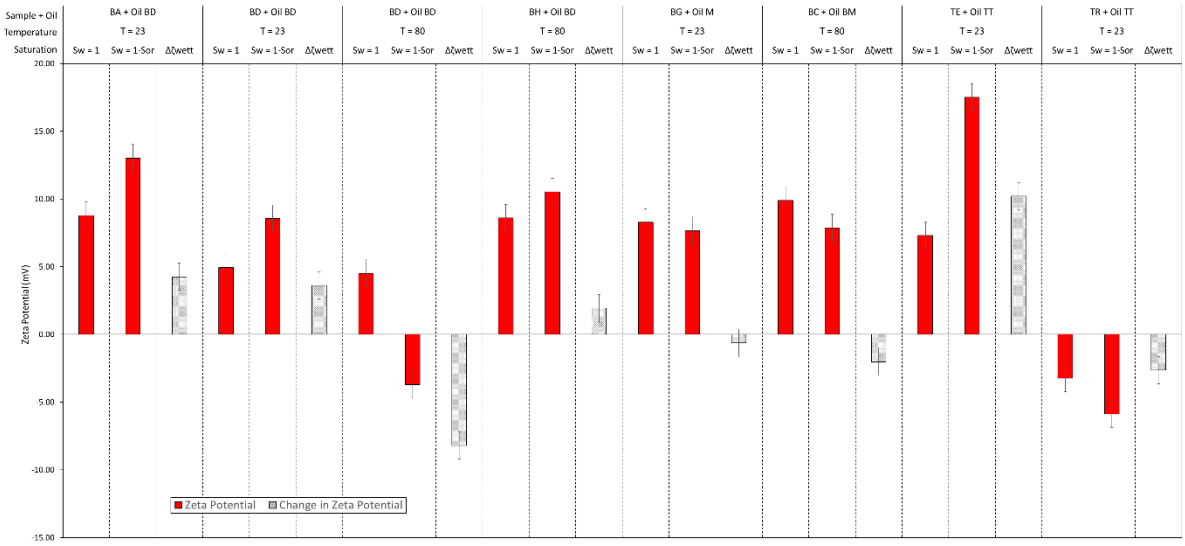

Figure 3-7: Zeta potential measurements made at $S_w = 1$ and $S_w = 1 - S_{or}$ in samples aged when saturated with formation brine and crude oil, along with the difference between these values (Δζwett). The temperature here reflects the temperature at which the zeta potential was measured. Aging of the samples was always undertaken at elevated temperature (see section 3.2).

In this work, three crude oils were used. Aging in Oil BM and formation brine consistently caused the zeta potential to become more negative, irrespective of the carbonate sample used or the experimental conditions. Aging in Oil TT and formation brine caused the zeta potential to become more positive in sample TE, but more negative in sample TR. This is the only combination of crude oil and carbonate sample in which the change in zeta potential after aging is sample specific across all the crude oils and carbonate samples tested here and by Jackson et al. (2016a). The change in zeta potential of samples aged in Oil BM was

measured at ambient and elevated temperature and was always of the same polarity. In contrast, aging in Oil BD and formation brine caused the zeta potential to become more positive at laboratory temperature, but more negative at elevated temperature (Figure 3-7). The magnitude of the change in zeta potential varied across samples, crude oils and experimental conditions as with the single-phase mineral-brine zeta potential measurements. Oil BM typically caused a smaller change in the zeta potential after aging of approximately -1mV whereas Oil BD caused a much larger change of up to +5mV. Oil TT showed a very large change in sample TE of +10mV but a smaller change in sample TR of -3mV.

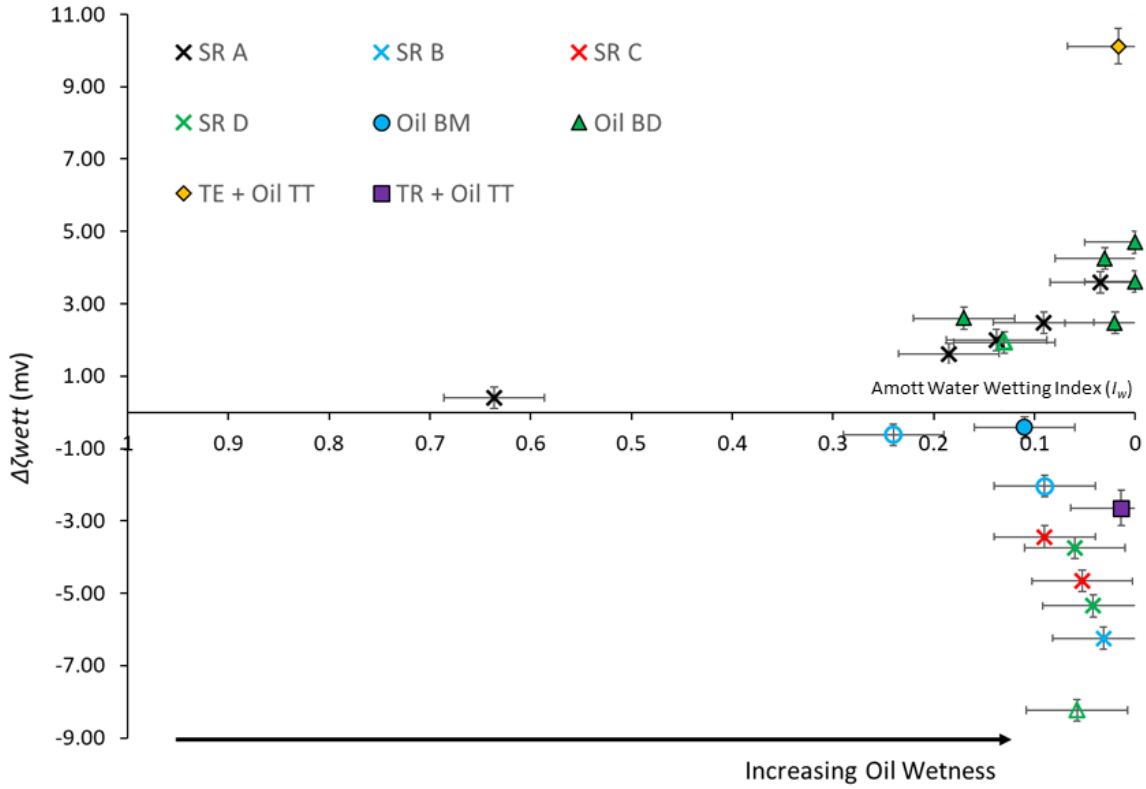

Figure 3-8: Change in zeta potential measured in formation brine after aging for a range of crude oils, carbonate samples, formation brine compositions and temperatures. Filled symbols represent data obtained at ambient temperature. Open symbols represent data obtained at elevated temperature. Data for oils SR-A to SR-D previously reported (Jackson et al. 2016a) and shown by crosses. TE+Oil TT denotes the results of aging sample TE in crude oil TT; TR+Oil TT denotes the results of aging sample TR in crude oil TT. All other crude oils showed similar behaviour irrespective of rock sample, so the rock sample is not reported.

A plot of $\Delta\zeta_{wett}$ against the Amott water wetting index (I_w) for each crude oil and shows two main trends (Figure 3-8). Filled data points represent measurements made at ambient temperature and open data points represent measurements made at elevated temperature. For ambient temperature results, two crude oils (SR-A, BD) show an increasingly positive zeta potential with decreasing I_w and increasing oil wetness. Four crude oils (SR-B, SR-C, SR-D and BM) show an increasingly negative zeta potential with decreasing I_w and increasing oil wetness. Oil TT deviates from these trends, showing both a positive and negative change in zeta potential after aging in formation brine that is dependent on carbonate sample type. Oil BD also exhibits both positive and negative changes dependent on the temperature, as noted previously.

Jackson and Vinogradov (2012) and Jackson et al. (2016a) interpreted the change in zeta potential after aging in terms of the zeta potential at the oil-brine interface. They argued that a positive change in $\Delta\zeta_{wett}$ is consistent with a positive zeta potential at the oil-brine interface and vice-versa because, after aging and wettability alteration, the oil-wet mineral surfaces return the zeta potential of the oil-brine interface rather than the mineral brine interface (**Figure 2-9**). However, it is important to note that the polarity of the oil-brine zeta potential interpreted in this way can be ambiguous. If the zeta potential is initially positive and becomes more positive after aging, then this unambiguously indicates a positive oil-brine zeta potential (e.g. oil BD and samples BA, BD and BH at laboratory temperature in Figure 3-7). Likewise, if the zeta potential is initially negative and becomes more negative after aging, then this unambiguously indicates a negative oil-brine zeta potential (e.g. oil TT and sample TR in Figure 3-7). If the zeta potential is initially positive and becomes negative after aging, then this unambiguously indicates a negative oil-brine zeta potential and vice-versa (e.g. oil BD and sample BH at elevated temperature in Figure 3-7). However, if the zeta potential is initially positive and becomes less positive after aging, then this could indicate a negative or less positive zeta potential at the oil-brine interface (e.g. oil BM in Figure 3-7); likewise, if the zeta potential is initially negative and becomes less negative after aging, then this could indicate a

positive or less negative zeta potential at the oil-brine interface. This ambiguity is acknowledged when recording the interpreted zeta potential for each crude oil (e.g. Table 3-2).

In addition to aging in formation brine Jackson et al. (2016a) also investigated the effect of wettability alteration on the zeta potential when aging in low salinity brine with two crude oils (SR-A and SR-D). They found that the change in the zeta potential after aging in low salinity brine was of the same polarity (but different magnitude) as when aged in formation brine, and thus concluded that the polarity of the zeta potential of the oil-brine interface was independent of brine composition or ionic strength at pH values relevant to carbonate oil reservoirs. This hypothesis was tested further here with several rock samples and crude oils. The zeta potential of these samples measured at $S_w = 1$ and $S_w = 1 - S_{or}$ along with the change in zeta potential after aging these samples in low salinity brine ($\Delta\zeta_{wett}$) is shown in Figure 3-9.

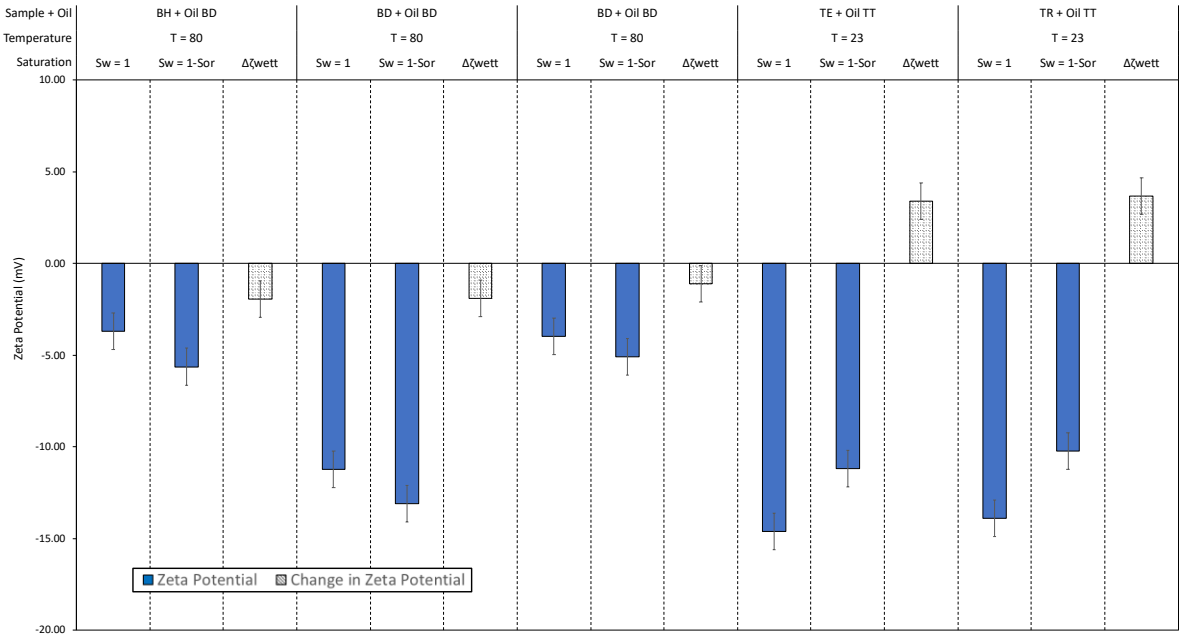

Figure 3-9: Zeta potential measurements made at $S_w = 1$ and $S_w = 1 - S_{or}$ in samples aged when saturated with low salinity brine and crude oil, along with the difference between these values ($\Delta\zeta$wett). The temperature here reflects the temperature at which the zeta potential was measured. Aging of the samples was always undertaken at elevated temperature (see section 3.2).

As with the measurements made after aging in formation brine, there is a potential ambiguity in the interpretation of the oil-brine interface polarity. In low salinity brine, the zeta potential of the mineral-brine interface is always negative. Those samples which show a more

negative zeta potential after aging and wettability alteration (Samples aged with Oil BD in Figure 3-9 unambiguously indicates a negative oil-brine zeta potential, however, in those samples where the zeta potential became less negative after aging (Samples aged with Oil TT in Figure 3-9) could represent either a positive or less negative oil-brine zeta potential. The change in zeta potential for samples saturated and aged in low salinity brine ($\Delta\zeta_{wett}$) as a function of I_w is plotted in Figure 3-10. Again, filled symbols represent measurements made at ambient temperature while open symbols represent those made at elevated temperature.

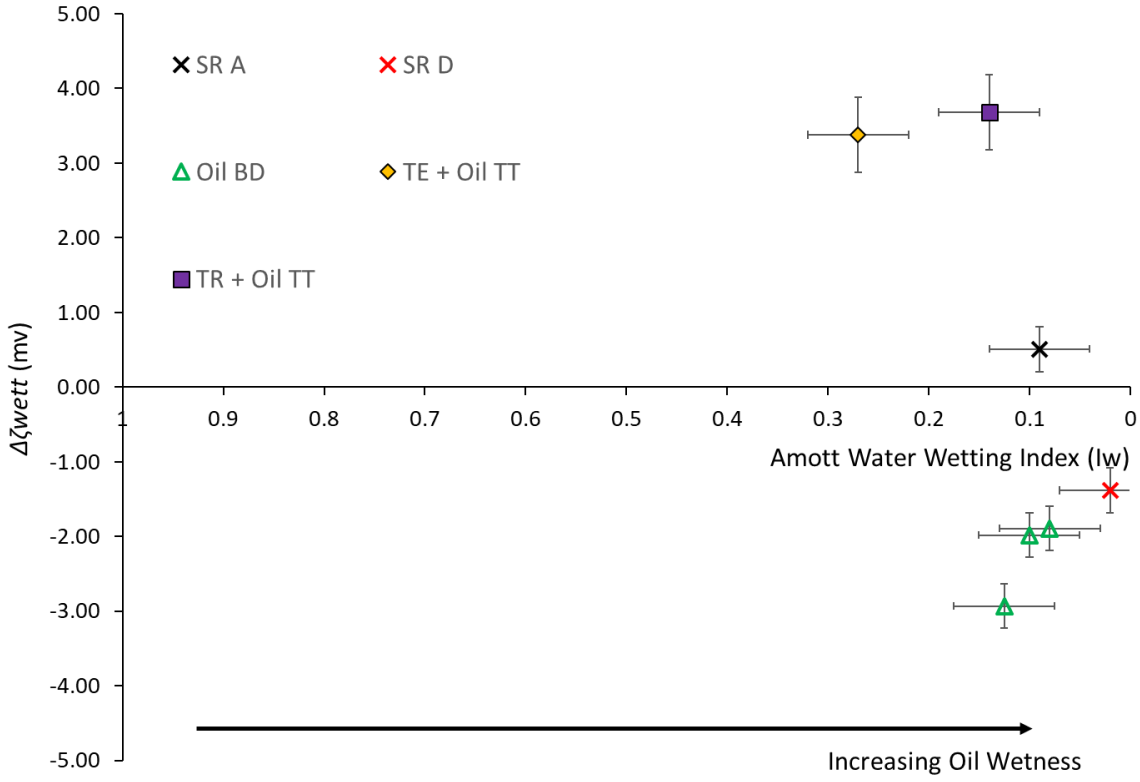

Figure 3-10: Change in zeta potential measured in low salinity brine after aging for a range of crude oils, carbonate core samples, low salinity brine compositions and temperatures. Filled symbols represent data obtained at ambient temperature. Open symbols represent data obtained at elevated temperature. Data for oils SR-A to SR-D previously reported by Jackson et al. (2016a) and shown by crosses. TE+Oil TT denotes the results of aging sample TE in crude oil TT; TR+Oil TT denotes the results of aging sample TR in crude oil TT.

The polarity of $\Delta\zeta_{wett}$ for a given crude oil is different depending on whether the aging was in formation or low salinity brine (Figure 3-10; compare like crude oils with Figure 3-8). After aging in formation brine, oil BD generally caused the zeta potential to become more positive; however, when aging in low salinity brine, the opposite trend was observed. Oil TT,

which was observed to show both a positive and negative change in zeta potential after aging in formation brine dependent on the core sample type, consistently caused the zeta potential to become more positive irrespective of core type after aging in low salinity brine and the change was of comparable magnitude (+3.5mV).

The data presented here and by Jackson et al. (2016a) report results showing the link between wettability alteration and changes in the zeta potential for seven different crude oils. When aging in formation brine, four of these oils (SR-B, SR-C, SR-D and BM) have consistently caused the zeta potential to become more negative in all samples; one (SR-A) consistently resulted in a more positive zeta potential, and two have shown both a more positive and more negative zeta potential depending on the rock sample or temperature (BD and TT). Samples aged with either Oil TT or Oil BD exhibit more positive or more negative zeta potentials depending on the core type, aging brine and conditions used. Assuming that the change in zeta potential after aging is indicative of the zeta potential of the oil-brine interface, then the data reported here suggest that the zeta potential of the oil-brine interface depends not only on the crude oil properties (as suggested by Jackson et al. (2016a)) but also on the host rock, brine salinity and/or composition, and temperature. Controls on the zeta potential at the oil-brine interface and the implications for CSW will be discussed later.

3.3.3 Controlled Salinity Corefloods

Two types of corefloods were performed in this work: (i) conventional secondary or tertiary low salinity waterfloods (LSW) where the injection brine is changed to increasingly dilute brines (either secondary: FB → LS or tertiary: FB → SW → LS) and (ii) inverted secondary or tertiary inverse waterfloods (iLSW) where the injection brine sequence is reversed, and increasingly concentrated brines are injected (secondary: LS → FB or tertiary: LS → SW → FB). In all corefloods, the samples were aged in the first injection brine.

Let us consider first the coreflood results from conventional LSW. Earlier results and other published results (e.g. (Alroudhan, Vinogradov, and Jackson 2016; Al Mahrouqi et al. 2017a) show that LSW yields a more negative zeta potential at the mineral-brine interface (Figure 3-3). Figure 3-11 reports examples of conventional LSW in both secondary and tertiary mode.

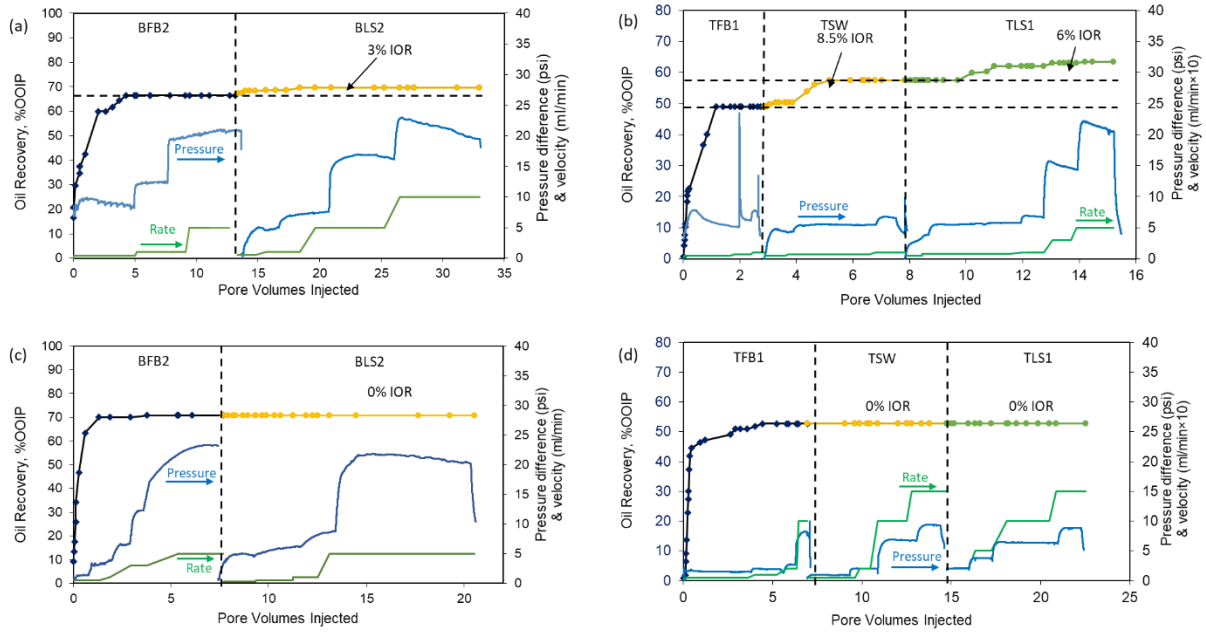

Figure 3-11: Examples of conventional LSW corefloods. Plots (a) and (b) show typical results using crude-oils, Oil BM and Oil TT respectively, interpreted to have a negative oil-brine zeta potential in the aging brine; plots (c) and (d) show typical results using crude-oils, Oil BD and Oil TT respectively, interpreted to have a positive oil-brine zeta potential. Results shown correspond to the summary in Table 3-2 (a) experiment 19; (b) experiment 21; (c) experiment 12 and (d) experiment 20. All corefloods shown here were performed at laboratory temperature.

In all of the LSW corefloods conducted, crude oils that were interpreted to have a negative zeta potential showed an increase in oil recovery (IOR) (e.g. Figure 3-11 (a) and (b))

whereas oils that were inferred to have a positive zeta potential showed no IOR (e.g. Figure 3-11 (c) and (d)). These trends were observed regardless of the specific brines, coreflooding mode and temperature. A notable result is for Oil BD, which was interpreted to have a positive zeta potential at laboratory conditions but a negative zeta potential at elevated temperature. The LSW at laboratory temperature showed no IOR, whereas at elevated temperature, LSW yielded an additional recovery of 2.2% (Figure 3-13).

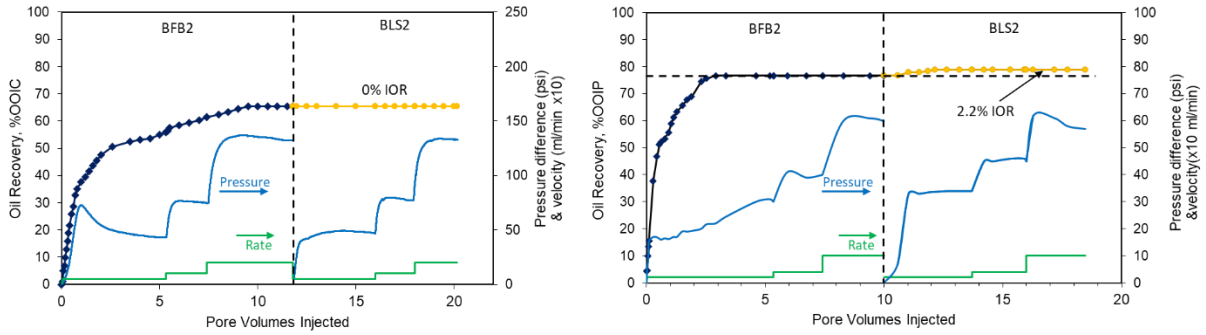

Figure 3-12: Conventional LSW in sample BD saturated with oil BD at (a) ambient temperature where the zeta potential of the oil-brine interface was determined to be positive (Experiment 11 in Table 3-2) and (b) at elevated temperature where the zeta potential of the oil-brine interface was determined to be negative (Experiment 16 in Table 3-2).

Figure 3-12 reports examples of inverse iLSW in both secondary and tertiary mode.

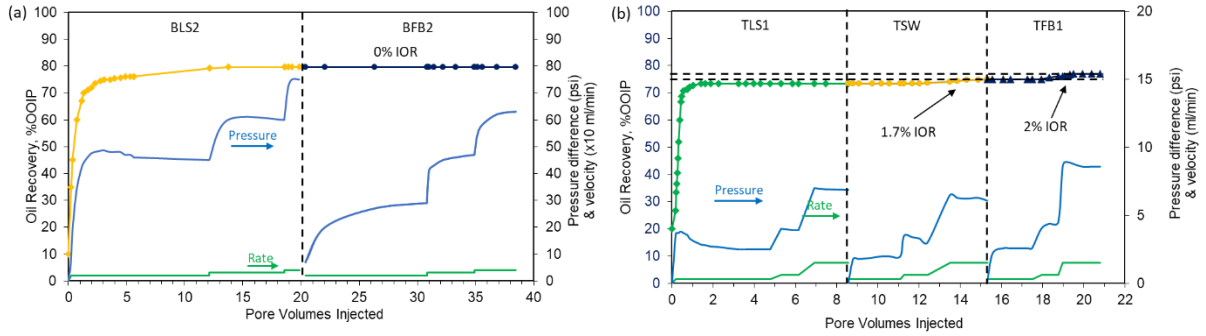

Figure 3-13: Examples of conventional iLSW corefloods. Plot (a) shows a typical result using crude-oils BD interpreted to have a negative oil-brine zeta potential in the aging brine (Experiment 15 in Table 3-2); plot (b) shows typical results using crude-oil TT interpreted to have a positive oil-brine zeta potential (Experiment 22 in Table 3-2). Plot (a) was performed at elevated temperature whilst plot (b) was performed at ambient temperature.

In the iLSW, crude oils interpreted to have a negative oil-brine zeta potential interface showed no IOR (e.g. Figure 3-13 (a)) whereas crude oils interpreted to have a positive oil-brine zeta potential typically showed IOR (e.g. Figure 3-13 (b)). The one exception was an iLSW with crude oil TT in sample TR (Figure 3-14). However, as discussed previously, the

interpreted zeta potential for the crude oil was ambiguous, as the sample zeta potential was negative and became more positive (but was still negative) after aging (Figure 3-9). Hence, in this case, it is possible that the polarity of the oil-brine zeta potential was incorrectly interpreted and is in fact negative.

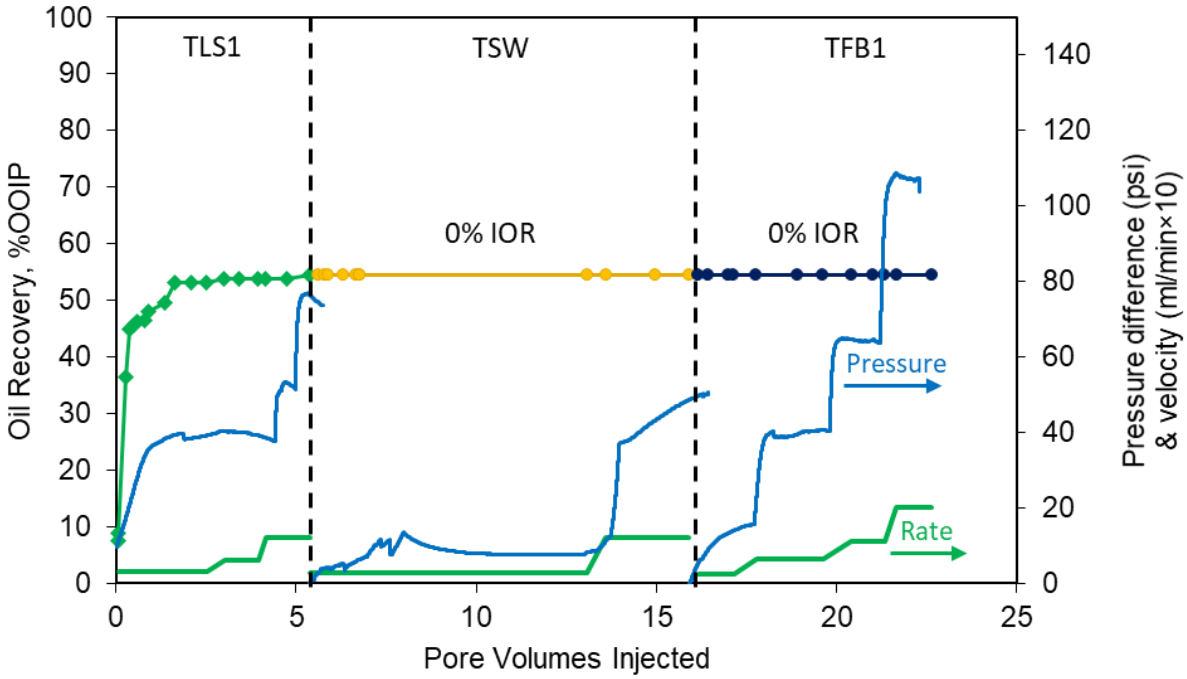

Figure 3-14: iLSW coreflood with crude oil TT in sample TR performed at ambient temperature (Experiment 23 in Table 3-2). The zeta potential became more positive after aging but did not yield an IOR response unlike other iLSW where the zeta potential became more positive after aging.

Crude oil BD was interpreted to have a positive oil-brine zeta potential after aging in formation brine in sample BH at elevated temperature (Figure 3-7) and showed no IOR in a conventional LSW (Figure 3-15a), consistent with the other results reported here and by Jackson et al. (2016a). The sample was then cleaned and aged in low salinity brine in the same sample, after which it was interpreted to have a negative oil-brine zeta potential (Figure 3-9). An iLSW coreflood was then conducted but no IOR was observed (Figure 3-15b), again consistent with the other results reported here and by Jackson et al. (2016a). Regardless of flooding sequence, no IOR was observed during CSW for crude oil BD in sample BH. The interpretation of the oil-brine zeta potential in both instances was unambiguous.

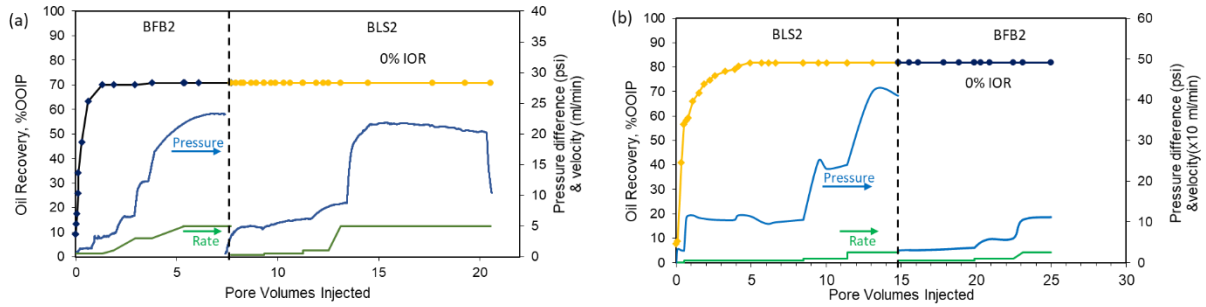

Figure 3-15: CSW using crude oil BD in sample BH. Plot (a) shows a conventional LSW (experiment 12 in Table 3-2); plot (b) shows an iLSW (Experiment 13 in Table 3-2). Corefloods were performed at elevated temperature.

For a given coreflood sequence and COBR system, a 'normalised zeta potential' can be defined, given by:

$$\zeta_n = \left| \frac{\Delta\zeta_{CSW}}{\Delta\zeta_{wett} * I_w} \right| \qquad (3\text{-}3)$$

where:

$$\Delta\zeta_{CSW} = \zeta^{Injection\ Brine} - \zeta^{Aging\ Brine} \qquad (3\text{-}4)$$

$$\Delta\zeta_{wett} = \zeta_{S_w=1-S_{or}} - \zeta_{S_w=1} \qquad (3\text{-}5)$$

where $\Delta\zeta_{CSW}$ is the change in the mineral-brine zeta potential caused by injection of a CSW brine, determined from single-phase measurements (e.g. Figure 3-3). Equation (3-4) is similar to that proposed by Jackson et al. (2016a) but with the inclusion of I_w, which accounts for the success of wettability alteration after aging. For successful CSW corefloods that yield IOR, a relationship is observed between the amount of IOR (%) and ζ_n, (Figure 3-16) regardless of the core type, crude oil, brine compositions, temperature or flooding sequence. Ambient temperature corefloods are given by triangular symbols and elevated temperature corefloods are shown by circular symbols.

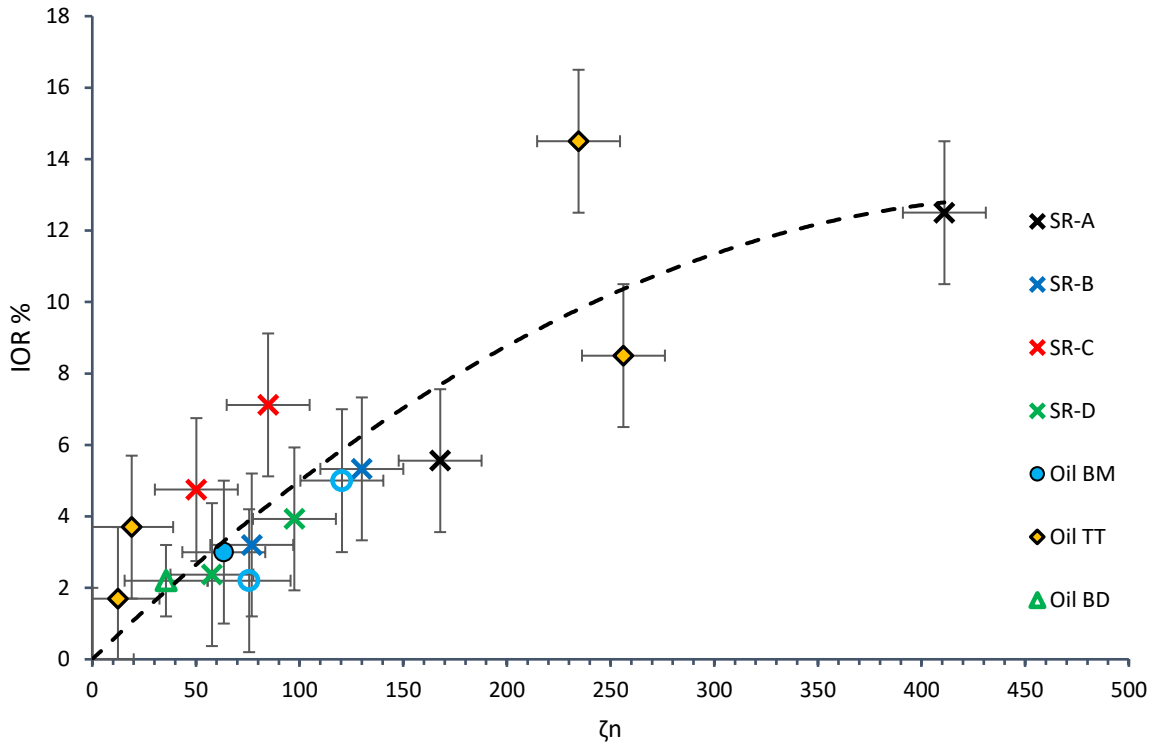

Figure 3-16: Incremental oil recovered from successful CSW as a function of normalised zeta potential. Filled symbols represent data obtained at ambient temperature. Open symbols represent data obtained at elevated temperature. Data for oils SR-A to SR-D previously reported (Jackson et al. 2016a) and shown by crosses.

The correlation between IOR and ζ_n is empirically determined and there is no theoretical derivation for equation (3-3). However, considering the electrostatic repulsion model of Jackson et al. (2016), there is some justification for the terms in equation (3-3). The model suggests that the changes in zeta potential of the mineral-brine and oil-brine interfaces are the key parameters in determining the success of CSW. The terms $\Delta\zeta_{wett}$ and $\Delta\zeta_{CSW}$ are the most appropriate pieces of data that capture these. Equation (3-3) differs from that of Jackson et al. (2016) by the inclusion of I_w in the denominator. However, if the detachment of oil from the mineral surface(s) is indeed the key mechanism controlling CSW then it follows that more oil-wet samples (those with smaller values of I_w) should offer a greater propensity for IOR by CSW. The wettability of the samples used by Jackson et al. (2016) were largely consistent so the impact of I_w on ζ_n may not have been noticed. Naturally there are limitations with equation (3-3), noticeably if a sample had an I_w of zero, then it should exhibit an infinite IOR potential, which is obviously physically unfeasible.

3.4 Discussion

Based on the suite of single and multiphase corefloods conducted to date, combining the new dataset obtained here with that reported by Jackson et al. (2016a), the following observations are made:

- Dilution of the injection brine yields a more negative mineral-brine zeta potential regardless of sample type or temperature for realistic formation and dilute brine compositions.
- All conventional LSW corefloods have shown an IOR response when the crude oil is interpreted to have a negative oil-brine zeta potential in the aging brine.
- All bar one iLSW corefloods have shown an IOR response when the crude oil is interpreted to have a positive oil-brine zeta potential in the aging brine. Interpretation of the crude-oil zeta potential was ambiguous in the one exception, and it likely had a negative oil-brine zeta potential that was not recognized from the change in zeta potential after aging.
- No IOR has been observed in any coreflood when the change in polarity of the mineral-brine zeta potential was opposite to that of the interpreted polarity of the oil-brine zeta potential in the aging brine.
- The effect of temperature on the success of LSW is directly linked to the effect of temperature on the zeta potential at the mineral-brine and oil-brine interfaces, such that the observations above are honoured.
- IOR during CSW can be correlated with a normalized change in zeta potential that accounts for the change in mineral-brine zeta potential in response to changing brine composition, the interpreted oil-brine zeta potential (represented by the change in zeta potential in response to aging in the crude oil) and the Amott water-wetting index.

The results and key observations for IOR during CSW reported here are consistent with those of Jackson et al. (2016a) (see Table 3-2 for a summary) and provide further support to their model for CSW, in which the change in brine composition must be chosen such that it yields an increased electrostatic repulsion between the mineral-brine and oil-brine interfaces, and that the polarity of the zeta potential at the oil-brine interface must also be determined in addition to the polarity of the mineral-brine interface. It is incorrect to assume the zeta potential of the oil-brine interface is always negative, and LSW failures observed previously may have been caused by a positive oil-brine zeta potential that had not been recognized.

Table 3-2: Summary of all CSW carbonate corefloods to date reporting the polarity of the oil interpreted from the change in zeta potential after aging, whether IOR was observed, and if these observations fit with the CSW model of Jackson et al. (2016a). 1-6 previously reported by Jackson et al. (2016a). Experiments marked with (*) represent experiments where there may be a potential ambiguity in the interpretation of the oil-brine zeta potential polarity.

Experiment Number	Core Sample	Oil	CSW type	Temperature	Interpreted Oil-Brine Zeta-Potential Polarity	IOR Observed?	Consistent with Model?
1	Estaillades	SR-A	Normal	Ambient	+	No	Yes
2	Estaillades	SR-A	Inverse	Ambient	+ (*)	Yes	Yes (*)
3	Estaillades	SR-B	Normal	Ambient	-	Yes	Yes
4	Estaillades	SR-C	Normal	Ambient	-	Yes	Yes
5	Estaillades	SR-D	Normal	Ambient	-	Yes	Yes
6	Estaillades	SR-D	Inverse	Ambient	+ (*)	No	Yes (*)
7	BA	BD	Normal	Ambient	+	No	Yes
8	BB	BD	Normal	Ambient	+	No	Yes
9	BC	BD	Normal	Ambient	+	No	Yes
10	BF	BD	Normal	Ambient	+	No	Yes
11	BD	BD	Normal	Ambient	+	No	Yes
12	BH	BD	Normal	80	+	No	Yes
13	BH	BD	Inverse	80	-	No	Yes
14	BD	BD	Inverse	80	-	No	Yes
15	BD	BD	Inverse	80	-	No	Yes
16	BD	BD	Normal	80	-	Yes	Yes
17	BC	BM	Normal	80	- (*)	Yes	Yes (*)
18	BC	BM	Normal	80	- (*)	Yes	Yes (*)
19	BG	BM	Normal	Ambient	- (*)	Yes	Yes (*)
20	TE	TT	Normal	Ambient	+	No	Yes
21	TR	TT	Normal	Ambient	-	Yes	Yes
22	TE	TT	Inverse	Ambient	+ (*)	Yes	Yes (*)
23	TR	TT	Inverse	Ambient	+ (*)	No	No (*)

Jackson et al. (2016a) assumed that the interpreted polarity of the oil-brine zeta potential was an intrinsic property of the crude oil and remained constant during CSW under reservoir relevant conditions. In these new results there is evidence of variation in the oil-brine zeta potential polarity dependent on the brine composition, temperature and, interestingly in some cases, the core sample used, suggesting this previous assumption is invalid. However, there is further ambiguity in the interpretation of the oil-brine interface polarity in some instances via the method used here. Experiment 23, the iLSW with sample TR and Oil TT, is the only experiment that does not fit with the model of Jackson et al. (2016a) based on the simple interpretation that the change in the zeta potential after aging is indicative of the oil-brine interface polarity used previously. However, if it is instead assumed that this oil is less negative than the mineral surface, this would yield the interpreted positive oil-brine zeta potential but the electrostatic model controlling IOR by CSW is still valid and successful in explaining the lack of observed IOR. The key discrepancy between the results presented here and those of Jackson et al. (2016a) lie within the interpretation of the oil-brine interface. The method used here is not a direct measurement of the oil-brine zeta potential. The streaming potential method probes the mineral-brine interface where the core is water wet and the oil-brine interface where the core is oil wet. This therefore allows for an interpretation of the polarity of the oil-brine interface but not an accurate measurement of the magnitude.

We have seen in Chapter 2 the scarcity of, and difficulty in obtaining, zeta potential measurements of the crude oil-brine interface at conditions relevant to subsurface reservoirs. The existing data and models tend to suggest that this is negatively charged at reservoir pH values greater than 5; the interpretation of a positively charged oil during the coreflood experiments shown here is somewhat contradictory to this literature data. However, positively charged oils have been observed by certain authors (Lu et al. 2017; Nasralla and Nasr-El-Din 2014b; Pooryousefy et al. 2018) in the presence of high concentrations of Ca^{2+} and Mg^{2+} (Figure 2-12). Charge inversion was observed at around a pCa/pMg of 0.5 which corresponds to a concentration of approximately 0.32 mol/L. This is comparable to the divalent cation

concentration present in the formation brines used in the experiments presented here (Table 3-1). Furthermore, the effect of temperature on the oil-brine zeta potential is unclear. The notion that the oil-brine zeta potential is negatively charged at reservoir conditions is not necessarily supported by relevant data.

It is evident that the current understanding of the oil-brine interface is insufficient for applications to true reservoir conditions. No clear trends between the oil, brine or mineral properties and the interpreted polarity of the oil-brine interface have been identified from the results shown here that would allow a prediction of the oil-brine polarity prior to conducting the experimental procedure. This is not necessarily surprising given bulk properties are poor indicators of interfacial properties (see section 2.2.4). It is unclear why Oil TT would exhibit both a positive and negative polarity dependent upon the core sample type when aged in compositionally similar cores with the same brine (Figure 3-7). The effect of aging on the oil-brine zeta potential is also not understood. Wettability alteration during aging is acknowledged to occur due to chemical reactions between the COBR components (e.g., Buckley et al.1989a; Buckley, et al. 1998; Drummond and Israelachvili 2004; Hiorth et al. 2010; Zhang and Austad 2006)) but the impact of this on the crude oil interfacial chemistry, and thus the zeta potential is unclear.

Additional modelling, and experimental data to constrain and validate those models, is required at conditions relevant to oil reservoirs. The methodology used here is advantageous in interpreting the polarity of the oil-brine zeta potential at reservoir conditions and correlating this to IOR, but has possible ambiguities in the interpretation, cannot provide an accurate estimate of the magnitude of the oil-brine zeta potential and is too time consuming and resource intensive to systematically study the impact of individual variables on the interpreted polarity. Independent experimental methods that can accurately measure the zeta potential of the oil-brine interface under reservoir relevant conditions are necessary to systematically probe the impact of brine composition and concentration, temperature and oil properties on

the zeta potential to better understand the behaviour of the interface and to predict and understand IOR by CSW.

3.5 Conclusions

It is important to determine how the relevant formation and injection brines used in CSW will modify the zeta potential of both the mineral-brine and oil-brine interfaces at reservoir conditions on intact samples.

The injection brine composition should be designed to yield a change in the mineral-brine zeta potential that is of the same polarity as the crude oil-brine interface polarity in order to increase oil recovery.

This change results in an increased electrostatic repulsion between the mineral and brine interfaces, acting to increase the stability of a thin water film acting between the two interfaces, resulting in a change towards a more water-wet core which is consistent with the majority of literature observations of CSW. The change in the electrostatic forces, not the total salinity, is more important for the success of CSW.

The crude oil-brine interface polarity of importance to CSW is that present after aging with the formation brine and rock core of interest, not the pristine crude oil-brine interface. The polarity of the crude oil-brine interface can vary depending upon the aging conditions used. No correlation between the oil/brine/rock properties and the polarity of the crude oil-brine interface inferred after aging have yet been identified. As such, there is currently no model to predict the crude oil-brine interface polarity of a given COBR system prior to measuring experimentally.

The polarity of the crude oil-brine interface is unlikely to be constant during CSW. It is currently unknown if, or how, modifying the injection brine composition may alter this. Additional data and models are required to increase our understanding.

Chapter 4 - Zeta Potential of Intact Natural Sandstones at Reservoir Conditions

Abstract

This chapter presents zeta potential measurements obtained on natural intact sandstone samples saturated with complex brines representative of those used in CSW and at ambient and elevated temperature. Compared to previous data available in literature, the dataset contains sandstone core samples covering a range of mineralogies, from clean, pure quartz to clay rich sandstones. Additionally, few data have been published which report the zeta potential of sandstones in the presence of natural subsurface brines. The zeta potential at high and low ionic strength both corelate with the bulk clay content. The former becomes more negative with increasing clay content whilst the latter becomes less negative with increasing clay content. Consequently, the change in zeta potential between high and low ionic strength brines, such as during a low salinity waterflood, decreases with increasing clay content and may be negligible in some cases. The results highlight the importance of ion-exchange between the bulk fluid and clay content in controlling the zeta potential of sandstones.

4.1 Introduction

In Chapter 2 we saw evidence from a range of studies and scales to suggest that the CSE is observed in sandstone reservoirs and that this is often associated with a change to a more water-wet state. As with carbonates, the mechanisms that have been hypothesised to control this wettability alteration remain ambiguous, but many are linked to changes in the zeta potential at the mineral- and oil-brine interfaces. The model of Jackson et al. (2016a) that was explored further in Chapter 3 suggests that CSW is successful if the zeta potential at the mineral-brine interface is modified in such a way to induce an electrostatic repulsion between the mineral-brine and oil-brine interfaces. There is no reason why this model should not apply

to sandstone reservoirs. The main difference between the two rock types are the origins and controls on the surface charge.

The controls on the zeta potential of the sandstone-brine interface were reviewed in section 2.2.3. It was seen that the zeta potential is typically negative and increases in magnitude with decreasing brine ionic strength. However, as was also noted, most of the data was obtained in simple NaCl brines at laboratory temperature. Few data exist at reservoir conditions. The relevant data that does, suggests the zeta potential may differ significantly from trends observed under ideal conditions, particularly for heterogenous sandstones containing high clay contents and other impurities (Alarouj et al. 2021). It has been argued that the presence of clay minerals is a necessary condition for the CSE in sandstones and the amount of IOR may correlate with the extent of clay content (see section 2.1.3 and Tang and Morrow 1999; Seccombe et al. 2008; Jackson et al. 2016a). Different clay minerals have different surface charges to quartz and other minerals present in sandstones (Figure 2-10). The micro-scale zeta potential of these different minerals, along with their quantity and distribution within the pore space, determine the macro-scale zeta potential of the whole core sample, the latter of which is of interest for most practical applications.

The aim of this chapter is therefore to report macro-scale zeta potential measurements of different sandstones at reservoir conditions. In particular, the impact of clay content on the zeta potential will be investigated due to its apparent importance for CSW. Natural, intact core samples of different outcrops are saturated with synthetic formation brines and low salinity brines representative of those used in CSW. Data are obtained at ambient laboratory temperature and elevated temperature relevant to oil reservoirs.

4.2 Materials and Methods

4.2.1 Brine Compositions

Table 4-1 shows the compositions of the brines used in this chapter to represent those found in natural systems. Two high ionic strength brines (HIS-1 & HIS-2) and two low ionic strength brines (LIS-1 & LIS-2) were prepared using DI water and reagent grade salts (Sigma-Aldrich). pH and conductivity were measured before and after zeta potential measurements using a Mettler-Toledo pH probe and a Metrohm 856 Conductivity Module. LIS-1 is a 70x diluted version of HIS-1.

Table 4-1: Compositions, pH, conductivity and ionic strength of brines used in this study. LIS-1 is a 70x diluted version of HIS-1.

	HIS-1	**HIS-2**	**LIS-1**	**LIS-2**
NaCl (mg/L)	57,884.1	70,489.9	833.6	548.7
KCl (mg/L)	743.6	N/A	10.7	N/A
$CaCl_2.2H_2O$ (mg/L)	13,205.1	30,271.7	190.2	39.3
$MgCl_2.6H_2O$ (mg/L)	2,007.5	10,111.8	28.9	157.4
TDS (mg/L)	69,536.7	110,873.3	1,001.4	745.4
Ionic Strength (mol/L)	1.3	2.0	0.018	0.015
pH	5.8 ± 0.2	5.5 ± 0.2	6.1 ± 0.2	6.2 ± 0.2
Conductivity (mS/cm)	77.5 ± 0.3	96.0 ± 0.3	2.1 ± 0.3	± 0.3

4.2.2 Rock Properties

Five different sandstone samples were used in this chapter. Core samples measuring 7.6 cm in length and 3.6 cm in diameter were prepared. Samples were cleaned with warm Toluene and Methanol under reflux for 48 hours to remove any impurities. Samples were then

left to dry at ambient laboratory conditions for another 48 hours before being saturated under vacuum with the brine of interest. At least 10 pore volumes (PVs) of fresh brine were pumped through the core samples before measurements began. Table 4-2 shows petrophysical properties and mineralogy data for the samples used.

Table 4-2: Petrophysical and mineralogical data for the sandstone samples used in this chapter.

Sample	Porosity	Permeability	Mineralogy
Fontainebleau (FB)	9%	70 mD	99.9%+ Quartz
Doddington (DODT)	21%	450 mD	93.6% Quartz 1.7% Feldspar 4.5% Clay
St. Bees (STB)	19%	70 mD	90% Quartz 5% White Mica 5% Clay
Berea (BERB)	20%	60 mD	88% Quartz 5% Carbonates 7% Clay
Castlegate (CAST)	24%	350 mD	90% Quartz 0.5% Carbonates 9% Clays

4.2.3 Zeta Potential Measurements

The zeta potential of the sandstone core samples was measured using the exact same procedure as described in section 3.2.2. Samples were saturated with the brine of interest and placed into a coreholder. Brine flow through the core was induced using a pump and the

pressure drop measured. Two Ag/AgCl electrodes situated either side of the coreholder recorded the voltage drop. Stabilised pressure and voltage drop measurements were recorded for several different brine flowrates. The voltage and pressure measurements were plotted against each other and the gradient of a linear regression through the points yielded the streaming potential coupling coefficient, *C*. Effluent brine conductivity and pH, along with the saturated rock conductivity were also measured. The zeta potential was then calculated using equation (3-2).

4.3 Results

4.3.1 Ambient Temperature Zeta Potential Measurements

Zeta potential measurements obtained at ambient laboratory temperature are shown in Figure 4-1. Red bars represent measurements obtained when the core samples were saturated with high ionic strength brines and blue bars represent measurements made with low ionic strength brines (Table 4-1). Measurements were obtained on several samples of the different outcrop rock types used in this chapter (Table 4-2).

The first observation is that all the zeta potential measurements are negative in polarity. This is consistent with previous data (Figure 2-10) and the hypothesis that sandstone surfaces are negatively charged due to deprotonation of the metal oxide surface sites (Stumm et al. 1992). There is significant variation in the magnitude of these zeta potential measurements. Considering those obtained with high ionic strength brines, different samples of the same rock type are generally consistent within experimental error. However, the zeta potential of different rock types ranges noticeably from approximately -2 mV in Fontainebleau samples to approximately -14 mV in Castlegate samples.

When saturated with low ionic strength brines, the zeta potential of a given sample generally becomes more negative and larger in magnitude. This increase in magnitude is again consistent with previous observations and conventional double layer expansion theory (Hunter 2013). There is also significant variation in the magnitude of these zeta potential measurements between different samples, with values ranging from -14 mV (FB-1; CAST-2; CAST-3) to -26 mV (FB-2; DODT-3; DODT-4). Compared to the high ionic strength measurements, there is more variation in the zeta potential of different samples of the same rock type, for example -14 mV in FB-1 to -26 mV in FB-2, and -14 mV in CAST-2 to -23 mV in CAST-1. This variation makes it difficult to identify any clear trends between the magnitude of the zeta potential and the rock type. FB-1 showed the smallest magnitude of any of the samples at -14 mV whilst FB-2 returned the largest magnitude of the samples of -26 mV.

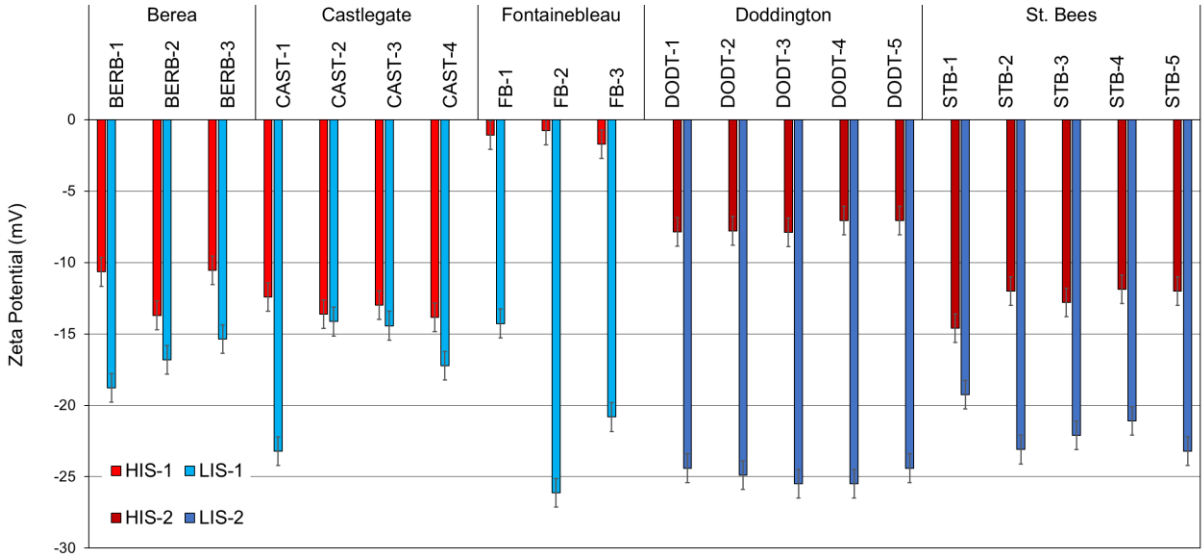

Figure 4-1: Zeta potential measurements obtained on natural, intact sandstone core samples at ambient laboratory temperature (23 ^{O}C) when saturated with high (red bars) and low (blue bars) ionic strength brines representative of those found in subsurface environments.

4.3.2 Elevated Temperature Zeta Potential Measurements

The zeta potential of the Berea, Castlegate and Fontainebleau samples saturated with the HIS-1 and LIS-1 brines (Table 4-1) was also measured at an elevated temperature of 70 ^{O}C. The Doddington and St. Bees samples were not measured at elevated temperature as this was not a focus of the experimental procedure where these samples were used. Figure 4-2 reports these results. The ambient temperature results from Figure 4-1 are also shown for comparison. As in Figure 4-1, red bars represent measurements with high ionic strength brines and blue bars represent measurements with low ionic strength brines. Filled bars represent measurements at ambient temperature whilst empty bars represent measurements at elevated temperature.

The zeta potential was again negative in all samples and the magnitude varied depending on rock type and sample. Fontainebleau samples typically returned a small zeta potential of about -2 mV, whereas Berea and Castlegate samples were more negative. There is more variation in the zeta potential of these rock types across different samples at elevated temperature than at ambient temperature. For most samples, the zeta potential was more

negative in low ionic strength brines than in high ionic strength brines as would be expected based on previous data and theories. However, there are some noticeable instances where the zeta potential was identical within experimental error in both brines (BERB-3; CAST-3) or where the zeta potential in low ionic strength was less negative and smaller in magnitude than at high ionic strength (CAST-2).

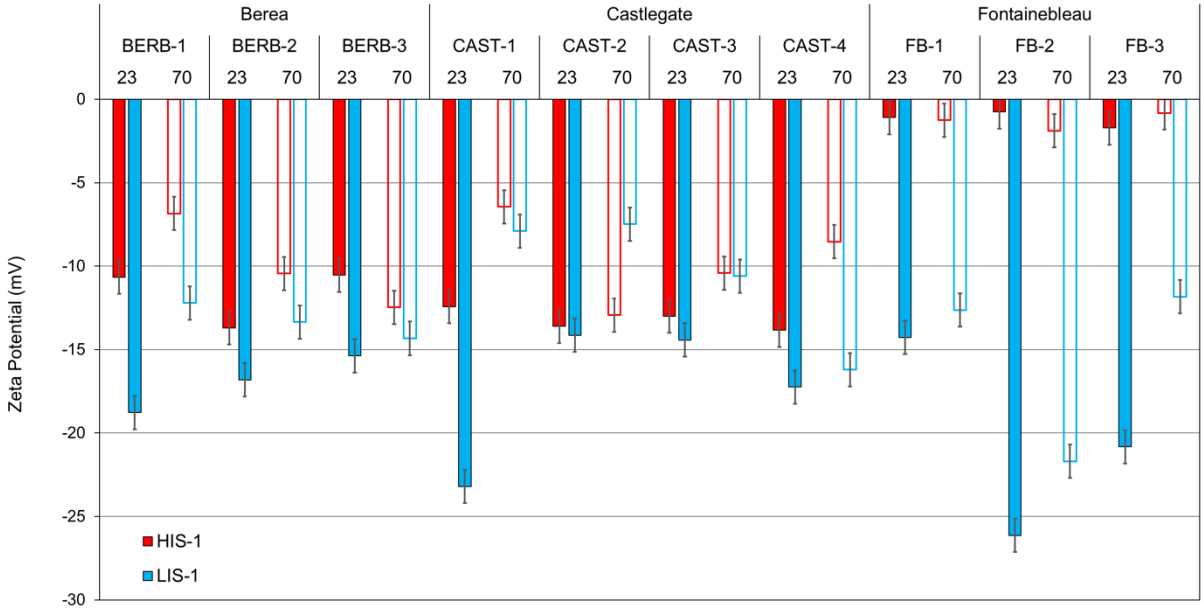

Figure 4-2: Zeta potential measurements obtained on natural, intact sandstone core samples at ambient laboratory temperature (filled bars, 23 ^{O}C) and elevated temperature (empty bars, 70 ^{O}C) when saturated with high (red bars) and low (blue bars) ionic strength brines representative of those found in subsurface environments.

4.3.3 Zeta Potential vs pH

The variability in the magnitude of the zeta potential between different rock types would be expected based on previous literature (Figure 2-10). The zeta potential of clean sandpacks and sandstones has previously been correlated with the pH of pure NaCl brines, and NaCl brines with the addition of $CaCl_2$ or $MgCl_2$ (Vinogradov et al. 2018; Glover 2018; Revil and Glover 1998). The sandpack data of Vinogradov et al. (2018) highlighting this correlation are shown in Figure 4-3 as black crosses, along with the main trendlines. They showed that the zeta potential at low ionic strength correlates linearly with pH. Increasing pH yielded an increasingly negative zeta potential. At high ionic strength the zeta potential was largely

independent of pH and most data grouped around pH 7 and exhibited a zeta potential around -10 mV.

The zeta potential measurements obtained here for natural core samples saturated with complex brines are also shown in Figure 4-3 as a function of pH for comparison to the literature data. These are plotted against the effluent brine pH. Again, red points represent measurements obtained with high ionic strength brines whilst blue points represent those obtained with low ionic strength brines. Filled symbols represent ambient temperature measurements (23 ^{O}C) and empty symbols represent elevated temperature measurements (70 ^{O}C).

The data from this study do not correlate with the previous trends of Vinogradov et al. (2018). In general, the zeta potential is smaller in magnitude than the sandpacks for a given pH, but there is no clear trend between the data. When saturated with low ionic strength brines, the pH is larger than with high ionic strength brines (7.5 – 8.5 compared to 6 - 7) and the zeta potential more negative. Again, the magnitude of the zeta potential across the samples varies significantly (-7 mV to -28 mV in low ionic strength brines). Zeta potential measurements obtained with high ionic strength brines are more scattered than previously data would suggest and appear largely independent of pH.

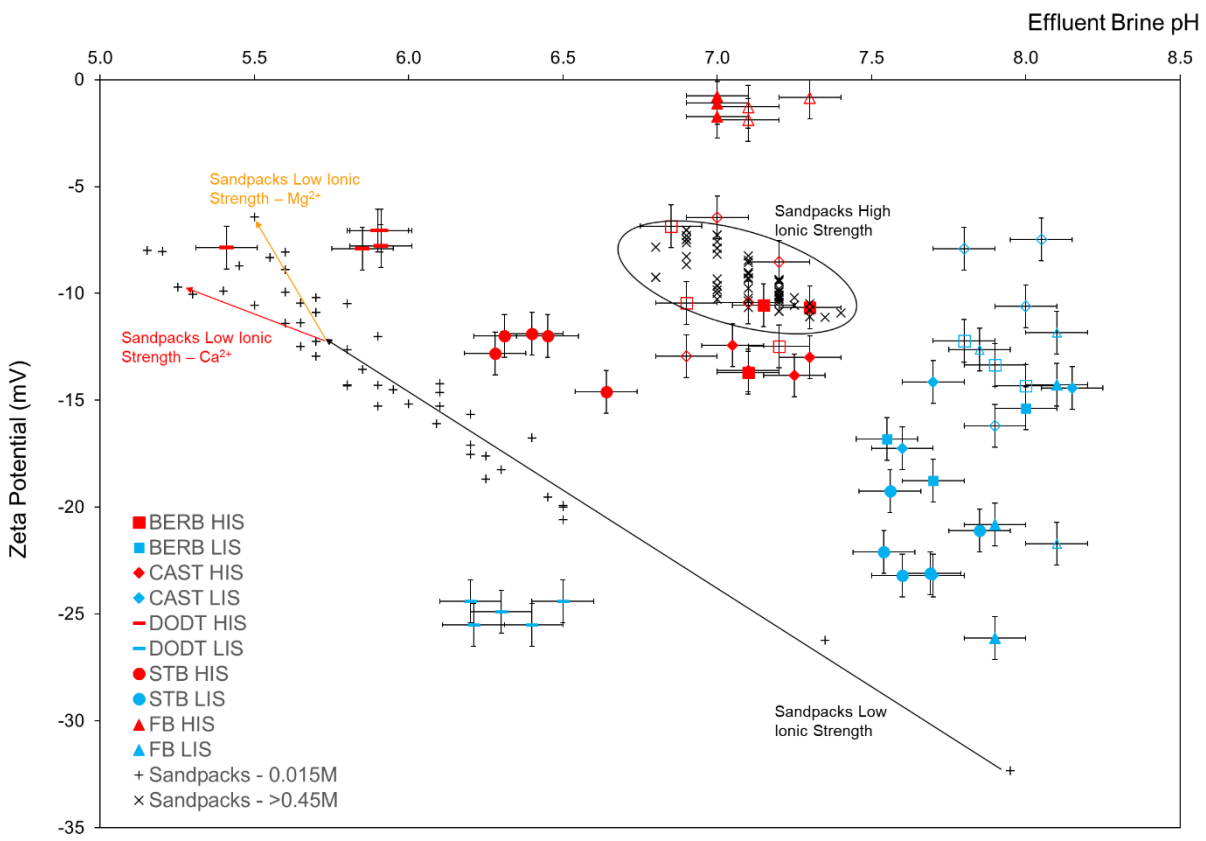

Figure 4-3: Zeta potential measurements as a function of pH. Black crosses and trendlines reported by Vinogradov et al. (2018). Red and blue points represent zeta potential measurements obtained with high and low ionic strength brines respectively. Filled and empty data represent zeta potential measurements obtained at ambient (23 ^{O}C) and elevated temperature (70 ^{O}C) respectively. Shapes represent different rock types: Berea (Squares); Castlegate (Diamonds); Doddington (Lines); St. Bees (Circles); Fontainebleau (Triangles).

4.3.4 Change in Zeta Potential with Ionic Strength

Figure 4-4 plots the difference in the zeta potential of a given sample when saturated with the high and low ionic strength brines as reported in Figure 4-1 and Figure 4-2. Yellow bars represent measurements obtained at ambient temperature and pink bars represent data obtained at elevated temperature. The difference in zeta potential is termed $\Delta\zeta_{IS}$ where:

$$\Delta\zeta_{IS} = \zeta_{LIS} - \zeta_{HIS} \qquad (4\text{-}1)$$

where the subscripts LIS and HIS represent zeta potential measurements obtained with low and high ionic strength brines respectively.

The zeta potential of most samples is more negative in low ionic strength brines yielding a negative $\Delta\zeta_{IS}$. Fontainebleau samples show the largest $\Delta\zeta_{IS}$ of between -10 mV and -25 mV; Doddington samples exhibit a $\Delta\zeta_{IS}$ between -11 mV and -18 mV; St. Bees exhibit a slightly smaller $\Delta\zeta_{IS}$ between -5 mV and -11 mV. Berea and Castlegate samples generally exhibit a much smaller $\Delta\zeta_{IS}$ with several samples exhibiting no difference outside of experimental error (BERB-3 at 70 ^{O}C; CAST-1 at 70 ^{O}C; CAST-2 at 23 ^{O}C and CAST-3 at both 23 ^{O}C & 70 ^{O}C). Notably, the zeta potential of CAST-2 at 70 ^{O}C is smaller in magnitude in low ionic strength than at high ionic strength yielding a positive value for $\Delta\zeta_{IS}$.

As with the individual zeta potential measurements at high and low ionic strength, the magnitude of $\Delta\zeta_{IS}$ varies noticeably between samples of the same rock type is evident. Sample FB-2 shows the largest difference of all samples of -25 mV, whereas FB-1 only changes by -13 mV in comparison. Likewise, CAST-1 changes by -10 mV whilst CAST-2 changes by +5 mV. There was no obvious reason for this variability. All samples were visually identical and obtained from the same block of each outcrop. The observed variability is likely indicative of the internal structural and mineralogical heterogeneity. The impact of this on the zeta potential is discussed later in the chapter.

One final observation from Figure 4-4 is that in all samples, except CAST-4, the magnitude of $\Delta\zeta_{IS}$ decreases at elevated temperature indicating the zeta potential is less dependent on the brine composition at elevated temperature. The impact of temperature on the zeta potential measurements is explored next.

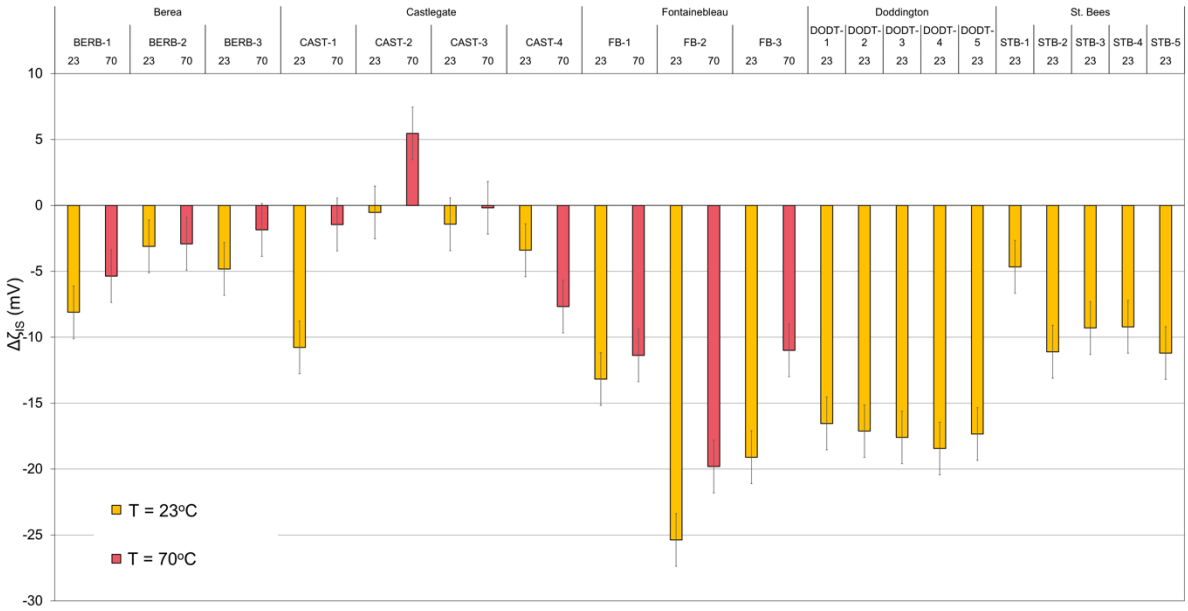

Figure 4-4: Difference between zeta potential measurements obtained on natural, intact sandstone core samples when saturated with high and low ionic strength brines representative of those found in subsurface environments. Yellow bars represent measurements obtained at ambient laboratory temperature (23 ^{O}C) and pink bars represent measurements obtained at elevated temperature (70 ^{O}C).

4.3.5 Change in Zeta Potential with Temperature

It has been observed that the zeta potential changes with temperature (Figure 4-2). To explore the effect of temperature, the difference between the zeta potential at high and low temperature is termed $\Delta\zeta_{Temp}$, where:

$$\Delta\zeta_{\mathrm{Temp}} = \zeta_{\mathrm{HT}} - \zeta_{\mathrm{LT}} \qquad (4\text{-}2)$$

where the subscripts HT and LT represent zeta potential measurements obtained at high and low temperature respectively. Figure 4-5 plots $\Delta\zeta_{Temp}$ for the Berea, Castlegate and Fontainebleau samples saturated with high and low ionic strength brines.

For most samples, $\Delta\zeta_{Temp}$ is positive or negligible indicating that increasing temperature generally makes the zeta potential smaller in magnitude/less negative or has no effect. As with the other results, there is large variation in the magnitude of $\Delta\zeta_{Temp}$ between different samples. However, the variation in $\Delta\zeta_{Temp}$ appears to be dependent on the individual samples rather than any clear distinction between rock type. For example, some samples

show a large $\Delta\zeta_{Temp}$ in both high and low ionic strength brines (e.g. CAST-1 changes by +6 mV and +15 mV respectively) indicating a strong temperature dependency of the sample. Other samples of the same rock type show a much smaller $\Delta\zeta_{Temp}$ (e.g. CAST-3 changes by +2.5 mV and +3.9 mV respectively) indicating a smaller temperature dependency. Several samples show little or no dependence outside of experimental error (e.g. FB-1; BERB-3). Other samples show a large dependence in low ionic strength brines but not in high ionic strength brines (+9 mV and +1 mV respectively for FB-3; +7 mV and +1 mV respectively in CAST-2). The zeta potential of BERB-2 changes by the same amount (+3 mV) when the temperature is increased in both high and low ionic strength brines. No change in the zeta potential outside of experimental error was observed when the temperature was increased for the Fontainebleau samples saturated at high ionic strength.

It has been previously observed that increasing temperature decreases the magnitude of the zeta potential in sandstones or sandpacks saturated with low ionic strength NaCl brines (Vinogradov and Jackson 2015; Vinogradov et al. 2018). In high ionic strength NaCl brines the zeta potential has been observed to be independent of temperature (Vinogradov and Jackson 2015; Vinogradov et al. 2018). Similar trends have also been observed for carbonate core samples (Al Mahrouqi et al. 2017a). In Figure 4-5, $\Delta\zeta_{Temp}$ is generally larger in low ionic strength brines for a given sample, in line with these observations, however, $\Delta\zeta_{Temp}$ is non-zero in several samples when measured with high ionic strength brines.

The change in zeta potential with temperature in sandstones has been shown to be caused by changes in the surface charge due to the temperature dependence of the brine pH (Vinogradov and Jackson 2015; Vinogradov et al. 2018). The pH of low ionic strength NaCl brines decreases with increasing temperature yielding a less negative zeta potential (see Figure 4-3 and Vinogradov et al. (2018)). The pH of high ionic strength NaCl brines is unaffected by temperature and therefore the zeta potential is independent of temperature (Vinogradov et al. 2018). However, as was shown in Figure 4-3 no correlation between the

zeta potential and the brine pH at ambient or elevated temperature was observed in these more complex core samples and brine compositions.

Despite no clear correlations between the rock type, brine composition or pH, these results suggest that elevated temperature in natural systems causes the zeta potential to become smaller in magnitude, with the effect stronger in low ionic strength brines.

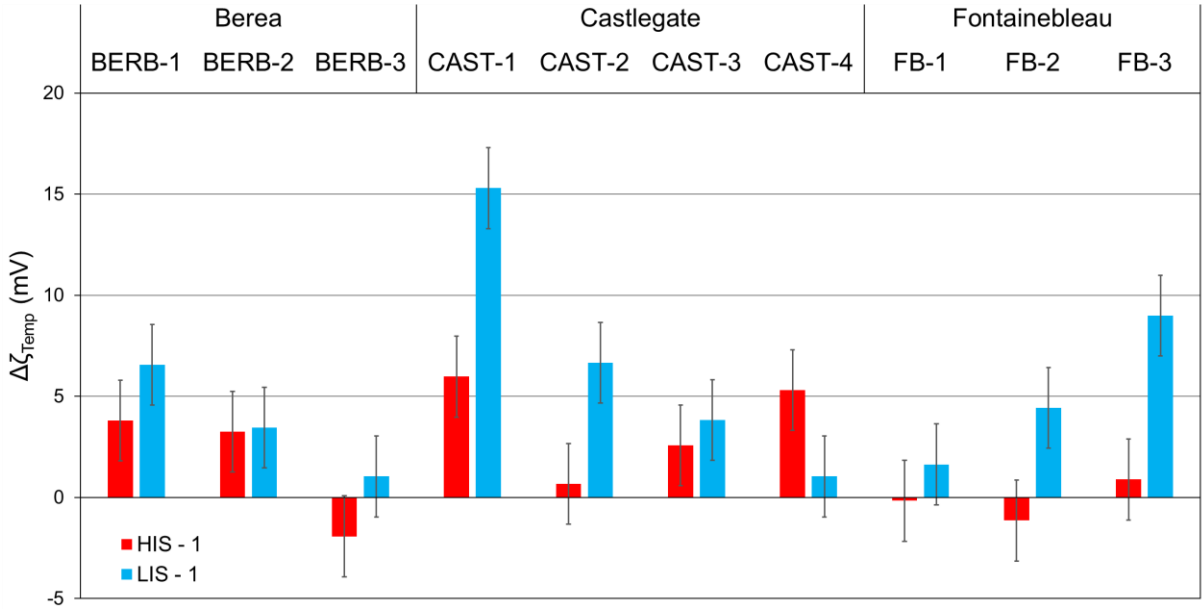

Figure 4-5: Difference between zeta potential measurements obtained on natural, intact sandstone core samples at ambient laboratory temperature (23 ^{O}C) and elevated temperature (70 ^{O}C) when saturated with high (red bars) and low (blue bars) ionic strength brines representative of those found in subsurface environments.

4.4 Discussion

4.4.1 Controls on the Zeta Potential of Natural Sandstones

The zeta potential measurements obtained here on natural sandstone cores at subsurface conditions are consistent with several trends previously observed on clean or crushed sandstones under ideal conditions. Namely (i) the macro-scale zeta potential is typically negative indicating most of the micro-scale mineral-surfaces are negatively charged (ii) increasing temperature decreases the magnitude of the macro-scale zeta potential in low ionic strength brines and (iii) the macro-scale zeta potential varies between different rock types. However, the data presented here show some observations that differ from previous trends. Firstly, increasing temperature also appears to decrease the magnitude of the macro-scale zeta potential in high ionic strength brines. Secondly, a lower ionic strength brine does not always yield a more negative zeta potential. Finally, individual samples of the same rock type can exhibit different macro-scale zeta potential measurements, highlighting the underlying heterogeneity in the micro-scale zeta potential distribution.

To explore the impact of the micro-scale zeta potential distribution on the macro-scale zeta potential of the different rock types, only the measurements obtained at ambient temperature are considered since elevated temperature measurements were not obtained on all rock types. The bulk clay content is considered to act as a proxy measure for the mineralogical heterogeneity of the samples. The samples are not differentiated by the specific types of clays present. Different clay minerals are known to exhibit different micro-scale zeta potential behaviour, thus a sample with a larger bulk clay content is expected to exhibit a broader range of micro-scale zeta potential values than a cleaner, quartz rich sample. It is the distribution of these minerals on the surface of the pore space, rather than the bulk content, that will ultimately determine their contribution to the macro-scale zeta potential. However, the surface area distribution of minerals within a pore space cannot be easily determined. It is assumed that an increased bulk clay content will correlate with an increase in the amount of

clay present in the pore space. The bulk clay content is therefore assumed to act as a measure for the fraction of the pore surface covered by clay. Thus, samples with a larger bulk clay fraction will exhibit a broader micro-scale zeta potential distribution than clean samples and will also contribute to a larger portion of the overall macro-scale zeta potential.

The impact of the bulk clay content on the zeta potential is shown in Figure 4-6. The average zeta potential of each rock type measured high ionic strength brines (red crosses) and low ionic strength brines (blue bars) is plotted against the bulk clay content. The average of the difference in zeta potential when measured with high and low ionic strength brines, $\Delta\zeta_{IS}$ (black circles) is also shown. Error bars show the variability in the samples, not errors in the experimental measurements.

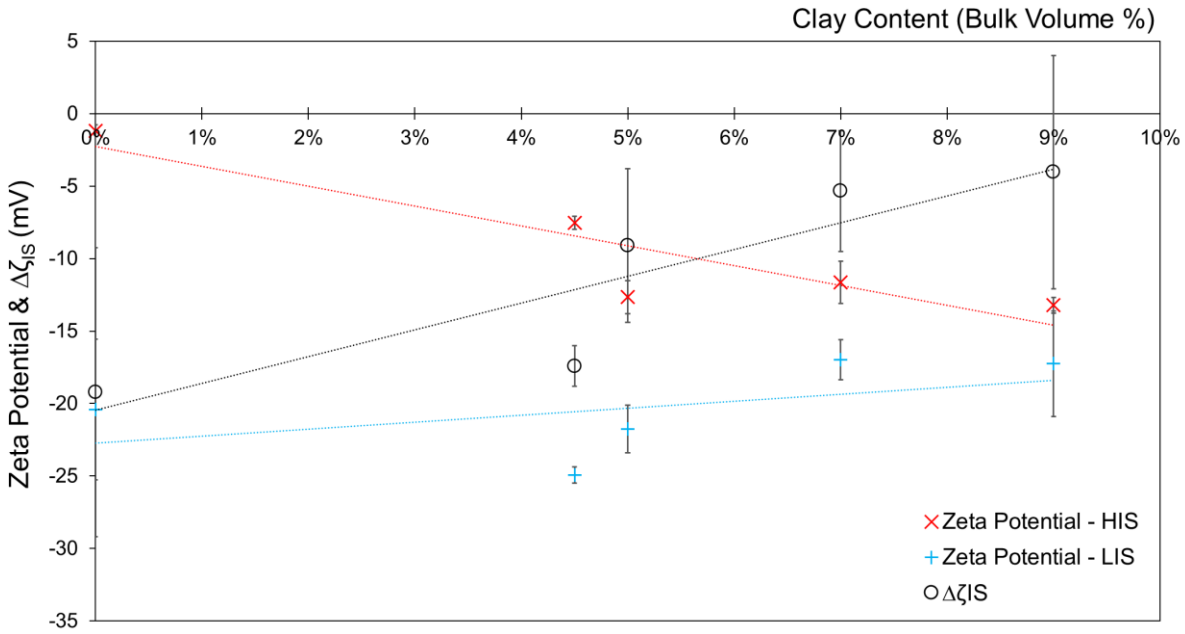

Figure 4-6: Average zeta potential of different rock types measured with high (red crosses) and low (blue crosses) ionic strength brines at ambient temperature plotted as a function of bulk clay content (bulk volume %). Difference between two measurements, ΔζIS, also shown (black circles).

The macro-scale zeta potential in high ionic strength brines becomes more negative with increasing clay content, whilst the macro-scale zeta potential in low ionic strength brines becomes less negative with increasing clay content, although to a lesser extent. $\Delta\zeta_{IS}$

decreases with increasing clay content as the high and low ionic strength zeta potential measurements converge.

The variability in the zeta potential of samples of the same rock type shown by the size of the error bars increases with increasing clay content. Rock types with a larger clay content will be more heterogeneous and should exhibit a broader and more complex micro-scale zeta potential distribution. It is unsurprising therefore that different core samples of clay rich sandstones may exhibit different macro-scale zeta potential measurements, yielding the increased variability.

In low ionic strength NaCl brines, it has been shown that a reduction in the ionic strength typically yields an increase in the magnitude of the zeta potential of both crushed and intact sandstones (Figure 2-10) This is consistent with conventional theories of double layer expansion due to a reduction in the extent of counter-ion screening (e.g. Hunter 2013). In sandstones, a reduction in the brine ionic strength often yields a more negative zeta potential since the sandstone surface is thought to be negatively charged (Stumm et al. 1992). However, it has been reported that the macro-scale zeta potential of Berea sandstone core samples measured with NaCl brines can become less negative with a reduction in the ionic strength (Li et al. 2018). It was shown that adsorption onto clay surfaces of trace Ca^{2+} ions sourced from the rock increased as the ionic strength decreased (Li et al. 2018). Adsorption of Ca^{2+} modifies the surface charge to make the micro-scale zeta potential of the clay minerals more positive. The extent of Ca^{2+} adsorption increases as the cation exchange capacity (CEC) increases (Eriksson 1952). Clay minerals generally have a high CEC due to a large, negatively charged surface area (Ammann et al. 2005; Borden and Giese 2001). Thus, clay minerals have many surface sites where cationic species can adsorb.

In clay rich samples saturated with low ionic strength brines, modification of the surface charge via divalent cation adsorption competes with the low counter-ion screening to determine the micro-scale zeta potential of a mineral surface. If there is sufficient Ca^{2+} adsorption on the micro-scale this can ultimately yield a more positive macro-scale zeta

potential. In the low ionic strength brines used in this chapter, approximately 20% of the ionic species are Ca^{2+} whilst a further 7% are Mg^{2+}. In comparison, Li et al. (2018) observed that only 2% Ca^{2+} in the bulk brine was sufficient to alter the macro-scale zeta potential. Divalent cation adsorption to the clay surfaces would therefore be expected, with the extent increasing with increasing clay content since the brine composition and ionic strength are largely consistent across experiments. The increasingly positive macro-scale zeta potential with increasing clay content is therefore ascribed to adsorption of Ca^{2+} and or Mg^{2+} ions to the clay surfaces, making the surface charge and micro-scale zeta potential more positive.

In high ionic strength brines, divalent cation adsorption at the micro-scale is suppressed due to the increased counter-ion screening of the surface electrical potential. Intermolecular effects such as ion-ion interactions (Siretanu et al. 2014; Ebeling et al. 2011) and steric forces (Bohinc et al. 2017; Borukhov et al. 1997) can become increasingly significant in determining the ion density and packing structure near a charged interface. These forces are particularly important when high concentrations of divalent cations are present (Van Lin et al. 2019; Perkin 2012; Smith et al. 2019; de Souza and Bazant 2020) as in the high ionic strength brines used here. Under such conditions, the distribution of ionic species near to an interface is primarily controlled by these intermolecular interactions and becomes largely independent of the electrostatic properties of the surface.

The high ionic strength brines used here are largely similar in composition and concentration so the ion distribution near the mineral surfaces will be similar in all samples. Divalent cation adsorption will be suppressed, and the extent of counter-ion screening will be the same in all experiments. Consequently, the micro-scale zeta potential at a mineral surface will therefore largely reflect the surface potential. The macro-scale zeta potential will be determined by the micro-scale surface potential distribution. Clay minerals have a large surface area and a larger number of surface sites than quartz (shown by the larger CEC e.g., Carroll 1959) which yields a more negative surface potential. Thus, when ionic adsorption and

electrostatic interaction with the mineral surface is suppressed under high ionic strength conditions, clay minerals should yield a more negative micro-scale zeta potential than quartz.

Rock types with a larger clay content will therefore exhibit a micro-scale zeta potential distribution that is more negative than pure quartz or clay free sandstones. Consequently, core samples of clay rich rock types will exhibit a more negative macro-scale zeta potential. This trend is clear in Figure 4-6 and has also been observed in other studies. Ur Rahman Awan et al. (2022) showed an increasingly negative zeta potential with increasing clay content for natural sandstone cores saturated with high ionic strength NaCl brines. Furthermore, the macro-scale zeta potential of soil packs has been shown to become more negative with increasing CEC when saturated with NaCl brines (Akbulut and Arasan 2010; Li et al. 2014; Tone et al. 1998).

Minerals with a low CEC, such as quartz, have limited capacity for cation adsorption. The micro-scale zeta potential of these surfaces is therefore controlled primarily by the surface charge and the extent of counter-ion screening, the latter of which is determined by the ionic strength of the brine. In the clean, pure quartz Fontainebleau samples, the zeta potential will be primarily controlled by the ionic strength since the surface charge should be largely unaffected by the brine composition or concentration. Indeed, $\Delta\zeta_{IS}$ is large indicating the zeta potential in low ionic strength brines is more negative than in high ionic strength brines; observations consistent with conventional double layer expansion and counter-ion reduction.

Conversely, as discussed, clay minerals with a higher CEC have a greater propensity for cation adsorption. The extent of divalent cation adsorption increases with increasing surface charge (which can be represented by the CEC), decreasing brine ionic strength and increasing divalent cation composition. When the brine ionic strength is decreased in these experiments, the increased divalent cation adsorption competes with the reduction in counter-ion screening to determine the micro-scale zeta potential. If a significant portion of the pore surface area is covered by clay, then these minerals will contribute more to the macro-scale zeta potential behaviour. The clay-rich Berea and Castlegate samples are expected to have a

larger portion of the pore surface area covered by clay. Therefore, at low ionic strength, cation adsorption is a primary control on the macro-scale zeta potential of these samples. If cation adsorption is significant, the macro-scale zeta potential may become more positive with decreasing brine ionic strength (see CAST-2, Figure 4-2).

The discrepancies between these observations and previous trends highlight the importance of measuring the macro-scale zeta potential on intact, natural samples under representative subsurface conditions. Crushing samples to measure the macro-scale zeta potential by electrophoresis changes the micro-scale zeta potential distribution by exposing fresh interfaces to the brine. The bulk clay volume of these samples is generally small (>10%) but has been observed to be an important control on the zeta potential. These subtle changes are lost when the sample is crushed, and the dominant interface is quartz. Moreover, crushing destroys the natural rock textures and heterogeneity within the sandstone. These can have an important effect on the micro-scale zeta potential distribution due to differences in the surface potential of faces/edges of mineral crystals (Li et al. 2020). Rock textures may be important in clay-rich samples where clay minerals may make up only a small amount of the bulk volume but may contribute a large proportion to the macro-scale zeta potential due to their high surface area.

Surface complexation modelling of the ion-exchange interactions between different mineral species and the ionic species in complex subsurface brines would be an important extension of this work to validate the interpretation of the experimental results. However, the discrepancy between zeta potential measurements made on crushed and intact sandstones cores suggest the interactions between different minerals may not be the only control. Coupling geochemical exchange reactions with a pore network that explores the distribution of mineral species on the pore surface may also be an important extension.

4.4.2 Implications for Controlled Salinity Waterflooding

It has been shown in chapter 3 that for successful CSW the injection brine composition must modify the zeta potential at the mineral-brine interface in such a way as to induce an electrostatic repulsion between the mineral-brine and oil-brine interfaces. The zeta potential of natural sandstones under appropriate reservoir conditions has been poorly understood. It is widely assumed that dilution of the injection brine (as in a conventional LSW) yields a more negative zeta potential at the sandstone-brine interface (Nasralla and Nasr-El-Din 2014a; Pooryousefy et al. 2018; Brady et al. 2015; Austad, RezaeiDoust, and Puntervold 2010).

The results presented here suggest that dilution of the injection brine may not necessarily yield a more negative zeta potential, particularly in clay-rich sandstones (Figure 4-4). Dilution of the injection brine may yield no significant change in the zeta potential or may make the zeta potential more positive. Furthermore, the change in zeta potential at elevated reservoir temperature may be even less significant (Figure 4-5). The parameter $\Delta\zeta_{IS}$ (equation 4-2) is analogous to $\Delta\zeta_{CSW}$ (equation 3-4). It was shown that the amount of additional oil recovered from carbonate core samples during CSW was proportional to $\Delta\zeta_{CSW}$. The results shown here for sandstones suggest that dilution of the injection brine may only yield a negligible $\Delta\zeta_{CSW}$ that is insufficient to generate a significant enough electrostatic repulsion to observe IOR. Moreover, $\Delta\zeta_{IS}$ was observed to be smaller in clay rich sandstones implying CSW may be less significant in these rock types, despite previous suggestions these sandstones are ideal candidates for CSW. However, clay rich sandstones are thought to be more oil-wet than clean sandstones (Anderson 1986b). It was seen in Chapter 3 the amount of IOR in carbonates also correlated with increasing oil-wetness (the majority of which were strongly oil-wet). The importance of clays for CSW may therefore be a competing balance between rendering the sandstone more oil-wet and allowing the zeta potential of the mineral surfaces to be modified to a significant enough extent to induce an electrostatic repulsion.

Instead of simply diluting the injection brine, modifying the zeta potential of sandstones may be more effective by modifying the composition of the injection brine. Specifically removing divalent cations to limit the extent of adsorption at lower ionic strength.

4.5 Conclusions

The macro-scale zeta potential of natural intact sandstone cores under representative subsurface conditions of brine composition, ionic strength and temperature can differ significantly from the micro-scale zeta potential behaviour of the constituent minerals under ideal conditions.

The zeta potential of sandstones at reservoir conditions is typically negative in polarity but does not always increase in magnitude with a reduction in ionic strength in clay-rich samples.

The zeta potential in high ionic strength brines becomes more negative with increasing clay content due to an increase in the negative surface charge. In low ionic strength brines, the zeta potential becomes more positive with increasing clay content due to increased adsorption of divalent cations to the more negatively charged surface.

Increasing the temperature makes the zeta potential less negative and smaller in magnitude, including under high ionic strength conditions. The difference between the zeta potential in high and low ionic strength brines at elevated temperature is suppressed.

These results have important implications for low salinity waterflooding in sandstone reservoirs.

Chapter 5 - Relationship Between Zeta Potential and Wettability in Porous Media: Insights from a Simple Bundle of Capillary Tubes Model

---

The results and ideas presented in this chapter have been published in the *Journal of Colloid and Interface Science* as:

Collini, H. and Jackson, M.D., 2022. Relationship Between Zeta Potential and Wettability in Porous Media: Insights From a Simple Bundle of Capillary Tubes Model. Journal of Colloid and Interface Science, 608, pp.605-621.

Abstract

This chapter presents a simple bundle of capillary tubes model that is used to explore the relationship between the wettability and the zeta potential of porous media that has been identified thus far. The novelty lies in the assignment of different surface charges to capillaries depending on wetting state. Integrating over all capillaries depending on fluid occupancy determines the macroscale properties of interest. The model shows a good match to the limited experimental data available and is used to determine the zeta potential of the oil-brine interface in the experiments presented in chapter 3. The oil-brine zeta potential is found to be positive in a majority of cases. Whilst the model provides a good match to the data in oil-wet cases, the results do not match the zeta potential behaviour of mixed-wet systems as well. The limitations of the model are discussed and suggestions for how the model can be extended are provided.

5.1 Introduction

Wetting describes the tendency of one fluid to spread over a solid surface in the presence of a second fluid. Wettability defines the degree of wetting. In Chapter 2 we saw the importance of wettability for controlling the pore scale distribution of fluids and the dynamics of multiphase flow (Blunt and Scher 1995; Blunt 2017; Dagan 2012). Furthermore, wettability alteration is observed during CSW.

In Chapter 3 we observed a relationship between the wettability of intact carbonate core samples, measured using the Amott water wetting index, (see section 3.3.2 and Amott 1959) and the macro-scale zeta potential of the samples, measured using the streaming potential method (SPM) (see Figure 3-8; Jackson and Vinogradov (2012); Jackson et al. (2016a)). The macro-scale zeta potential measured in porous media or powder suspensions represents a complex average over the micro (mineral-surface)-scale zeta potentials, that may vary across different minerals in heterogeneous (multi-mineral) samples, or across the different faces of a given mineral in homogenous (single mineral) samples (Li et al. 2020). It has been suggested through a simple qualitative pore scale model that oil-wet mineral surfaces return the micro-scale zeta potential of the oil-brine interface. Changes in the macro-scale zeta potential of a core sample with wettability alteration therefore indicate the polarity of the oil-brine zeta potential (Jackson and Vinogradov (2012) and Jackson et al. (2016a)).

Although this simple model can explain, conceptually, the observed experimental behaviour, it does not provide a quantitative relationship between macro-scale zeta potential and wettability in porous media. Such a relationship requires a pore-scale model, the development of which is the main aim of this chapter. A pore-scale model can also yield new insight into the relationship between macro-scale zeta potential and water saturation, for which there are almost no experimental data. The lack of experimental data relating macro-scale zeta potential and water saturation in porous media provides further motivation for the development of a pore-scale model.

Given that this is the first model of its type, the model is derived from the simplest possible description of the rock pore-space that captures the necessary physics: a bundle of capillary tubes of different size. Although it is a much-simplified representation of the pore-space of a reservoir rock, the model is useful because it allows the governing equations to be derived from first principles (see Hunter (1981a) for examples in single phase flow). A capillary tubes model is the simplest possible approach to relate micro-scale (mineral-surface-scale) and macro-scale (continnum-scale) properties of wettability and zeta potential; such models have been extensively used to investigate and quantify streaming potentials during single and multi-phase flow in water-wet systems (Allègre et al. 2015; Cheng et al. 2018; Jougnot et al. 2012; Jougnot et al. 2020; Revil et al. 2007; Soldi et al. 2018; Vinogradov et al. 2021; Jouniaux and Ishido 2012; Revil and Linde 2006; Linde et al. 2007). Understanding the behaviour of such simple models underpins the development and application of pore-scale models that capture more realistic representations of pore geometry, fluid occupancy and connectivity (Blunt et al. 2002).

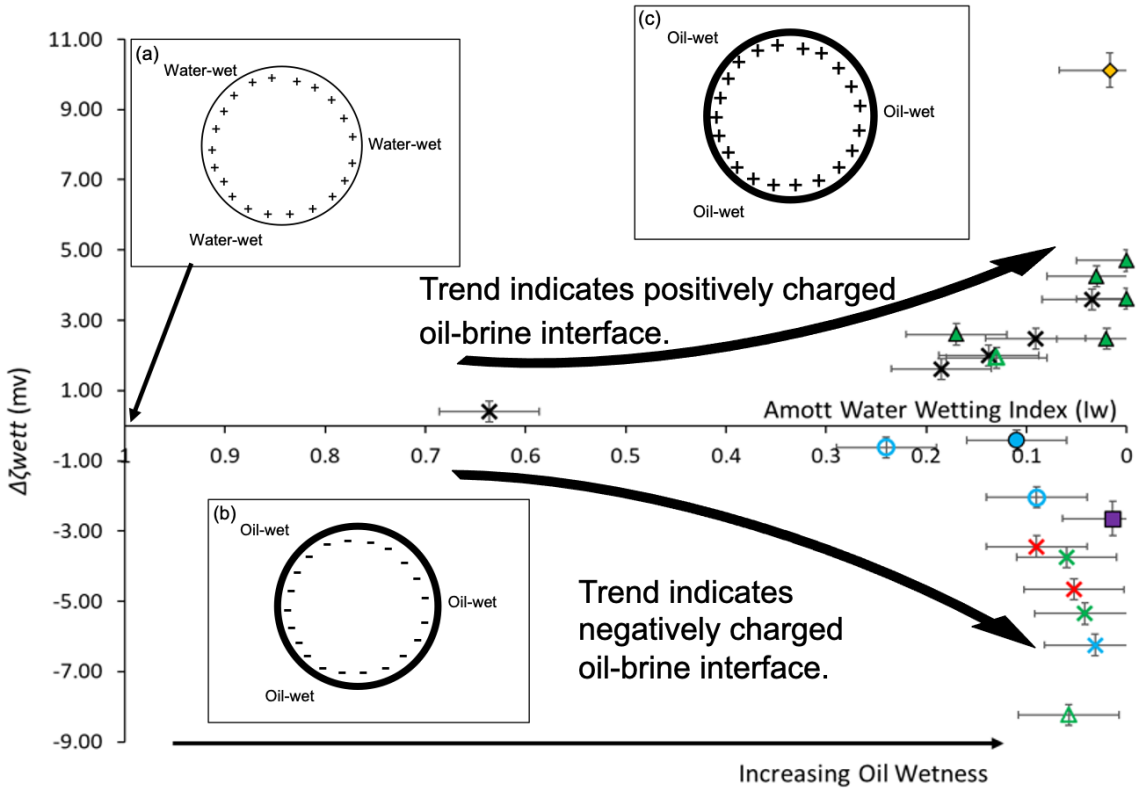

Figure 5-1: Experimental data (adapted from Figure 3-8) showing the change in macro-scale zeta potential measured on intact natural carbonate cores after drainage and aging with crude oil and natural saline brine. Triangles represent measurements made at room temperature and circles represent measurements made at elevated temperature (>70 ^{O}C). The different colours represent different crude oils (see Chapter 3 for more details). Data plotted as a function of the Amott water wetting index (Iw). Inset (a) is a schematic of a model capillary that is water-wet and brine saturated. The mineral surface of the capillary has a positive micro-scale zeta potential in this example, consistent with the experimental data reported in Chapter 3 for the carbonate cores investigated. Insert (b) represents samples in which the measured macro-scale zeta potential becomes more negative after wettability alteration. The micro-scale oil-brine zeta potential is negative, so the macro-scale zeta potential becomes more negative as more of the mineral surfaces become oil-wet. Insert (c) represents samples in which the measured macro-scale zeta potential becomes more positive after wettability alteration. The micro-scale oil-brine zeta potential is positive and larger in magnitude than the mineral-brine zeta potential, so the macro-scale zeta potential becomes more positive as more of the mineral surfaces become oil-wet.

5.2 Bundle of Capillary Tubes Model

The bundle of capillary tubes model used in this paper is derived from similar models used in previous studies (Jackson 2010; Jackson 2008; Vinogradov et al. 2021). The macro-scale properties of interest here are water saturation, Amott water-wetting index, and zeta potential. The Amott water wetting index (Amott 1959) is defined in equation (2-2a).

To determine the macro-scale properties, it is necessary to calculate total and water-saturated pore (capillary) volumes, and the electrokinetic coupling in water-saturated capillaries. The key equations and derivations are outlined from first principles. The model derivation first considers a single capillary tube with radius r_c, occupied by a single phase; then integrates over all capillaries with different phase occupancy and values of r_c to determine the macro-scale properties for the entire model. The simple capillary tubes model is extended beyond previous studies by assigning a different micro-scale zeta potential to water- and oil-wet capillaries, and calculating the resulting macro-scale wettability index and zeta potential to provide the first quantitative relationship between wettability and zeta potential for a simple model of a porous medium.

5.2.1 Volume and Electrokinetic Coupling in a Single Capillary

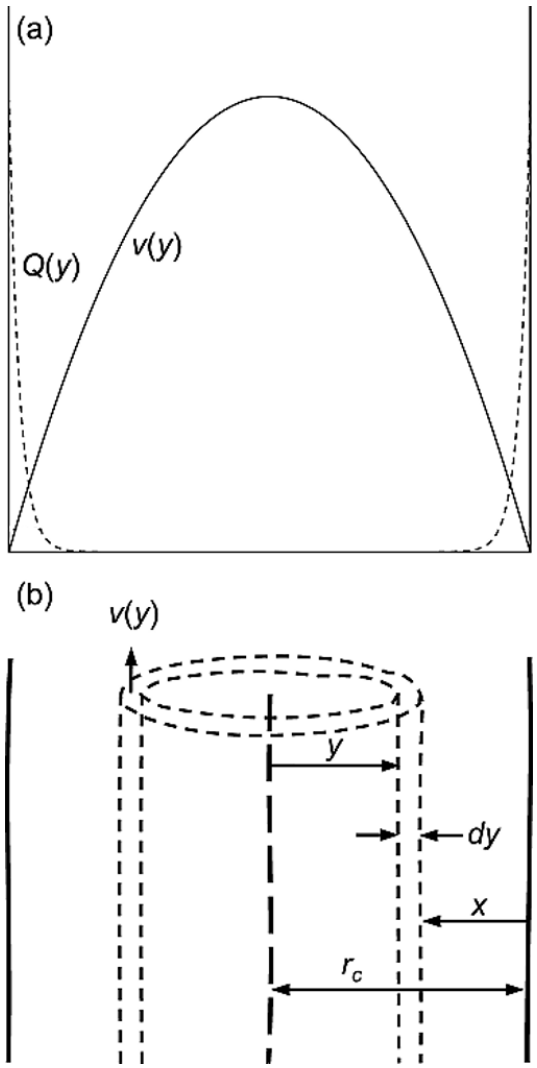

Figure 5-2: (a) Flow velocity v(y) (solid line) and excess countercharge Q(y) (dashed line) within a brine-occupied capillary, invoking the thin double-layer assumption and a constant surface charge density. The width of the thin double layer has been greatly exaggerated. (b) Calculation of the streaming current. Modified from Jackson (2010).

Let us begin by considering a single, water-occupied capillary of length L_c and radius r_c. The volume of the capillary is trivially given by

$$V_c = \pi r_c^2 L_c \quad (5\text{-}1)$$

Assume that only water (brine) and oil are present in the model, denoted by the subscripts *w* and *o* respectively. Each capillary is occupied by a single, mobile, fluid phase, but the capillaries can be wetted by a thin layer of either phase. This wetting layer is immobile

and volumetrically insignificant relative to the total volume of the capillary, and thus does not contribute to the phase saturation. The capillary tube is assumed to be initially water-wet and can become oil-wet only if it has been invaded by oil.

The streaming potential within the capillary arises from the electrical charge on the capillary surface. In this model, the capillaries are assumed to be comprised of homogenous calcium carbonate and assume a constant surface charge density. Calcium carbonate was chosen to be consistent with the experimental data against which the model predictions are compared (see Chapter 3; Revil and Cerepi (2004) and Jackson et al. (2016a). Although it is immobile and volumetrically insignificant, the wetting layer is important because it dictates the surface charge. Water-wet, brine-occupied capillaries exhibit the charge at the carbonate-brine interface. Conversely, oil-wet, brine-occupied capillaries exhibit the charge at the oil-brine interface: polar species present in the oil can modify the surface charge during wettability alteration (Figure 5-1; Figure 2-9).

The charge on the capillary surface results in the development of an electrical double layer (EDL). The EDL is assumed to comprises a layer of fixed, immobile ions (the 'Stern layer' (Hunter 1981a), separated at the Stern plane from a 'diffuse layer' of mobile ions (Figure 2-7). The "thin double layer assumption" is invoked to describe the excess charge in the diffuse layer, $Q(y)$, which is valid when the thickness of the electrical double layer is much smaller than the local radius of curvature. This assumption has been shown to be valid in reservoir rocks (Jackson and Leinov 2012).

During brine flow, relative motion of the excess charge in the diffuse layer along the shear plane yields a streaming current. The location of the shear plane is a variable often tuned to match experimental zeta potential data (Revil, Pezard, and Glover 1999). The simplest assumption is that the shear plane coincides with the Stern plane and thus, the effective radius of each capillary can be defined the distance from the Stern plane to the centre line of the capillary (Figure 5-2). Oil is assumed to be non-conductive and to carry no electrical charge, consistent with experimental data (Jackson et al. 2011) consequently, the flow of oil

through oil occupied capillaries does not generate a streaming current and is not considered here.

Applying boundary conditions of steady laminar flow of brine into and out of the capillary, the streaming current through a single capillary is given by (Hunter 1981a):

$$I_{S,C} = \int_0^{r_c} 2\pi y Q(y) v(y)\, dy \qquad (5\text{-}2)$$

The velocity profile, *v(y),* across the capillary is described by Poiseulle's law (Figure 5-2a):

$$v(y) = \frac{1}{4\mu_b}(r_c^2 - y^2)\frac{\Delta P}{L_c} \qquad (5\text{-}3)$$

where μ_b is the viscosity of the brine, *y* is the distance from the centre of the capillary (Figure 5-2) and ΔP is the pressure drop along the capillary of length L_c.

The double layer is confined to a thin region near the wall of the capillary and, following (Hunter 1981a) and numerous other textbooks, invoking this assumption can linearize Poiseulle's equation close to the capillary wall to give

$$({r_c}^2 - y^2) \approx 2r_c(r_c - y) \qquad (5\text{-}4)$$

Substituting $x = (r_c - y)$, equation (5-2) becomes

$$I_{S,C} = \int_0^{r_c} \frac{2\pi(r_c - x) r_c x \Delta P}{2\mu_b L_c} Q(x)\, dx \qquad (5\text{-}5)$$

The thin nature of the double layer can be used to further linearize the streaming current, giving

$${r_c}^2\left(x - \frac{x^2}{r_c}\right) \approx {r_c}^2 x \qquad (5\text{-}6)$$

The charge density in the EDL *Q(x)* can be described by Poisson's equation (Hunter 1981a):

$$\varepsilon_b \frac{d^2V}{dx^2} = Q(x) \qquad (5\text{-}7)$$

where ε_b is the permittivity of the brine which is assumed constant, and V is the electrical potential in the diffuse layer. Substituting equations (5-6) and (5-7) into equation (5-5) and integrating by parts yields an expression for the streaming current through a single capillary, in terms of the zeta potential of the capillary surface, the brine viscosity and permittivity, and the pressure gradient along the capillary.

In water-wet capillaries, the micro-scale zeta potential of the capillary surface corresponds to the carbonate mineral-brine interface (ζ_{mb}) whereas in oil-wet capillaries, the micro-scale zeta potential of the capillary surface corresponds to the oil-brine interface (ζ_{ob}). The streaming current in each case is given, respectively, by

$$I_{S,C} = \frac{-\varepsilon_b \zeta_{mb} \pi r_c^2 \Delta P}{\mu_b L_c} \qquad (5\text{-}8a)$$

$$I_{S,C} = \frac{-\varepsilon_b \zeta_{ob} \pi r_c^2 \Delta P}{\mu_b L_c} \qquad (5\text{-}8b)$$

The boundary conditions are zero current flow into or out of the capillary and no charge accumulation at the end of the capillary (Hunter 1981a). The streaming current must then be balanced by a conduction current of equal magnitude but opposite direction. The conduction current in a single capillary is given by Ohm's law (Hunter 1981a):

$$I_{C,C} = \pi r_c^2 \sigma_b \frac{\Delta V}{L_c} + 2\pi r_c \sigma_s \frac{\Delta V}{L_c} \qquad (5\text{-}9)$$

where ΔV is the streaming potential difference across the capillary, σ_b is the conductivity of the brine and σ_s is the surface conductivity due to the presence of the EDL. Oil-occupied capillaries are non-conductive.

Equating the streaming and conduction currents, consistent with the boundary conditions, and rearranging yields:

$$\frac{\Delta V}{\Delta P} = C = \frac{\varepsilon_b \zeta_{mb}}{\mu_b (\sigma_b + \frac{2\sigma_s}{r})} \qquad (5\text{-}10a)$$

$$\frac{\Delta V}{\Delta P} = C = \frac{e_b \zeta_{ob}}{\mu_b(\sigma_b + \frac{2\sigma_s}{r})} \qquad (5\text{-}10b)$$

for water-wet, brine-occupied, and oil-wet, brine-occupied capillaries respectively, where *C* is termed the streaming potential coupling coefficient. Neglecting surface electrical conductivity, as is typical in highly conductive, saline brines, simplifies these equations to the well-known Helmholtz-Smoluchowski equation:

$$\frac{\Delta V}{\Delta P} = C = \frac{\varepsilon_b \zeta_{mb}}{\mu_b \sigma_b} \qquad (5\text{-}11a)$$

$$\frac{\Delta V}{\Delta P} = C = \frac{\varepsilon_b \zeta_{ob}}{\mu_b \sigma_b} \qquad (5\text{-}11b)$$

for water-wet and oil-wet capillaries, respectively. If surface electrical conductivity is negligible, the relationship between the coupling coefficient and zeta potential is independent of the capillary tube properties i.e. the model microstructure (Hunter 1981a).

5.2.2 Bundle of Capillary Tubes

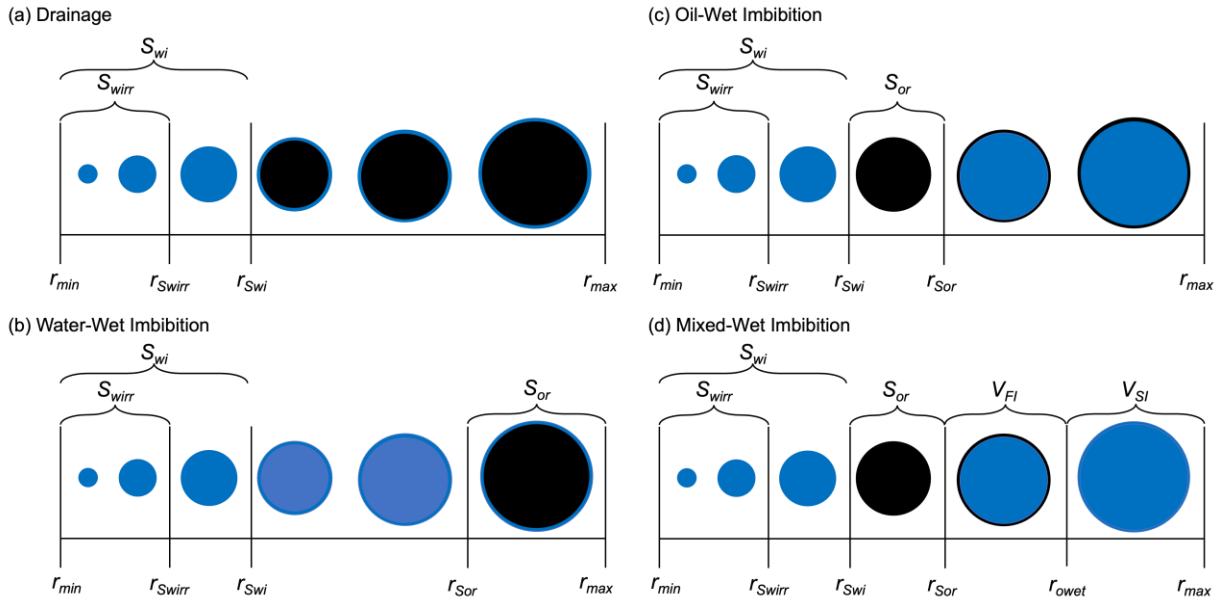

Figure 5-3: Schematic of the bundle of capillary tubes model for (a) drainage and (b-d) waterflooding with different wetting states. (b) shows the case where all capillaries remain water-wet after drainage and aging; (c) shows the case where oil-invaded capillaries become oil-wet after drainage and aging, and (d) shows the case where only the smaller pores become oil-wet after drainage and aging to yield a mixed-wet model.

The single capillary model is now extended to a bundle containing N capillaries orientated in the same direction, with no intersections between capillaries, which results in unidirectional mass and charge transport. The capillaries have different radii to allow for varying fluid occupancy. The number of capillaries with radius between r_c and $r_c + \mathrm{d}r_c$ is given by $n(r_c)\mathrm{d}r_c$ such that integrating over all capillaries gives:

$$\int_{r_{min}}^{r_{max}} n(r_c)\mathrm{d}r_c = N \qquad (5\text{-}12)$$

where r_{min} and r_{max} are the minimum and maximum capillary radii respectively. This model considers 1000 capillaries, the radii of which are determined by a simple capillary size distribution of the form:

$$n(r)dr_c = D\left(\frac{r - r_{max}}{r_{min} - r_{max}}\right)^c \qquad (5\text{-}13)$$

where *c* takes integer values between 0 and 12 (Jackson 2010) and *D* is a constant dependent on the values of *N* and *c*. Larger values of *c* skew the distribution to increase the frequency of smaller pores which is observed in many geological porous media (Dullien 2012). This simple expression allows us to quantitatively investigate the effect of the pore-size distribution on the model zeta potential and wettability.

The mobile phase occupying each capillary is determined assuming capillary equilibrium. There is no need to specify or calculate a capillary number, but it is assumed to be sufficiently large enough for capillary equilibrium. During drainage, when the (initially) non-wetting oil phase invades the (initially) water-wet capillaries, the oil invades the capillaries in order of size, from largest to smallest (Jackson and Blunt 2002; Figure 5-3a). During waterflooding (defined here as invasion of water into the capillaries regardless of wetting state resulting in an increase in the water saturation), the water invades water-wet capillaries first (spontaneous imbibition) in the order smallest to largest (Figure 3a), before invading oil-wet capillaries in the order largest to smallest (Figure 5-3b).

The general procedure for calculating the macro-scale bulk and transport properties of the model (described in Jackson, 2008) is simple: the property is defined for a single capillary as shown in the preceding section, and then the macro-scale value is determined by integrating over all capillaries that contribute.

The water saturation is given by the volume of water-occupied capillaries divided by the total capillary (pore) volume, noting that water may occupy the largest or smallest capillaries depending on the wettability. The radius of the smallest water-wet capillary that is occupied by oil is defined r_{omin} and this is varied to vary the water saturation in water-wet models. Similarly, r_{omax} is defined to be the radius of the largest oil-wet capillary that is occupied by oil, and this is varied to vary the water saturation in oil-wet models. In mixed-wet models, both r_{omin} and r_{omax} are varied to vary the water saturation in water- and oil-wet portions of the model, as described in a later section. Given this, the water saturation is generally expressed as:

$$S_w = \frac{\int_{r_{min}}^{r_{omin}} r_c^2 n(r_c) dr_c + \int_{r_{omax}}^{r_{max}} r_c^2 n(r_c) dr_c}{\int_{r_{min}}^{r_{max}} r_c^2 n(r_c) dr_c} \quad (5\text{-}14)$$

with the expression for a given wetting state obtained by adjusting the values of r_{omin} and r_{omax}. These values are discussed for specific wetting scenarios in later sections.

The macro-scale properties of Amott water-wetting index and zeta potential are calculated in similar fashion. These calculations are explained in the following section. Before doing so, the modelling of initial, irreducible and residual water and/or oil saturation are considered. Expressions for other macro-scale model properties such as porosity and permeability can be found in (Jackson 2010) but are not relevant here.

5.2.2.1 Initial, Irreducible & Residual Saturations

Without suitable modification, the bundle of capillary tubes does not allow for the trapping of phases observed in natural porous media: drainage continues until all the capillaries are occupied by the invading oil phase and $S_w = 0$; likewise, waterflooding continues until all the capillaries are occupied by the invading water phase and $S_w = 1$. In real porous media, water is trapped in the smaller pores and the corners of larger pores during drainage. The minimum water saturation, typically termed the irreducible water saturation, S_{wirr} , is therefore some value greater than zero. In some cases, during drainage, the invading oil does not displace all the mobile water, resulting in some initial water saturation $S_{wi} > S_{wirr}$.

5.2.2.2 Irreducible Water Saturation

To account for the irreducible water saturation, a minimum radius, r_{Swirr}, which can be invaded by oil during drainage is defined (Figure 5-3a); capillaries with smaller radii than this minimum value represent the small pores in rocks that are not invaded during primary drainage, yielding an irreducible water saturation given by:

$$S_{wirr} = \frac{\int_{r_{min}}^{r_{Swirr}} r_c^2 n(r_c) dr_c}{\int_{r_{min}}^{r_{max}} r_c^2 n(r_c) dr_c} \qquad (5\text{-}15)$$

Capillaries with $r_c < r_{Swirr}$ remain water-wet and water-occupied and this water is trapped and immobile: it contributes to the electrical conductivity of the model but not to the streaming current. The value of r_{Swirr} can be adjusted to match experimental data for S_{wirr}.

5.2.2.3 Initial Water Saturation

To account for an initial water saturation $S_{wi} > S_{wirr}$, a minimum radius of capillaries, r_{Swi}, is defined to represent those which are invaded by oil during drainage; capillaries with smaller radii than this minimum value represents the smaller pores in rocks that are nonetheless larger than those occupied by irreducible water and could be invaded during primary drainage, yielding an initial water saturation given by:

$$S_{wi} = \frac{\int_{r_{min}}^{r_{Swi}} r_c^2 n(r_c) dr_c}{\int_{r_{min}}^{r_{max}} r_c^2 n(r_c) dr_c} \qquad (5\text{-}16)$$

Capillaries with $r_{Swirr} < r_c < r_{omin}$ remain water-wet and water-occupied but the water is mobile and contributes to the electrical conductivity and streaming current. If oil displaces water from all mobile capillaries, $r_{Swi} = r_{Swirr}$ and equation (5-16) reduces to equation (5-15). The value of r_{Swi} can be tuned to match experimental data for S_{wi}.

5.2.2.4 Residual Oil Saturation

During waterflooding, residual oil is trapped either by snap-off when the oil ganglia in water-wet pores become disconnected, or when flow through wetting layers in oil-wet pores becomes too slow (Blunt et al. 2002). The water saturation during waterflooding returns to some maximum value given by $S_w = 1 - S_{or}$, where S_{or} is the residual oil saturation. The capillary tubes model cannot capture the details of snap-off and layer flow. Instead, the

approach used to account for the residual oil saturation depends on the wetting state of the model.

In a water-wet model, a maximum radius of oil-occupied capillaries, $r_{Sor,}$ is defined to represent those that can be invaded by water during waterflooding (Figure 5-3b), assuming that capillary forces cause the wetting water to initially invade the smaller capillaries leaving oil trapped in the larger capillaries. Conversely, in an oil-wet model, a minimum radius of oil-occupied capillaries, $r_{Sor,}$ is defined to represent those that can be invaded by water during waterflooding (Figure 5-3c), assuming that capillary forces cause the non-wetting water to initially invade the larger capillaries, leaving oil trapped in the smaller capillaries. This approach yields a residual oil saturation given by:

$$S_{or} = \frac{\int_{r_{Sor}}^{r_{max}} r_c^2 n(r_c) dr_c}{\int_{r_{min}}^{r_{max}} r_c^2 n(r_c) dr_c} \qquad \text{(water-wet)} \qquad (5\text{-}17a)$$

$$S_{or} = \frac{\int_{r_{Swirr}}^{r_{Sor}} r_c^2 n(r_c) dr_c}{\int_{r_{min}}^{r_{max}} r_c^2 n(r_c) dr_c} \qquad \text{(oil-wet, } S_{wi} = S_{wirr}\text{)} \qquad (5\text{-}17b)$$

$$S_{or} = \frac{\int_{r_{Swi}}^{r_{Sor}} r_c^2 n(r_c) dr_c}{\int_{r_{min}}^{r_{max}} r_c^2 n(r_c) dr_c} \qquad \text{(oil-wet, } S_{wi} > S_{wirr}\text{)} \qquad (5\text{-}17c)$$

Capillaries containing immobile residual oil do not contribute to either the electrical conductivity or streaming current. The value of r_{Sor} can be adjusted to match experimental data for S_{or}.

5.2.3 Macro-Scale (Model) Zeta Potential and Amott Water Wetting Index

The streaming current is determined by integrating over all capillaries that are occupied by mobile brine ($r_c > r_{Swirr}$), since oil is assumed to be non-conductive. Water-wet capillaries contribute to the streaming current that arises from the surface charge at the mineral-brine interface; oil-wet capillaries contribute to the streaming current that arises from the surface

charge at the oil-brine interface. The total streaming current for the model is the sum of these two contributions, since only water or oil can wet the capillary surface.

Consistent with the boundary conditions defined for a single capillary and assuming the pressure drop across the model is constant, the total streaming current is balanced by the total conduction current. The conduction current is determined by integrating over all brine-occupied capillaries, irrespective of whether the brine is mobile ($r_c > r_{Swirr}$) or irreducible ($r_c < r_{Swirr}$). The exact expressions depend on the model wetting state, which is discussed next.

As shown later, the model predictions are independent of the absolute size of the capillaries and the size distribution. This is because surface electrical conductivity is assumed negligible for the saline brines of interest, so the streaming and conduction currents follow the same paths through the pore-space and so scale in the same way (Jackson 2010; Jougnot et al. 2019; Vinogradov et al. 2021). It is assumed that capillaries are similar in diameter to reservoir rock pores and so small enough to justify the assumption that phase occupancy is dictated by capillary equilibrium; the model is also assumed large enough to correspond to a representative elementary volume (REV). Similar assumptions underpin more complex pore-scale models (Blunt et al. 2002).

5.2.3.1 Drainage and Water-Wet Waterflooding

It is assumed the model remains water-wet during drainage (Figure 5-3a). To calculate the macroscopic zeta potential of the entire model, equation (5-8a) is integrated over all mobile, brine-occupied capillaries to determine the streaming current of the model. The value of r_{omin} is varied to vary the water saturation such that $r_{Swirr} < r_c < r_{omin}$. The streaming current of the model as a function of water saturation is given by:

$$I_{S,M}(S_w) = \int_{r_{Swirr}}^{r_{omin}} \frac{-\varepsilon_b \zeta_{mb} \pi r_c^2 \Delta P}{\mu_b L_c} d(r_c) \qquad (5\text{-}18)$$

Likewise, the total conduction current of the model is calculated by integrating equation (5-9) over all brine-occupied capillaries, varying r_{omin} to vary the water saturation, yielding:

$$I_{C,M}(S_w) = \int_{r_{min}}^{r_{omin}} \pi r_c^2 \sigma_b \frac{\Delta V}{L_c} d(r_c) + \int_{r_{min}}^{r_{omin}} 2\pi r_c \sigma_s \frac{\Delta V}{L_c} d(r_c) \qquad (5\text{-}19)$$

Equations (5-18) and (5-19) must balance to honour the boundary conditions of zero current flow and zero charge accumulation, but to enforce this it is necessary to account for the irreducible water saturation. Equations (5-18) and (5-19) are scaled by the total volume of capillaries through which the streaming and conduction currents act at S_w = 1, such that the normalised streaming and conductions currents are, respectively, given by:

$$I_{S,Mn}(S_w) = \frac{\int_{r_{Swirr}}^{r_{omin}} \frac{-\varepsilon_b \zeta_{mb} \pi r_c^2 \Delta P}{\mu_b L_c} d(r_c)}{\int_{r_{Swirr}}^{r_{max}} r_c^2 d(r_c)} \qquad (5\text{-}20)$$

$$I_{C,Mn}(S_w) = \frac{\left(\int_{r_{min}}^{r_{omin}} \pi r_c^2 \sigma_b \frac{\Delta V}{L_c} d(r_c) + \int_{r_{min}}^{r_{omin}} 2\pi r_c \sigma_s \frac{\Delta V}{L_c} d(r_c)\right)}{\left(\int_{r_{min}}^{r_{max}} r_c^2 d(r_c) + \int_{r_{min}}^{r_{max}} r_c d(r_c)\right)} \qquad (5\text{-}21)$$

Equating equations (5-20) and (5-21) and re-arranging yields the following expression for the macro-scale coupling coefficient:

$$\frac{\Delta V}{\Delta P} = C(S_w) = \frac{\varepsilon_b \zeta_{mb} \left(\frac{\int_{r_{Swirr}}^{r_{omin}} r_c^2 n(r_c) dr_c}{\int_{r_{Swirr}}^{r_{max}} r_c^2 n(r_c) dr_c}\right)}{\mu_b \left(\frac{\sigma_b \int_{r_{min}}^{r_{omin}} r_c^2 n(r_c) dr_c + \sigma_s \int_{r_{min}}^{r_{omin}} r_c}{\int_{r_{min}}^{r_{max}} r_c^2 n(r_c) dr_c + \int_{r_{min}}^{r_{max}} r_c}\right)} \qquad (5\text{-}22)$$

Equation (5-22) is the Helmholtz-Smoluchowski equation for the water-wet bundle of capillaries model and accounts for the saturation dependence of the streaming potential coupling coefficient. The corresponding water saturation is given by equation (5-14) with r_{omax} = r_{max}.

If r_{omin} = r_{max}, then S_w = 1 from equation (5-14), and equation (5-22) simplifies to equation (5-10a) for a single brine occupied, water-wet capillary. Given that the model predictions will be compared against measured data obtained using saline brines, surface electrical conductivity is ignored and so σ_s = 0. Substituting for *C* in equation (5-22) and re-

arranging gives the macro-scale zeta potential of the water-wet model as a function of the micro-scale zeta potential of the mineral-brine interface (ζ_{mb}):

$$\zeta(S_w) = \frac{\zeta_{mb}\left(\frac{\int_{r_{Swirr}}^{r_{omin}} r_c^2 n(r_c)dr_c}{\int_{r_{Swirr}}^{r_{max}} r_c^2 n(r_c)dr_c}\right)}{\left(\frac{\int_{r_{min}}^{r_{omin}} r_c^2 n(r_c)dr_c}{\int_{r_{min}}^{r_{max}} r_c^2 n(r_c)dr_c}\right)} \qquad (5\text{-}23)$$

Equation (5-23) applies during both drainage and waterflooding, so long as the capillaries are all water-wet. However, during waterflooding, it is possible to limit the maximum value of r_{omin} to account for the residual oil saturation, such that $r_{omin} \leq r_{Sor}$ (Figure 5-3b). As before, the corresponding water saturation is given by equation (5-14) with $r_{omax} = r_{max}$.

At the irreducible water saturation, all water-wet capillaries occupied by mobile oil will spontaneously imbibe a volume of brine given by:

$$V_{WSI} = \int_{r_{Swirr}}^{r_{Sor}} \pi r_c^2 L_c n(r_c) dr_c \qquad (5\text{-}24)$$

The total volume of capillaries that can be invaded by brine during spontaneous imbibition and forced waterflooding is equivalent to the total volume of capillaries occupied by mobile oil (i.e. that do not contain immobile water or residual oil so have $r_{Swirr} < r_c < r_{Sor}$). The total volume of brine that can invade is therefore given by

$$V_{WSI} + V_{WFI} = \int_{r_{Swirr}}^{r_{Sor}} \pi r_c^2 L_c n(r_c) dr_c \qquad (5\text{-}25)$$

Given this, and the definition in equation (2-2a), the corresponding Amott water-wetting index for a water-wet model is given by

$$I_w = \frac{\int_{r_{Swirr}}^{r_{Sor}} r_c^2 n(r_c) dr_c}{\int_{r_{Swirr}}^{r_{Sor}} r_c^2 n(r_c) dr_c} \qquad (5\text{-}26)$$

which trivially returns the value of 1 in the water-wet case.

5.2.3.2 Oil-Wet Waterflooding

If the oil-occupied capillaries become oil-wet after drainage (i.e. the crude oil causes wettability alteration, Figure 5-3c) then the macro-scale zeta potential during waterflooding is calculated using the same approach as outlined for the water-wet case: integrate the streaming current over all capillaries occupied by mobile brine, and the conduction current over all brine-occupied capillaries. However, oil-wet capillaries now contribute to the streaming current that arises from the oil-brine zeta potential. If $r_{Swi} = r_{Swirr}$, then the initial water saturation equals the irreducible water saturation and only oil-wet capillaries contribute to the streaming current. However, if $r_{Swi} > r_{Swirr}$ then the initial water saturation is higher than the irreducible water saturation ($S_{wi} > S_{wirr}$), so the water-wet, brine-occupied capillaries (i.e. those with $r_{Swirr} < r_c < r_{Swi}$) also contribute to the streaming current that arises from the mineral-brine zeta potential. The value of r_{omax} is varied to vary the water saturation, as the invading brine now invades oil-wet capillaries in the order largest to smallest. Following the same approach as outlined for the water-wet case, the following expressions for the macro-scale zeta potential as a function of the micro-scale zeta potentials of the mineral-brine (ζ_{mb}) and oil-brine (ζ_{ob}) interfaces are obtained:

$$\zeta(S_w) = \frac{\zeta_{ob}\left(\frac{\int_{r_{romax}}^{r_{max}} r_c^2 n(r_c) dr_c}{\int_{r_{Swirr}}^{r_{max}} r_c^2 n(r_c) dr_c}\right)}{\left(\frac{\int_{r_{min}}^{r_{Swirr}} r_c^2 n(r_c) dr_c + \int_{r_{romax}}^{r_{max}} r_c^2 n(r_c) dr_c}{\int_{r_{min}}^{r_{max}} r_c^2 n(r_c) dr_c}\right)} \qquad (S_{wi} = S_{wirr}) \qquad (5\text{-}27a)$$

$$\zeta(S_w) = \frac{\zeta_{mb}\left(\frac{\int_{r_{Swirr}}^{r_{Swi}} r_c^2 n(r_c) dr_c}{\int_{r_{Swirr}}^{r_{max}} r_c^2 n(r_c) dr_c}\right) + \zeta_{ob}\left(\frac{\int_{r_{romax}}^{r_{max}} r_c^2 n(r_c) dr_c}{\int_{r_{Swirr}}^{r_{max}} r_c^2 n(r_c) dr_c}\right)}{\left(\frac{\int_{r_{min}}^{r_{Swi}} r_c^2 n(r_c) dr_c + \int_{r_{romax}}^{r_{max}} r_c^2 n(r_c) dr_c}{\int_{r_{min}}^{r_{max}} r_c^2 n(r_c) dr_c}\right)} \qquad (S_{wi} > S_{wirr}) \qquad (5\text{-}27b)$$

where it is possible to limit the minimum value of r_{omax} to account for the residual oil saturation such that $r_{omax} \geq r_{Sor}$. The corresponding water saturation is given by equation (5-14), with $r_{omin} = r_{Swirr}$ if $S_{wi} = S_{wirr}$ and $r_{omin} = r_{Swi}$ if $S_{wi} > S_{wirr}$.

In this oil-wet model, irrespective of the value of S_{wi}, there are no oil-occupied, but water-wet capillaries that can spontaneously imbibe water, so the corresponding Amott water wetting index trivially returns the value of 0.

5.2.3.3 Mixed-Wet Waterflooding

Mixed wettability in the model occurs when some of the oil-occupied capillaries do not undergo wettability alteration to become oil-wet after aging. Controls on wettability alteration for a given crude oil and formation brine are complex and include the mineral surface properties and the local topology of the pore-space (Rücker et al. 2020; Buckley 1996; Hirasaki 1991; Schmatz et al. 2015; Zhang et al. 2006). This simple model cannot account for these complexities, so two 'end-member' cases of mixed wettability are considered: (i) the smallest-oil occupied capillaries remain water-wet after aging and (ii) the largest oil-occupied capillaries remain water-wet after aging (e.g. Figure 5-3d). As will be shown in the results, the model predictions are identical irrespective of which of these two approaches is chosen to handle mixed-wettability; the results for mixed-wetting are independent of the distribution of water- and oil-wet capillaries.

To account for mixed wettability, a new radius r_{owet} is defined. In mixed-wetting case (i), all capillaries with $r_{Swi} < r_c < r_{owet}$ remain water-wet after aging and all capillaries with $r_c > r_{owet}$ become oil-wet. Oil occupied, but water-wet, capillaries will spontaneously imbibe water whilst oil-wet capillaries occupied by mobile oil will imbibe additional water under an applied pressure. Following the same approach described in the previous sections, the Amott water-wetting index for case (i) is given by:

$$I_w = \frac{\int_{r_{Swi}}^{r_{owet}} r_c^2 n(r_c) dr_c}{\int_{r_{Swi}}^{r_{owet}} r_c^2 n(r_c) dr_c + \int_{r_{Sor}}^{r_{max}} r_c^2 n(r_c) dr_c} \quad (5\text{-}28)$$

where r_{owet} can be adjusted to match experimental data for I_w.

Water-wet capillaries return the zeta potential of the mineral-brine interface whilst oil-wet capillaries return the zeta potential of the oil-brine interface so. The water saturation is varied by varying r_{omin} in water-wet capillaries such that $r_{omin} \leq r_{owet}$ and vary r_{omax} in oil-wet capillaries such that $r_{omax} \geq r_{Sor}$ noting that the invading water will occupy water-wet capillaries first at capillary equilibrium. The value of r_{Sor} is adjusted to match experimental data for S_{or}. The macro-scale zeta potential is given by:

$$\zeta(S_w) = \frac{\zeta_{mb}\left(\frac{\int_{r_{Swirr}}^{r_{omin}} r_c^2 n(r_c) dr_c}{\int_{r_{Swirr}}^{r_{max}} r_c^2 n(r_c) dr_c}\right) + \zeta_{ob}\left(\frac{\int_{r_{Sor}}^{r_{omax}} r_c^2 n(r_c) dr_c}{\int_{r_{Swirr}}^{r_{max}} r_c^2 n(r_c) dr_c}\right)}{\left(\frac{\int_{r_{min}}^{r_{omin}} r_c^2 n(r_c) dr_c + \int_{r_{Sor}}^{r_{omax}} r_c^2 n(r_c) dr_c}{\int_{r_{min}}^{r_{max}} r_c^2 n(r_c) dr_c}\right)} \qquad (5\text{-}29)$$

The corresponding water saturation is given by equation (5-14).

If $r_{owet} = r_{Sor}$ then equation (5-29) reduces to equation (5-23) and we recover the water-wet model ($I_w = 1$). If $r_{owet} = r_{Swirr}$ then equation (5-29) reduces to equation (5-27a) while if $r_{owet} = r_{Swi}$ then equation (5-28) reduces to equation (5-27b); in both cases, we recover the oil-wet model ($I_w = 0$).

For mixed-wetting case (ii), all capillaries with $r_{Swi} < r_c < r_{owet}$ become oil-wet after aging and all capillaries with $r_c > r_{owet}$ remain water-wet. The Amott water wetting index in this case is given by:

$$I_w = \frac{\int_{r_{owet}}^{r_{max}} r_c^2 n(r_c) dr_c}{\int_{r_{owet}}^{r_{max}} r_c^2 n(r_c) dr_c + \int_{r_{Sor}}^{r_{owet}} r_c^2 n(r_c) dr_c} \qquad (5\text{-}30)$$

and the macro-scale zeta potential by:

$$\zeta(S_w) = \frac{\zeta_{mb}\left(\frac{\int_{r_{owet}}^{r_{max}} r_c^2 n(r_c) dr_c}{\int_{r_{Swirr}}^{r_{max}} r_c^2 n(r_c) dr_c}\right) + \zeta_{ob}\left(\frac{\int_{r_{Sor}}^{r_{omax}} r_c^2 n(r_c) dr_c}{\int_{r_{Swirr}}^{r_{max}} r_c^2 n(r_c) dr_c}\right)}{\left(\frac{\int_{r_{owet}}^{r_{max}} r_c^2 n(r_c) dr_c + \int_{r_{Sor}}^{r_{omax}} r_c^2 n(r_c) dr_c}{\int_{r_{min}}^{r_{max}} r_c^2 n(r_c) dr_c}\right)} \qquad (S_{wi} = S_{wirr}) \qquad (5\text{-}31a)$$

$$\zeta(S_w) = \frac{\zeta_{mb}\left(\frac{\int_{r_{Swirr}}^{r_{Swi}} r_c^2 n(r_c)dr_c}{\int_{r_{Swirr}}^{r_{max}} r_c^2 n(r_c)dr_c}\right) + \zeta_{mb}\left(\frac{\int_{r_{owet}}^{r_{max}} r_c^2 n(r_c)dr_c}{\int_{r_{Swirr}}^{r_{max}} r_c^2 n(r_c)dr_c}\right) + \zeta_{ob}\left(\frac{\int_{r_{Sor}}^{r_{omax}} r_c^2 n(r_c)dr_c}{\int_{r_{Swirr}}^{r_{max}} r_c^2 n(r_c)dr_c}\right)}{\left(\frac{\int_{r_{min}}^{r_{Swi}} r_c^2 n(r_c)dr_c + \int_{r_{owet}}^{r_{max}} r_c^2 n(r_c)dr_c + \int_{r_{Sor}}^{r_{omax}} r_c^2 n(r_c)dr_c}{\int_{r_{min}}^{r_{max}} r_c^2 n(r_c)dr_c}\right)} \quad (S_{wi} > S_{wirr}) \quad (5\text{-}31b)$$

The corresponding water saturation is given by equation (5-14).

If $r_{owet} = r_{Swi}$ then equations (5-31a) and (5-31b) reduce to equation (5-23) and we recover the water-wet model ($I_w = 1$); if $r_{owet} = r_{max}$ then equations (5-31a) and (5-31b) reduce to equations (5-27a) and (5-27b) respectively, and we recover the oil-wet model ($I_w = 0$).

5.3 Results

5.3.1 Water-Wet and Oil-Wet Models Drained to S_{wirr}

The first case considered is when rock samples are drained to the irreducible water saturation, S_{wirr}, with crude oil before aging at elevated temperature to induce wettability alteration. This procedure is common to many petrophysical laboratories and studies (e.g. Tang and Morrow (1999). This is modelled by assuming all capillaries are initially water-wet and water occupied and are then invaded by crude oil until all of the mobile capillaries are occupied by oil, yielding $r_{omin} = r_{Swirr}$ and $r_{omax} = r_{max}$ (Figure 5-3a). The impact of wettability alteration on the zeta potential measured during the subsequent waterflooding process is considered for the simplest, limiting scenarios in which none, or all, of the oil-invaded capillaries undergo wettability alteration, yielding completely water- or oil-wet models with I_w = 1 or 0 respectively.

For the example results, a value of ζ_{mb} = +7 mV is used for the micro-scale zeta potential of the mineral-brine interface, as reported for carbonate samples saturated with a saline natural brine (>2 mol/L) (Jackson et al. 2016a) and consistent with other measurements of carbonate rocks saturated with typical saline natural brines (see Chapter 3 and Alroudhan, Vinogradov, and Jackson (2016); Al Mahrouqi et al. (2017a). Since the magnitude and polarity of the micro-scale zeta potential of the oil-brine interface, ζ_{ob}, are uncertain at the conditions of interest, a range of values are considered. This issue is discussed later in the chapter. The macro-scale zeta potential is reported as a function of water saturation, with the waterflooding curves returning to a water saturation of 1. In natural rock samples, this would not occur due to trapping of residual oil, but the curve can simply be terminated at the chosen residual oil saturation ($S_w = 1 - S_{or}$) to interpret results for a specific example.

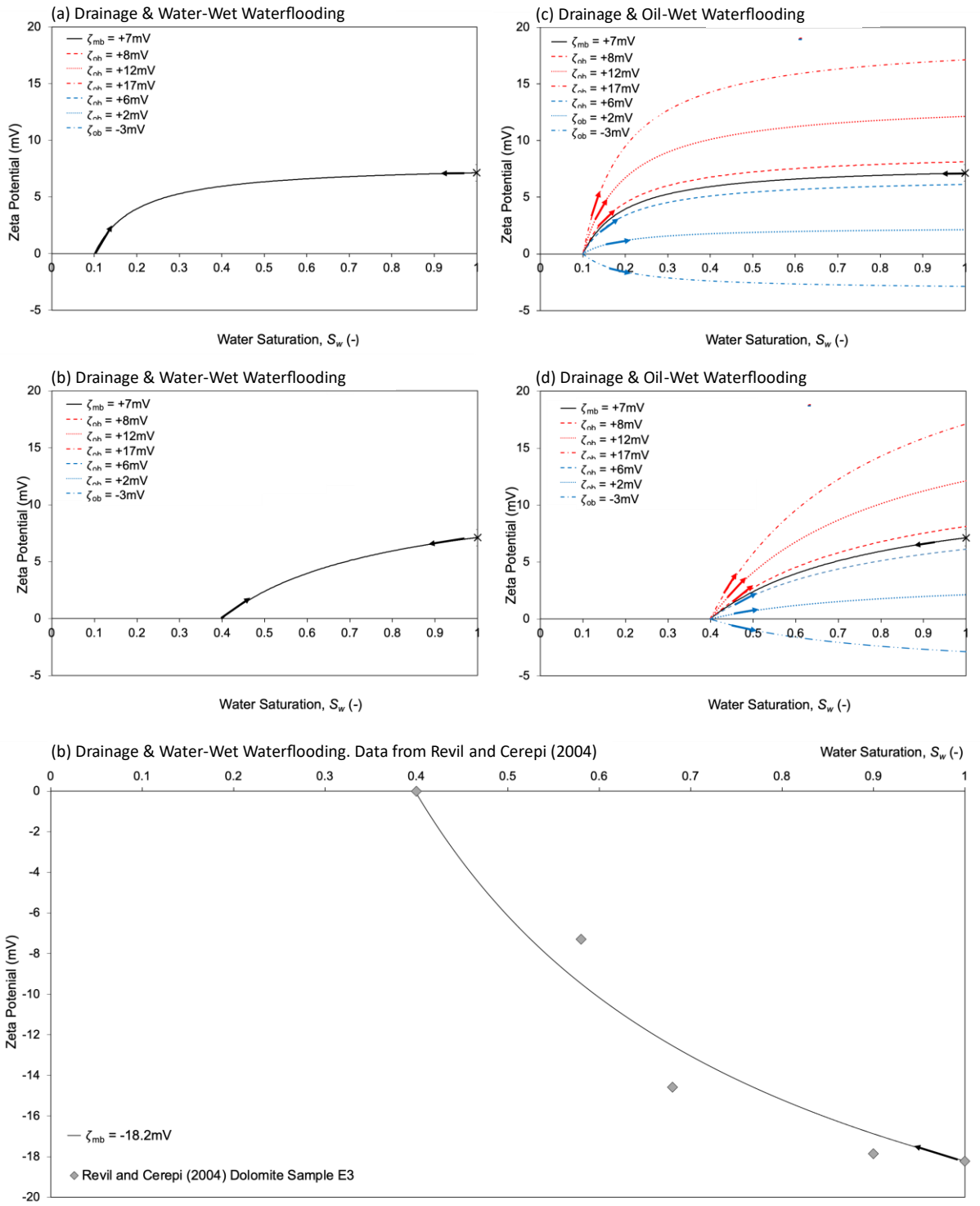

Figure 5-4: Macro-scale (model) zeta potential as a function of water saturation for an example with micro-scale mineral-brine zeta potential ζmb = +7 mV for (a) drainage and water-wet waterflooding with S_{wirr} = 0.1; (b) drainage and water-wet waterflooding with S_{wirr} = 0.4; (c) drainage and oil-wet waterflooding with S_{wirr} = 0.1; (d) drainage and oil-wet waterflooding with S_{wirr} = 0.4 and a range of values of oil-brine zeta potential. Plot (e) shows drainage with S_{wirr} = 0.4, compared against experimental data obtained from Revil and Cerepi (2004) and using their measured value of ζ_{mb} = -18.2 mV in the model. Measured zeta potential values were calculated from their reported streaming potential measurements using the Helmholtz-Smoluchowski equation (5-11a), assuming negligible surface electrical conductivity consistent with their measured conductivity data and using published correlations for brine viscosity and permittivity (Saunders et al. 2012). Arrows show direction of water saturation change. Red curves represent models where $\zeta_{ob} > \zeta_{mb}$; blue curves represent models where $\zeta_{ob} < \zeta_{mb}$.

The macro-scale (model) zeta potential obtained during water-wet drainage and both water- and oil-wet waterflooding monotonically decreases with decreasing water saturation and falls to zero at the irreducible water saturation (Figure 5-4). The capillary size distribution has no effect on the macro-scale zeta potential irrespective of wetting state or water saturation i.e. the model microstructure has no impact on the results when bulk electrical conductivity dominates, consistent with numerous previous experimental and modelling studies (Hunter 1981a). The reason the microstructure plays no role is that the streaming and conduction currents follow the same paths through the pore-space (Vinogradov et al. 2021; Jougnot et al. 2019). The focus here on saline brines with high electrical conductivity means that surface electrical conductivity is small compared to the bulk electrical conductivity, as has been observed in numerous studies (Vinogradov and Jackson 2011; Jackson and Vinogradov 2012; Al Mahrouqi et al. 2017a; Revil and Cerepi 2004).

The model predictions against compared against measured macro-scale zeta potential values obtained from steady-state, gas-brine streaming potential measurements on a water-wet dolomite rock sample reported by Revil and Cerepi (2004) (their sample E3) (Revil and Cerepi 2004). They measured the streaming potential coupling coefficient at full and partial saturation during drainage using 5 g/L (0.086 mol/L) NaCl electrolyte and nitrogen.

The model predictions were obtained by setting S_{wirr} = 0.4 and using a micro-scale mineral-brine zeta potential of ζ_{mb} = -18.2mV, consistent with the experimentally determined values. There are no other adjustable parameters in the model. The model predictions and experimental data show good agreement for this water-wet sample, despite the simplicity of the model. Note that Revil and Cerepi (2004) did not report error bars. There are no comparable data for oil-wet samples against to test the model predictions against.

Figure 5-4 shows that the modelled and measured macro-scale zeta potentials decrease in magnitude with decreasing water saturation. This is because the streaming and conduction currents both decrease as the water saturation decreases, but the streaming

current decreases more rapidly than the conduction current as the irreducible (immobile) water contributes to the latter but not the former. At the irreducible saturation, there is no flow of water, so the streaming current and hence the sample zeta potential fall to zero (Jackson 2010). Varying the value of S_{wirr} acts only to stretch or compress the curves (Figure 5-4) consistent with previous findings (Vinogradov et al. 2021). When the irreducible water saturation is large, the macro-scale zeta potential decreases in magnitude more rapidly with decreasing water saturation and *vice-versa*. In the limiting case of zero irreducible water saturation, the macro-scale zeta potential is constant and independent of water saturation as both the streaming and conduction currents decrease at the same rate (Jackson 2010).

The saturation dependence of the model macro-scale zeta potential during water-wet drainage and waterflooding is identical irrespective of the chosen micro-scale oil-brine zeta potential (Figure 5-4a,b,e). In both processes, all capillaries are water-wet and so the streaming current is controlled only by the zeta potential at the mineral-brine interface.

In contrast, the saturation dependence of the model macro-scale zeta potential during (water-wet) drainage and oil-wet waterflooding can be strongly hysteretic depending on the difference between the micro-scale oil-brine and mineral-brine zeta potentials (Figure 5-4c,d). If the oil-brine zeta potential is more positive than the mineral-brine zeta potential, then the macro-scale zeta potential becomes relatively more positive with increasing water saturation; conversely, if the oil-brine zeta potential is less positive or negative, then the macro-scale zeta potential becomes relatively less positive with increasing water saturation and may even invert to return a negative value. The reason is that the oil-occupied capillaries all become oil-wet after drainage, so the streaming current during waterflooding is controlled only by the micro-scale zeta potential at the oil-brine interface. The results suggest that, if the residual oil saturation was very small, it would be possible to determine the zeta potential of the oil-brine interface by measuring the streaming potential on a strongly oil-wet porous sample. However, rock samples aged in natural crude oils rarely show purely water- or oil-wet conditions, so we need to investigate the effect of mixed wettability on the model zeta potential.

5.3.2 Mixed-Wet Models

This section tests the effect of having an initial water saturation that is larger than the irreducible saturation. Having determined that model results are not significantly affected by its value, the irreducible water saturations is fixed so that S_{wirr} = 0.3 as a representative average, and the same micro-scale mineral-brine zeta potential of ζ_{mb} = +7 mV is used as in the previous section. As before, the saturation dependence of the macro-scale zeta potential is shown with the waterflooding curves returning to a water saturation of 1, but the curve can simply be terminated at the chosen residual oil saturation ($S_w = 1 - S_{or}$) to interpret results for a specific example.

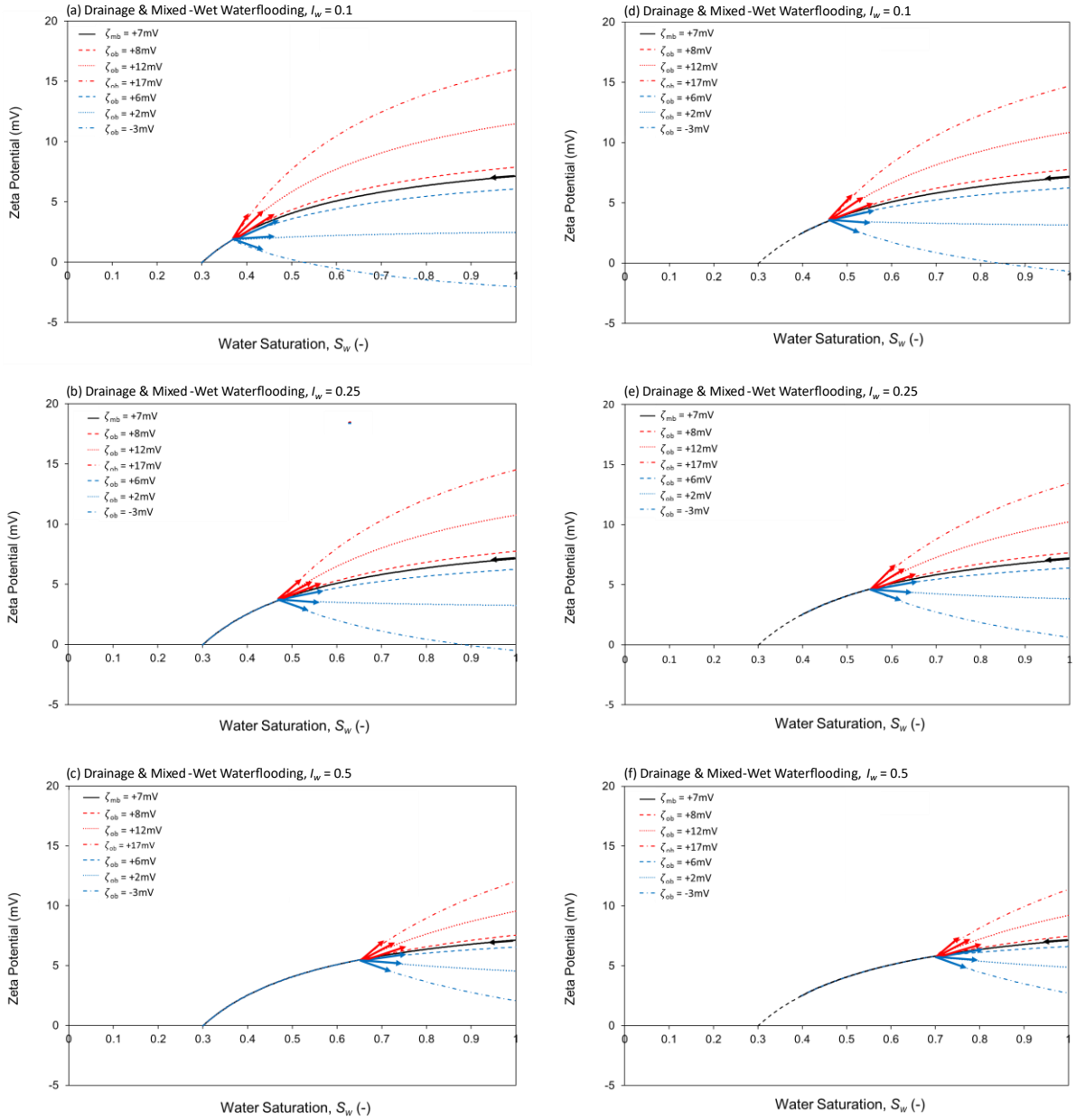

Figure 5-5: Macro-scale (model) zeta potential as a function of water saturation for (a-c) (water-wet) drainage and mixed-wet waterflooding for samples drained to S_{wirr} = 0.3 with I_w = 0.1, 0.25 and 0.5 respectively and for (d-f) (water-wet) drainage and mixed-wet waterflooding for samples drained to S_{wi} = 0.4 with S_{wirr} = 0.3 and I_w = 0.1, 0.25 and 0.5 respectively. The dashed portion of the drainage curve shows the path that would be followed if drainage were to continue to S_{wirr}. Arrows show direction of water saturation change. Red curves represent models where the micro-scale $\zeta_{ob} > \zeta_{mb}$; blue curves represent models where $\zeta_{ob} < \zeta_{mb}$.

Again, the capillary size distribution has no effect on the saturation dependence of the macro-scale zeta potential; the results are also identical irrespective of the approach used to model mixed-wetting (cases (i) and (ii) described above). The model microstructure, including

the wettability-dependent distribution of oil and brine, once again plays no role, for the same reason given in the previous section: the streaming and conduction currents follow the same paths through the rock pore space. Microstructure only impacts the predicted macro-scale zeta potential if the streaming and conduction currents follow different paths.

In contrast to the end-member water- and oil-wet cases investigated in the previous section, there is hysteresis between (water-wet) drainage and mixed-wet waterflooding (Figure 5-5). The macro-scale zeta potential during drainage is again controlled only by the micro-scale zeta potential at the mineral-brine interface; however, during waterflooding, the macro-scale zeta potential arises from a combination of the micro-scale mineral-brine zeta potential in the water-wet capillaries and oil-brine zeta potential in the oil-wet capillaries.

The waterflooding curves initially follow the drainage curve because the invading water displaces oil from water-wet capillaries first, so only the micro-scale mineral-brine zeta potential contributes to the streaming current. Once the water-wet capillaries are all occupied, the waterflooding curves diverge from the drainage curve because the invading water enters oil-wet capillaries, so the micro-scale oil-brine zeta potential also contributes to the streaming current. As before, if the oil-brine zeta potential is more positive than the mineral-brine zeta potential, then the macro-scale zeta potential becomes relatively more positive with increasing water saturation; conversely, if the oil-brine zeta potential is less positive or negative, then the macro-scale zeta potential becomes relatively less positive with increasing water saturation.

The results more closely reflect water-wet waterflooding with increasing I_w and/or S_{wi} because fewer capillaries become oil-wet after drainage (Figure 5-5). A negative micro-scale zeta potential at the oil-brine interface is not always sufficient to invert the polarity of the macro-scale zeta potential. There must be enough capillaries that become oil-wet and/or the micro-scale oil-brine zeta potential must be sufficiently large and different to the mineral-brine zeta potential to have a significant impact on the macro-scale zeta potential. These results suggest that the macro-scale zeta potential measured on a mixed-wet sample is unlikely to reflect the magnitude of the micro-scale oil-brine zeta potential and may not reflect its polarity even when

measured at the residual oil saturation, when water occupies many of the oil-wet pores. The relationship between wettability and the macro-scale zeta potential measured at the residual saturation is tested further in the next section.

5.3.3 Interpretation of the Micro-Scale Zeta Potential of the Oil-Brine Interface

Thus far the capillary tubes model has been used to predict general trends between macro-scale zeta potential, wetting state and the micro-scale zeta potentials of the individual mineral- and oil-brine interfaces. In this section, the model is tuned to the experimental data of Jackson et al. (2016) and the new results presented in Chapter 3 to determine the magnitude and polarity of the micro-scale oil-brine zeta potential, as it was not possible to directly measure this in these experiments.

For a given experiment, the measured values of S_{wirr}; S_{wi}; S_{or}; ζ_{mb} (S_w = 1) and I_w are used and the values of the critical capillary radii r_{min}; r_{Swirr}; r_{Swi}; r_{Sor} and r_{max} are adjusted to develop a mixed-wet model bespoke to that experiment. The only model parameter that was not experimentally measured was the micro-scale oil-brine zeta potential, ζ_{ob}, so this is tuned such that the model macro-scale zeta potential matches the measured macro-scale zeta potential at S_w = 1 - S_{or} (see selected examples in Figure 6; one for each oil used across the two experimental studies). Note that the sample of Oil D used by Jackson et al. (2016a) was different to Oil BD used in Chapter 3 (Table 3-1) so these are distinguished as Oil D(J) and Oil BD.

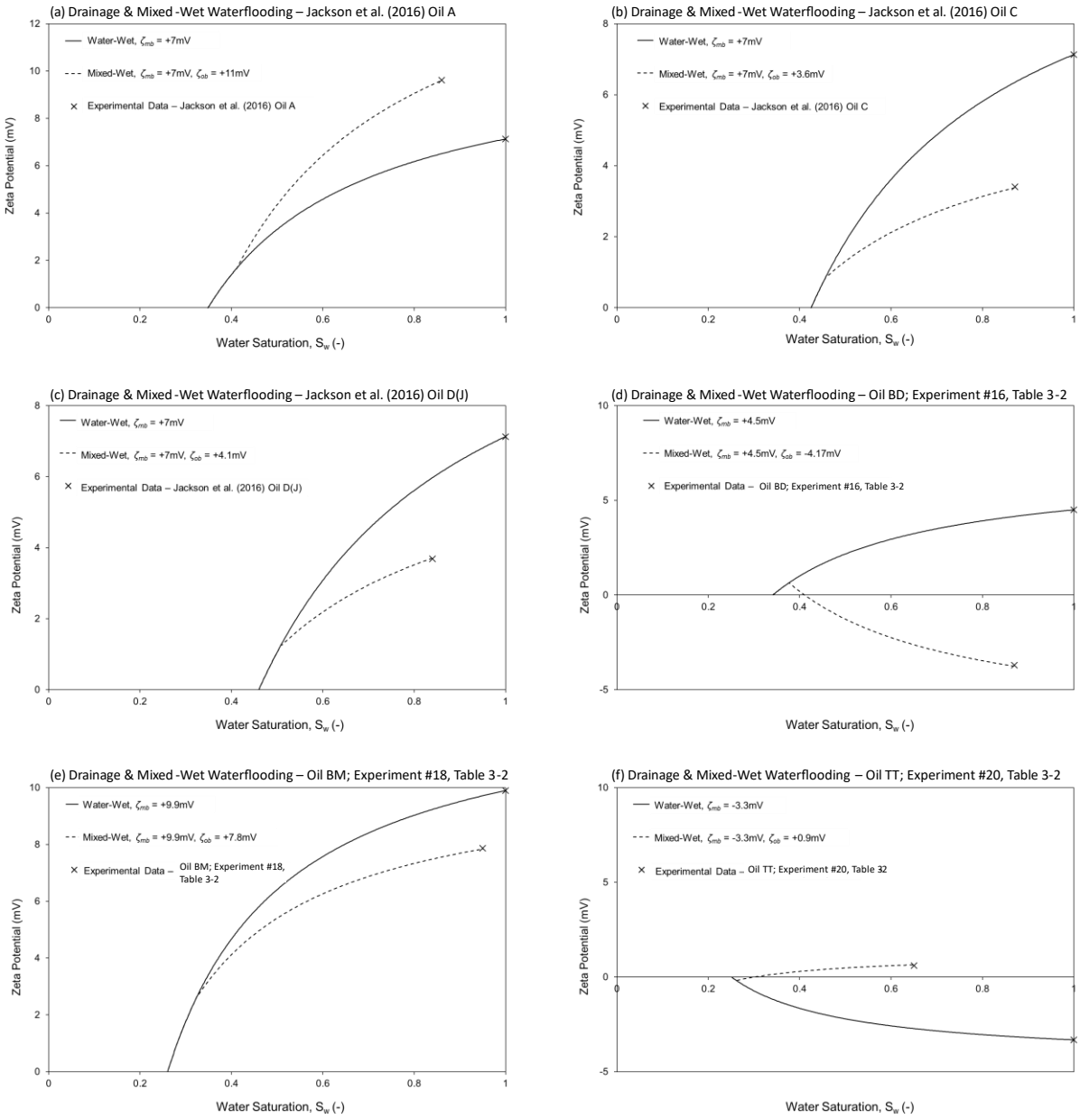

Figure 5-6: Water-wet drainage (solid black lines) and mixed-wet waterflooding (dashed lines) models showing macro-scale zeta potential as a function of water saturation S_w, compared against experimentally measured macro-scale zeta potential from (a) Jackson et al. (2016b) Oil A; (b) Jackson et al. (2016b) Oil C; (c) Jackson et al. (2016b) Oil D(J); (d) Oil BD, Table 3-1; (e) Oil BM, Table 3-1; (f) Oil TT, Table 3-1. The model properties were adjusted in each case to match the measured S_{wirr}, S_{wi}, I_w and ζ_{mb} (S_w = 1) and the unknown value of micro-scale oil-brine zeta potential ζ_{ob} was tuned such that the model macro-scale zeta potential matches the experimentally measured macro-scale zeta potential at $S_w = 1 - S_{or}$.

The value of the micro-scale oil-brine zeta potential determined using this approach for all experiments reported in Table 3-2 is shown in Figure 5-7.

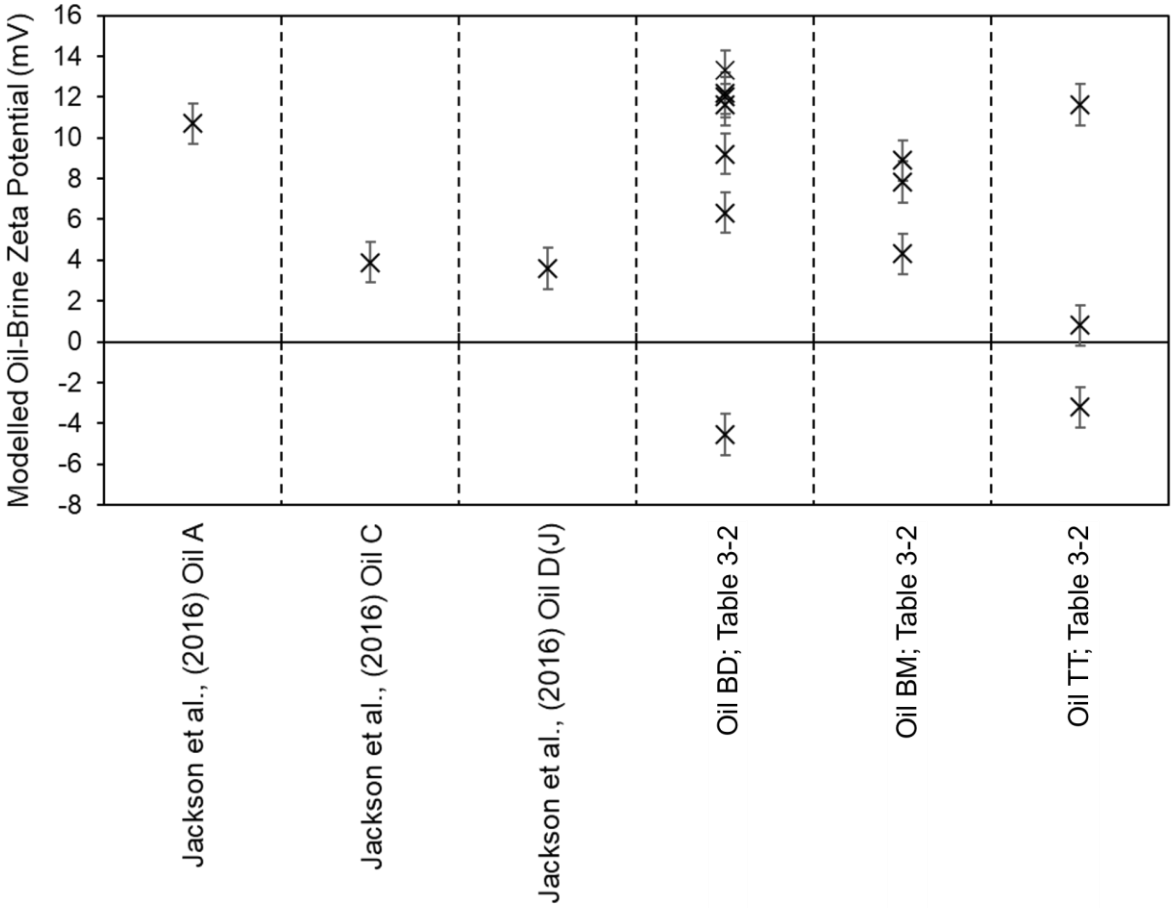

Figure 5-7: Modelled micro-scale oil-brine zeta potential values for the different crude oils tested by Jackson et al. (2016a) and in Chapter 3. Different datapoints for a given crude oil correspond to experiments using different rock samples, brine compositions or temperature. 16 values of oil-brine zeta potential are reported in total.

The capillary tubes model suggests positive values for the micro-scale oil-brine zeta potential in most of the experiments tested, up to a maximum of +13.1 mV (determined for the Oil BD experiment with carbonate sample BA at ambient laboratory temperature in Table 3-2, experiment #7). Only two experiments, using crude oils BD and TT, are interpreted to have negative micro-scale oil-brine zeta potential (determined for the Oil BD experiment reported in Table 3-2, with carbonate sample BD at 80 ^{O}C (experiment #16) and the Oil TT experiment with sample TE at ambient temperature (experiment #20) with a minimum value of -4.1 mV. The spread of oil-brine zeta potential values interpreted here is not surprising given the range

of brine compositions and temperatures tested in the experiments, but the fact that the zeta potentials are mostly positive is unexpected.

As discussed previously, the polarity of the oil-brine zeta potential in these experiments was interpreted using a very simple, qualitative approach: if the macro-scale zeta potential became more positive after aging then the micro-scale oil-brine zeta potential was interpreted to be positive, and *vice-versa*. In the 16 experiments conducted using high salinity formation brine, the crude oils tested were interpreted to have a positive oil-brine zeta potential in nine experiments and a negative oil-brine zeta potential in seven experiments (Table 3-2). However, in five of the seven experiments in which a negative macro-scale zeta potential was interpreted, it was noted that the micro-scale oil-brine zeta potential was not unambiguously negative; it could be positive but have smaller magnitude than the (positive) mineral-brine zeta potential (see section 3.3.2). In these experiments, the macro-scale zeta potential after aging remained positive but became smaller in magnitude after aging.

The micro-scale oil-brine zeta potential in the five ambiguous experiments were interpreted to be negative (Table 3-2) but the model here instead predicts a positive oil-brine zeta potential that is smaller in magnitude than the mineral-brine zeta potential. Hence, the model only predicts a negative oil-brine zeta potential in two of the experiments. The polarity of the modelled oil-brine zeta potential obtained here is consistent with the polarity interpretations only when these were unambiguous (see Table 3-2 and Jackson et al. (2016a)) The importance of this issue for predicting oil recovery during CSW is considered in the discussion.

5.3.4 Link Between Macro-Scale Zeta Potential and Wettability

Finally, the capillary tubes model is applied to investigate the link between the measured sample wettability, and the measured change in sample (macro-scale) zeta potential caused by wettability alteration ($\Delta\zeta_{wett}$), after aging in crude oil. The model predictions

are compared to the experimental data shown in Figure 5-1. A single representative model is considered with S_{wirr} = 0.3, S_{wi} = 0.33, S_{or} = 0.9; these values are broadly consistent with the experimental data. It is assumed that the micro-scale mineral-brine zeta potential ζ_{mb} is positive, consistent with the model results reported in previous sections and the use of carbonate rock samples in the experiments, and three scenarios are considered for the micro-scale oil-brine zeta potential: (i) the oil-brine interface is of the same polarity as the mineral-brine interface but greater in magnitude ($\zeta_{ob} > \zeta_{mb}$); (ii) the oil-brine interface is of the same polarity as the mineral-brine interface but smaller in magnitude ($\zeta_{ob} < \zeta_{mb}$), and (iii) the oil-brine interface has opposite polarity. The model results are shown in Figure 5-8 along with the experimental data re-plotted from Figure 5-1.

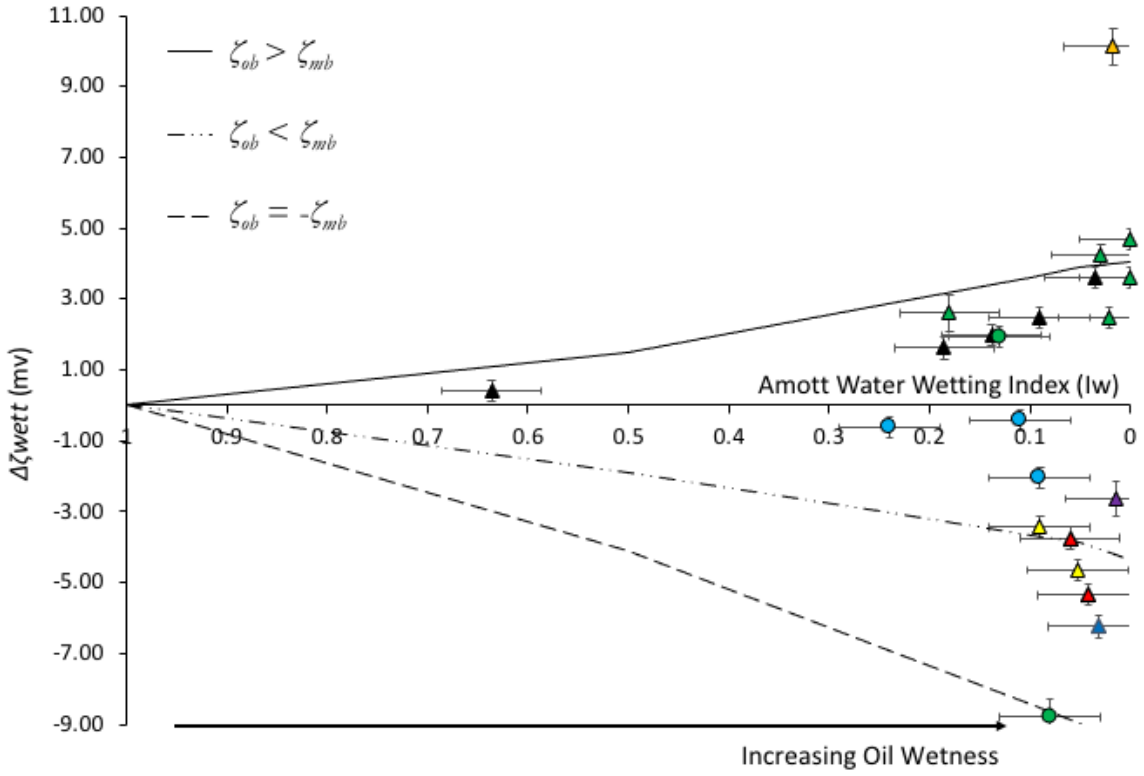

Figure 5-8: Change in macro-scale zeta potential before and after aging and wettability alteration, $\Delta\zeta wett$, as a function of Amott Water Wetting Index, I_w. Model takes inputs of S_{wirr} = 0.3, S_{wi} = 0.33, S_{or} = 0.1 and a positive micro-scale mineral-brine zeta potential ζ_{mb}. Points correspond to experimental data from Chapter 3 as reported in Figure 3-8 showing the change in macro-scale zeta potential measured on intact natural carbonate cores after drainage and aging with crude oil. Triangles represent measurements made at room temperature and circles represent measurements made at elevated reservoir temperature >70 ^{O}C. Different colours represent different crude oils.

The model broadly captures the observed trends in the experimental data: when the micro-scale oil-brine zeta potential is more positive than the mineral-brine zeta potential, the macro-scale zeta potential becomes relatively more positive with increasing oil-wetness; conversely, if the micro-scale oil-brine zeta potential is less positive, the macro-scale zeta potential becomes relatively less positive with increasing oil-wetness. If the polarity of the micro-scale oil-brine zeta potential is negative, then the macro-scale zeta potential becomes relatively less positive with increasing oil-wetness but is more negative for a given wettability and may invert to return a negative value if the model is sufficiently oil-wet. If a negative value for the micro-scale mineral-brine interface was assumed instead, the same general trends would still be observed but with the polarity inverted.

Although the model captures the overall trends, it fails to quantitatively match the experimental data. The model predicts a close to linear trend between $\Delta\zeta_{wett}$ and I_w irrespective of the value of micro-scale oil-brine or mineral-brine zeta potential, whereas the experimental data exhibit a trend more comparable to a linear-log relationship. The model overpredicts the change in macro-scale zeta potential in the mixed-wet regime ($0.1 < I_w < 0.8$) and does not reproduce the sharp changes in $\Delta\zeta_{wett}$ in the strongly oil-wet region ($I_w < 0.1$). The limitations of the model that may be responsible for these discrepancies and their implications for understanding the link between macro-scale zeta potential and wettability of porous media are discussed further in the next section.

5.4 Discussion

The bundle of capillary tubes model presented here reports, for the first time, a quantitative relationship between the macro (continuum)-scale zeta potential interpreted from streaming potential measurements on intact porous media, and changes in the wetting state of the mineral surfaces. The model is simplistic in its representation of rock pore-space but serves as a foundation from which to develop more advanced models and yields a number of insights into the relationship between zeta potential and wettability.

When water is strongly wetting, the macro-scale zeta potential of the porous medium reflects the micro-scale zeta potential of the mineral-brine interface, whereas when oil is strongly wetting, the macro-scale zeta potential reflects the micro-scale zeta potential of the oil-brine interface (Figure 5-4). Mixed-wet porous media yield a macro-scale zeta potential that is a combination of the micro-scale zeta potentials of both the mineral- and oil-brine interfaces, and which increasingly reflects the micro-scale zeta potential of the oil-brine interface as the porous medium becomes increasingly oil-wet, and *vice-versa* (Figure 5-5). If the micro-scale zeta potential of the oil-brine interface is of the same polarity but larger in magnitude than the micro-scale zeta potential of the mineral-brine interface, then the macro-scale zeta potential increases in magnitude with increasing oil-wetness, and *vice-versa*. If the polarities of the micro-scale oil-brine and mineral-brine interfaces are opposed, then inversion of the macro-scale zeta potential can occur with sufficient oil-wetness. These observations have been previously hypothesised based on qualitative interpretations of experimental data (see Chapter 3; (Jackson and Vinogradov 2012; Jackson et al. 2016a) but have not been supported by pore-scale modelling until now.

We have seen the importance of the oil-brine zeta potential for controlling CSW in carbonates in Chapter 3. IOR was observed to occur during conventional LSW only when the micro-scale oil-brine zeta potential was interpreted to be negative (see Table 3-2 Chapter 3 and Jackson et al. (2016a)). Conversely, when the micro-scale oil-brine zeta potential was interpreted to be positive, IOR was only observed by increasing brine salinity in an inverse

LSW. The capillary tubes model presented here predicts a positive oil-brine zeta potential in most of the experiments reported by Jackson et al. (2016a) and in Table 3-2.

We have also seen in Chapter 2 that confirming the interpretations of the oil-brine zeta potential reported here with independent experimental measurements is challenging. Few data at appropriate reservoir conditions exist with which to validate these interpretations against. Those that do exist suggest the oil-brine zeta potential is negative. However, some experimental data, and surface complexation models of the oil-brine interface suggest that high concentrations of divalent cations may invert the polarity of the interface. This has been discussed in Chapter 2 and Chapter 3.

The experimental data showing positive values of the oil-brine interface suggests these may be as high as +14.7 mV (see Figure 2-12, Chapter 2 and Pooryousefy et al. (2018). The oil-brine zeta potential values predicted by the capillary tubes model (Figure 5-7) fall within this range. These results suggest that the oil-brine zeta potential is more commonly positive than has previously been thought. As has been suggested, the many published examples of CSW where the injection brine was diluted, and no additional oil recovery was observed may have contained an unknown positively charged oil (Chapter 3 and Jackson et al. (2016a)).

The model also provides insight into the relationship between macro-scale zeta potential and the wettability of the porous medium, which may be useful in developing a tool to determine reservoir wettability *in-situ* by measuring the zeta potential via downhole measurements of the streaming potential, obtained using a wireline tool such as a Modular Formation Dynamics Tester. Two probes equipped with pressure transducers and suitable non-polarising electrodes could be used to impose flow in the reservoir and measure the resulting pressure and voltage differences (Chen et al. 2005) From these data, supplemented by measurements of the rock and formation brine conductivity, the zeta potential of the reservoir rocks in-situ could be determined. If a robust correlation between zeta potential and wettability can be identified, then the in-situ wettability could also be characterised (Jackson and Vinogradov 2012; Jackson et al. 2011; Vinogradov and Jackson 2011).

The model captures the overall trend between zeta potential and wettability observed experimentally, but deviates in the mixed-wet regime, where it tends to overpredict the change in zeta potential $\Delta\zeta_{wett}$ for a given wettability I_w and does not capture the sharp changes in $\Delta\zeta_{wett}$ with small changes in I_w in strongly oil-wet conditions. This discrepancy may be due to the way in which wettability is accounted for. It is assumed that oil in water-wet capillaries is completely displaced during waterflooding when, in natural rocks, water enters pores by thickening the wetting water film and trapping oil droplets or ganglia in the pore centres. Since the model does not account for trapped oil, it may be underpredicting the number of water-wet pores for a given I_w, particularly in the mixed wet regime (Figure 5-8). Moreover, I_w may not be the best measure of wettability, as it characterises wettability using rock samples at the cm - m scale, yet many of the mineral scale properties and mechanisms that control wettability and development of the electrical double layer occur at the sub nm scale (see chapter 2). Characterising wettability across scales is a common and persistent problem for understanding multiphase flow. The sharp changes in zeta potential observed in response to very small changes in I_w in strongly oil wet samples suggest that important physical changes are occurring at the mineral-surface scale that have a strong effect on the macro-scale zeta potential but are not captured by macro-scale changes in I_w.

Ultimately, it should not be expected that the model predictions quantitatively reproduce experimental data because a bundle of capillary tubes is an overly simplistic approximation to real porous media. It does not include any of the interconnectivity of the pore space, pore geometry, or geochemical and textural heterogeneity in real rocks that has a profound effect on flow properties, particularly during multi-phase flow. During drainage, connate water can become trapped in the corners and asperities of pores that cannot be invaded by oil and therefore cannot become oil-wet during aging (Dullien, 2012). This water remains trapped and immobile during subsequent waterflooding, altering the flow paths of the invading water and the interfaces which it encounters, thus altering the macro-scale zeta potential. Likewise, oil may become trapped in small pores located upstream of larger pores,

preventing the flow of water and eliminating their contribution to the streaming current, thus further affecting the zeta potential. In water-wet portions, oil droplets may be trapped in the centres of the pores and/or ganglia of oil may snap-off. The presence of residual oil in the pore space as water flows around the ganglia will affect both the streaming and conduction currents through that pore space. Furthermore, the oil may contribute to the streaming current through its own surface charge. The complexities of such a system will likely affect the zeta potential and cannot be captured by such a simplistic model.

Pore connectivity in real porous media has an important effect on fluid flow in subsequent drainage and waterflooding processes. The observation that the capillary size distribution has no effect on the macroscale zeta potential is valid when the streaming and conduction currents follow the same path through the pore space. In the bundle of capillary tubes model this occurs since only one mobile fluid phase is present in each capillary and there is no interconnectivity of capillaries. Inclusion of such effects in a more complex model may be expected to yield some dependency of the zeta potential on the capillary (or pore) size distribution.

Future work could use more realistic pore network models to capture the effects of these complex flow paths on electrokinetic phenomena (e.g. Zhang, 2017). Such models would be relatively easy to develop based on existing techniques. An improved pore scale model that considers a triangular pore space and allows for corner flow of oil/water and/or trapping of fluids can more accurately describe multi-phase flow in individual pores and represent mixed wettability within an individual pore, rather than the simple assumption of a single wetting state in a given capillary employed in the work here (Blunt et al. 2002). Alternatively, 3-D models that describe complex pore networks based on high resolution imaging are well established (Blunt et al. 2013). Interconnectivity of such pores through a 3-D network based on real porous media will affect the flow paths of fluids during drainage and waterflooding. A wettability map based on micro-CT images (e.g. Singh et al. 2016) could be applied to the pore network and, utilising the same approach as employed here, different

surface charges could be applied depending on the wetting state of the pore surfaces. The governing equations for the streaming and conduction currents can then be solved during subsequent waterflooding.

More advanced modelling would go some way to yielding insight into the dominant controls on the zeta potential under mixed wettability and may improve understanding of the apparent positive charge of the crude oils that have been observed in experimental results (Chapter 3). Since these results were obtained at the residual oil saturation where only water is flowing through the pore space, a more advanced pore network with surface charges assigned to pores based on their wetting state would be a useful starting point to further investigate these observations. More complex single pore descriptions may be more applicable to oilfield applications where multiple fluids flow simultaneously.

One final point to note is that whilst the application of such models has been focused on understanding wettability alteration on the zeta potential, they could equally be applied to understanding the impact of mineralogical heterogeneity on the zeta potential. For example, in sandstones, the distribution of clays and other mineral impurities within the pore space could be assigned to understand their impact.

5.5 Conclusions

This chapter has presented the first pore-scale model linking measured, macro-scale zeta potential with the micro-scale zeta potential on individual mineral surfaces. The micro-scale zeta potential depends on whether a mineral surface is water- or oil-wet: water-wet surfaces are assigned the mineral-brine zeta potential, but oil-wet surfaces are assigned the oil-brine zeta potential. The pore-space is modelled as a bundle of capillary tubes of varying size which allows expressions for the macro-scale zeta potential, brine saturation and wettability to be derived from first principles without the need for numerical modelling. Despite its simplicity, the model captures experimentally measured relationships between macro-scale zeta potential and water saturation in water-wet intact carbonate rocks (Revil and Cerepi 2004). The model was used to determine the relationship between macro-scale zeta potential and water saturation for different macro-scale wetting states, and the relationship between macro-scale zeta potential and wettability at the residual oil saturation, to interpret experimentally measured data on intact carbonate rock samples (Figure 3-8; Jackson and Vinogradov (2012); Jackson et al. (2016a)).

Regardless of wettability, the model predicts that the macro-scale zeta potential decreases with decreasing water saturation, falling to zero at the irreducible water saturation when there is no flow of water, consistent with experimental data from intact sandstone and carbonate samples (Revil and Cerepi 2004; Vinogradov and Jackson 2011). In water-wet models, the macro-scale zeta potential measured at full water saturation corresponds to the micro-scale zeta potential of the mineral-brine interface, confirming the use of the streaming potential method to determine micro-scale zeta potential of intact porous samples. Moreover, the saturation-dependence of the macro-scale zeta potential is the same irrespective of whether the water saturation is decreasing (drainage) or increasing (waterflooding).

Wettability alteration causes hysteretic behaviour in the saturation-dependence of the macro-scale zeta potential because mineral surfaces that becomes oil-wet after drainage return the micro-scale zeta potential of the oil-brine interface. Moreover, the macro-scale zeta

potential exhibits a clear relationship with wettability, because wettability reflects the ratio of water-wet to oil-wet surfaces (pores).

Fitting the model to the experimental data in Figure 3-8 allowed the micro-scale oil-brine zeta potentials in these experiments to be estimated, returning values between -4.1 mV and +13.9 mV despite literature data indicating this is typically negative (Chapter 2). Positive values of the oil-brine zeta potential have important implications for surface complexation models of the crude oil surface (Bonto et al. 2019; Brady and Krumhansl 2012; Tetteh, Veisi, et al. 2020) and for the design of controlled salinity waterflooding in oil reservoirs (Tetteh and Barati 2019; Mahani, Keya, et al. 2017b; Collini et al. 2020; Sari et al. 2017).

The model predicts a clear relationship between zeta potential and wettability but does not perfectly match experimental data, particularly in the mixed-wet regime. This is unsurprising given the simplified representation of the pore space, but the work provides a foundation for the development of more complex pore-scale models (Blunt 2017; Blunt et al. 2002; Blunt and Scher 1995).

Chapter 6 - Streaming Potential Measurements of the Crude Oil-Brine Interface

Abstract

This chapter outlines a process to measure the zeta potential of the crude oil-brine interface using the streaming potential method (SPM). The SPM is sensitive to the wetting state of porous media so strongly oil wet substrates are prepared and coated with crude oil. The zeta potential of these substrates is interpreted to represent the zeta potential of the crude oil-brine interface. Results are compared and benchmarked against established electrophoretic measurements of zeta potential on crude oil-brine emulsions and show a good match. Zeta potential measurements are reported up to high ionic strengths of 2 mol/L where conventional methods are limited. It is found that Ca^{2+} acts as a PDI to the crude oil surface and makes the zeta potential more positive. The bulk oil properties are found to be poor indicators of interfacial activity. Method presents a foundation to explore the zeta potential of the crude oil-brine interface (and other fluid-fluid interfaces) at hostile conditions of high ionic strength and temperature. Results can be used to better inform and constrain surface complexation models and design the injection brine composition for controlled salinity waterflooding.

6.1 Introduction

It is apparent that the zeta potential of the oil-brine interface is an important control on the success of CSW, yet, understanding of its polarity and magnitude at conditions relevant to subsurface oil reservoirs is limited. Conventional experimental methods to measure the zeta potential largely rely on electrophoresis and often make use of a Zetasizer (e.g. Nasralla and Nasr-El-Din (2014a). This approach relies on the ability to maintain a stable dispersion of oil droplets in brine which can be challenging under subsurface conditions of high ionic strength and/or temperature. Evidence from streaming potential measurements on carbonate core

samples (Chapter 3) and pore network modelling (Chapter 5) suggests that the zeta potential of the oil-brine interface may be positive under such conditions and more common than previously thought. However, these methods only provide an interpretation or prediction of the oil-brine interface, not a direct measurement. There exists therefore, a need for experimental methods which can directly and accurately probe the zeta potential of the crude oil-brine interface at subsurface conditions. The aim of this chapter is to develop such an approach to measure the oil-brine zeta potential using the streaming potential method.

Numerous papers have shown that the streaming potential method can measure the zeta potential of intact porous media with high ionic strength brines containing multiple salts and at elevated temperatures up to 120 ^{O}C (Al Mahrouqi et al. 2017a; Alroudhan, Vinogradov, and Jackson 2016; Vinogradov et al. 2010; Vinogradov and Jackson 2015; Vinogradov et al. 2018). Furthermore, it has been shown that the streaming potential method is sensitive to the wetting state of the porous media (Jackson and Vinogradov 2012; Jackson et al. 2016a); Figure 3-8). Streaming potential measurements obtained on a strongly oil-wet porous media that has been coated with crude oil should reflect the zeta potential of the oil-brine interface. This chapter will outline an approach to create such a substrate by chemically treating a natural sandstone core sample to render it neutrally charged and strongly oil wetting. These substrates are then coated with various crude oils. The zeta potential of these oil coated substrates is measured using the streaming potential method with simple NaCl/$CaCl_2$ brines up to 2 mol/L ionic strength. The results are benchmarked and compared at lower ionic strength (0.001 and 0.02 mol/L) against zeta potential measurements obtained using a conventional approach with a Zetasizer.

6.2 Materials & Methods

6.2.1 Substrate Preparation

The porous media used for the underlying substrate were Fontainebleau sandstone cores (D = 3.7 cm; L = 7.6 cm) with typical values for porosity of 9% and permeability of 200 +/- 20 mD. Fontainebleau was chosen primarily for its high quartz purity and chemical homogeneity (>99.9% SiOH). Additionally, the permeability of the samples is high enough to allow for relatively easy fluid saturation, whilst being sufficiently low enough to generate a significant pressure drop during streaming potential measurements without having to use excessively high flowrates.

The Fontainebleau cores were cleaned with toluene and methanol using a Soxhlet apparatus and dried. The cores were then saturated with 5% di-methyl-di-chloridesilane in heptane (Silanization Solution-1, Sigma Aldrich) in a vacuum over at a pressure of -1 bar (-0.1MPa) for at least 24 hours. The cores were then allowed to air dry at room temperature until a constant mass had been obtained to remove excess solvent (typically 24 – 48 hours). Typical values of porosity and permeability after silanising were 6% and 185 mD respectively. The silanised samples were then saturated again in the vacuum over at a pressure of -1 bar (-0.1MPa) with the crude oil of interest for at least 48 hours.

The wettability of these oil-coated silanised cores was characterised using the Amott water wetting index (see section 2.1.1.2II). Samples were submerged in a 0.001 mol/L NaCl electrolyte for three weeks and the volume of water spontaneously imbibed measured. In all cases, no water was imbibed. This yields an I_w value of zero (equation 2-2a) thus confirming the silanised cores are strongly oil wetting on a macro scale. Furthermore, droplets of water placed onto the outer surface of the silanised samples were not observed to spread providing further indication of oil-wetness. Previous studies have also used silanes to render strongly oil wet natural sandstone cores (Grate et al. 2013).

Following SI, the oil-saturated, silanised samples were then flooded with 10^{-3} mol/L NaCl electrolyte at a low rate (0.01 mL/min) for several days until no oil was flowing in the effluent. High flowrate 'bumps' were then performed (up to 30 mL/min) to ensure all mobile oil was displaced. This process was repeated in the other direction of flow. Typically, 20% of the initial oil remained in the core and electrolyte permeability values at the residual oil saturation were approximately 50 mD.

Figure 6-1 shows a model schematic of a pore space/channel of a crude oil coated, silanised Fontainebleau sandstone following the above preparation method. Silanes react strongly with water molecules and thus react with the SiOH/SiO surface groups of the sandstone. Consequently, this reaction neutralises the surface charge of the sandstone, whilst the exposed methyl groups render the surface non-polar, neutrally charged and oil-wetting. When saturated with crude oil, the oil will spread over the silane surface and the residual oil that remains after displacement with brine exists as a thin wetting film. During streaming potential measurements, the excess charge carried by flowing electrolyte arises due to the charge at the crude oil-brine interface.

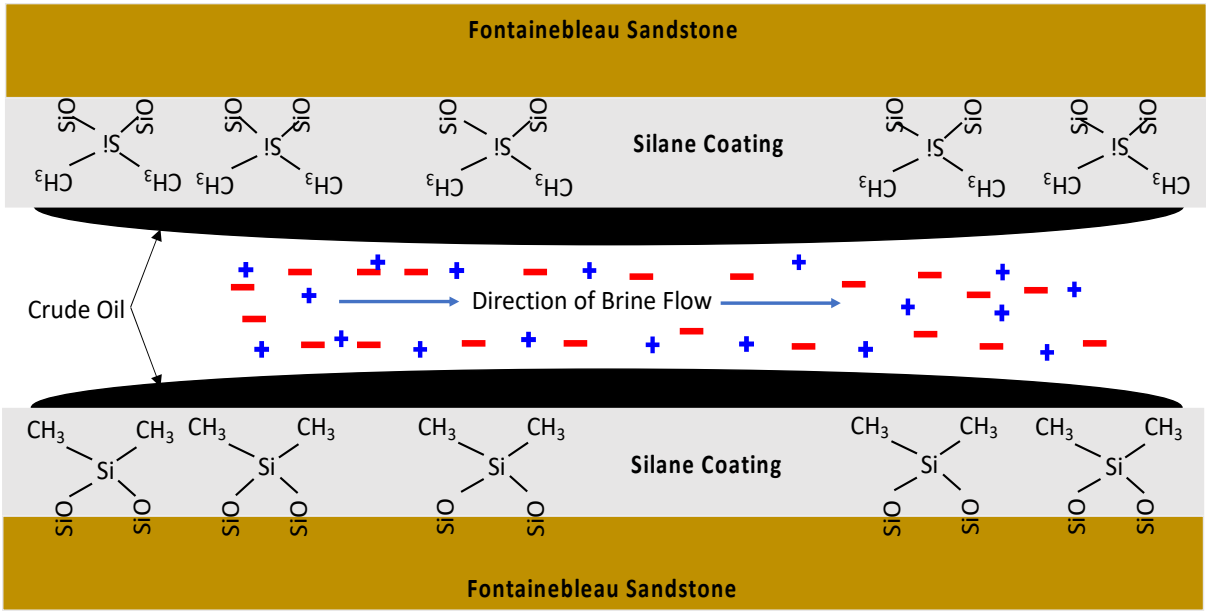

Figure 6-1: Schematic of a pore space of a crude oil coated, silanised Fontainebleau sandstone sample. The excess charge carried by the electrolyte flow originates only from the crude oil-brine interface due to the strongly oil-wetting nature and neutral charge of the underlying silane coating.

6.2.2 Electrolyte Ionic Strength and Composition

Synthetic electrolytes were prepared using deionised water and reagent grade salts (Sigma-Aldrich) to the desired ionic strength and composition. Conductivity (Metrohm 856 Conductivity Module) and pH (Mettler Toledo) were measured before and after experiments to ensure consistency. Natural pH values were typically between 5 – 6. Measurements were obtained using brines containing NaCl and $CaCl_2$ salts of varying composition but at constant ionic strengths of 0.001; 0.02; 0.5 and 2 mol/L, the latter three corresponding to the typical ionic strengths of low-salinity, seawater and reservoir formation brines respectively. The ionic strength was held constant as this control the size of the electrical double layer whilst the NaCl and $CaCl_2$ concentrations were varied to change the percentage of the total ionic strength contributed by the $CaCl_2$. Streaming potential measurements for each sample were performed initially with 0.001 mol/L NaCl and then gradually increasing the calcium concentration at a fixed ionic strength, before increasing to the next ionic strength of interest. Completing the measurements in this sequence minimises the effect of contamination by any residual electrolyte from the previous experiment. The pH was unaltered from the natural pH of the brine/oil system.

6.2.3 Crude Oils

Table 6-1 shows the physical properties of the crude oils used in this study. Table 6-2 shows the SARA analysis of the crude oils.

Table 6-1: Crude oil physical properties used in this study. Oils BD, BM and TT previously used in Chapter 3 (Table 3-1).

Oil	Viscosity (cP)	Density (kg/m3)	AN (mgKOH/g)	BN (mgKOH/g)
BM	N/A	N/A	0.20	1.80
BG	13 (70 ^{O}C)	870 (70 ^{O}C)	0.01	2.00
BP	11 (70 ^{O}C)	910 (30 ^{O}C)	0.19	2.60
BD	N/A	N/A	0.05	0.60
TT	1.56 (70 ^{O}C)	803 (70 ^{O}C)	0.34	0.41

Table 6-2: SARA analysis of crude oils used in this study. Oils BD, BM and TT previously used in Chapter 3 (Table 3-1).

Oil	Saturates (%)	Aromatics (%)	Resins (%)	Asphaltenes (%)	Total Resins + Asphaltenes (%)
BM	16.8	50.0	23.2	7.1	30.2
BG	22.0	41.0	20.0	17.0	37.0
BP	30.0	34.0	25.0	11.0	36.0
BD	43.5	46.0	10.1	0.4	10.5
TT	48.4	48.1	2.8	0.7	3.5

6.2.4 Zeta Potential Measurements

The streaming potential method of Vinogradov et al. (2010) that was used throughout this thesis and is described in detail in section 3.2.2 was used to measure the zeta potential of the oil coated silanised samples. Since these are based on natural intact Fontainebleau cores they are easily inserted into the existing setup.

The samples are inserted into a core holder with an applied confining pressure of 20 bar (2 MPa). Two Ag/AgCl electrodes situated either side out of the direct flowlines and measure the electrical voltage difference across the core. An external pump is used to induce brine flow through the sample and the pressure difference across the core is measured. The flow is allowed to stabilise where the pressure and voltage differences are recorded, this is

repeated for several different flow rates, typically five to eight per streaming potential measurement. The direction of electrolyte flow through the sample is reversed at each flow rate to check the pressure and voltage responses are symmetric with respect to flow direction, ensuring there are no electrode polarisation effects. Plotting the values of stabilised voltage difference against the values of stabilised pressure difference for each flow rate allows determination of the streaming potential coupling coefficient (*C*), given by the gradient of a linear regression through the data. The zeta potential can then be calculated using a modified form of the classical Helmholtz-Smoluchowski equation (equation 3-2).

Following a streaming potential measurement, samples were re-saturated with the next electrolyte of interest by flooding the sample for at least 250 mL (>10 pore volumes) in both directions. Effluent pH and conductivity were measured to ensure consistency with the inlet values.

6.2.5 Zetasizer Measurements

Zeta potential measurements were also obtained using a conventional approach with a Zetasizer to benchmark the streaming potential measurements against. The same oils and brines were used but only for ionic strengths of 0.001 and 0.02 mol/L where it was relatively easy to maintain a stable dispersion. The zeta potential was measured using a Zetasizer NanoZS (Malvern Analytical) with 15 subruns per measurement and three measurements per sample. For each oil/brine combination, two vials containing 20 mL of brine and 4 droplets (~0.1 - 0.2 mL) of crude oil were prepared. These were emulsified using a Turraxx Ultra stirrer at 10,000 rpm for 30 seconds. The emulsions were then left to settle for a few minutes before a 1 mL sample was drawn and inserted into the Zetasizer. Two samples from each vial were measured yielding a total of four samples and twelve zeta potential measurements per oil/brine combination. Measurements where the underlying distribution was deemed ‘poor’ were

excluded from the results. The zeta potential is reported as the average of these measurements ± two standard errors.

6.3 Results

6.3.1 Streaming Potential Measurements

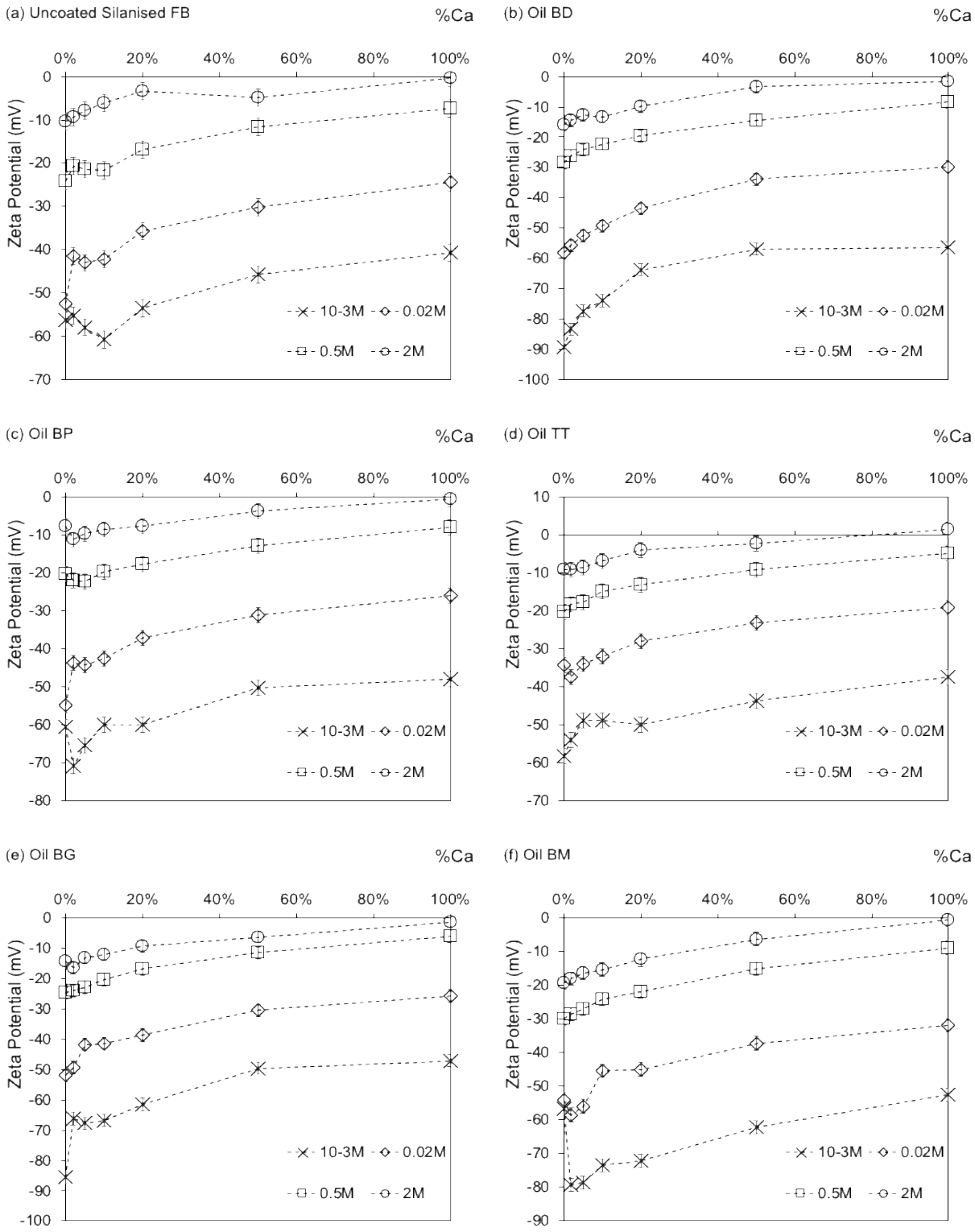

Figure 6-2: Zeta potential as a function of Ca^{2+} percentage at constant ionic strengths for a range of oil coated, silanised Fontainebleau core samples.

Figure 6-2 reports zeta potential measurements made on the oil coated silanised Fontainebleau core samples. Figure 6-2(a) reports zeta potential measurements obtained on a silanised Fontainebleau core that was not exposed to or coated with crude oil. Results are plotted as a function of the percentage contribution to the ionic strength that comes from Ca^{2+} ions. The pH in these experiments was unaltered from its natural value and did not change from the natural brine pH. The pH was typically between 5.1 and 6. Experimental data including the specific pH of each measurement can be found in the appendix. The decision to alter the Ca^{2+} concentration as opposed to the pH (as is commonly done in many literature studies, see Figure 2-11) was made due to the difficulty of altering the pH in natural subsurface environments. Adjusting the concentration of other potential determining ions (PDIs), such as Ca^{2+}, to control the zeta potential is more relevant to practical applications.

Despite the neutral charge of the uncoated silanised sample a non-zero zeta potential is observed (Figure 6-2 (a)). The zeta potential becomes smaller in magnitude with increasing ionic strength and increasingly more positive with increasing Ca^{2+} concentration. Both trends have been observed for non-polar oils, the air-water interface and other neutrally charged surfaces in the presence of aqueous solutions. The negative charge at a neutral interface has primarily been attributed to the affinity of the hydroxyl ion (OH^-) at pH > 3 (see section 2.2.4.1 for further discussion). The magnitude of the zeta potential measured on the silane sample (Figure 6-2 (a)) in dilute brines (0.001 – 0.02 mol/L) is comparable to electrophoretic data reported for non-polar oils at similar conditions. The zeta potential measurements obtained on the silane sample are therefore thought to represent the zeta potential of any neutral surface in the presence of an aqueous electrolyte. The zeta potential in this case does not depend on the properties of the surface itself, rather the properties of the fluid.

The same general trends observed for the silane sample are also evident for the oil coated silane samples (Figure 6-2 (b)-(f)). The zeta potential becomes smaller in magnitude with increasing ionic strength and increasingly more positive with increasing Ca^{2+} concentration. The magnitude of the zeta potential varies between the different samples. The

zeta potential falls between -50 mV (Oils BP/BM) and -90 mV (Oil BD) in 0.001 mol/L NaCl brines, increasing to between -35 mV (Oil TT) and -60 mV (Oil BD) when the ionic strength is increased to 0.02 mol/L. In $CaCl_2$ brines, the zeta potential ranges between -40 mV (Oil TT) and -60 mV (Oil BM) at 0.001 mol/L and between -20 mV (Oil TT) and -35 mV (Oil BM) at 0.02 mol/L. This variation in the magnitude of zeta potential shows that the presence of crude oil modifies the surface charge of the silane substrate and varies depending on the oil. Such variation is unsurprising given zeta potential data reported in literature (Figure 2-11) and the magnitude of the zeta potential measured on the oil coated silane samples is comparable to those data. A full comparison between the zeta potential measurements in Figure 6-2(b)-(f) and those published in literature will be discussed later in this chapter.

The zeta potential measurements obtained at high ionic strengths (>0.1 mol/L) are non-zero for all samples. In all but one case these are negative in polarity. The only exception is for the sample coated with Oil TT where a small but positive value of +0.6 mV is reported for the 2 mol/L $CaCl_2$ brine. This corresponds to a Ca^{2+} concentration of 0.67 mol/L, similar to the concentration at which positive zeta potential measurements have been observed in literature (Figure 2-12). There is confidence in the polarity of this measurement since the gradient of the linear regression between stabilised values of ΔV and ΔP (equation 3-2) shows a clear change from negative to positive during the streaming potential measurements.

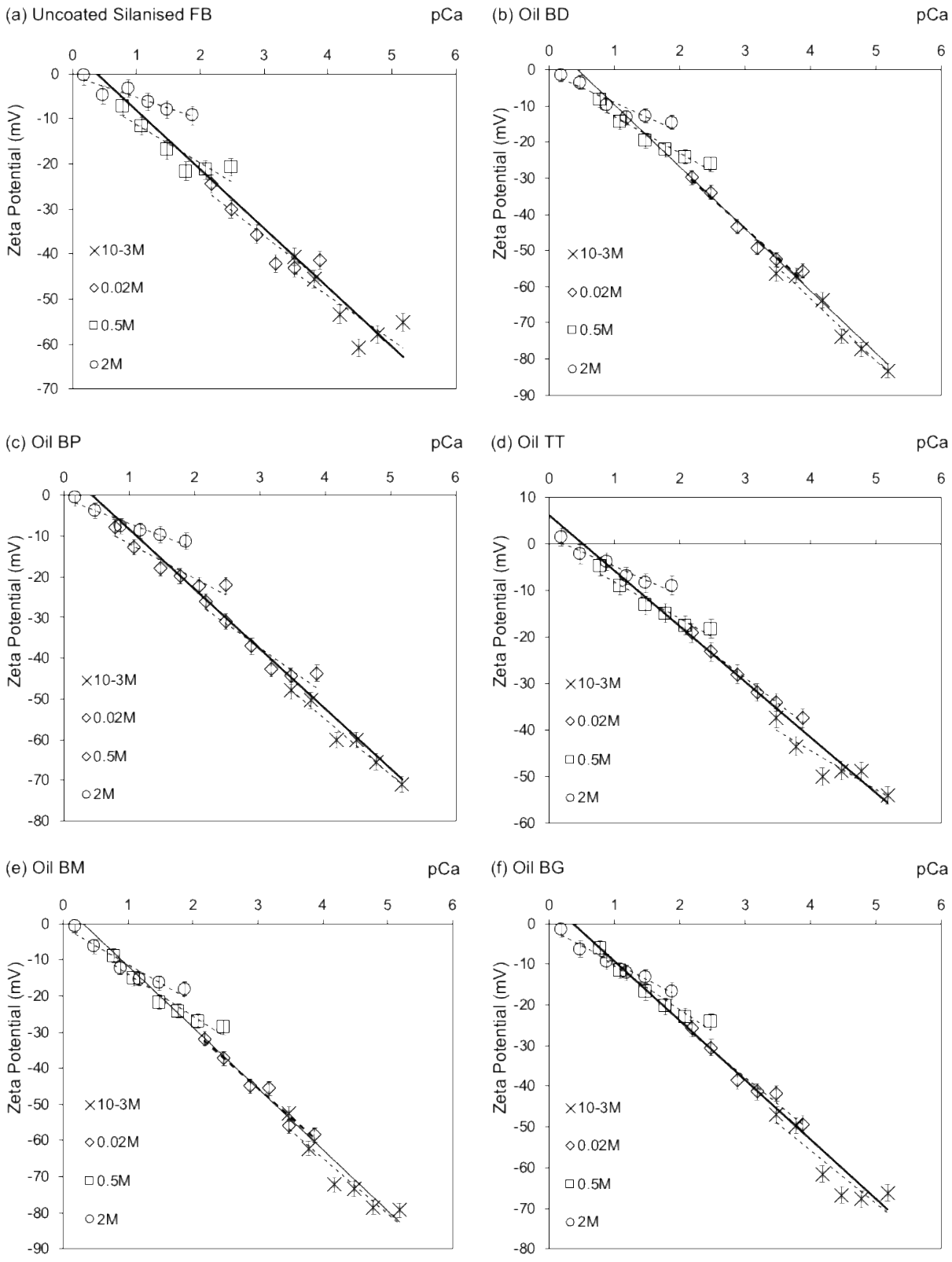

Figure 6-3: Zeta Potential measurements reported in Figure 6-2 plotted as a function of pCa.

The zeta potential results reported in Figure 6-2 are shown in Figure 6-3 plotted as a function of pCa - the negative logarithm of Ca^{2+} concentration in mol/L. For all samples, including the uncoated silane sample, there is a clear linear dependence of the zeta potential with pCa. This is also observed in literature data (Figure 2-12). The gradient of the linear trend lines plotted for each ionic strength decreases with increasing ionic strength showing the sensitivity of the zeta potential to calcium decreases with increasing ionic strength.

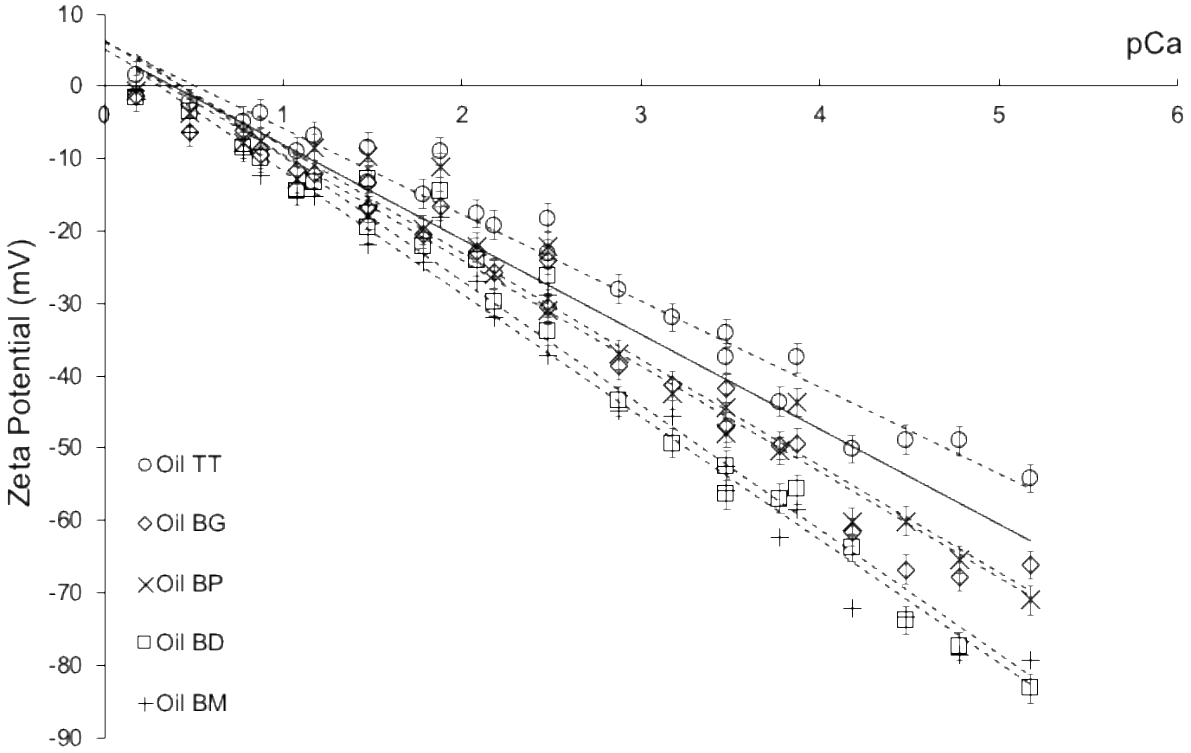

Figure 6-4: Zeta potential measurements as a function of pCa for all crude oil coated silanised Fontainebleau samples. Solid black line shows trend line of zeta potential measurements for the uncoated silane sample with the individual points removed for clarity.

Figure 6-4 collates the results shown in Figure 6-3 for the different samples to compare against one another. Linear trendlines are plotted through all the data for a given sample regardless of ionic strength. The trend line for the uncoated silane sample is shown for reference as the solid black line, but we the individual points have been removed for visual clarity.

The difference between the uncoated silane samples and the coated silane samples highlights the change in the zeta potential behaviour due to the presence of crude oil. Furthermore, the variation between the crude oils evidences the different zeta potential behaviour. Only the addition of Oil TT causes the zeta potential to become more positive than the silane sample, this was also the only sample to return a positive zeta potential measurement. Oils BP and BG, and Oils BD and BM show apparently similar behaviour.

A linear relationship between the zeta potential and pPDI is indicative of a Nernstein relationship and has been previously observed for carbonates (Alroudhan, Vinogradov, and Jackson 2016). The gradient of the zeta potential can be described by:

$$\left.\frac{d\zeta}{dpPDI}\right|_{\zeta \to 0} = \frac{-2.303\frac{k_B T}{ze}}{\left(1+\frac{C_d}{C_s}\right)\exp(\kappa\delta)} \qquad (6\text{-}1)$$

where *k* is the Boltzmann constant, *T* the absolute temperature, *z* the valence of the PDI, *e* the elementary charge on an electron, κ the inverse Debye length, C_d and C_s are the capacitance per unit area of the diffuse and Stern layer respectively and δ the distance of the shear plane from the Stern plane.

The linear relationship between zeta potential and pCa observed in Figure 6-4 suggest the crude oil-brine interface also exhibits Nernstian behaviour to the Ca^{2+} ion. The Stern layer capacitance for a given oil can therefore be calculated from the gradient of the linear regression (Figure 6-4) and equation (6-1). The diffuse layer capacitance is assumed to be approximated by $\kappa\varepsilon$ where ε is the electrolyte permittivity (Alroudhan, Vinogradov, and Jackson 2016). The simplest assumption that the Stern plane coincides with the shear plane is employed yielding a δ = zero (Figure 2-7).The Stern layer capacitance calculated in this way are reported in Table 6-3.

C_s ranges from 0.03 F/m^2 for Oil TT saturated with 0.001 mol/L ionic strength electrolyte to 1.86 F/m^2 for Oil BM saturated with 2 mol/L ionic strength electrolyte. These values are smaller, but of a similar order of magnitude, than those calculated by Alroudhan,

Vinogradov, and Jackson (2016) who determined a Stern layer capacitance of 2.75 F/m^2 for the calcite surface in contact with a 2 mol/L ionic strength electrolyte. This suggests the crude oil surface does not have as strong a capacity for the Ca^{2+} ion as the calcite surface. Takeya et al. (2019) use a value of 2.253 F/m^2 for the Stern layer capacitance in their model of the crude oil surface, irrespective of ionic strength. The difference in the Stern layer capacitance for different oils further highlights the different surface properties and extent of interaction with the Ca^{2+} ion between the oils.

Table 6-3: Stern layer capacitances determined from the gradient of trend lines fitted to the experimental data in Figure 6-4 and equation 6-1.

Oil	Ionic Strength (mol/L)	Gradient (mV/decade)	C_s (F/m^2)
BD	0.001	-17.4	0.11
	0.02	-16.2	0.41
	0.5	-10.2	0.90
	2	-8.2	1.31
BP	0.001	-13.7	0.07
	0.02	-11.3	0.21
	0.5	-8.6	0.70
	2	-6.1	0.89
TT	0.001	-8.4	0.03
	0.02	-10.9	0.20
	0.5	-8.0	0.63
	2	-6.2	0.91
BG	0.001	-13.1	0.06
	0.02	-13.2	0.28
	0.5	-10.8	0.98
	2	-8.4	1.35
BM	0.001	-15.5	0.08
	0.02	-16.0	0.40
	0.5	-11.6	1.10
	2	-10.2	1.80

6.3.2 Comparison with Zetasizer Measurements

To explore whether the steaming potential measurements made on the oil coated silane samples do indeed return the zeta potential of the crude oil-brine interface, the zeta potential of oil-brine emulsions was also measured with a Zetasizer for comparison. Data were obtained for all five oils with the lower ionic strength brines (0.001 – 0.02 mol/L) at the same conditions to ensure comparability.

Figure 6-5 shows some examples of the zeta potential distributions obtained during the Zetasizer measurements. The software has a built-in test for normality that determines whether the data for a given distribution is ‘good’ or ‘poor’. Figure 6-5 (a) and (b) show examples of ‘good’ distributions obtained on emulsions of Oil TT. A mean of -31mV and a standard deviation of approximately 7.5 mV was obtained over the 15 sub-runs. These examples are typical of the more accurate Zetasizer measurements and represent the lower end of the standard deviation range. Oil TT was the lightest of the oils used in this chapter and was typically the easiest to emulsify, the most stable and produced the most accurate and repeatable results.

Figure 6-5 (c) and (d) show examples of ‘poor’ zeta potential distributions. The data shown in (c) for an emulsion made with Oil BG is highly scattered and shows a wide range of zeta potential measurements. This is represented by the large standard deviation of 155 mV. Furthermore, the mean of this measurement (-27 mV) differs significantly from the mode (95 mV). Considering the mean on its own this measurement would not appear unreasonable based on literature data (Figure 2-11) however it is clear from the distribution that such a measurement is poor quality. There was no obvious reason why these poor measurements occurred. Regardless, results such as this were surprisingly common, particularly for the more viscous and darker oils BP, BG and BM that were harder to emulsify and quickly aggregated. The internal calculation of the zeta potential assumes droplets are spherical which may not have been the case for such oils and may have contributed to the poor measurements.

Measurements where the distribution was deemed ‘poor’ were not included in the results presented later in this section. However, by considering only the ‘summary results’ of mean zeta potential, conductivity, and electrophoretic mobility provided by the software it would not necessarily be clear that such a broad and poor underlying distribution was present. The measurement shown in Figure 6-5 (d) obtained on an emulsion of Oil BP looks at first glance to be reasonably normally distributed but is deemed ‘poor’ due to the large standard deviation of 70 mV. As with Figure 6-5 (c), the mean on its own appears to be of a magnitude one might expect. Again, there was no obvious reason for such a broad distribution. Measurements such as Figure 6-5 (c) and (d) highlight the variability and challenges in measuring the zeta potential of an oil-brine emulsion.

To further emphasise this point, Figure 6-5(e) and (f) show examples of measurements where the underlying data distribution was deemed ‘good’ but there is still significant variability. Figure 6-5 (e) is from a measurement made on and emulsion with Oil BM with a mean of -25 mV and a standard deviation of 15 mV whilst Figure 6-5(f) is from an emulsion with Oil BP with a mean of -57 mV and a standard deviation of 21 mV. Broader distributions such as these were typical of ‘good’ measurements on the more viscous and darker Oils BP, BG and BM.

It has been reported that the amount of oil dispersed in the brine, along with the droplet size, can significantly affect the value of the measured zeta potential with increasing oil fraction and increasing droplet size yielding a larger magnitude in the zeta potential (Onaizi 2022; Kumar and Mahto 2017; Kundu, Kumar, and Mishra 2015). The three viscous and darker Oils (BP, BG and BM) were noticeably more difficult to emulsify and less stable than Oil TT. The broader distributions observed for these three oils may have been due to a broader particle size distribution. Oil BD exhibited behaviour somewhere between Oil TT and Oils BP, BG and BM. It was relatively easy to emulsify but was typically more variable than Oil TT. Photos showing examples of the emulsions for each of the oils can be found in Appendix C (Figure C 1).

Zetasizer measurements on a given sample were generally consistent due to the accuracy of the device. However, different samples from the same emulsion could yield significantly different results, even if the underlying distribution was ‘good’. Many literature studies only report the range in zeta potential measurements from one sample (Kundu, Kumar, and Mishra 2015; Nasralla and Nasr-El-Din 2014a; Takeya et al. 2019). In some cases there is no discussion of repeat measurements or samples (Takeya et al. 2019). Conducting experiments in this way may be underestimating the error in the zeta potential of the emulsion. Moreover, if the underlying distribution was not considered when analysing data, poor distributions such as those shown in Figure 6-5(c) and (d) may have been reported as good results if the mean zeta potential appeared to be in the expected range. The only study that discusses the impact of the underlying distribution is that of Kolltveit (2016) who note many of the same challenges discussed here.

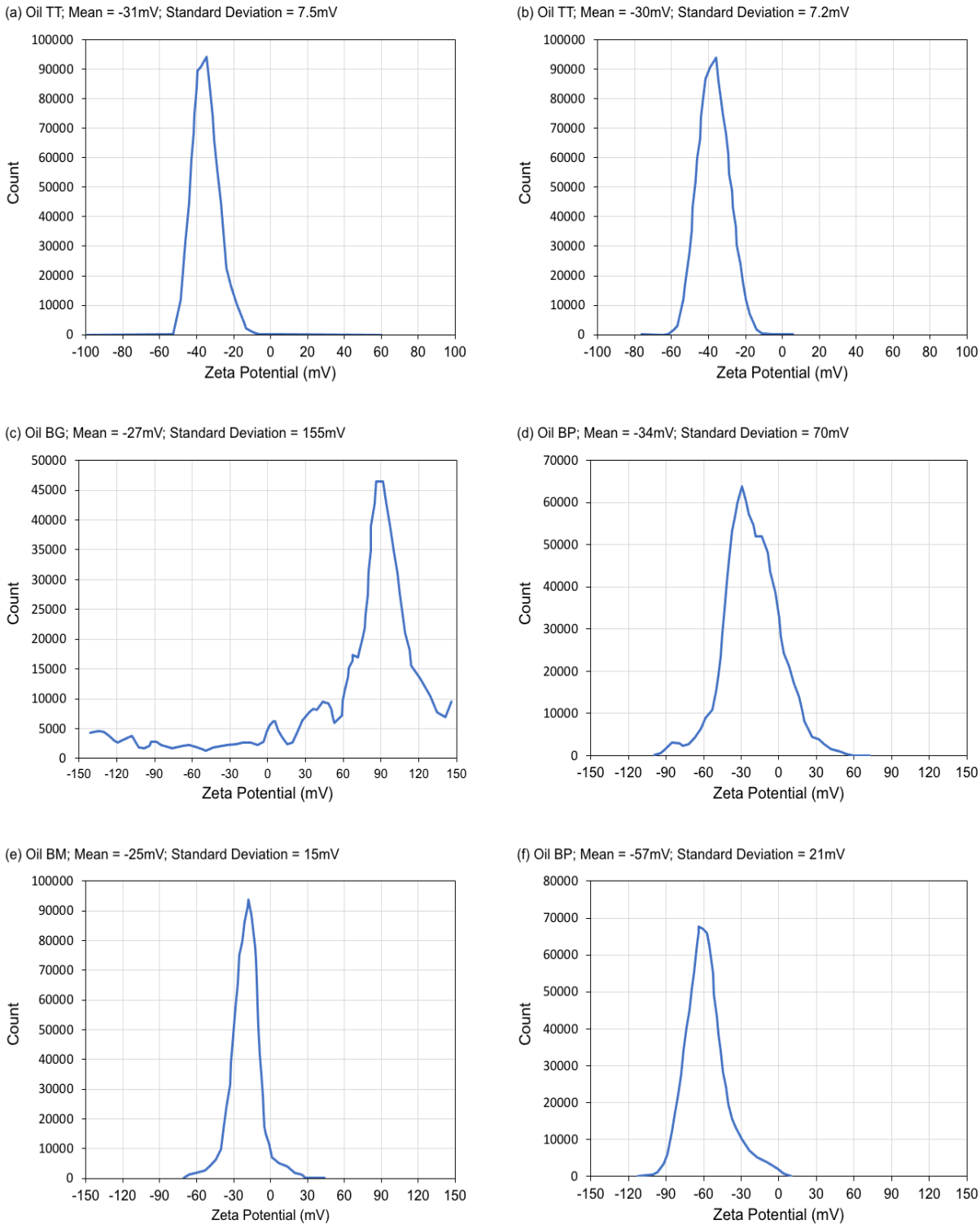

Figure 6-5: Examples of the underlying zeta potential distributions measured during Zetasizer measurements on oil-brine emulsions. (a) Oil TT; Mean = -31 mV; Std.dev = 7.5 mV (b) Oil TT; Mean = -30 mV; Std.dev = 7.2 mV (c) Oil BG; Mean = -27 mV; Std.dev = 155 mV (d) Oil BP; Mean = -34 mV; Std.dev = 70 mV (e) Oil BM; Mean = -25 mV; Std.dev = 15 mV (f) Oil BP; Mean = -57 mV; Std.dev = 21 mV.

It should be noted that the streaming potential measurements do not yield any insight into the underlying zeta potential distribution. The measurements reflect the mean zeta potential across the whole porous media. The streaming potential results will therefore be compared to the mean zeta potential of the Zetasizer measurements. Figure 6-6 compares these for Oil TT. The error in the streaming potential measurements reflects the accuracy of the electrodes. The zetasizer data are reported as the mean of the 12 measurements (excluding any with a 'poor' underlying distribution) with the range given as two standard errors.

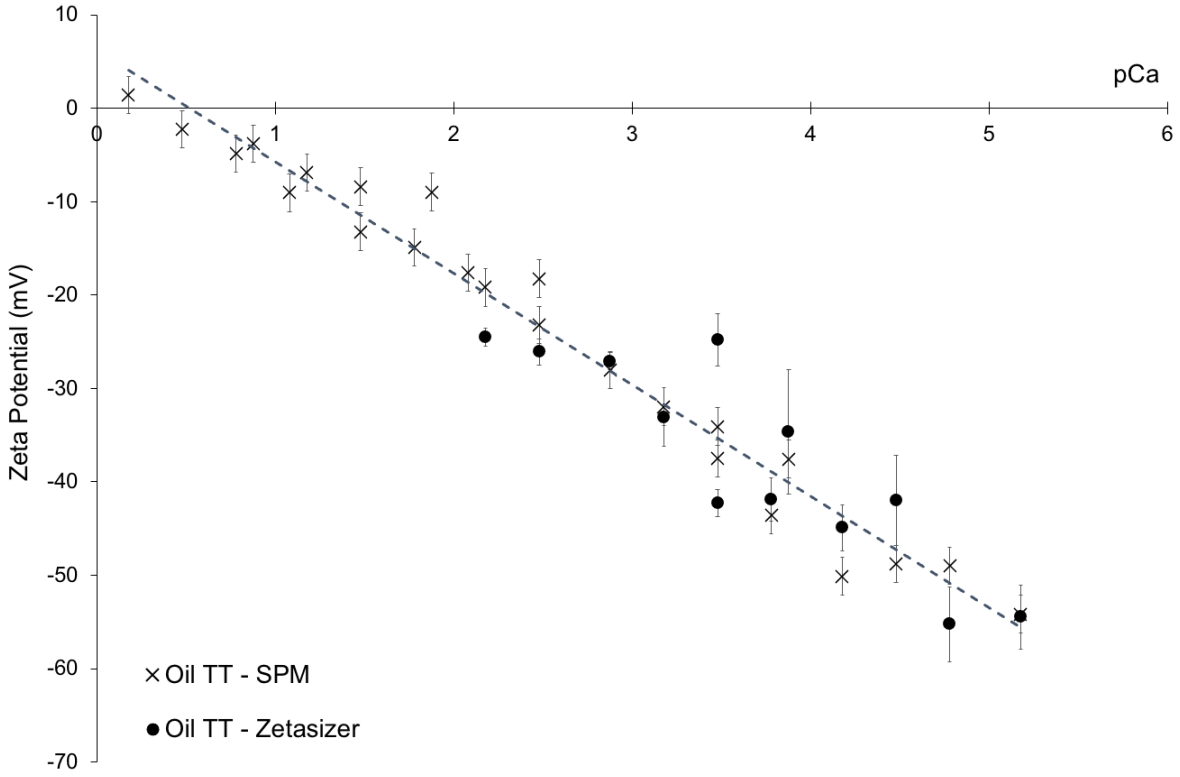

Figure 6-6: Comparison of streaming potential measurements and Zetasizer measurements of the zeta potential of Oil TT as a function of pCa.

A good match between the two experimental methods is observed with the Zetasizer data aligning nearly identically with the SPM trendline. Oil TT was the lightest of the five oils, the easiest to emulsify and produced the most stable emulsions. Typically, Oil TT also returned the narrowest zeta potential distributions during measurements and repeat measurements

across the four samples for each data point were largely consistent and reproducible. The consistency between the data provides confidence that the oil-coated silane substrates used in the SPM measurements do indeed return the zeta potential of the oil-brine interface.

Conversely, the remaining four oils that were more viscous and more challenging to emulsify well did not produce as consistent data. These data are compared in Figure 6-7 and all four oils are collated on the one plot. Filled symbols represent the Zetasizer data and open symbols show the SPM data previously shown in Figure 6-4.

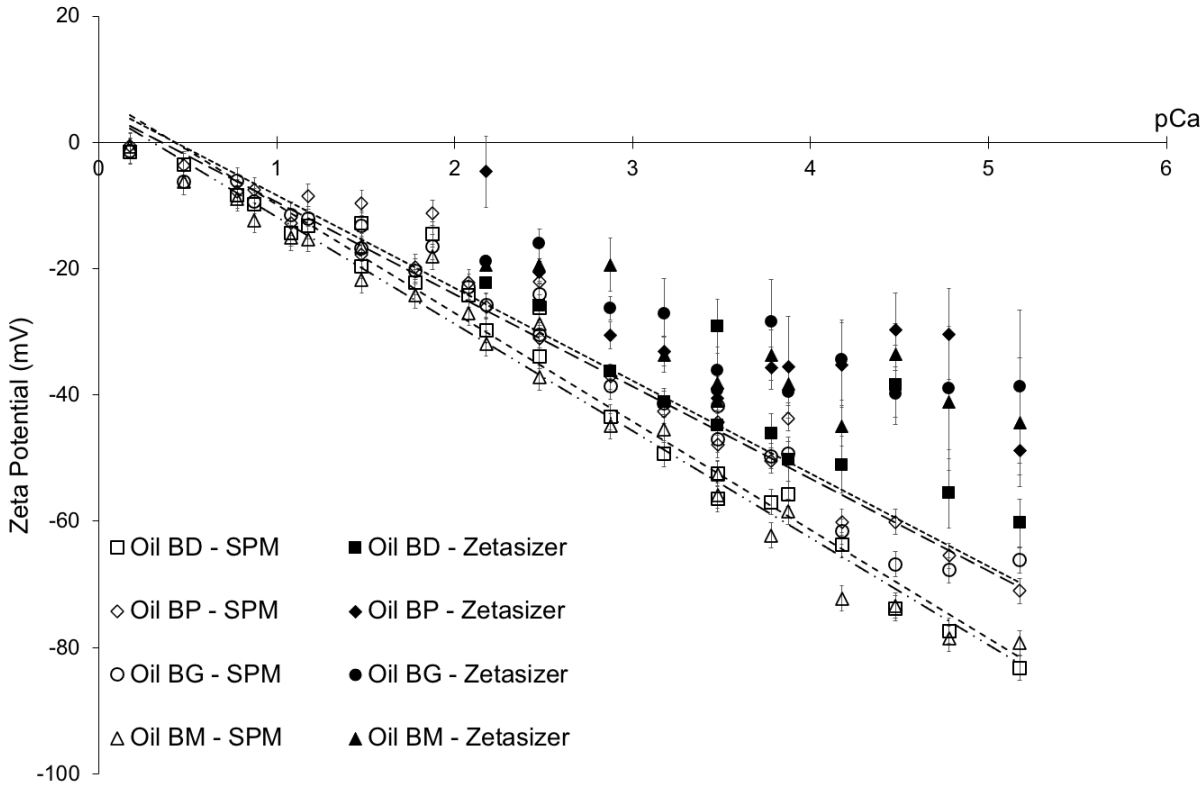

Figure 6-7: Comparison of streaming potential measurements (open symbols) and Zetasizer measurements (filled symbols) for Oils BD (Squares); BP (Diamonds); BG (Circles) and BM (Triangles).

The Zetasizer data is not as consistent with the streaming potential data for these four oils. The Zetasizer data is generally smaller in magnitude than the streaming potential data and does not exhibit the linear Nernstein behaviour seen in the SPM data. The Zetasizer data for these oils is more scattered and less accurate than for Oil TT. Given the errors and challenges in obtaining high quality data for oils BD, BP BG and BM there is limited confidence

in the accuracy of the Zetasizer data for these oils. The lack of consistent Nernstein behaviour that has been seen in the SPM data, the Zetasizer data for Oil TT, and in literature measurements (Figure 2-12) further questions the accuracy of these data.

6.4 Discussion

6.4.1 Comparison to Literature Data

The zeta potential results obtained here using the streaming potential method are qualitatively consistent with three main trends observed in the literature data (i) the zeta potential of the oil-brine interface is typically negative at pH > 5 (ii) the magnitude decreases with increasing ionic strength (iii) addition of calcium yields a more positive zeta potential, with a strong linear correlation observed between the zeta potential and pCa (Figure 2-11 & Figure 2-12). Figure 6-8 below compares the new data with literature data previously shown inFigure 2-12. The grey shaded region represents the new data bounded by the steepest trendline (Oil BM) and the shallowest trendline (Oil TT). The small black crosses represent the individual data points in Figure 6-4 (excluding that ofAlroudhan, Vinogradov, and Jackson (2016)). Literature data are plotted as before in Figure 2-12 with the different studies referenced in the legend. The dashed black line represents the linear trend line plotted through all literature data measured at a pH of 4 whilst the black dot-dash line represents those measured at a pH above 7. The dotted line represents the trendline through all the new streaming potential data, obtained at a pH of 5 - 6.

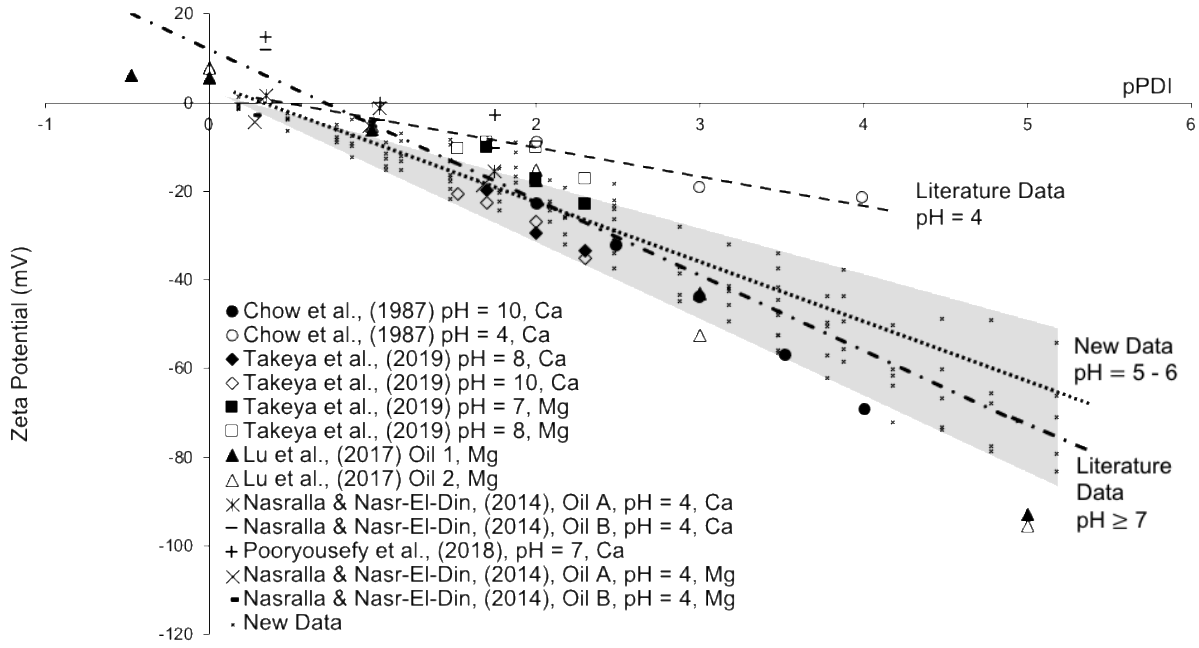

Figure 6-8: Zeta Potential measurements from Figure 6-4 (small crosses) plotted against data obtained from literature previously shown in Figure 2-12. The grey shaded region represents the locus of points for the new data reported here. The dotted line shows the trendline through all the new data. The dashed black line represents the linear trend line plotted through all literature data measured at a pH of 4 whilst the black dot-dash line represents those measured at a pH above 7.

The new data plot in the region between the literature data obtained at pH > 7 and pH = 4. Given the pH in these experiments was typically in the range 5 - 6 this is consistent with what might be expected. Previous SCM's have suggested that increasing the pH increases the number of negatively charged acid species at the interface, making the zeta potential more negative, and increasing the sensitivity to divalent cations such as Ca^{2+} (Brady et al. 2015, Bonto et al. 2019, Tetteh et al. 2020) Regardless of cation type, the literature data obtained at pH > 7 is generally more negative in magnitude and shows a steeper gradient between zeta potential and pPDI than this data, suggesting a greater sensitivity to the PDI at higher pH values consistent with these previous theories. At a pH of 4, the literature data are smaller in magnitude with a smaller sensitivity to the PDI concentration than the new data, consistent with the concept of a reduced number of negatively charged acid species at the interface. The variability between different oils is unsurprising given their different properties and compositions. The consistency between the new data and what has previously been observed

provides further confidence to the ability of the streaming potential to accurately measure the zeta potential of the oil-brine interface.

6.4.2 Impact of Oil Properties

The protonation/deprotonation of the surface-active base/acid species are thought to be the primary control on the surface charge of the oil-brine interface. The acid number (AN) and base number (BN) reflect the bulk concentrations of these species and are therefore thought to correlate with the surface-active concentrations of the species, and subsequently the surface charge. Figure 6-9 plots the zeta potential data measured with NaCl brines as a function of the AN, BN and AN/BN ratio both qualitatively and quantitatively. Figure 6-10 shows similar plots for the data measured with $CaCl_2$ brines.

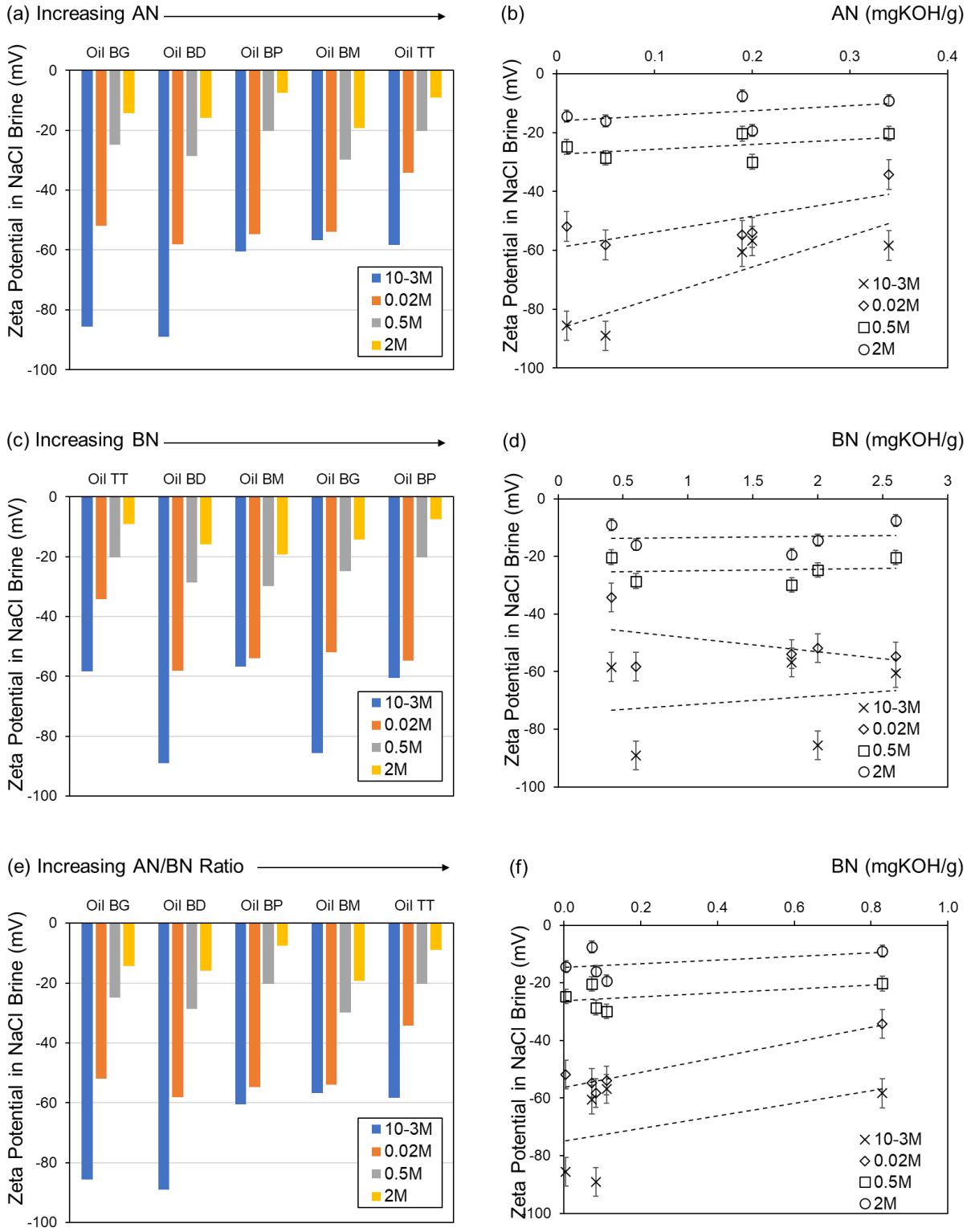

Figure 6-9: Zeta potential measurements obtained on oil coated silanised Fontainebleau cores saturated with NaCl brines of varying ionic strengths plotted against (a-b) the AN of the oil (c-d) the BN of the oil and (e-f) the AN/BN ratio of the oil (Table 6-1).

It appears that oils with a larger AN generally return a less negative zeta potential for a given ionic strength (Figure 6-9 and Figure 6-10, top plots) although the effect decreases with increasing ionic strength (Figure 6-9 and Figure 6-10, top plots). In high ionic strength brines (>0.5 mol/L) the zeta potential is largely independent of the AN. The zeta potential appears also to be largely independent of the BN regardless of ionic strength (Figure 6-9 and Figure 6-10, middle plots). Consequently, the zeta potential correlates with the AN/BN ratio in a similar way to the AN, since it is insensitive to the BN. These same general trends are observed in both NaCl and $CaCl_2$ brines, although the magnitudes are smaller in the latter. The consistency in the trends between NaCl and $CaCl_2$ brines suggests these trends are primarily related to the surface charge rather than any interaction with specific ions. However, the charge inversion between Oils BD, BP, BG and BM and Oil TT in 2 mol/L $CaCl_2$ (Figure 6-10, middle plots) provide evidence there is some dependency and interaction with ionic species.

The correlation with the AN is surprising based on previous theories for the oil-brine interface. It would be expected that a larger number of acid species in the bulk would yield a larger number of acid species at the interface. At a pH 5 - 6 where these data were obtained, the surface acid species are thought to deprotonate and exhibit a negative charge (equation 2-8b). Thus, an oil with a higher AN would be expected to return a more negative zeta potential, contradicting what has been observed here. However, a higher number of acid species at the interface would also be expected to interact more with cations in the brine. Such interaction may neutralise (Na^+; equation 2-12a) or form positive complexes (Ca^{2+}; Chapter 2, equation 2-10a) with the surface species yielding a less negative surface and zeta potential. The trends observed in Figure 6-9 and Figure 6-10 may suggest that both Na^+ and Ca^{2+} act as PDIs to the oil surface.

Similar arguments have been proposed for the base species. A higher BN would be expected to correlate with an increased number of base species at the surface. However, at pH 5-6, the majority of base species are neutrally charged and therefore do contribute

significantly to the development of surface charge (equation 2-8a). Thus, the number of surface base species should not significantly affect the zeta potential of the oil-brine interface. The insensitivity of the zeta potential to the BN observed here is consistent with such theories.

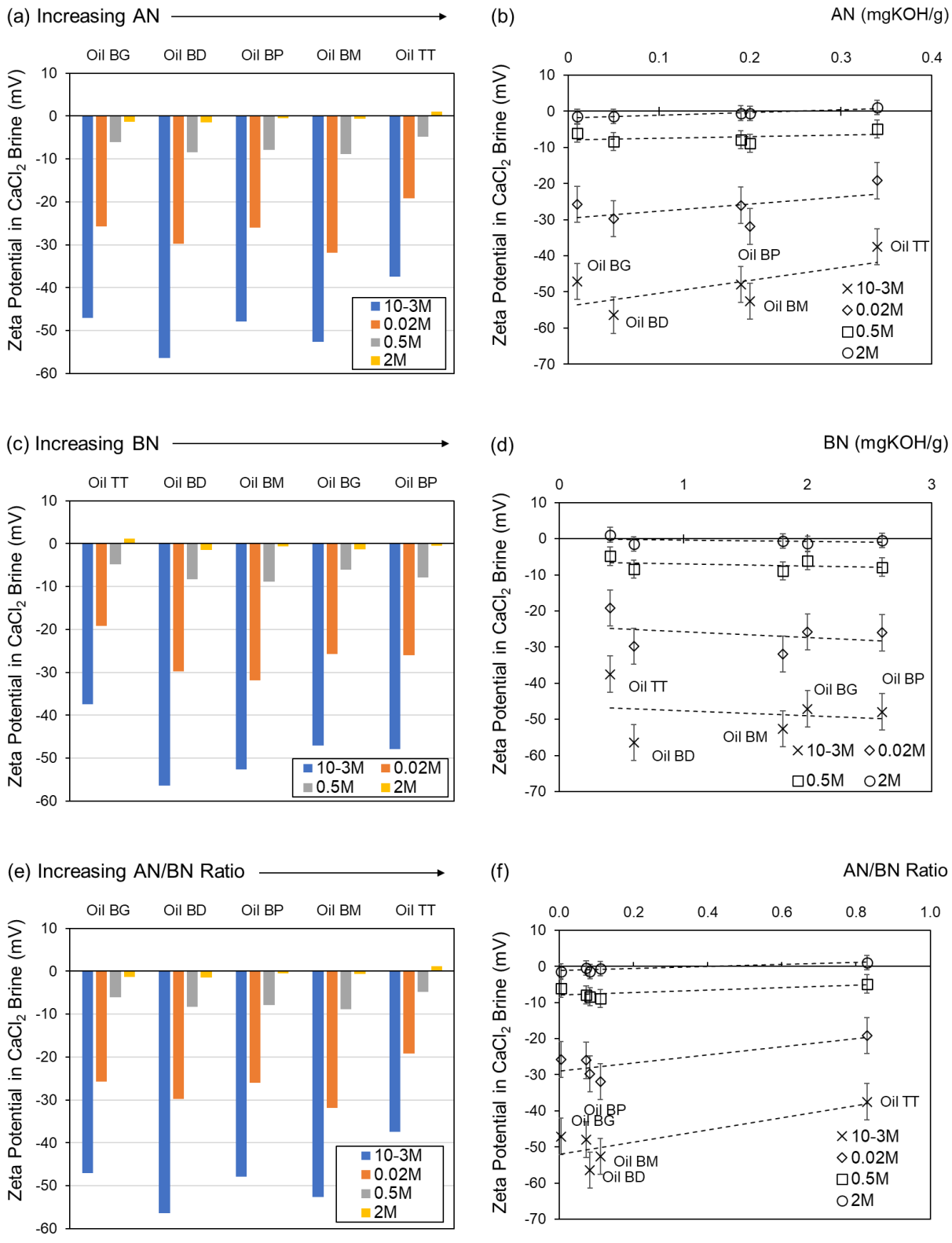

Figure 6-10: Zeta potential measurements obtained on oil coated silanised Fontainebleau cores saturated with $CaCl_2$ brines of varying ionic strengths plotted against (a-b) the AN of the oil (c-d) the BN of the oil and (e-f) the AN/BN ratio of the oil.

The linear Nernstein relationship between the zeta potential and the pCa observed in Figure 6-4 should also be dependent on the surface charge and surface properties of the different oils as these will determine the Stern layer capacitance. To examine any correlations with the oil properties, the gradient of the trendlines shown in Figure 6-4 are plotted against the AN, BN and AN/BN ratio in Figure 6-11. The intercept of these trendlines with the x-axis in Figure 6-4 is also plotted. This correlates to the pCa at the point of zero charge (pZc = zero zeta potential) and represents the concentration of Ca^{2+} required to neutralise the surface charge.

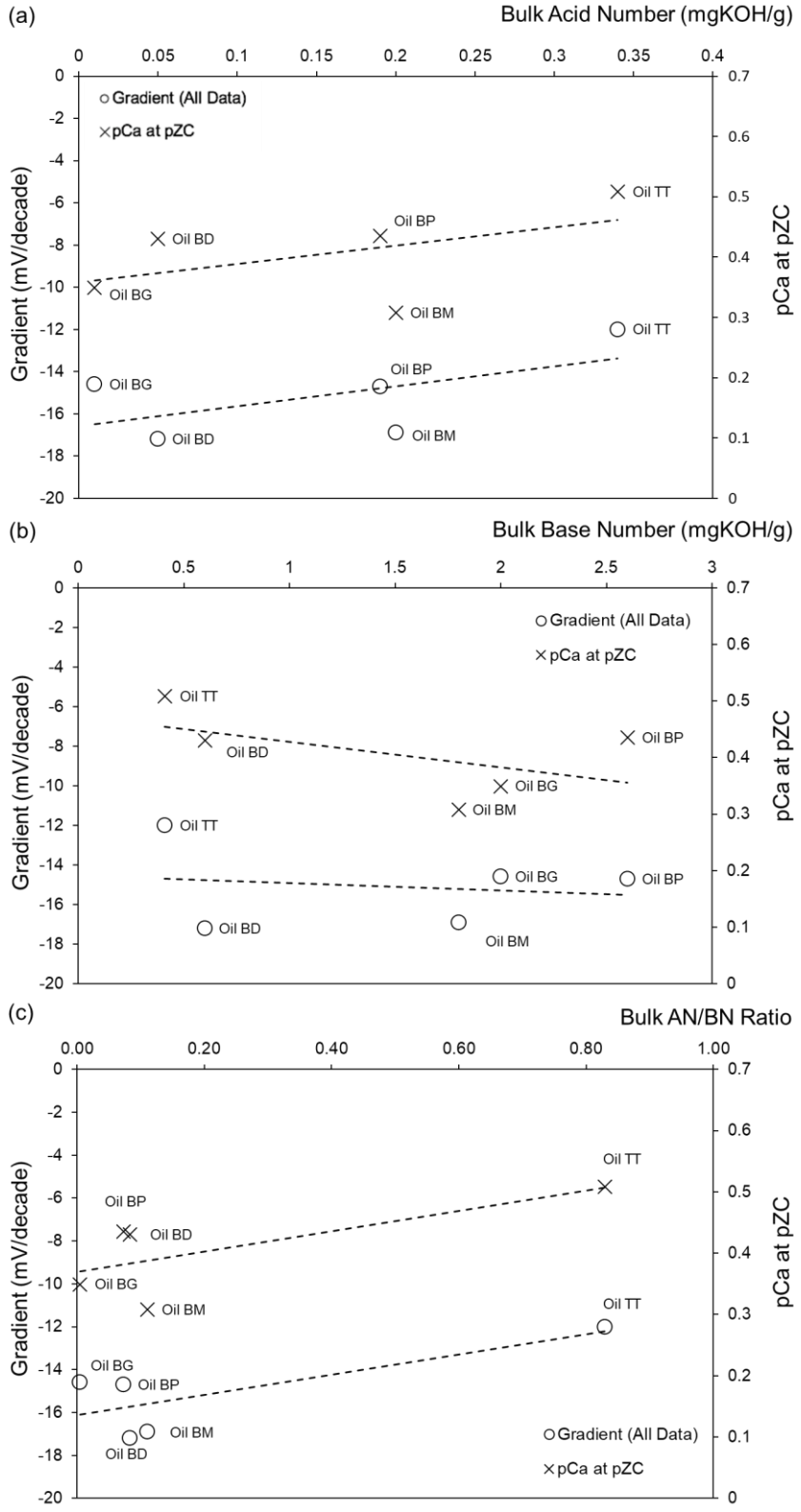

Figure 6-11: The gradient and the pCa at the point of zero charge (pZC) for the different oil coated silanised Fontainebleau cores, determined from the trend lines plotted in Figure 6-4 showing the relationship between zeta potential against pCa, against the (a) AN (b) BN and (c) AN/BN ratio of the different crude oils.

There is a clear positive correlation between both the gradient and the pCa at pZc and the AN and AN/BN ratio. The gradient appears independent of the BN whilst the pCa shows a slight negative trend with the BN, although the dependency is weaker than that of the AN and the data is scattered. As before, the comparable trends with the AN and the AN/BN ratio follow given that the BN appears largely insignificant in controlling the two properties.

Assuming the bulk AN does indeed correlate with the amount of negative charge at the crude oil surface, it follows that the amount of calcium required to neutralise this negative charge should increase with the AN (and AN/BN ratio). This is consistent with the observations in and provides further evidence to the notion that Ca^{2+} is a PDI to the oil surface. The expected increase in surface charge with increasing AN would also be expected to yield an increase in the Stern layer capacitance. Yet, in Figure 6-11 it can be seen that increasing AN yields a smaller gradient, which correlates with the Stern layer capacitance (Table 6-3). It is not clear why this discrepancy occurs but may highlight the difficulties in interpreting the surface properties from the bulk species (see section 2.2.4).

Despite many authors arguments, limited evidence suggests the bulk AN and BN are useful indicators of the surface charge of an oil. Oil TT has an AN that is ~34 times higher than Oil BG, yet the zeta potential is generally less negative, particularly in NaCl brines. This may suggest that Oil BG may actually have a higher number of acid species at the interface. Alternatively, PDIs may have a stronger affinity to the surface of Oil TT to modify its surface charge. Bonto et al. (2019) suggested an approach to determine the number of surface sites based on the bulk AN and BN. Their SCM firstly constrains the number of surface acid sites to 0.5 - 2.5 sites/nm^2 (correlating to an AN of 0.05 – 3 respectively) and the number of surface base sites to 0 – 2 sites/nm^2 (BN of 0 and 3 respectively) with the number of sites varying linearly with the AN or BN in these ranges. They then apply a further constraint to prevent the number of base sites exceeding the number of acid sites. Finally, if the number of base sites is greater than the acid sites, they set the acid sites equal to the base sites. Utilising this

approach, the number of acid and base sites that we may expect at the surface for the oils used in this study is calculated. The results are shown in Table 6-4.

Table 6-4: Predicted number of acid and base surface sites for the different oils used in this study using the approach of Bonto et al. (2019).

Oil	AN (mgKOH/g)	BN (mgKOH/g)	Surface Acid Sites (sites/nm^2)	Surface Base Sites (sites/nm^2)	Surface Acid/Base Site Ratio
TT	0.34	0.41	0.70	0.27	2.55
BD	0.05	0.60	0.50	0.40	1.25
BM	0.20	1.80	1.20	1.20	1.00
BG	0.01	2.00	1.33	1.33	1.00
BP	0.19	2.6	1.73	1.73	1.00

In three of the oils (BM, BG and BP), the AN is much less than the BN and thus the approach of Bonto et al. (2019) predicts much fewer acid species at the surface. The model requires that the number of surface acid sites must be equal to the number of surface base sites, despite the much higher BN in these oils. The surface acid/base site ratio for these oils is therefore 1. For the remaining two oils (BD and TT) the model calculates a larger number of acid sites than base sites at the interface and thus these species dominate, however the absolute number of both acid and base surface sites is smaller than in the other three oils.

This approach does not yield any clearer correlations with the observed data or trends. The larger number of surface acid sites for Oils BM, BG and BP may explain why these exhibit more negative zeta potential measurements than Oil TT, yet it is unclear why Oil BD, which is predicted to have the fewest number of surface acid sites, was one of the most negative oils (Figure 6-4). Furthermore, Oil BD showed similar zeta potential behaviour to Oil BM despite

the significant differences between their bulk physical properties (Table 6-1) and interpreted surface properties (Table 6-4). Likewise, Oils BG and BP showed similar zeta potential behaviour despite their different properties. It is apparent that the bulk AN and BN appear to be poor indicators or interfacial activity. This is unsurprising given the broad range of bulk material captured when measuring these properties. A potential limitation of the trends interpreted from these results is that all the oils used in this study have a relatively small AN. It is not uncommon for crude oils to exhibit AN up to 3 (and higher) and so it is unclear the extent to which these observations would propagate into this regime.

6.4.3 Implications for Controlled Salinity Waterflooding (CSW)

The zeta potential of the crude oil-brine zeta potential is of significant interest to many industries and applications but has gained particular attention regarding understanding improved oil recovery (IOR) by controlled salinity waterflooding (CSW). We have seen in Chapter 3 that for successful CSW in carbonate reservoirs, the zeta potential at the mineral-brine interface should be modified in such a way that it increases the electrostatic repulsion between the oil-brine and mineral-brine interfaces i.e., if the oil-brine interface is negatively charged, then the brine composition should be altered to make the zeta potential at the mineral-brine interface more negative, usually by diluting or reducing the total brine salinity. This mechanism was proposed based on an interpretation of the crude oil-brine zeta potential polarity from changes in the zeta potential of a carbonate core sample after wettability alteration. Samples that became more positive with increasing oil-wetness were interpreted to have a positive zeta potential at the oil-brine whilst samples that became more negative with increasing oil-wetness were interpreted to have a negative zeta potential at the oil-brine interface.

The oil-brine zeta potential interpreted in this way was found to be positively charged in several instances (Table 3-2). Furthermore, in Chapter 5, pore network modelling investigating the observed link between the zeta potential of a core sample and its wettability was used to model the magnitude of the oil-brine zeta potential (Figure 5-7). This modelling found that in most cases, the oil-brine zeta potential in reservoir formation brines – containing multiple ionic species with a total ionic strength above 2 mol/L - was predicted to be positively charged, ranging from +2 to +14mV (Figure 5-7). Both of these approaches suggested positive values for the oil-brine zeta potential may be more common in real subsurface environments than literature measurements obtained at low ionic strength, ideal laboratory conditions previously indicated.

The streaming potential method used here allows the zeta potential of the oil-brine interface to be probed at conditions relevant to natural reservoirs. However, the new data presented here indicate that in most instances, the oil-brine zeta potential is negatively charged at reservoir pH values of 5 - 6. In the presence of 2 mol/L $CaCl_2$ (representing the ionic strength and calcium concentration of natural formation brines) only one oil (Oil TT) returned a positive, but small, zeta potential of +0.6 mV.

Whilst the conditions used here do not directly represent those of the subsurface, it appears that there is a discrepancy between the 'pristine' oil-brine zeta potential measured on model systems and the *'in-situ'* oil-brine zeta potential interpreted from zeta potential measurements made on systems that represent 'real' COBR conditions. Given the complexity of real systems there may be a number of factors that contribute to such discrepancy. In particular, the oil-brine zeta potential may not be independent of the mineral-brine zeta potential. In Chapter 3, Oil TT was interpreted from coreflood experiments to exhibit a positive oil-brine zeta potential when the underlying carbonate surface was positively charged, and a negative oil-brine zeta potential when negatively charged (Figure 3-7). It is plausible that the distribution of polar components in the crude oil may be affected by the local electric field from the carbonate surface, and thus the oil-brine zeta potential is affected by the mineral-brine interface. This effect has only been observed in Oil TT which, of all the oils used in this work, has an AN/BN ratio closest to 1 (Table 6-1). The distribution of these species at the surface of Oil TT may be more susceptible to a local electric field than for other oils where one type of species dominates. This question has not yet been investigated by any experimental or modelling studies.

The streaming potential method allows the zeta potential of the oil-brine interface to be probed at conditions of salinity, composition and temperature that are more appropriate to the subsurface than can typically achieved by electrophoretic measurements. This work provides a foundation to systematically exploring the impact of these parameters to improve understanding of the oil-brine interface behaviour and better inform modelling studies. Such

next steps may yield insight into the challenges associated with predicting and optimising CSW.

6.5 Conclusions

Existing data of the crude oil-brine zeta potential is limited and unrepresentative of the conditions encountered in natural subsurface environments.

The zeta potential of the crude oil-brine interface can be measured using the streaming potential method by measuring the zeta potential of a neutral, strongly oil-wet porous substrate that has been coated with crude oil. Such a substrate can be prepared by chemically treating a natural sandstone core with a silane.

The zeta potential of various crude oils was measured with NaCl and $CaCl_2$ brines up to 2 mol/L at pH 5 -6. Measurements were validated at low ionic strength using a Zetasizer.

Conventional Zetasizer measurements of the oil-brine interface can be highly variable and dependent upon the properties of the oil-brine emulsion.

The zeta potential of the oil-brine interface is typically negative at pH 5-6 and increases in magnitude with decreasing ionic strength.

A linear relationship between zeta potential and pCa exists which varies with crude oil properties.

Increased AN appears to yield a more positive crude oil-brine zeta potential.

The results provide a foundation to systematically probe the controls on the crude oil-brine zeta potential. This has important implications for understanding and optimising improved oil recovery by controlled salinity waterflooding and developing surface complexation models for the oil-brine interface.

Chapter 7 - Summary, Conclusions & Further Work

7.1 Summary and Conclusion

The main focus of this work was to explore the relationship between the zeta potential of the mineral-brine and oil-brine interfaces and the wetting state of natural core samples. The implications of these relationships were primarily considered for the design and optimisation of controlled salinity waterflooding (CSW) process to improve oil recovery (IOR). A significant number of streaming potential measurements and coreflood experiments have been conducted to yield insight into these relationships. Pore network and surface complexation models have also been utilised to understand and contextualise experimental results in more detail.

Considering carbonates, an extensive suite of zeta potential measurements and complementary corefloods have been reported. The zeta potential was measured on outcrop and reservoir core samples saturated with formation brines, seawaters and low salinity brines of interest to CSW at ambient and elevated reservoir temperatures. The zeta potential is typically positive in high salinity formation brines and becomes more negative with a reduction in the brine salinity. In all cases, dilution yields a more negative zeta potential regardless of sample, brine composition or temperature. This reduction is attributed to the removal of Ca^{2+} and/or Mg^{2+}. Wettability alteration with crude oil yields a measurable change in the zeta potential. Samples become either more positive or more negative. The direction of change is interpreted to be indicative of the polarity of the oil-brine zeta potential. Contradictory to previous literature, the oil-brine zeta potential at reservoir conditions was interpreted to be positive in a number of instances. For certain oils, the interpreted oil-brine zeta potential polarity was observed to be dependent upon the composition of the aging brine, the measurement temperature and the core sample.

The interpreted polarity of the oil-brine interface appears to be an important parameter in determining the success of CSW in carbonates. IOR by CSW was observed only if the zeta potential at the mineral-brine interface was modified in such a way as to induce an electrostatic repulsion between the mineral-brine and oil-brine interfaces. I.e. if the oil-brine interface was interpreted to be negative, then IOR was observed only if the zeta potential at the mineral-brine interface became more negative when the injection brine was modified, and *vice-versa*. The amount of IOR during successful corefloods was correlated with the change in zeta potential at the mineral-brine interface, the change in zeta potential caused by wettability alteration and the wettability of the core sample. Of those parameters, the latter two are properties of the crude oil/brine/rock (COBR) system and cannot be modified. Thus, to maximise recovery, the injection brine composition should be designed to maximise the change in zeta potential at the mineral-brine interface.

The zeta potential of intact natural sandstones is typically negative when saturated with reservoir formation brines and low salinity brines at ambient and elevated reservoir temperature. However, in comparison to previous measurements under simple ideal conditions, the zeta potential does not correlate with pH. Instead, the zeta potential correlates with the bulk clay content – assumed to be a measure of both the mineralogical heterogeneity and surface charge. In high salinity formation brines, the zeta potential becomes increasingly more negative with increasing clay content whereas in low salinity brines the opposite trend is observed. Consequently, the difference in zeta potential decreases with increasing clay content. Dilution of the injection brine during CSW in sandstones may not yield a significant change in the zeta potential at the mineral-brine interface.

Pore network modelling was used to investigate the relationship between the zeta potential and wetting state. A bundle of capillary tubes (BOCT) model was developed where different capillaries were assigned a different surface charge depending on their wetting state. The macro-scale zeta potential and wettability were determined by integrating over all capillaries. This model was applied to the zeta potential measurements obtained on carbonate

cores and was used to interpret the zeta potential of the oil-wet capillaries, the only model parameter that was not experimentally measured. The zeta potential of oil-wet capillaries was assumed to represent the zeta potential of the oil-brine interface which was found to be positive in most cases. The results suggest that positive values of the oil-brine interface under reservoir conditions may be more common than previously thought from literature data. Whilst the interpretation of the oil-brine zeta potential was the primary application of the BOCT model, it can also be used to determine the macroscopic zeta potential of porous media where there is an underlying micro-scale zeta potential distribution at the mineral-surfaces, such as in heterogeneous porous media.

Finally, the zeta potential of the oil-brine interface was measured using the streaming potential method. Natural sandstone cores were chemically treated with a silane to render a strongly oil-wet substrate. These substrates were coated with crude oil, and the zeta potential of these samples measured. The results were benchmarked against electrophoretic measurements under dilute conditions showing a good match where the electrophoretic measurements were of good quality. The streaming potential method is advantageous over electrophoretic methods in both the parameter space that can be probed and the ease of conducting measurements. Results showed a strong linear relationship between the zeta potential of the oil-brine interface and the pCa (negative logarithm of the calcium concentration). The magnitude of the zeta potential varies between crude oils highlighting the differences in their composition and interfacial properties. However, the bulk physical properties are poor indicators of interfacial properties and thus it is challenging to interpret the zeta potential without measuring it experimentally. Despite indications from coreflood experiments and pore network modelling that the oil-brine zeta potential was commonly positive in high salinity reservoir formation brines, this was not observed in the streaming potential measurements. There is an apparent discrepancy between the *'in-situ'* oil-brine zeta potential measured in coreflood experiments representative of real systems, and the 'pristine' oil-brine zeta potential measured directly in model systems.

7.2 Implications for Controlled Salinity Waterflooding

The methodology and workflow presented in chapter 3 appears to provide a successful approach for predicting the success of CSW in carbonates. Measuring the change in zeta potential of a core sample after wettability alteration can be interpreted to represent the polarity of the oil-brine zeta potential. The injection brine should subsequently be designed in such a way as to modify the zeta potential at the mineral-brine interface to yield the same polarity as the oil-brine interface. For example, if the oil-brine zeta potential is interpreted to be negative, the injection brine should yield a more negative zeta potential at the mineral-brine interface. A more negative mineral-brine zeta potential can be achieved by reducing the total ionic strength or modifying the concentration of PDIs, particularly Ca^{2+} and/or Mg^{2+}. Likewise, if the oil-brine zeta potential is interpreted to be positive then the injection brine composition should be designed to make the zeta potential at the mineral-brine interface more positive. This could be achieved by increasing the concentration of Ca^{2+} and/or Mg^{2+}. Maxising the change in the zeta potential at the mineral-brine interface should yield optimal recovery. Strongly oil-wet carbonate reservoirs appear appropriate candidates for their IOR potential.

There are still questions regarding the controls on the zeta potential of the oil-brine interface, but the approach presented in chapter 6 provides a method to measure this at reservoir relevant conditions. More work is needed to fully understand how this translates into the oil-brine zeta potential in the subsurface. Interpreting the zeta potential from bulk oil properties that are typically measured in industry is inadequate. Better modelling may go some way to understanding the interfacially active and important components in crude oil.

The model and workflow appears to work well in strongly oil-wet carbonates but questions remain about how this will translate to mixed- or water-wet reservoir systems, such as sandstones. Additional zeta potential measurements on such systems at single- and multi-phase conditions, along with more advanced pore and pore network models are important next steps to improve understanding of CSW process in these systems.

7.3 Suggestions for Future Work

The majority of the open questions that have arisen from this work regard the controls on the oil-brine zeta potential under reservoir conditions, however, there are still some gaps of knowledge regarding the controls on the mineral-brine zeta potential in sandstones. Outlined below are some of the important open questions and suggestions for future work.

- We have seen from single-phase measurements that the zeta potential of clay-rich sandstones does not necessarily change when the injection brine is diluted, and may even become more positive. This anomalous observation was attributed to divalent cation adsorption on the clay surfaces. A more robust and systematic study probing the competing effects of cation adsorption and counter charge reduction on the zeta potential may confirm such hypotheses and yield further insight into the controls on the sandstone zeta potential. Such results would also better inform surface complexation models of the sandstone-brine interface such as that of Brady and Krumhansl (2012).
- The model proposed in chapter 3 relating changes in zeta potential to observations of IOR during CSW in carbonates appears fairly robust, it is not clear how this model applies in sandstones. The mineral-brine zeta potential does not necessarily change significantly by diluting the injection brine as mentioned prior. Furthermore, sandstones do not tend to become as oil-wet. Thus, the interpretation of the oil-brine zeta potential may be challenging. Given that the mineral-brine zeta potential is typically negative, any interpretation of a positive oil-brine interface will be ambiguous unless charge inversion is observed. The model presented in chapter 3 should be tested for sandstones to explore its applicability, with a particular emphasis on the bulk clay content since this was identified as a key control on the zeta potential.
- The pore network model developed in chapter 5 performed poorly in the mixed-wet regime. This is likely due to the oversimplification of real porous media by the bundle of capillary tubes model. More sophisticated pore network models could be developed based on the same principle of applying a different surface charge to different wetting

states. This would allow the zeta potential in the mixed-wet regime to be better understood. Moreover, it may yield better insight into the zeta potential of the oil-brine interface in sandstone core samples.

- The model could alternatively be applied to investigate the impact of the underlying micro-scale zeta potential distribution caused by mineralogical heterogeneity on the macroscopic zeta potential of porous media. For example, the relationship(s) between the zeta potential and clay content in sandstones could be investigated by assigning different surface charges to different minerals e.g. quartz, clay…
- The zeta potential of the oil-brine interface is poorly understood, particularly at conditions appropriate to the subsurface. The approach outline in chapter 6 to measure the zeta potential of the oil-brine interface with the streaming potential method allows for a new parameter space to be explore. There are a number of areas of interest including:
    - Understanding the impact of different ionic species present in natural brines (e.g. Mg^{2+}, SO_4^{2-}, CO_3^{2-}, K^+…).
    - Measuring the zeta potential in subsurface representative formation brines, seawaters and low salinity brines.
    - Understanding the impact of temperature.
- Bulk physical properties are poor indicators of the interfacial activity at the oil-brine interface. Better measures or improved understanding of the interfacially active components of crude oil may yield better insight into the understanding and modelling of the oil-brine zeta potential.
- The discrepancy between the *'in-situ'* oil-brine zeta potential from corefloods and the 'pristine' oil-brine zeta potential from streaming potential measurements is an important area of future work. The zeta potential of the oil-brine interface in subsurface formation brines should firstly be measured to confirm this discrepancy is present.

- The polarity of the oil-brine interface of Oil TT in chapter 3 was interpreted as positive when the mineral-brine interface was positive and negative when the mineral-brine interface was negative. It is plausible that the oil-brine interface in the subsurface may be affected by the zeta potential of the mineral-brine interface. The polar components in the crude oil may be distributed differently near the local electrical field originating from the mineral surface than in the bulk oil or in an oil-brine emulsion. This question has not been raised before. Indeed, the majority of studies assume both properties are independent of one another. The influence of the mineral-brine zeta potential on the oil-brine zeta potential could be an important source of the discrepancy mentioned in the previous point.

References

Abdallah, Wael, Jill S Buckley, Andrew Carnegie, John Edwards, Bernd Herold, Edmund Fordham, Arne Graue, Tarek Habashy, Nikita Seleznev, and Claude Signer. 1986. 'Fundamentals of wettability', *Technology*, 38: 268.

Abdallah, Wael, and Ahmed Gmira. 2014. 'Wettability assessment and surface compositional analysis of aged calcite treated with dynamic water', *Energy & Fuels*, 28: 1652-63.

Abdel-Raouf, Manar El-Sayed. 2012. *Crude Oil Emulsions - Composition Stability and Characterization* (IntechOpen).

Akbulut, Suat, and Seracettin Arasan. 2010. 'The variations of cation exchange capacity, pH, and zeta potential in expansive soils treated by additives', *International journal of civil and structural engineering*, 1: 139.

Al Mahrouqi, D., J. Vinogradov, and M. D. Jackson. 2017a. 'Zeta potential of artificial and natural calcite in aqueous solution', *Adv Colloid Interface Sci*, 240: 60-76.

Al Mahrouqi, Dawoud, Jan Vinogradov, and Matthew D Jackson. 2016. 'Temperature dependence of the zeta potential in intact natural carbonates', *Geophysical Research Letters*, 43: 11,578-11,87.

———. 2017b. 'Zeta potential of artificial and natural calcite in aqueous solution', *Advances in colloid and interface science*, 240: 60-76.

Alarouj, Mutlaq, Harry Collini, and Matthew D Jackson. 2021. 'Positive Zeta Potential in Sandstones Saturated with Natural Saline Brine', *Geophysical Research Letters*, 48: e2021GL094306.

Alhammadi, A.M., AlRatrout, A., Singh, K. et al. In situ characterization of mixed-wettability in a reservoir rock at subsurface conditions. Sci Rep 7, 10753 (2017).

Allègre, Vincent, Laurence Jouniaux, F Lehmann, P Sailhac, and R Toussaint. 2015. 'Influence of water pressure dynamics and fluid flow on the streaming-potential response for unsaturated conditions', *Geophysical Prospecting*, 63: 694-712.

Alotaibi, M. B., and A. A. Yousef. 2017. 'The Role of Individual and Combined Ions in Waterflooding Carbonate Reservoirs: Electrokinetic Study', *SPE Reservoir Evaluation & Engineering*, 20: 77-86.

Alotaibi, Mohammed B, Dongkyu Cha, Abdulkarim M Alsofi, and Ali A Yousef. 2018. 'Dynamic interactions of inorganic species at carbonate/brine interfaces: An electrokinetic study', *Colloids and Surfaces A: Physicochemical and Engineering Aspects*, 550: 222-35.

Alotaibi, Mohammed B, Hisham A Nasr-El-Din, and James J Fletcher. 2011. 'Electrokinetics of limestone and dolomite rock particles', *SPE Reservoir Evaluation & Engineering*, 14: 594-603.

AlRatrout, Ahmed, Ali Q Raeini, Branko Bijeljic, and Martin J Blunt. 2017. 'Automatic measurement of contact angle in pore-space images', *Advances in Water Resources*, 109: 158-69.

Alroudhan, A., J. Vinogradov, and M. D. Jackson. 2016. 'Zeta potential of intact natural limestone: Impact of potential-determining ions Ca, Mg and SO4', *Colloids and Surfaces A: Physicochemical and Engineering Aspects*, 493: 83-98.

Alshakhs, Mohammed J, and Anthony R Kovscek. 2016. 'Understanding the role of brine ionic composition on oil recovery by assessment of wettability from colloidal forces', *Advances in Colloid and Interface Science*, 233: 126-38.

Ammann, L, F Bergaya, and G Lagaly. 2005. 'Determination of the cation exchange capacity of clays with copper complexes revisited', *Clay Minerals*, 40: 441-53.

Amott, Earl. 1959. 'Observations relating to the wettability of porous rock', *Transactions of the AIME*, 216: 156-62.

Andersen, Simon Ivar, Mahavadi Sharath Chandra, John Chen, Ben Y Zeng, Fenglou Zou, Mmilili Mapolelo, Wael Abdallah, and Johannes Jan Buiting. 2016. 'Detection and

impact of carboxylic acids at the crude oil–water interface', *Energy & Fuels*, 30: 4475-85.
Anderson, William. 1986a. 'Wettability literature survey-part 2: Wettability measurement', *Journal of petroleum technology*, 38: 1246-62.
Anderson, William G. 1986b. 'Wettability literature survey-part 1: rock/oil/brine interactions and the effects of core handling on wettability', *Journal of petroleum technology*, 38: 1125-44.
Andrew, Matthew, Branko Bijeljic, and Martin J Blunt. 2014. 'Pore-scale contact angle measurements at reservoir conditions using X-ray microtomography', *Advances in Water Resources*, 68: 24-31.
Andrews, Edward, Ann Muggeridge, Gaetano Garfi, Alistair Jones, and Samuel Krevor. 2021. 'Pore-Scale X-ray Imaging of Wetting Alteration and Oil Redistribution during Low-Salinity Flooding of Berea Sandstone', *Energy & Fuels*, 35: 1197-207.
Austad, T, S Strand, EJ Høgnesen, and P Zhang. 2005. "Seawater as IOR fluid in fractured chalk." In *SPE international symposium on oilfield chemistry*. OnePetro.
Austad, T., S. F. Shariatpanahi, S. Strand, C. J. J. Black, and K. J. Webb. 2012. 'Conditions for a Low-Salinity Enhanced Oil Recovery (EOR) Effect in Carbonate Oil Reservoirs', *Energy & Fuels*, 26: 569-75.
Austad, Tor, Alireza RezaeiDoust, and Tina Puntervold. 2010. "Chemical mechanism of low salinity water flooding in sandstone reservoirs." In *SPE improved oil recovery symposium*. OnePetro.
Awolayo, Adedapo, Hemanta Sarma, and Ali AlSumaiti. 2016. 'An Experimental Investigation into the Impact of Sulfate Ions in Smart Water to Improve Oil Recovery in Carbonate Reservoirs', *Transport in Porous Media*, 111: 649-68.
Awolayo, Adedapo, Hemanta Sarma, and Ali M AlSumaiti. 2014. "A laboratory study of ionic effect of smart water for enhancing oil recovery in carbonate reservoirs." In *SPE EOR Conference at Oil and Gas West Asia*. OnePetro.
Bartels, W-B, H Mahani, S Berg, and SM Hassanizadeh. 2019. 'Literature review of low salinity waterflooding from a length and time scale perspective', *Fuel*, 236: 338-53.
Bartels, W-B, Hassan Mahani, Steffen Berg, Robin Menezes, Jesse A van der Hoeven, and Ali Fadili. 2017. 'Oil configuration under high-salinity and low-salinity conditions at pore scale: a parametric investigation by use of a single-channel micromodel', *Spe Journal*, 22: 1362-73.
Bartels, W-B, Maja Rücker, Steffen Berg, H Mahani, A Georgiadis, A Fadili, N Brussee, A Coorn, H Van Der Linde, and C Hinz. 2017. 'Fast X-ray micro-CT study of the impact of brine salinity on the pore-scale fluid distribution during waterflooding', *Petrophysics-The SPWLA Journal of Formation Evaluation and Reservoir Description*, 58: 36-47.
Berg, S., A. W. Cense, E. Jansen, and K. Bakker. 2010. 'Direct Experimental Evidence of Wettability Modification By Low Salinity', *Petrophysics*, 51: 9.
Bernard, George G. 1967. "Effect of floodwater salinity on recovery of oil from cores containing clays." In *SPE California Regional Meeting*. OnePetro.
Bertheussen, Are, Sébastien Simon, and Johan Sjöblom. 2017. 'Equilibrium partitioning of naphthenic acids and bases and their consequences on interfacial properties', *Colloids and Surfaces A: Physicochemical and Engineering Aspects*, 529: 45-56.
Blunt, Martin J. 1997. 'Pore level modeling of the effects of wettability', *SPE Journal*, 2: 494-510.
———. 2017. *Multiphase flow in permeable media: A pore-scale perspective* (Cambridge University Press).
Blunt, Martin J, Matthew D Jackson, Mohammad Piri, and Per H Valvatne. 2002. 'Detailed physics, predictive capabilities and macroscopic consequences for pore-network models of multiphase flow', *Advances in water resources*, 25: 1069-89.
Blunt, Martin J, and Harvey Scher. 1995. 'Pore-level modeling of wetting', *Physical Review E*, 52: 6387.

Bohinc, Klemen, Guilherme Volpe Bossa, and Sylvio May. 2017. 'Incorporation of ion and solvent structure into mean-field modeling of the electric double layer', *Advances in colloid and interface science*, 249: 220-33.

Boleve, Alexandre, Agnès Crespy, André Revil, F Janod, and Jean-Luc Mattiuzzo. 2007. 'Streaming potentials of granular media: Influence of the Dukhin and Reynolds numbers', *Journal of Geophysical Research: Solid Earth*, 112.

Bonto, María, Ali A. Eftekhari, and Hamidreza M. Nick. 2019. 'An overview of the oil-brine interfacial behavior and a new surface complexation model', *Scientific reports*, 9: 6072.

Borden, D, and RF Giese. 2001. 'Baseline studies of the clay minerals society source clays: cation exchange capacity measurements by the ammonia-electrode method', *Clays and clay minerals*, 49: 444-45.

Borukhov, Itamar, David Andelman, and Henri Orland. 1997. 'Steric effects in electrolytes: A modified Poisson-Boltzmann equation', *Physical review letters*, 79: 435.

Bouckaert, Stéphanie, Araceli Fernandez Pales, Christophe McGlade, Uwe Remme, Brent Wanner, Laszlo Varro, Davide D'Ambrosio, and Thomas Spencer. 2021. 'Net Zero by 2050: A Roadmap for the Global Energy Sector'.

Boujelben, Ahmed, Steven McDougall, Michael Watson, Igor Bondino, and Nicolas Agenet. 2018. 'Pore network modelling of low salinity water injection under unsteady-state flow conditions', *Journal of Petroleum Science and Engineering*.

Brady, Patrick V, and James L Krumhansl. 2012. 'A surface complexation model of oil–brine–sandstone interfaces at 100 C: Low salinity waterflooding', *Journal of Petroleum Science and Engineering*, 81: 171-76.

Brady, Patrick V., Norman R. Morrow, Andrew Fogden, Vivianne Deniz, Nina Loahardjo, and Winoto. 2015. 'Electrostatics and the Low Salinity Effect in Sandstone Reservoirs', *Energy & Fuels*, 29: 666-77.

Brooks, D. E., and G. V. F. Seaman. 1973. 'The effect of neutral polymers on the electrokinetic potential of cells and other charged particles: I. Models for the zeta potential increase', *Journal of Colloid and Interface Science*, 43: 670-86.

Buckley, J. S., Y. Liu, and S. Monsterleet. 1998. 'Mechanisms of Wetting Alteration by Crude Oils'.

Buckley, J. S., K. Takamura, and N. R. Morrow. 1989a. 'Influence of Electrical Surface Charges on the Wetting Properties of Crude Oils', *SPE Reservoir Engineering*, 4: 332-40.

Buckley, J.S., Y. Liu, X. Xie, and N.R. Morrow. 1997. 'Asphaltenes and Crude Oil Wetting - The Effect of Oil Composition', *Spe Journal*, 2: 107-19.

Buckley, Jill S. 1996. 'Mechanisms and consequences of wettability alteration by crude oils', Heriot-Watt University.

Buckley, JS, and Y Liu. 1998. 'Some mechanisms of crude oil/brine/solid interactions', *Journal of Petroleum Science and Engineering*, 20: 155-60.

Buckley, JS, K Takamura, and NR Morrow. 1989b. 'Influence of electrical surface charges on the wetting properties of crude oils', *SPE reservoir engineering*, 4: 332-40.

Carroll, Dorothy. 1959. 'Ion exchange in clays and other minerals', *Geological Society of America Bulletin*, 70: 749-79.

Chandrasekhar, Sriram, Himanshu Sharma, and Kishore K Mohanty. 2018. 'Dependence of wettability on brine composition in high temperature carbonate rocks', *Fuel*, 225: 573-87.

Chaverot, P, Alain Cagna, Sylvie Glita, and Francis Rondelez. 2008. 'Interfacial tension of bitumen− water interfaces. Part 1: Influence of endogenous surfactants at acidic pH', *Energy & Fuels*, 22: 790-98.

Chávez-Miyauchi, Tomás E, Abbas Firoozabadi, and Gerald G Fuller. 2016. 'Nonmonotonic elasticity of the crude oil–brine interface in relation to improved oil recovery', *Langmuir*, 32: 2192-98.

Chen, Lifeng, Guicai Zhang, Lei Wang, Wenming Wu, and Jijiang Ge. 2014. 'Zeta potential of limestone in a large range of salinity', *Colloids and Surfaces A: Physicochemical and Engineering Aspects*, 450: 1-8.

Chen, Min-Yi, Bhavani Raghuraman, Ian Bryant, Michael G Supp, and Jose Navarro. 2005. "Wireline apparatus for measuring steaming potentials and determining earth formation characteristics." In.: Google Patents.

Chen, Yongqiang, Quan Xie, and Vahid J Niasar. 2021. 'Insights into the nano-structure of oil-brine-kaolinite interfaces: Molecular dynamics and implications for enhanced oil recovery', *Applied Clay Science*, 211: 106203.

Chen, Yongqiang, Quan Xie, Wanfen Pu, and Ali Saeedi. 2018. 'Drivers of pH increase and implications for low salinity effect in sandstone', *Fuel*, 218: 112-17.

Cheng, Siyuan, Mengyin Fu, and F. A. Kulacki. 2018. 'Characterization of a porous transducer using a capillary bundle model: Permeability and streaming potential prediction', *International Journal of Heat and Mass Transfer*, 118: 349-54.

Chow, Ross S, and Koichi Takamura. 1988. 'Electrophoretic mobilities of bitumen and conventional crude-in-water emulsions using the laser Doppler apparatus in the presence of multivalent cations', *Journal of colloid and interface science*, 125: 212-25.

Chvedov, D., S. Ostap, and T. Le. 2001. 'Surface properties of red mud particles from potentiometric titration', *Colloids and Surfaces A: Physicochemical and Engineering Aspects*, 182: 131-41.

Collini, Harry, Shuai Li, Matthew D Jackson, Nicolas Agenet, Bilal Rashid, and John Couves. 2020. 'Zeta potential in intact carbonates at reservoir conditions and its impact on oil recovery during controlled salinity waterflooding', *Fuel*, 266: 116927.

Coreño, Juan, Antonia Martínez, Ana Bolarín, and Félix Sánchez. 2001. 'Apatite nucleation on silica surface: a ζ potential approach', *Journal of Biomedical Materials Research: An Official Journal of The Society for Biomaterials, The Japanese Society for Biomaterials, and The Australian Society for Biomaterials and the Korean Society for Biomaterials*, 57: 119-25.

Creux, Patrice, Jean Lachaise, Alain Graciaa, James K Beattie, and Alex M Djerdjev. 2009. 'Strong specific hydroxide ion binding at the pristine oil/water and air/water interfaces', *The Journal of Physical Chemistry B*, 113: 14146-50.

Creux, Patrice, Jean Lachaise, Alain Graciaa, and James K. Beattie. 2007. 'Specific Cation Effects at the Hydroxide-Charged Air/Water Interface', *The Journal of Physical Chemistry C*, 111: 3753-55.

Czarnecki, Jan. 2009. 'Stabilization of water in crude oil emulsions. Part 2', *Energy & Fuels*, 23: 1253-57.

Dagan, Gedeon. 2012. *Flow and transport in porous formations* (Springer Science & Business Media).

de Souza, J Pedro, and Martin Z Bazant. 2020. 'Continuum theory of electrostatic correlations at charged surfaces', *The Journal of Physical Chemistry C*, 124: 11414-21.

Delgado, Á V, F González-Caballero, RJ Hunter, LK Koopal, and J Lyklema. 2007. 'Measurement and interpretation of electrokinetic phenomena', *Journal of colloid and interface science*, 309: 194-224.

Derkani, Maryam H, Ashleigh J Fletcher, Wael Abdallah, Bastian Sauerer, James Anderson, and Zhenyu J Zhang. 2018. 'Low salinity waterflooding in carbonate reservoirs: Review of interfacial mechanisms', *Colloids and Interfaces*, 2: 20.

Ding, Hongna, and Sheik Rahman. 2017. 'Experimental and theoretical study of wettability alteration during low salinity water flooding-an state of the art review', *Colloids and Surfaces A: Physicochemical and Engineering Aspects*, 520: 622-39.

Donaldson, Erle C, Rex D Thomas, and Philip B Lorenz. 1969. 'Wettability determination and its effect on recovery efficiency', *Society of Petroleum Engineers Journal*, 9: 13-20.

Drummond, Carlos, and Jacob Israelachvili. 2004. 'Fundamental studies of crude oil–surface water interactions and its relationship to reservoir wettability', *Journal of Petroleum Science and Engineering*, 45: 61-81.

Dubey, ST, and PH Doe. 1993. 'Base number and wetting properties of crude oils', *SPE reservoir engineering*, 8: 195-200.

Dullien, Francis AL. 2012. *Porous media: fluid transport and pore structure* (Academic press).

Duman, Osman, and Sibel Tunç. 2009. 'Electrokinetic and rheological properties of Na-bentonite in some electrolyte solutions', *Microporous and Mesoporous Materials*, 117: 331-38.

Ebeling, Daniel, Dirk Van den Ende, and Frieder Mugele. 2011. 'Electrostatic interaction forces in aqueous salt solutions of variable concentration and valency', *Nanotechnology*, 22: 305706.

Eriksson, Erik. 1952. 'CATION-EXCHANGE EQUILIBRIA ON CLAY MINERALS', *Soil Science*, 74: 103-14.

Farooq, Umer, Sébastien Simon, Medad T Tweheyo, Johan Sjöblom, and Gisle Øye. 2013. 'Electrophoretic measurements of crude oil fractions dispersed in aqueous solutions of different ionic compositions—evaluation of the interfacial charging mechanisms', *Journal of Dispersion Science and Technology*, 34: 1376-81.

Farooq, Umer, Medad T. Tweheyo, Johan Sjöblom, and Gisle Øye. 2011. 'Surface Characterization of Model, Outcrop, and Reservoir Samples in Low Salinity Aqueous Solutions', *Journal of Dispersion Science and Technology*, 32: 519-31.

Fathi, S. Jafar, T. Austad, and S. Strand. 2011. 'Water-Based Enhanced Oil Recovery (EOR) by "Smart Water": Optimal Ionic Composition for EOR in Carbonates', *Energy & Fuels*, 25: 5173-79.

Foxall, Thomas, Gordon C Peterson, Henry M Rendall, and Alec L Smith. 1979. 'Charge determination at calcium salt/aqueous solution interface', *Journal of the Chemical Society, Faraday Transactions 1: Physical Chemistry in Condensed Phases*, 75: 1034-39.

Fredriksen, Sunniva B., Arthur U. Rognmo, and Martin A. Fernø. 2018. 'Pore-scale mechanisms during low salinity waterflooding: Oil mobilization by diffusion and osmosis', *Journal of Petroleum Science and Engineering*, 163: 650-60.

Gan, Wei, Wei Wu, Fangyuan Yang, Deping Hu, Hui Fang, Zhenggang Lan, and Qunhui Yuan. 2017. 'The behavior of hydroxide and hydronium ions at the hexadecane–water interface studied with second harmonic generation and zeta potential measurements', *Soft Matter*, 13: 7962-68.

Gandomkar, Asghar, and Mohammad Reza Rahimpour. 2015. 'Investigation of low-salinity waterflooding in secondary and tertiary enhanced oil recovery in limestone reservoirs', *Energy & Fuels*, 29: 7781-92.

Garfi, G., John, C.M., Rücker, M., Lin, Q., Spurin, C., Berg, S. and Krevor, S., 2022. Determination of the spatial distribution of wetting in the pore networks of rocks. Journal of Colloid and Interface Science.

Garzanti, Eduardo. 2019. 'Petrographic classification of sand and sandstone', *Earth-science reviews*, 192: 545-63.

Gaudin, AM, and DW Fuerstenau. 1955. 'Streaming potential studies. Quartz flotation with cationic collectors', *Mining Eng.*, 7.

Glover, P. W. J. 2018. 'Modelling pH-Dependent and Microstructure-Dependent Streaming Potential Coefficient and Zeta Potential of Porous Sandstones', *Transport in Porous Media*, 124: 31-56.

Glover, Paul WJ, Emilie Walker, and Matthew D Jackson. 2012. 'Streaming-potential coefficient of reservoir rock: A theoretical model', *Geophysics*, 77: D17-D43.

Grate, Jay W, Marvin G Warner, Jonathan W Pittman, Karl J Dehoff, Thomas W Wietsma, Changyong Zhang, and Mart Oostrom. 2013. 'Silane modification of glass and silica surfaces to obtain equally oil-wet surfaces in glass-covered silicon micromodel applications', *Water Resources Research*, 49: 4724-29.

Gray-Weale, Angus, and James K Beattie. 2009. 'An explanation for the charge on water's surface', *Physical Chemistry Chemical Physics*, 11: 10994-1005.

Guo, Jixiang, Qing Liu, Mingyuan Li, Zhaoliang Wu, and Alfred A Christy. 2006. 'The effect of alkali on crude oil/water interfacial properties and the stability of crude oil emulsions', *Colloids and Surfaces A: Physicochemical and Engineering Aspects*, 273: 213-18.

Haagh, Martinus Everardus Johannes, Igor Sîretanu, MHG Duits, and F Mugele. 2017. 'Salinity-dependent contact angle alteration in oil/brine/silicate systems: the critical role of divalent cations', *Langmuir*, 33: 3349-57.

Havre, Trond Erik, Johan Sjöblom, and Jens Emil Vindstad. 2003. 'Oil/water-partitioning and interfacial behavior of naphthenic acids', *Journal of Dispersion Science and Technology*, 24: 789-801.

Hilner, E, Martin Peter Andersson, Tue Hassenkam, Jesper Matthiesen, PA Salino, and Susan Louise Svane Stipp. 2015. 'The effect of ionic strength on oil adhesion in sandstone–the search for the low salinity mechanism', *Scientific reports*, 5: 1-9.

Hiorth, A, LM Cathles, and MV Madland. 2010. 'The impact of pore water chemistry on carbonate surface charge and oil wettability', *Transport in porous media*, 85: 1-21.

Hirasaki, GJ. 1991. 'Wettability: fundamentals and surface forces', *SPE formation evaluation*, 6: 217-26.

Hunter, Robert J. 2013. *Zeta potential in colloid science: principles and applications* (Academic press).

Hunter, Robert J. 1981a. *Zeta potential in colloid science : principles and applications* (Academic Press: London ; New York).

———. 1981b. *Zeta potential in colloid science : principles and applications* (Academic Press: London).

———. 1993. *Introduction to modern colloid science* (Oxford University Press: Oxford).

Hutin, Anthony, Jean-François Argillier, and Dominique Langevin. 2014a. 'Mass transfer between crude oil and water. Part 1: Effect of oil components', *Energy & Fuels*, 28: 7331-36.

———. 2014b. 'Mass transfer between crude oil and water. Part 2: Effect of sodium dodecyl benzenesulfonate for enhanced oil recovery', *Energy & Fuels*, 28: 7337-42.

Jaafar, Mohd Zaidi, Matthew David Jackson, Jon Saunders, Jan Vinogradov, and Christopher C Pain. 2009. "Measurements of streaming potential for downhole monitoring in intelligent wells." In *SPE Middle East Oil and Gas Show and Conference*. Society of Petroleum Engineers.

Jackson, M. D., D. Al-Mahrouqi, and J. Vinogradov. 2016a. 'Zeta potential in oil-water-carbonate systems and its impact on oil recovery during controlled salinity water-flooding', *Sci Rep*, 6: 37363.

Jackson, M. D., J. Vinogradov, G. Hamon, and M. Chamerois. 2016a. 'Evidence, mechanisms and improved understanding of controlled salinity waterflooding part 1: Sandstones', *Fuel*, 185: 772-93.

Jackson, Matthew D. 2008. 'Characterization of multiphase electrokinetic coupling using a bundle of capillary tubes model', *Journal of Geophysical Research: Solid Earth*, 113.

Jackson, Matthew D, Dawoud Al-Mahrouqi, and Jan Vinogradov. 2016b. 'Zeta potential in oil-water-carbonate systems and its impact on oil recovery during controlled salinity water-flooding', *Scientific Reports*, 6: 37363.

Jackson, Matthew D, and Martin J Blunt. 2002. 'Elliptic regions and stable solutions for three-phase flow in porous media', *Transport in porous media*, 48: 249-69.

Jackson, Matthew D, Murtaza Y Gulamali, Eli Leinov, Jonathan H Saunders, and Jan Vinogradov. 2012. 'Spontaneous potentials in hydrocarbon reservoirs during waterflooding: Application to water-front monitoring', *Spe Journal*, 17: 53-69.

Jackson, Matthew D, and Eli Leinov. 2012. 'On the validity of the “thin” and “thick” double-layer assumptions when calculating streaming currents in porous media', *International Journal of Geophysics*, 2012.

Jackson, Matthew D, Jan Vinogradov, Jonathan H Saunders, and Mohd Z Jaafar. 2011. 'Laboratory measurements and numerical modeling of streaming potential for downhole monitoring in intelligent wells', *SPE Journal*, 16: 625-36.

Jackson, Matthew D. 2010. 'Multiphase electrokinetic coupling: Insights into the impact of fluid and charge distribution at the pore scale from a bundle of capillary tubes model', *Journal of Geophysical Research: Solid Earth*, 115.

Jackson, Matthew D., and Jan Vinogradov. 2012. 'Impact of wettability on laboratory measurements of streaming potential in carbonates', *Colloids and Surfaces A: Physicochemical and Engineering Aspects*, 393: 86-95.

Jackson, MD, Jan Vinogradov, G Hamon, and M Chamerois. 2016b. 'Evidence, mechanisms and improved understanding of controlled salinity waterflooding part 1: Sandstones', *Fuel*, 185: 772-93.

Jadhunandan, PP, and Norman R Morrow. 1995. 'Effect of wettability on waterflood recovery for crude-oil/brine/rock systems', *SPE reservoir engineering*, 10: 40-46.

Jougnot, Damien, Niklas Linde, André Revil, and Claude Doussan. 2012. 'Derivation of soil-specific streaming potential electrical parameters from hydrodynamic characteristics of partially saturated soils', *Vadose Zone Journal*, 11: 0-0.

Jougnot, Damien, Aida Mendieta, Philippe Leroy, and Alexis Maineult. 2019. 'Exploring the effect of the pore size distribution on the streaming potential generation in saturated porous media, insight from pore network simulations', *Journal of Geophysical Research: Solid Earth*, 124: 5315-35.

Jougnot, Damien, Delphine Roubinet, Luis Guarracino, and Alexis Maineult. 2020. 'Modeling streaming potential in porous and fractured media, description and benefits of the effective excess charge density approach.' in, *Advances in Modeling and Interpretation in Near Surface Geophysics* (Springer).

Jouniaux, Laurence, and Tsuneo Ishido. 2012. 'Electrokinetics in earth sciences: a tutorial', *International Journal of Geophysics*, 2012.

Kafili Kasmaei, Azadeh, and Dandina N Rao. 2015. 'Is wettability alteration the main cause for enhanced recovery in low-salinity waterflooding?', *SPE Reservoir Evaluation & Engineering*, 18: 228-35.

Kasha, Ahmed, Hasan Al-Hashim, Wael Abdallah, Reza Taherian, and Bastian Sauerer. 2015. 'Effect of Ca2+, Mg2+ and SO42− ions on the zeta potential of calcite and dolomite particles aged with stearic acid', *Colloids and Surfaces A: Physicochemical and Engineering Aspects*, 482: 290-99.

Katende, Allan, and Farad Sagala. 2019. 'A critical review of low salinity water flooding: Mechanism, laboratory and field application', *Journal of Molecular Liquids*, 278: 627-49.

Khilar, K. C., R. N. Vaidya, and H. S. Fogler. 1989. 'Colloidally-induced fines release in porous media', *Journal of Petroleum Science and Engineering*, 4: 213-21.

Kia, S. F., H. S. Fogler, and M. G. Reed. 1987. 'Effect of Salt Composition on Clay Release in Berea Sandstones', *SPE*, 16254.

Klemme, HD, and Gregory F Ulmishek. 1991. 'Effective petroleum source rocks of the world: stratigraphic distribution and controlling depositional factors (1)', *AAPG Bulletin*, 75: 1809-51.

Kokal, Sunil, and Abdulaziz Al-Kaabi. 2010. 'Enhanced oil recovery: challenges & opportunities', *World Petroleum Council: Official Publication*, 64: p64-69.

Kokal, Sunil, Thompson Tang, Laurier Schramm, and Selim Sayegh. 1995. 'Electrokinetic and adsorption properties of asphaltenes', *Colloids and Surfaces A: Physicochemical and Engineering Aspects*, 94: 253-65.

Kolltveit, Yvonne. 2016. 'Relationship between crude oil composition and physical-chemical properties', The University of Bergen.

Kosmulski, Marek, and Per Dahlsten. 2006. 'High ionic strength electrokinetics of clay minerals', *Colloids and Surfaces A: Physicochemical and Engineering Aspects*, 291: 212-18.

Kosmulski, Marek, Edward Maczka, Krystyna Marczewska-Boczkowska, and Jarl B Rosenholm. 2003. 'Electrokinetic potentials of mineral oxides and calcium carbonate in artificial seawater', *Marine pollution bulletin*, 46: 120-22.

Kumar, Shailesh, and Vikas Mahto. 2017. 'Use of a novel surfactant to prepare oil-in-water emulsion of an Indian heavy crude oil for pipeline transportation', *Energy & Fuels*, 31: 12010-20.

Kundu, Partha, Vimal Kumar, and Indra Mani Mishra. 2015. 'Modeling the steady-shear rheological behavior of dilute to highly concentrated oil-in-water (o/w) emulsions: Effect of temperature, oil volume fraction and anionic surfactant concentration', *Journal of Petroleum Science and Engineering*, 129: 189-204.

Lager, A, KJ Webb, and CJJ Black. 2007. "Impact of brine chemistry on oil recovery." In *IOR 2007-14th European symposium on improved oil recovery*, cp-24-00020. European Association of Geoscientists & Engineers.

Lager, Arnaud, Kevin J Webb, CJJ Black, Mike Singleton, and Kenneth S Sorbie. 2008. 'Low salinity oil recovery-an experimental investigation1', *Petrophysics-The SPWLA Journal of Formation Evaluation and Reservoir Description*, 49.

Lashkarbolooki, Mostafa, Masoud Riazi, Farzad Hajibagheri, and Shahab Ayatollahi. 2016. 'Low salinity injection into asphaltenic-carbonate oil reservoir, mechanistical study', *Journal of Molecular Liquids*, 216: 377-86.

Lebedeva, Evgenia V., and Andrew Fogden. 2011. 'Micro-CT and Wettability Analysis of Oil Recovery from Sand Packs and the Effect of Waterflood Salinity and Kaolinite', *Energy & Fuels*, 25: 5683-94.

Li, Shuai, Harry Collini, and Matthew D Jackson. 2018. 'Anomalous zeta potential trends in natural sandstones', *Geophysical Research Letters*, 45: 11,068-11,73.

Li, Shuai, Matthew D Jackson, and Nicolas Agenet. 2020. 'Role of the calcite-water interface in wettability alteration during low salinity waterflooding', *Fuel*, 276: 118097.

Li, Shuai, Philippe Leroy, Frank Heberling, Nicolas Devau, Damien Jougnot, and Christophe Chiaberge. 2016. 'Influence of surface conductivity on the apparent zeta potential of calcite', *Journal of colloid and interface science*, 468: 262-75.

Li, Z. Y., J. Y. Li, Y. Liu, and R. K. Xu. 2014. 'Measurements of the streaming potential of clay soils from tropical and subtropical regions using self-made apparatus', *Environ Sci Pollut Res Int*, 21: 10461-9.

Ligthelm, Dick Jacob, Jan Gronsveld, Jan Hofman, Niels Brussee, Fons Marcelis, and Hilbert van der Linde. 2009. "Novel waterflooding strategy by manipulation of injection brine composition." In *EUROPEC/EAGE conference and exhibition*. OnePetro.

Linde, Niklas, Damie Jougnot, Andre Revil, SK Matthäi, Tanvi Arora, Didier Renard, and Claude Doussan. 2007. 'Streaming current generation in two-phase flow conditions', *Geophysical Research Letters*, 34.

Lu, Yingda, Nariman Fathi Najafabadi, and Abbas Firoozabadi. 2017. 'Effect of temperature on wettability of oil/brine/rock systems', *Energy & Fuels*, 31: 4989-95.

Ma, SM, X Zhang, NR Morrow, and X Zhou. 1999. 'Characterization of wettability from spontaneous imbibition measurements', *Journal of Canadian Petroleum Technology*, 38.

Mahani, H., A. L. Keya, S. Berg, and R. Nasralla. 2017a. 'Electrokinetics of Carbonate/Brine Interface in Low-Salinity Waterflooding: Effect of Brine Salinity, Composition, Rock Type, and pH on zeta-Potential and a Surface-Complexation Model', *Spe Journal*, 22: 53-68.

Mahani, Hassan, Arsene Levy Keya, Steffen Berg, Willem-Bart Bartels, Ramez Nasralla, and William R. Rossen. 2015. 'Insights into the Mechanism of Wettability Alteration by Low-Salinity Flooding (LSF) in Carbonates', *Energy & Fuels*, 29: 1352-67.

Mahani, Hassan, Arsene Levy Keya, Steffen Berg, and Ramez Nasralla. 2017b. 'Electrokinetics of carbonate/brine interface in low-salinity waterflooding: Effect of brine salinity, composition, rock type, and pH on ζ-potential and a surface-complexation model', *SPE Journal*, 22: 53-68.

———. 2018. 'Electrokinetics of carbonate/brine interface in low-salinity waterflooding: Effect of brine salinity, composition, rock type, and pH on?-potential and a surface-complexation model', *Spe Journal*, 22: 53-68.

Mahani, Hassan, R Menezes, S Berg, Ali Fadili, R Nasralla, D Voskov, and Vahid Joekar-Niasar. 2017. 'Insights into the impact of temperature on the wettability alteration by low salinity in carbonate rocks', *Energy & Fuels*, 31: 7839-53.

Manciu, Marian, and Eli Ruckenstein. 2012. 'Ions near the air/water interface: I. Compatibility of zeta potential and surface tension experiments', *Colloids and Surfaces A: Physicochemical and Engineering Aspects*, 400: 27-35.

Martin, John C. 1959. "The effects of clay on the displacement of heavy oil by water." In *Venezuelan annual meeting*. OnePetro.

McBride, Earle F. 1963. 'A classification of common sandstones', *Journal of Sedimentary Research*, 33: 664-69.

McGuire, PL, JR Chatham, FK Paskvan, DM Sommer, and FH Carini. 2005. "Low salinity oil recovery: An exciting new EOR opportunity for Alaska's North Slope." In *SPE western regional meeting*. OnePetro.

Mehraban, Mohammad Fattahi, Shahab Ayatollahi, and Mohammad Sharifi. 2019. 'Role of divalent ions, temperature, and crude oil during water injection into dolomitic carbonate oil reservoirs', *Oil & Gas Science and Technology–Revue d'IFP Energies nouvelles*, 74: 36.

Mirzaei-Paiaman, Abouzar, and Behzad Ghanbarian. 2021. 'A new methodology for grouping and averaging capillary pressure curves for reservoir models', *Energy Geoscience*, 2: 52-62.

Moeini, Farzaneh, Abdolhossein Hemmati-Sarapardeh, Mohammad-Hossein Ghazanfari, Mohsen Masihi, and Shahab Ayatollahi. 2014. 'Toward mechanistic understanding of heavy crude oil/brine interfacial tension: The roles of salinity, temperature and pressure', *Fluid phase equilibria*, 375: 191-200.

Morrow, Norman R. 1990. 'Wettability and its effect on oil recovery', *Journal of petroleum technology*, 42: 1476-84.

Morse, John W. 2018. 'The kinetics of calcium carbonate dissolution and precipitation.' in, *Carbonates* (De Gruyter).

Morse, John W, and Fred T Mackenzie. 1990. *Geochemistry of sedimentary carbonates* (Elsevier).

Mugele, Frieder, Bijoyendra Bera, Andrea Cavalli, Igor Siretanu, Armando Maestro, Michel Duits, Martien Cohen-Stuart, Dirk van den Ende, Isabella Stocker, and Ian Collins. 2015. 'Ion adsorption-induced wetting transition in oil-water-mineral systems', *Scientific reports*, 5: 1-8.

Muggeridge, Ann, Andrew Cockin, Kevin Webb, Harry Frampton, Ian Collins, Tim Moulds, and Peter Salino. 2014. 'Recovery rates, enhanced oil recovery and technological limits', *Philosophical Transactions of the Royal Society A: Mathematical, Physical and Engineering Sciences*, 372: 20120320.

Nande, Soumitra B., and Samarth D. Patwardhan. 2021. 'A review on low salinity waterflooding in carbonates: challenges and future perspective', *Journal of Petroleum Exploration and Production Technology*.

Nasralla, Ramez A, and Hisham A Nasr-El-Din. 2014a. 'Double-layer expansion: is it a primary mechanism of improved oil recovery by low-salinity waterflooding?', *SPE Reservoir Evaluation & Engineering*, 17: 49-59.

Nasralla, Ramez A, Ekaterina Sergienko, Shehadeh K Masalmeh, Hilbert A van der Linde, Niels J Brussee, Hassan Mahani, Bart M Suijkerbuijk, and Ibrahim S Al-Qarshubi. 2016. 'Potential of low-salinity waterflood to improve oil recovery in carbonates: Demonstrating the effect by qualitative coreflood', *Spe Journal*, 21: 1643-54.

Nasralla, Ramez A, Jeroen R Snippe, and Rouhi Farajzadeh. 2015. "Coupled geochemical-reservoir model to understand the interaction between low salinity brines and carbonate rock." In *SPE Asia Pacific enhanced oil recovery conference*. OnePetro.

Nasralla, Ramez A., Mohammed Abdullah Bataweel, and Hisham A. Nasr-El-Din. 2011. "Investigation of Wettability Alteration by Low Salinity Water." In *Offshore Europe*. Aberdeen, UK: Society of Petroleum Engineers.

Nasralla, Ramez A., Hassan Mahani, Hilbert A. van der Linde, Fons H. M. Marcelis, Shehadeh K. Masalmeh, Ekaterina Sergienko, Niels J. Brussee, Sebastiaan G. J. Pieterse, and Saptarshi Basu. 2018. 'Low salinity waterflooding for a carbonate reservoir:

Experimental evaluation and numerical interpretation', *Journal of Petroleum Science and Engineering*.

Nasralla, Ramez A., and Hisham A. Nasr-El-Din. 2014b. 'Impact of cation type and concentration in injected brine on oil recovery in sandstone reservoirs', *Journal of Petroleum Science and Engineering*, 122: 384-95.

Nazarova, Marfa, Patrick Bouriat, and Patrice Creux. 2018. 'Electrical Double-Layer Expansion Impact on the Oil–Quartz Adhesion for High- and Low-Salinity Brines', *Energy & Fuels*, 32: 7319-25.

Nenningsland, Andreas L, Sebastien Simon, and Johan Sjoblom. 2010. 'Surface properties of basic components extracted from petroleum crude oil', *Energy & Fuels*, 24: 6501-05.

Onaizi, Sagheer A. 2022. 'Effect of oil/water ratio on rheological behavior, droplet size, zeta potential, long-term stability, and acid-induced demulsification of crude oil/water nanoemulsions', *Journal of Petroleum Science and Engineering*, 209: 109857.

Perkin, Susan. 2012. 'Ionic liquids in confined geometries', *Physical Chemistry Chemical Physics*, 14: 5052-62.

Pooryousefy, Ehsan, Quan Xie, Yongqiang Chen, Ahmad Sari, and Ali Saeedi. 2018. 'Drivers of low salinity effect in sandstone reservoirs', *Journal of Molecular Liquids*, 250: 396-403.

Puntervold, Tina, Skule Strand, and Tor Austad. 2007. 'Water flooding of carbonate reservoirs: Effects of a model base and natural crude oil bases on chalk wettability', *Energy & Fuels*, 21: 1606-16.

Ravari, Reza Rostami. 2011. 'Water-Based EOR in Limestone by Smart Water: A study of surface chemistry'.

Revil, A, and A Cerepi. 2004. 'Streaming potentials in two-phase flow conditions', *Geophysical Research Letters*, 31.

Revil, A, and PWJ Glover. 1998. 'Nature of surface electrical conductivity in natural sands, sandstones, and clays', *Geophysical Research Letters*, 25: 691-94.

Revil, A, and N Linde. 2006. 'Chemico-electromechanical coupling in microporous media', *Journal of colloid and interface science*, 302: 682-94.

Revil, A., P. A. Pezard, and P. W. J. Glover. 1999. 'Streaming potential in porous media: 1. Theory of the zeta potential', *Journal of Geophysical Research: Solid Earth*, 104: 20021-31.

Revil, André, Niklas Linde, Adrian Cerepi, D Jougnot, S Matthäi, and S Finsterle. 2007. 'Electrokinetic coupling in unsaturated porous media', *Journal of colloid and interface science*, 313: 315-27.

RezaeiDoust, A, T Puntervold, S Strand, and T Austad. 2009. 'Smart water as wettability modifier in carbonate and sandstone: A discussion of similarities/differences in the chemical mechanisms', *Energy & Fuels*, 23: 4479-85.

Robbana, Enis, Todd Buikema, Chris Mair, Dale Williams, Dave Mercer, Kevin Webb, Aubrey Hewson, and Chris Reddick. 2012. "Low salinity enhanced oil recovery-laboratory to day one field implementation-LoSal EOR into the Clair Ridge Project." In *Abu Dhabi International Petroleum Conference and Exhibition*. OnePetro.

Rønningsen, Hans Petter, Johan Sjöblom, and Li Mingyuan. 1995. 'Water-in-crude oil emulsions from the Norwegian continental shelf 11. Ageing of crude oils and its influence on the emulsion stability', *Colloids and Surfaces A: Physicochemical and Engineering Aspects*, 97: 119-28.

Rücker, M., W. B. Bartels, G. Garfi, M. Shams, T. Bultreys, M. Boone, S. Pieterse, G. C. Maitland, S. Krevor, V. Cnudde, H. Mahani, S. Berg, A. Georgiadis, and P. F. Luckham. 2020. 'Relationship between wetting and capillary pressure in a crude oil/brine/rock system: From nano-scale to core-scale', *Journal of colloid and interface science*, 562: 159-69.

Saikia, Bikash D, Jagannathan Mahadevan, and Dandina N Rao. 2018. 'Exploring mechanisms for wettability alteration in low-salinity waterfloods in carbonate rocks', *Journal of Petroleum Science and Engineering*, 164: 595-602.

Salathiel, RA. 1973. 'Oil recovery by surface film drainage in mixed-wettability rocks', *Journal of petroleum technology*, 25: 1216-24.

Sandengen, Kristian, Anders Kristoffersen, Karen Melhuus, and Leif O Jøsang. 2016. 'Osmosis as mechanism for low-salinity enhanced oil recovery', *Spe Journal*, 21: 1227-35.

Sari, Ahmad, Quan Xie, Yongqiang Chen, Ali Saeedi, and Ehsan Pooryousefy. 2017. 'Drivers of low salinity effect in carbonate reservoirs', *Energy & Fuels*, 31: 8951-58.

Saunders, JH, MD Jackson, MY Gulamali, Jan Vinogradov, and CC Pain. 2012. 'Streaming potentials at hydrocarbon reservoir conditions', *Geophysics*, 77: E77-E90.

Schmatz, Joyce, Janos L Urai, Steffen Berg, and Holger Ott. 2015. 'Nanoscale imaging of pore-scale fluid-fluid-solid contacts in sandstone', *Geophysical Research Letters*, 42: 2189-95.

Seccombe, James C., Arnaud Lager, Kevin John Webb, Gary Jerauld, and Esther Fueg. 2008. "Improving Wateflood Recovery: LoSalTM EOR Field Evaluation." In *SPE Symposium on Improved Oil Recovery*.

Seccombe, Jim, Arnaud Lager, Gary Jerauld, Bharat Jhaveri, Todd Buikema, Sierra Bassler, John Denis, Kevin Webb, Andrew Cockin, Esther Fueg, and Frank Paskvan. 2010. "Demonstration of Low-Salinity EOR at Interwell Scale, Endicott Field, Alaska." In *SPE Improved Oil Recovery Symposium*.

Selem, A.M., Agenet, N., Gao, Y., Raeini, A.Q., Blunt, M.J. and Bijeljic, B., 2021. Pore-scale imaging and analysis of low salinity waterflooding in a heterogeneous carbonate rock at reservoir conditions. Scientific Reports, 11(1), pp.1-14.

Seyyedi, Mojtaba, Stefano Tagliaferri, Jimmie Abatzis, and Sidsel Marie Nielsen. 2018. 'An integrated experimental approach to quantify the oil recovery potential of seawater and low-salinity seawater injection in North Sea chalk oil reservoirs', *Fuel*, 232: 267-78.

Shariatpanahi, SF, P Hopkins, H Aksulu, S Strand, T Puntervold, and T Austad. 2016. 'Water based EOR by wettability alteration in dolomite', *Energy & Fuels*, 30: 180-87.

Sheng, J. J. 2014. 'Critical review of low-salinity waterflooding', *Journal of Petroleum Science and Engineering*, 120: 216-24.

Simanzhenkov, Vasily, and Raphael Idem. 2003. *Crude oil chemistry* (Crc Press).

Singh, Navpreet, and Hemanta Kumar Sarma. 2021. "Successful in the Lab, Not as Effective in the Field? Uncertainties in the Field Observations of Low Salinity Water Flooding in Sandstone and Carbonate Reservoirs-A Critical Analysis." In *SPE Western Regional Meeting*. OnePetro.

Siretanu, I., D. Ebeling, M. P. Andersson, S. L. Stipp, A. Philipse, M. C. Stuart, D. van den Ende, and F. Mugele. 2014. 'Direct observation of ionic structure at solid-liquid interfaces: a deep look into the Stern Layer', *Sci Rep*, 4: 4956.

Smalley, P Craig, Ann H Muggeridge, Sølvi S Amundrud, Mariann Dalland, Ole S Helvig, Eli J Høgnesen, Per Valvatne, and Arvid Østhus. 2020. "EOR Screening Including Technical, Operational, Environmental and Economic Factors Reveals Practical EOR Potential Offshore on the Norwegian Continental Shelf." In *SPE Improved Oil Recovery Conference*. OnePetro.

Smith, Alexander M, Plinio Maroni, Gregor Trefalt, and Michal Borkovec. 2019. 'Unexpectedly Large Decay Lengths of Double-Layer Forces in Solutions of Symmetric, Multivalent Electrolytes', *The Journal of Physical Chemistry B*, 123: 1733-40.

Snosy, M. Fouad, Mahmoud Abu El Ela, Ahmed El-Banbi, and Helmy Sayyouh. 2020. 'Comprehensive investigation of low-salinity waterflooding in sandstone reservoirs', *Journal of Petroleum Exploration and Production Technology*, 10: 2019-34.

Sohrabi, Mehran, Pedram Mahzari, Seyed A Farzaneh, John R Mills, Pantelis Tsolis, and Shaun Ireland. 2017. 'Novel insights into mechanisms of oil recovery by use of low-salinity-water injection', *Spe Journal*, 22: 407-16.

Soldi, M, D Jougnot, and L Guarracino. 2018. 'An analytical effective excess charge density model to predict the streaming potential generated by unsaturated flow', *Geophysical Journal International*, 216: 380-94.

Sondi, Ivan, Jasenka Biscan, and Velimir Pravdic. 1995. 'Electrokinetics of Pure Clay Minerals Revisited', *Journal of Colloid & Interface Science*, 178.

Song, Jin, Yongchao Zeng, Le Wang, Xindi Duan, Maura Puerto, Walter G. Chapman, Sibani L. Biswal, and George J. Hirasaki. 2017. 'Surface complexation modeling of calcite zeta potential measurements in brines with mixed potential determining ions (Ca2+, CO32−, Mg2+, SO42−) for characterizing carbonate wettability', *Journal of Colloid and Interface Science*, 506: 169-79.

Sorbie, Kenneth Stuart, and IR Collins. 2010. "A proposed pore-scale mechanism for how low salinity waterflooding works." In *SPE improved oil recovery symposium*. OnePetro.

Strand, Skule, Eli J Høgnesen, and Tor Austad. 2006. 'Wettability alteration of carbonates—Effects of potential determining ions (Ca2+ and SO42−) and temperature', *Colloids and Surfaces A: Physicochemical and Engineering Aspects*, 275: 1-10.

Stumm, Werner, Laura Sigg, and Barbara Sulzberger. 1992. *Chemistry of the solid-water interface : processes at the mineral-water and particle-water interface in natural systems* (Wiley: New York ;).

Szymula, Marta, Wladyslaw Janusz, and Jerzy Jabloriski. 2000. 'Electrochemical properties of asphaltene particles in aqueous solutions', *Journal of Dispersion Science and Technology*, 21: 785-802.

Takahashi, Masayoshi. 2005. 'ζ Potential of Microbubbles in Aqueous Solutions: Electrical Properties of the Gas−Water Interface', *The Journal of Physical Chemistry B*, 109: 21858-64.

Takeya, Miku, Mai Shimokawara, Yogarajah Elakneswaran, Toyoharu Nawa, and Satoru Takahashi. 2019. 'Predicting the electrokinetic properties of the crude oil/brine interface for enhanced oil recovery in low salinity water flooding', *Fuel*, 235: 822-31.

Takeya, Miku, Mai Shimokawara, Yogarajah Elakneswaran, Hirofumi Okano, and Toyoharu Nawa. 2019. 'Effect of acid number on the electrokinetic properties of crude oil during low salinity waterflooding', *Energy & Fuels*.

Tang, Guo-Qing, and Norman R. Morrow. 1999. 'Influence of brine composition and fines migration on crude oil/brine/rock interactions and oil recovery', *Journal of Petroleum Science and Engineering*, 24: 99-111.

Tetteh, Joel T, and Reza Barati. 2019. 'Crude-oil/brine interaction as a recovery mechanism for low-salinity waterflooding of carbonate reservoirs', *SPE Reservoir Evaluation & Engineering*, 22: 877-96.

Tetteh, Joel T, Patrick V Brady, and Reza Barati Ghahfaorkhi. 2020. 'Review of low salinity waterflooding in carbonate rocks: mechanisms, investigation techniques, and future directions', *Advances in Colloid and Interface Science*: 102253.

Tetteh, Joel T, Sherifa E Cudjoe, Saman A Aryana, and Reza Barati Ghahfarokhi. 2021. 'Investigation into fluid-fluid interaction phenomena during low salinity waterflooding using a reservoir-on-a-chip microfluidic model', *Journal of Petroleum Science and Engineering*, 196: 108074.

Tetteh, Joel T, Masoumeh Veisi, Patrick V Brady, and Reza Barati Ghahfarokhi. 2020. 'Surface reactivity analysis of the crude oil–brine–limestone interface for a comprehensive understanding of the low-salinity waterflooding mechanism', *Energy & Fuels*, 34: 2739-56.

Tetteh, Joel T., Sirwan Alimoradi, Patrick V. Brady, and Reza Barati Ghahfarokhi. 2020. 'Electrokinetics at calcite-rich limestone surface: Understanding the role of ions in modified salinity waterflooding', *Journal of Molecular Liquids*, 297: 111868.

Thanh, Luong Duy, and Rudolf Sprik. 2016. 'Zeta potential in porous rocks in contact with monovalent and divalent electrolyte aqueous solutions', *Geophysics*, 81: D303-D14.

Tone, Kisato, Masanobu Kamori, Yasuo Shibasaki, Yasuo Takeda, and Osamu Yamamoto. 1998. 'EFFECT OF THE SURFACE POTENTIAL ON THE CATION EXCHANGE CAPACITY OF KAOLIN MINERALS', *Clay Science*, 10: 327-35.

Vaidya, R. N., and H. S. Fogler. 1992. 'Fines Migration and Formation Damage: Influence of pH and Ion Exchange', *SPE Production Engineering*: 325-30.

Van Lin, Simone R, Kara K Grotz, Igor Siretanu, Nadine Schwierz, and Frieder Mugele. 2019. 'Ion-specific and ph-dependent hydration of mica–electrolyte interfaces', *Langmuir*, 35: 5737-45.

Vernhet, Aude, C Bellon-Fontaine, and A Doren. 1994. 'Comparison of three electrokinetic methods to determine the zeta potential of solid surfaces', *Journal de chimie physique*, 91: 1728-47.

Vinogradov, J, and MD Jackson. 2011. 'Multiphase streaming potential in sandstones saturated with gas/brine and oil/brine during drainage and imbibition', *Geophysical Research Letters*, 38.

Vinogradov, J., M. Z. Jaafar, and M. D. Jackson. 2010. 'Measurement of streaming potential coupling coefficient in sandstones saturated with natural and artificial brines at high salinity', *Journal of Geophysical Research*, 115.

Vinogradov, J., and M. D. Jackson. 2015. 'Zeta potential in intact natural sandstones at elevated temperatures', *Geophysical Research Letters*, 42: 6287-94.

Vinogradov, Jan, Rhiannon Hill, and Damien Jougnot. 2021. 'Influence of Pore Size Distribution on the Electrokinetic Coupling Coefficient in Two-Phase Flow Conditions', *Water*, 13: 2316.

Vinogradov, Jan, Matthew D Jackson, and Manuel Chamerois. 2018. 'Zeta potential in sandpacks: Effect of temperature, electrolyte pH, ionic strength and divalent cations', *Colloids and Surfaces A: Physicochemical and Engineering Aspects*, 553: 259-71.

Walker, E., and P. W. J. Glover. 2017. 'Measurements of the Relationship Between Microstructure, pH, and the Streaming and Zeta Potentials of Sandstones', *Transport in porous media*, 121: 183-206.

Webb, KJ, CJJ and Black, and H Al-Ajeel. 2004. "Low salinity oil recovery-log-inject-log." In *SPE/DOE Symposium on Improved Oil Recovery*. OnePetro.

Wei, Bing, Laiming Lu, Qinzhi Li, Hao Li, and Xuewen Ning. 2017. 'Mechanistic study of oil/brine/solid interfacial behaviors during low-salinity waterflooding using visual and quantitative methods', *Energy & Fuels*, 31: 6615-24.

Wenzel, Robert N. 1949. 'Surface roughness and contact angle', *The Journal of Physical Chemistry*, 53: 1466-67.

Yang, Fan, Plamen Tchoukov, Heather Dettman, Robel B Teklebrhan, Lan Liu, Tadeusz Dabros, Jan Czarnecki, Jacob Masliyah, and Zhenghe Xu. 2015. 'Asphaltene subfractions responsible for stabilizing water-in-crude oil emulsions. Part 2: Molecular representations and molecular dynamics simulations', *Energy & Fuels*, 29: 4783-94.

Yang, Fan, Plamen Tchoukov, Erica Pensini, Tadeusz Dabros, Jan Czarnecki, Jacob Masliyah, and Zhenghe Xu. 2014. 'Asphaltene subfractions responsible for stabilizing water-in-crude oil emulsions. Part 1: interfacial behaviors', *Energy & Fuels*, 28: 6897-904.

Yousef, Ali A, Salah Al-Saleh, and Mohammed Al-Jawfi. 2011a. "Smart waterFlooding for carbonate reservoirs: Salinity and role of ions." In *SPE middle east oil and gas show and conference*. OnePetro.

Yousef, Ali A, Salah Al-Saleh, Abdulaziz Al-Kaabi, and Mohammed Al-Jawfi. 2011a. 'Laboratory investigation of the impact of injection-water salinity and ionic content on oil recovery from carbonate reservoirs', *SPE Reservoir Evaluation & Engineering*, 14: 578-93.

Yousef, Ali A., Salah Al-Saleh, and Mohammed Al-Jawfi. 2011b. "New Recovery Method for Carbonate Reservoirs through Tuning the Injection Water Salinity: Smart WaterFlooding." In *SPE EUROPEC/EAGE Annual Conference and Exhibition*.

———. 2012. "Improved/Enhanced Oil Recovery from Carbonate Reservoirs by Tuning Injection Water Salinity and Ionic Content." In *SPE Improved Oil Recovery Symposium*.

Yousef, Ali A., Salah Hamad Al-Saleh, Abdulaziz Al-Kaabi, and Mohammed Saleh Al-Jawfi. 2011b. 'Laboratory Investigation of the Impact of Injection-Water Salinity and Ionic Content on Oil Recovery From Carbonate Reservoirs', *SPE Reservoir Evaluation & Engineering*, 14: 578-93.

Yuan, Yuehua, and T Randall Lee. 2013. 'Contact angle and wetting properties.' in, *Surface science techniques* (Springer).

Yukselen-Aksoy, Y., and A. Kaya. 2011. 'A study of factors affecting on the zeta potential of kaolinite and quartz powder', *Environmental Earth Sciences*, 62: 697-705.

Zhang, D Leslie, Shunhua Liu, Maura Puerto, Clarence A Miller, and George J Hirasaki. 2006. 'Wettability alteration and spontaneous imbibition in oil-wet carbonate formations', *Journal of Petroleum Science and Engineering*, 52: 213-26.

Zhang, Peimao, and Tor Austad. 2006. 'Wettability and oil recovery from carbonates: Effects of temperature and potential determining ions', *Colloids and Surfaces A: Physicochemical and Engineering Aspects*, 279: 179-87.

Appendices

Appendix A

Raw experimental data from the single-phase and multiphase zeta potential measurements reported in chapter 3 have been deposited in the Imperial College London data repository and can be found at 10.14469/hpc/10337.

Appendix B

Table B 1: Single phase sandstone-brine zeta potential data presented in Chapter 4.

Sample	Temperature (°C)	Saturation Brine	*C*, V/Pa	ζ, mV	Porosity	k (mD)	pH	Fluid Conductivity (mS/cm)	Sat Rock Conductivity (mS/cm)	Formation Factor (F)
BERB-1	23	HIS-1	-7.97E-10	-10.66	14%	60	7.3	77.8	4.4	17.8
		LIS-1	-5.32E-08	-18.77	14%	60	7.7	2.3	0.1	15.6
	70	HIS-1	-1.45E-09	-6.85	14%	45	6.9	130.0	4.1	31.9
		LIS-1	-5.22E-08	-12.21	14%	45	7.8	6.4	0.3	24.8
BERB-2	23	HIS-1	-1.01E-09	-13.70	17%	60	7.1	78.4	4.5	17.3
		LIS-1	-5.16E-08	-16.81	17%	20	7.6	2.1	0.1	15.0
	70	HIS-1	-1.16E-09	-10.44	17%	45	6.9	126.0	7.7	16.3
		LIS-1	-5.22E-08	-13.35	17%	40	7.9	3.6	0.3	12.8
BERB-3	23	HIS-1	-7.97E-10	-10.55	19%	65	7.2	77.2	4.8	16.2

		LIS-1	-4.93E-08	-15.37	19%	40	8.0	2.3	0.1	16.0
	70	HIS-1	-1.27E-09	-12.47	19%	40	7.2	132.0	9.0	14.7
		LIS-1	-4.00E-08	-14.33	19%	40	8.0	5.3	0.4	12.5
CAST_1	23	HIS-1	-9.42E-10	-12.43	26%	400	7.1	77.0	7.3	10.5
		LIS-1	-5.48E-08	-23.20	26%	300	7.7	1.8	0.3	6.0
	70	HIS-1	-9.66E-10	-6.45	26%	250	7.0	128.0	9.5	13.5
		LIS-1	-3.04E-08	-7.90	26%	200	7.8	3.8	0.5	8.0
CAST_2	23	HIS-1	-1.01E-09	-13.61	26%	400	7.1	78.0	9.1	8.5
		LIS-1	-1.78E-08	-14.14	26%	300	7.7	4.5	0.7	6.5
	70	HIS-1	-1.45E-09	-12.94	26%	300	6.9	126.0	15.2	8.3
		LIS-1	-4.83E-08	-7.48	26%	250	8.1	3.8	0.3	11.2
CAST_3	23	HIS-1	-9.86E-10	-13.00	20%	500	7.3	77.0	8.0	9.7
		LIS-1	-3.91E-08	-14.43	20%	350	8.2	1.7	0.3	6.0
	70	HIS-1	-1.16E-09	-10.42	20%	220	7.1	130.0	13.9	9.3
		LIS-1	-4.96E-08	-10.60	20%	190	8.0	3.7	0.4	8.7
CAST_4	23	HIS-1	-1.02E-09	-13.84	20%	550	7.3	79.0	9.0	8.8
		LIS-1	-4.58E-08	-17.24	20%	520	7.6	2.0	0.3	6.3
	70	HIS-1	-9.56E-10	-8.53	20%	300	7.2	133.0	15.0	8.9
		LIS-1	-4.38E-08	-16.20	20%	300	7.9	7.0	0.8	8.7
FB_1	23	HIS-1	-8.28E-11	-1.09	10%	125	7.0	77.0	1.9	39.9
		LIS-1	-5.31E-08	-14.27	10%	145	8.1	2.0	0.1	40.0
	70	HIS-1	-1.24E-10	-1.26	10%	105	7.1	135.0	3.7	37.0
		LIS-1	-6.13E-08	-12.63	10%	110	7.9	4.0	0.1	44.4
FB_2	23	HIS-1	-5.80E-11	-0.76	9%	75	7.0	76.4	1.5	52.3
		LIS-1	-9.60E-08	-26.13	9%	75	7.9	2.0	0.0	54.9
	70	HIS-1	-1.71E-10	-1.89	9%	45	7.1	142.5	2.9	49.8
		LIS-1	-1.02E-07	-21.70	9%	70	8.1	4.5	0.1	63.6
FB_3	23	HIS-1	-1.31E-10	-1.72	10%	100	7.0	77.0	2.5	30.6

		LIS-1	-5.07E-08	-20.82	10%	170	7.9	2.6	0.1	26.0
	70	HIS-1	-1.02E-10	-0.83	10%	115	7.3	140.0	3.8	36.5
		LIS-1	-4.42E-08	-11.83	10%	110	8.1	6.0	0.2	37.3
DODT-1	23	HIS-2		-7.86	21%	450	5.4			22.0
		LIS-2		-24.40	21%	450	6.2			15.0
DODT-2	23	HIS-2		-7.78	21%	450	5.9			21.5
		LIS-2		-24.90	21%	450	6.3			10.0
DODT-3	23	HIS-2		-7.90	21%	450	5.9			19.0
		LIS-2		-25.50	21%	450	6.2			18.0
DODT-4	23	HIS-2		-7.06	21%	450	5.9			23.0
		LIS-2		-25.50	21%	450	6.4			10.0
DODT-5	23	HIS-2		-7.06	21%	450	5.9			22.3
		LIS-2		-24.40	21%	450	6.5			10.1
STB-1	23	HIS-2		-14.60	19%	70	6.6			32.0
		LIS-2		-19.26	19%	70	7.6			10.1
STB-2	23	HIS-2		-12.00	19%	70	6.3			24.5
		LIS-2		-23.10	19%	70	7.7			10.0
STB-3	23	HIS-2		-12.80	19%	70	6.3			21.0
		LIS-2		-22.10	19%	70	7.5			9.1
STB-4	23	HIS-2		-11.89	19%	70	6.4			23.0
		LIS-2		-21.10	19%	70	7.9			10.0
STB-5	23	HIS-2		-12.00	19%	70	6.5			34.0
		LIS-2		-23.20	19%	70	7.6			11.0

Appendix C

Raw experimental data from the streaming potential measurements made on the oil coated silanised Fontainebleau sandstones have been deposited in the Imperial College London data repository and can be found at 10.14469/hpc/10348.

Table C 1: Oil-brine zeta potential data shown in Chapter 6.

					SPM			Zetasizer		
Oil	**Ionic Strength (mol/L)**	**xCa**		**pCa**	**Zeta (mV)**	**pH**	**Zeta Error (mV)**	**Zeta (mV)**	**pH**	**Zeta Error (mV)**
Oil M	10-3M		0%	N/A	-56.83	5.7	2.00	-49.29	4.80	4.15
			2%	5.18	-79.27	5.9	2.00	-44.37	5.10	10.20
			5%	4.78	-78.57	5.6	2.00	-41.15	5.20	10.84
			10%	4.48	-73.38	5.6	2.00	-33.55	5.60	4.83
			20%	4.18	-72.23	5.5	2.00	-44.92	5.60	3.18
			50%	3.78	-62.22	5.9	2.00	-33.73	5.50	4.01
			100%	3.48	-52.58	5.7	2.00	-38.08	5.40	1.75
	0.02M		0%	N/A	-53.95	5.7	2.00	-41.72	5.70	5.87
			2%	3.88	-58.48	5.7	2.00	-38.25	5.60	2.96
			5%	3.48	-55.90	5.8	2.00	-40.96	6.00	2.06
			10%	3.18	-45.50	5.7	2.00	-33.64	6.10	2.74
			20%	2.88	-44.93	5.5	2.00	-19.41	5.60	4.22
			50%	2.48	-37.25	5.6	2.00	-19.50	5.70	2.91
			100%	2.18	-31.89	5.7	2.00	-19.38	5.40	0.82
	0.5M		0%	N/A	-29.92	5.7	2.00	N/A		
			2%	2.48	-28.74	5.6	2.00			
			5%	2.08	-27.00	5.8	2.00			
			10%	1.78	-24.21	5.7	2.00			
			20%	1.48	-21.83	5.5	2.00			
			50%	1.08	-15.15	5.4	2.00			

		100%	0.78	-8.90	5.5	2.00			
		0%	N/A	-19.32	6.2	2.00			
		2%	1.88	-18.11	6.0	2.00			
		5%	1.48	-16.44	5.9	2.00			
	2M	10%	1.18	-15.30	6.0	2.00			
		20%	0.88	-12.33	5.9	2.00			
		50%	0.48	-6.30	5.7	2.00			
		100%	0.18	-0.62	5.7	2.00			
		0%	N/A	-60.52	6.0	2.00	-40.22	5.50	6.85
		2%	5.18	-71.01	5.7	2.00	-48.77	5.30	3.87
		5%	4.78	-65.47	5.5	2.00	-30.37	5.50	7.17
	10-3M	10%	4.48	-60.11	5.5	2.00	-29.70	5.20	5.85
		20%	4.18	-60.15	5.6	2.00	-35.29	5.20	6.67
		50%	3.78	-50.38	5.7	2.00	-35.75	5.20	3.33
		100%	3.48	-47.93	6.2	2.00	-38.95	5.30	3.42
		0%	N/A	-54.78	5.8	2.00	-49.51	5.40	3.86
		2%	3.88	-43.69	5.5	2.00	-35.61	5.50	8.03
		5%	3.48	-44.39	5.5	2.00	-40.58	5.10	4.02
Oil P	0.02M	10%	3.18	-42.57	5.6	2.00	-33.06	5.20	2.31
		20%	2.88	-37.06	5.7	2.00	-30.51	5.30	2.14
		50%	2.48	-30.99	5.7	2.00	-20.61	5.20	1.69
		100%	2.18	-26.03	5.7	2.00	-4.62	5.10	5.63
		0%	N/A	-20.34	5.4	2.00			
		2%	2.48	-22.08	5.4	2.00			
		5%	2.08	-22.19	5.4	2.00			
	0.5M	10%	1.78	-19.78	5.4	2.00		N/A	
		20%	1.48	-17.78	5.5	2.00			
		50%	1.08	-12.73	5.4	2.00			
		100%	0.78	-7.84	5.4	2.00			
	2M	0%	N/A	-7.52	6.3	2.00			

		2%	1.88	-11.22	5.7	2.00			
		5%	1.48	-9.64	5.5	2.00			
		10%	1.18	-8.57	5.3	2.00			
		20%	0.88	-7.55	5.5	2.00			
		50%	0.48	-3.72	5.3	2.00			
		100%	0.18	-0.52	5.2	2.00			
Oil T	10-3M	0%	N/A	-58.38	5.7	2.00	-60.52	5.40	5.19
		2%	5.18	-54.16	5.6	2.00	-54.48	5.50	3.45
		5%	4.78	-49.01	5.5	2.00	-55.23	5.80	4.00
		10%	4.48	-48.82	5.5	2.00	-41.98	5.40	4.85
		20%	4.18	-50.10	6.4	2.00	-44.92	5.70	2.45
		50%	3.78	-43.61	6.2	2.00	-41.89	5.50	2.33
		100%	3.48	-37.48	5.7	2.00	-24.83	5.50	2.80
	0.02M	0%	N/A	-34.24	5.7	2.00	-36.76	5.60	2.78
		2%	3.88	-37.56	5.7	2.00	-34.64	5.50	6.68
		5%	3.48	-34.09	5.6	2.00	-42.28	5.30	1.49
		10%	3.18	-31.96	5.5	2.00	-33.07	5.40	3.11
		20%	2.88	-28.03	5.5	2.00	-27.08	5.80	0.93
		50%	2.48	-23.21	5.5	2.00	-26.08	5.90	1.42
		100%	2.18	-19.19	5.6	2.00	-24.52	6.00	1.00
	0.5M	0%	N/A	-20.28	6.5	2.00			
		2%	2.48	-18.25	6.1	2.00			
		5%	2.08	-17.59	6.3	2.00			
		10%	1.78	-14.91	5.6	2.00			
		20%	1.48	-13.22	5.5	2.00		N/A	
		50%	1.08	-9.06	5.3	2.00			
		100%	0.78	-4.86	5.4	2.00			
	2M	0%	N/A	-9.03	5.4	2.00			
		2%	1.88	-8.99	5.4	2.00			
		5%	1.48	-8.40	5.4	2.00			

		10%	1.18	-6.89	5.4	2.00			
		20%	0.88	-3.82	5.5	2.00			
		50%	0.48	-2.26	5.4	2.00			
		100%	0.18	1.43	5.4	2.00			
Oil G	10-3M	0%	N/A	-85.63	5.3	2.00	-40.80	5.30	9.06
		2%	5.18	-66.18	5.5	2.00	-38.70	5.30	12.09
		5%	4.78	-67.76	5.4	2.00	-38.90	5.20	9.83
		10%	4.48	-66.79	5.1	2.00	-39.80	5.00	3.69
		20%	4.18	-61.58	5.5	2.00	-34.47	5.00	6.30
		50%	3.78	-49.67	5.2	2.00	-28.48	5.20	6.74
		100%	3.48	-47.09	5.6	2.00	-39.19	5.10	2.12
	0.02M	0%	N/A	-51.92	5.5	2.00	-43.40	5.10	3.03
		2%	3.88	-49.36	5.4	2.00	-39.53	5.20	3.26
		5%	3.48	-41.76	5.8	2.00	-36.06	5.30	3.60
		10%	3.18	-41.35	5.3	2.00	-27.09	5.20	5.55
		20%	2.88	-38.63	5.5	2.00	-26.29	5.20	1.87
		50%	2.48	-30.52	5.4	2.00	-16.06	5.20	2.37
		100%	2.18	-25.78	5.7	2.00	-18.80	5.00	0.94
	0.5M	0%	N/A	-24.80	5.8	2.00			
		2%	2.48	-24.03	5.6	2.00			
		5%	2.08	-22.90	5.6	2.00			
		10%	1.78	-20.37	5.5	2.00			
		20%	1.48	-16.82	5.7	2.00			
		50%	1.08	-11.51	5.7	2.00			
		100%	0.78	-6.07	5.2	2.00		N/A	
	2M	0%	N/A	-14.40	6.0	2.00			
		2%	1.88	-16.57	5.5	2.00			
		5%	1.48	-13.18	5.5	2.00			
		10%	1.18	-12.09	5.5	2.00			
		20%	0.88	-9.34	5.6	2.00			

		50%	0.48	-6.30	5.4	2.00			
		100%	0.18	-1.37	4.9	2.00			
Oil D	10-3M	0%	N/A	-89.10	6.4	2.00	-68.16	5.50	3.85
		2%	5.18	-83.23	6.1	2.00	-60.27	5.50	3.76
		5%	4.78	-77.38	5.1	2.00	-55.55	5.60	5.48
		10%	4.48	-73.84	5.3	2.00	-38.46	5.40	6.28
		20%	4.18	-63.74	5.3	2.00	-51.03	5.40	4.54
		50%	3.78	-56.95	5.1	2.00	-46.11	5.40	3.20
		100%	3.48	-56.45	5.6	2.00	-29.16	5.40	4.24
	0.02M	0%	N/A	-58.21	5.9	2.00	-43.32	5.30	5.03
		2%	3.88	-55.71	5.5	2.00	-50.19	5.50	3.49
		5%	3.48	-52.43	5.5	2.00	-44.75	5.50	3.21
		10%	3.18	-49.31	5.5	2.00	-41.09	5.50	2.07
		20%	2.88	-43.48	5.6	2.00	-36.23	5.40	1.14
		50%	2.48	-33.86	5.5	2.00	-25.79	5.30	4.55
		100%	2.18	-29.76	5.6	2.00	-22.34	5.30	0.83
	0.5M	0%	N/A	-28.57	5.6	2.00			
		2%	2.48	-26.16	5.5	2.00			
		5%	2.08	-24.16	5.5	2.00			
		10%	1.78	-22.18	5.5	2.00			
		20%	1.48	-19.58	5.4	2.00			
		50%	1.08	-14.41	5.4	2.00			
		100%	0.78	-8.38	5.3	2.00		N/A	
	2M	0%	N/A	-15.95	5.6	2.00			
		2%	1.88	-14.52	5.4	2.00			
		5%	1.48	-12.83	5.5	2.00			
		10%	1.18	-13.26	5.5	2.00			
		20%	0.88	-9.86	5.5	2.00			
		50%	0.48	-3.50	5.4	2.00			
		100%	0.18	-1.47	5.6	2.00			

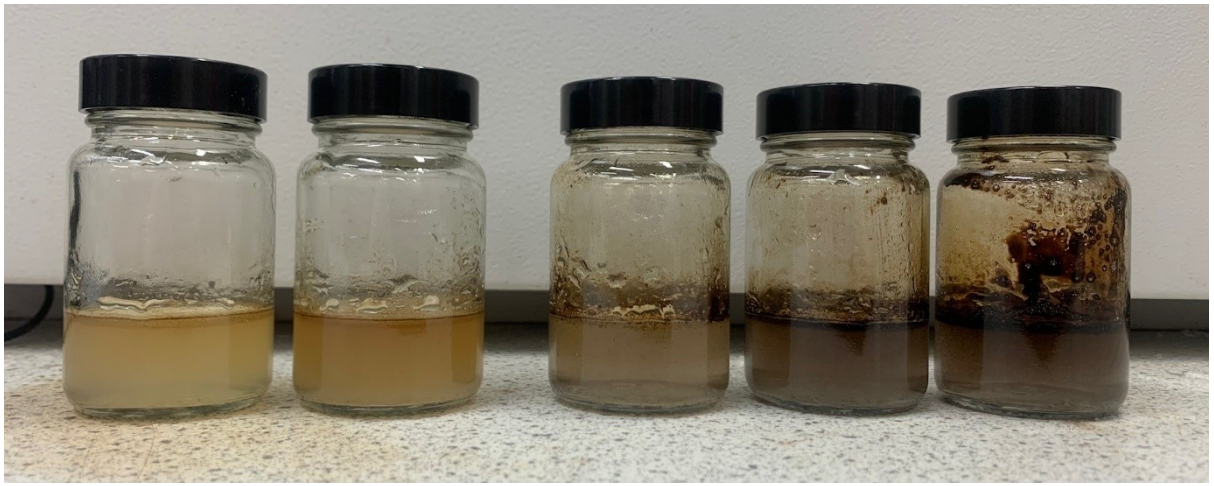

Figure C 1: Emulsions of the five different oils in 0.001M NaCl brine. From far left: Oil T; Oil D; Oil M; Oil P; Oil G.